



NAM

Collapse Shaking Table Test on a URM Cavity Wall Structural (LNEC-BUILD1) Representative of a Dutch Terraced House

**U. Tomassetti, A. A. Correia, F. Graziotti, A. I. Marques, M. Mandirola
and P. X. Candeias**

Eucentre

(European Centre for Training and Research in Earthquake Engineering)

LNEC

(Laboratório Nacional de Engenharia Civil / National Laboratory of Civil Engineering)

Date September 2017

Editors Jan van Elk & Dirk Doornhof

General Introduction

Many of the buildings in the Groningen field area are terraced unreinforced masonry buildings. A program to assess the response of these building to earthquakes was therefore initiated. This program built on the experimental and modelling program into the properties of URM building materials, wall elements and wall units.

A typical Groningen terraced house built using materials from the Groningen area by builders from the Groningen area, was tested at the shake-table of Eucentre in Pavia, Italy (Ref. 1). Although the building was at the end of this test program seriously damaged, the building had not collapsed. This left questions on the remaining capacity of the structure and its ability to resist larger seismic movements before (partially) collapsing. The test in Eucentre was therefore followed-up with further tests at the laboratory of LNEC in Lisbon, Portugal. Here the upper floors of the building tested in Eucentre were re-built in the LNEC laboratory and subjected to movements measured at the base of the upper floors in Eucentre.

This report describes experimental tests carried out in the LNEC laboratory in Lisbon (Portugal). These tests have been purposely extended to include partial collapse of the test specimen. This occurred at much higher shaking levels (peak ground acceleration) than those that are expected in the Groningen area.

The main reasons for extending these tests to higher shaking levels are as follows:

- Tests to seismic actions higher than expected allow one to measure the available excess capacity for the buildings to resist the earthquake action, which is fundamental to appropriately calibrate numerical models of the buildings, and then account for the fact that some buildings of a given typology may be of poorer construction or use lower quality building materials, and are thus weaker than anticipated for buildings of that typology. If the experimental tests show that the specimen is able to withstand even these severe ground motions, then the calibrated numerical models can confidently be used to confirm that that even the weakest building in the same typology will be able to resist the ground motions expected in Groningen.
- The Eucentre and LNEC laboratories in Pavia (Italy) and Lisbon (Portugal) have been set up with the primary objective to study the impact of tectonic earthquakes in Southern Europe in the area from Portugal – Italy – Greece to Turkey. The research for Groningen could have delayed progress relevant to the impact of tectonic earthquakes in this region. However, by extending these tests to larger ground motion values, more typical of tectonic earthquakes, we have made these experiments also relevant to Southern Europe and other areas of the world, where tectonic earthquakes cause higher ground motions.

After the collapse test of the upper floors of the terraced house, also the roof construction was individually tested.

References

1. Eucentre Shake-table Test of Terraced House Modelling Predictions and Analysis Cross Validation, staff from ARUP, Eucentre (Pavia) and TU Delft, November 2015 [this document also includes; (1) Instruments full-scale test-house Eucentre Laboratory, (2) Protocol for Shaking Table Test on Full Scale Building (Eucentre) V_1, and (3) Selection of Acceleration Time-Series for Shake Table Testing of Groningen Masonry Building at the EUCENTRE, Pavia, all three by staff from Eucentre (Pavia)],
2. Collapse shake-table testing of terraced house (LNEC-BUILD1), Eucentre and LNEC (U. Tomassetti, A. A. Correia, F. Graziotti, A.I. Marques, M. Mandirola, P.X. Candeias), 1st September 2017.
3. LNEC-BUILD1: Modelling predictions and analysis cross-validation, ARUP, TU Delft, Eucentre and Mosayk (several staff members from all four institutions), 8th September 2017.
4. Using the Applied Element Method to model the shake-table testing of two full-scale URM houses (EUC-BUILD1 and EUC-BUILD2), Mosayk (D. Malomo, R. Pinho), 31st October 2017.
5. Using the Applied Element Method to model the collapse shake-table testing of a URM cavity wall structure (LNEC-BUILD1), Mosayk (D. Malomo, R. Pinho), 31st October 2017.
6. Shake-table test up to collapse on a roof substructure of a Dutch terraced house (LNEC-BUILD2), Eucentre and LNEC (A.A. Correia, A.I. Marques, V. Bernardo, L. Grottoli, U. Tomassetti, F. Graziotti), 31st October 2017.
7. Using the Applied Element Method to model the collapse shake-table testing of a terraced house roof substructure (LNEC-BUILD2), Mosayk (D. Malomo, R. Pinho), 31st October 2017.



NAM

Title	Collapse Shaking Table Test on a URM Cavity Wall Structural (LNEC-BUILD1) Representative of a Dutch Terraced House	Date	September 2017
		Initiator	NAM
Autor(s)	U. Tomassetti, A. A. Correia, F. Graziotti, A. I. Marques, M. Mandirola and P. X. Candeias	Editors	Jan van Elk and Dirk Doornhof
Organisation	Eucentre (European Centre for Training and Research in Earthquake Engineering) LNEC (Laboratório Nacional de Engenharia Civil / National Laboratory of Civil Engineering)	Organisation	NAM
Place in the Study and Data Acquisition Plan	<p><u>Study Theme:</u> Seismic Response of Buildings (URM)</p> <p><u>Comment:</u></p> <p>Many of the buildings in the Groningen field area are terraced unreinforced masonry buildings. A program to assess the response of these building to earthquakes was therefore initiated. This program built on the experimental and modelling program into the properties of URM building materials, wall elements and wall units.</p> <p>A typical Groningen terraced house built using materials from the Groningen area by builders from the Groningen area, was tested at the shake-table of Eucentre in Pavia, Italy (Ref. 1). Although the building was at the end of this test program seriously damaged, the building had not collapsed. This left questions on the remaining capacity of the structure and its ability to resist larger seismic movements before (partially) collapsing. The test in Eucentre was therefore followed-up with further tests at the laboratory of LNEC in Lisbon, Portugal. Here the upper floors of the building tested in Eucentre were re-built in the LNEC laboratory and subjected to movements measured at the base of the upper floors in Eucentre.</p> <p>This report describes experimental tests carried out in the LNEC laboratory in Lisbon (Portugal). These tests have been purposely extended to include partial collapse of the test specimen. This occurred at much higher shaking levels (peak ground acceleration) than those that are expected in the Groningen area.</p> <p>The main reasons for extending these tests to higher shaking levels are as follows:</p> <ul style="list-style-type: none"> • Tests to seismic actions higher than expected allow one to measure the available excess capacity for the buildings to resist the earthquake action, which is 		

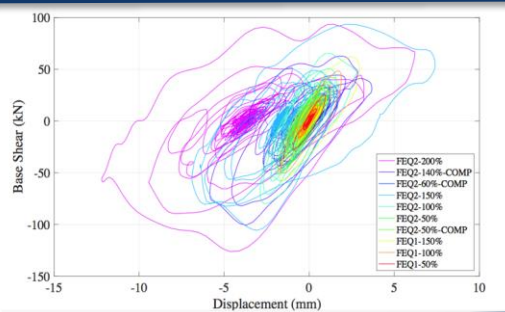
	<p>fundamental to appropriately calibrate numerical models of the buildings, and then account for the fact that some buildings of a given typology may be of poorer construction or use lower quality building materials, and are thus weaker than anticipated for buildings of that typology. If the experimental tests show that the specimen is able to withstand even these severe ground motions, then the calibrated numerical models can confidently be used to confirm that that even the weakest building in the same typology will be able to resist the ground motions expected in Groningen.</p> <ul style="list-style-type: none"> • The Eucentre and LNEC laboratories in Pavia (Italy) and Lisbon (Portugal) have been set up with the primary objective to study the impact of tectonic earthquakes in Southern Europe in the area from Portugal – Italy – Greece to Turkey. The research for Groningen could have delayed progress relevant to the impact of tectonic earthquakes in this region. However, by extending these tests to larger ground motion values, more typical of tectonic earthquakes, we have made these experiments also relevant to Southern Europe and other areas of the world, where tectonic earthquakes cause higher ground motions. <p>After the collapse test of the upper floors of the terraced house, also the roof construction was individually tested.</p>
Directly linked research	<p>(1) Shake table tests (2) Fragility curves for building typologies (URM) (3) Risk Assessment</p>
Used data	Experiments
Associated organisation	NAM
Assurance	Eucentre

COLLAPSE SHAKING TABLE TEST ON A URM CAVITY WALL STRUCTURE REPRESENTATIVE OF A DUTCH TERRACED HOUSE

Document authors

U. Tomassetti, A. A. Correia, F. Graziotti, A. I. Marques, M. Mandirola, P. X. Candeias

Research Report



COLLAPSE SHAKING TABLE TEST ON A URM CAVITY WALL BUILDING REPRESENTATIVE OF A DUTCH TERRACED HOUSE

U. Tomassetti, A. A. Correia, F. Graziotti, A. I. Marques, M. Mandirola, P. X. Candeias

According to law, EUCENTRE Foundation trademark cannot be reproduced, copied or utilized, without the written permission of the EUCENTRE Foundation, which is the owner, except in accordance with established contract conditions pertaining to the production of this document.

September, 2017, Pavia

TABLE OF CONTENTS

TABLE OF CONTENTS	III
LIST OF TABLES	V
LIST OF FIGURES	VII
1 CONSTRUCTION OF THE BUILDING PROTOTYPE	15
1.1 SCOPE AND MOTIVATION OF THE LNEC TEST	15
1.2 GEOMETRY OF THE SPECIMEN.....	16
1.3 BUILDING CONSTRUCTION DETAILS	18
1.4 BUILDING PROTOTYPE FINISHING.....	23
2 MATERIALS CHARACTERISATION	25
2.1 MORTAR CHARACTERISATION TESTS	26
2.1.1 CHARACTERISATION AND IDENTIFICATION OF SAMPLES BEFORE HARDENING	26
2.1.2 TESTS FOR THE DETERMINATION OF THE BULK DENSITY OF FRESH MORTAR	29
2.1.3 TESTS FOR THE DETERMINATION OF THE CONSISTENCE OF FRESH MORTAR (BY FLOW TABLE) ..	30
2.1.4 CHARACTERISATION AND IDENTIFICATION OF SPECIMENS (HARDENED MORTAR)	31
2.1.5 TESTS FOR THE DETERMINATION OF DYNAMIC MODULUS OF ELASTICITY	33
2.1.6 TESTS FOR THE DETERMINATION OF FLEXURAL AND COMPRESSIVE STRENGTHS	37
2.2 BLOCK CHARACTERISATION TESTS	46
2.2.1 CHARACTERISATION AND IDENTIFICATION OF SPECIMENS.....	46
2.2.2 TEST FOR THE DETERMINATION OF MOISTURE CONTENT.....	48
2.2.3 TEST FOR DETERMINATION OF THE WATER ABSORPTION CAPILLARITY COEFFICIENT	50
2.3 MASONRY CHARACTERISATION TESTS.....	51
2.3.1 CHARACTERISATION AND IDENTIFICATION OF SPECIMENS.....	51
2.3.2 TEST FOR THE DETERMINATION OF COMPRESSIVE STRENGTH.....	55
2.3.3 TEST FOR THE DETERMINATION OF SHEAR STRENGTH.....	78
2.3.4 TESTS FOR THE DETERMINATION OF BOND STRENGTH.....	87
2.4 ANALYSIS OF THE MATERIALS CHARACTERISATION RESULTS	93
3 INSTRUMENTATION OF THE SPECIMEN	94
4 TEST PROCEDURE	104
4.1 SHAKING TABLE INPUT SEQUENCE	104
4.2 CHARACTERISATION OF THE INDUCED GROUND MOTION TESTS	107
5 TEST RESULTS	109

5.1 SPECIMEN DYNAMIC IDENTIFICATION	109
5.1.1 INTRODUCTION AND METHODOLOGY	109
5.1.1.1 Frequency-Domain Decomposition method (FDD)	111
5.1.1.2 Enhanced Frequency-Domain Decomposition method (EFDD)	112
5.1.2 DYNAMIC IDENTIFICATION RESULTS	113
5.1.2.1 Removal of slab temporary support	113
5.1.2.2 Ambient vibrations on the laboratory floor	116
5.1.2.3 1 st dynamic identification (Test 1).....	118
5.1.2.4 2 nd dynamic identification (Test 3).....	122
5.1.2.5 7 th dynamic identification (Test 14)	125
5.1.2.6 8 th dynamic identification (Test 18)	128
5.2 DAMAGE EVOLUTION	132
5.3 DESCRIPTION OF THE COLLAPSE MECHANISM	136
5.4 FURNITURE PERFORMANCE	139
5.5 SHAKING TABLE PERFORMANCE.....	140
5.6 DISPLACEMENT AND ACCELERATION HISTORIES.....	144
5.7 DEFORMED SHAPE	150
5.8 POST-PROCESSING OF THE EXPERIMENTAL DATA OF THE FEQ2-300% TEST	156
5.9 HYSTERETIC RESPONSE	159
5.10 ROOF RESPONSE	162
5.11 IDENTIFICATION OF SPECIMEN DAMAGE LIMIT STATES.....	165
5.12 DERIVATION OF EDP ACCORDING TO SPECIMEN PERFORMANCE	166
<u>REFERENCES</u>	<u>168</u>

LIST OF TABLES

Table 1.1 Masses of the different structural elements characterising the specimen.	16
Table 1.2 Masses of the different elements characterising the roof of the specimen.	23
Table 2.1 Masonry mechanical properties.....	26
Table 2.2 Adopted amount of water for each type of mortar.....	27
Table 2.3 Determination of the water / product ratio for each corresponding mortar mix collection of samples.	29
Table 2.4 Results obtained for the determination of bulk density of all mortars.	30
Table 2.5 Results obtained in the determination of the consistency of fresh mortar for all samples collected.	31
Table 2.6 Summary of the average dynamic modulus of elasticity obtained for the two types of bedding mortar collected directly from the full-scale model for the different ages.....	36
Table 2.7 Summary of the average dynamic modulus of elasticity obtained for the two types of bedding mortar collected directly from the characterisation specimens for the different ages.	37
Table 2.8 Summary of the compressive and flexural strength averages obtained for the two types of bedding mortars collected directly from the full-scale model for different ages.	45
Table 2.9 .Summary of the compressive and flexural strength averages obtained for the two types of bedding mortars collected directly from characterisation specimens for different ages.....	45
Table 2.10 Characteristics of the two types of blocks selected for the tests.	47
Table 2.11 Bulk density for calcium silicate and clay blocks.....	48
Table 2.12 Weighing until constant mass is reached for the calcium silicate blocks.	49
Table 2.13 Weighing until constant mass is reached for the clay bricks.	49
Table 2.14 Percentage of moisture content of the two types of blocks.	50
Table 2.15 Results for the determination of the water absorption coefficient by capillarity for the two types of blocks.....	51
Table 2.16 Dimensions and masses of the two types of wallettes constructed for the compression strength tests.	53
Table 2.17 Dimensions and masses of calcium silicate and clay triplets for the shear strength tests.	55
Table 2.18 Dimensions and masses of the two types of wallettes built for the bond wrench tests.	55
Table 2.19 Summary of the results of the bulk density for the two types of specimens.	55
Table 2.20 Summary of the compressive strength for the calcium silicate wallettes.....	60
Table 2.21 Summary of the modulus of elasticity for calcium silicate wallettes.....	66
Table 2.22 Summary of the compressive strength for the clay wallettes.	68
Table 2.23 Summary of the modulus of elasticity for clay wallettes.	78
Table 2.24 Summary of the shear strength obtained for the calcium silicate triplets.....	85
Table 2.25 Summary of the shear strength obtained for the clay triplets.	86
Table 2.26 Summary of average cohesion values and internal friction angles for the two types of triplets.....	87

Table 2.27 Bond strength for the calcium silicate triplets.....	92
Table 2.28 Bond strength for the clay triplets	92
Table 2.29 Summary of bond strength in the two types of tested specimens.	93
Table 3.1 Summary of the accelerometers and their location.....	96
Table 3.2 Summary of the displacement transducers and their location.....	98
Table 3.3 Summary of the content of the remaining columns of the experimental data matrices...	99
Table 4.1 Applied testing sequence.	106
Table 4.2 Summary of the floor motion testing sequence dynamic characteristics.	107
Table 4.3 Summary of the floor motion dynamic characteristics.....	108
Table 5.1 Summary of vibration modes' characteristics for dynamic identification on the laboratory floor.	117
Table 5.2 Summary of vibration modes' characteristics for 1 st dynamic identification (Test 1).	120
Table 5.3 MAC coefficients for 1 st dynamic identification (Test 1).....	120
Table 5.4 Summary of vibration modes' characteristics for 2 nd dynamic identification (Test 3). ...	123
Table 5.5 MAC coefficients for 2 nd dynamic identification (Test 3).....	124
Table 5.6 Summary of vibration modes' characteristics for 7 th dynamic identification (Test 14)...	126
Table 5.7 MAC coefficients for 7 th dynamic identification (Test 14).....	127
Table 5.8 Summary of vibration modes' characteristics for 8 th dynamic identification (Test 18)...	129
Table 5.9 MAC coefficients for 8 th dynamic identification (Test 18).....	130
Table 5.10 Evolution of the fundamental mode of vibration of the model during the shaking table test.	131
Table 5.11 List of the backbone curve coordinates.	162
Table 5.12 List of the roof backbone curve coordinates.	165

LIST OF FIGURES

Figure 1.1 A typical terraced house in Groningen: (a) illustration of the front façade; (b) plan view.	15
Figure 1.2 Views of the full-scale specimen built in Eucentre, Pavia, Italy.....	16
Figure 1.3 Views of the full-scale specimen built in LNEC, Lisbon, Portugal: (a) North-East elevation; (b) East elevation; (c) North elevation; (d) South-West elevation.	17
Figure 1.4 Plan view of the ground floor. The arrow indicates the direction of the shaking table motion.....	18
Figure 1.5 Elevation views of the specimen’s CS inner leaf.	18
Figure 1.6 Elevation views of the specimen’s clay outer leaf.....	18
Figure 1.7 Construction details of the specimen: (a) positioning of cavity steel ties; (b) building phase of inner CS leaf; (c) laying of the first-floor slab; (d) construction of the first floor (e) geometry of steel tie; (f) construction of the first-floor level; (f) inner and outer leaves before the laying of the RC slab.....	19
Figure 1.8 Details of the connections between the precast RC slabs and the longitudinal CS walls: (a,c) from the inside and (b,d) from the outside.....	20
Figure 1.9 Details of the roof structure: (a) geometry of the timber diaphragm; (b) connection between the timber beams and the West gable.....	21
Figure 1.10 Plan view of the roof structure: geometry of the openings; the blue dots indicate the location of the nails connecting the planks with the beams.	21
Figure 1.11 Construction of the roof and views of specimen after the laying of the tiles.	22
Figure 1.12 Plan view of the ground floor with furniture.....	24
Figure 2.1 Types of product used in each bedding mortar.....	27
Figure 2.2 Construction of the full scale model at the time of collection of mortar samples.	27
Figure 2.3 Construction of characterisation specimens at the time of mortar sampling.....	28
Figure 2.4 Molding of masonry specimens: (a) pestle and (b) mold.....	28
Figure 2.5 Carrying out the determination of bulk density of fresh mortar.....	30
Figure 2.6 Determination of consistence of fresh mortar by scattering: (a) schematic representation of equipment; (b) test run.	31
Figure 2.7 Part of mortar specimens.	32
Figure 2.8 Curing conditions of mortar specimens.	32
Figure 2.9 Carrying out the test to determine the dynamic modulus of elasticity and plot obtained.	33
Figure 2.10 Test results for the determination of the dynamic modulus of elasticity of bedding mortar for the calcium silicate blocks (MS) after 10 days of age.	34
Figure 2.11 Test results for the determination of the dynamic modulus of elasticity of bedding mortar for the calcium silicate blocks (MS) after 20 days of age.	34
Figure 2.12 Test results for the determination of the dynamic modulus of elasticity of bedding mortar for the calcium silicate blocks (MS) after 28 days of age.....	35

Figure 2.13 Test results for the determination of the dynamic modulus of elasticity of bedding mortar for the clay bricks (MCL) after 10 days of age.	35
Figure 2.14 Test results for the determination of the dynamic modulus of elasticity of bedding mortar for the clay bricks (MCL) after 20 days of age.	36
Figure 2.15 Test results for the determination of the dynamic modulus of elasticity of bedding mortar for the clay bricks (MCL) after 28 days of age.	36
Figure 2.16 Relation between dynamic moduli of elasticity and maturation time for the two bedding mortars removed from the full scale model and the characterisation test specimens.	37
Figure 2.17 Test for determination of flexural strength: (a) scheme of positioning of the specimen and (b) specimen being tested.	38
Figure 2.18 Test for compressive strength: (a) test scheme and (b) specimen being tested.	39
Figure 2.19 Flexural strength test results for bedding mortar specimens used with calcium silicate blocks (MS) after 10 days of age.	39
Figure 2.20 Flexural strength test results for bedding mortar specimens used with calcium silicate blocks (MS) after 20 days of age.	40
Figure 2.21 Flexural strength test results for bedding mortar specimens used with calcium silicate blocks (MS) after 28 days of age.	40
Figure 2.22 Compressive strength and modulus of elasticity test results for bedding mortar specimens used with calcium silicate blocks (MS) after 10 days of age.	41
Figure 2.23 Compressive strength and modulus of elasticity test results for bedding mortar specimens used with calcium silicate blocks (MS) after 20 days of age.	41
Figure 2.24 Compressive strength and modulus of elasticity test results for bedding mortar specimens used with calcium silicate blocks (MS) after 28 days of age.	41
Figure 2.25 Distribution of the flexural and compressive strength of bedding mortars used with calcium silicate bricks (MS) after 28 days of age.	42
Figure 2.26 Flexural strength test results for bedding mortar specimens used with clay bricks (MCL) after 10 days of age.	42
Figure 2.27 Flexural strength test results for bedding mortar specimens used with clay bricks (MCL) after 20 days of age.	43
Figure 2.28 Flexural strength test results for bedding mortar specimens used with clay bricks (MCL) after 28 days of age.	43
Figure 2.29 Compressive strength and modulus of elasticity test results for bedding mortar specimens used with clay bricks (MCL) after 10 days of age.	43
Figure 2.30 Compressive strength and modulus of elasticity test results for bedding mortar specimens used with clay bricks (MCL) after 20 days of age.	44
Figure 2.31 Compressive strength and modulus of elasticity test results for bedding mortar specimens used with clay bricks (MCL) after 28 days of age.	44
Figure 2.32 Distribution of the flexural and compressive strengths of bedding mortars for the clay bricks (MCL) after 28 days of age.	44
Figure 2.33 Relation between flexural and compressive strengths and maturation time of bedding mortars for the calcium silicate blocks (MS) removed from the full-scale model and the characterisation test specimens.	45
Figure 2.34 Relation between flexural and compressive strength and maturation time of bedding mortars for the clay bricks (MCL) removed from the full-scale model and the characterisation test specimens.	46
Figure 2.35 Blocks used and indication of their dimensions.	46

Figure 2.36 Collection of test pieces.	47
Figure 2.37 Blocks units.	47
Figure 2.38 Drying the blocks in a ventilated oven.	48
Figure 2.39 Weighing of blocks.	49
Figure 2.40 Determination of the water absorption coefficient by capillarity of the carrier.	50
Figure 2.41 Types of masonry specimens (wallettes and triplets) built for testing.	52
Figure 2.42 Construction of wallettes and triplets.	52
Figure 2.43 Example of characterisation (measure and weight) of all specimens.	53
Figure 2.44 Schematic with the identification of the parameters measured in the various specimens.	54
Figure 2.45 Regularisation of the wallettes faces.	56
Figure 2.46 Final regularisation of the wallettes faces on top of the testing machine.	56
Figure 2.47 Lack of verticality in wallettes.	57
Figure 2.48 – Scheme and numbering of the transducers placed on each face of the two types of the wallettes.	57
Figure 2.49 Scheme with the location of the transducers placed on each face of the calcium silicate wallettes.	58
Figure 2.50 Scheme with the location of the transducers placed on each face of the clay wallettes.	58
Figure 2.51 Instrumentation placed on each face of the calcium silicate wallettes.	58
Figure 2.52 Instrumentation placed on each face of the clay wallettes.	59
Figure 2.53 Application of force as a function of time applied to calcium silicate wallettes.	59
Figure 2.54 Calcium silicate block wallette (WS_1) during the test and after failure.	60
Figure 2.55 Calcium silicate block wallette (WS_2) during the test and after failure.	60
Figure 2.56 Vertical stress vs. vertical and horizontal strains for wallette WS_1.	61
Figure 2.57 Vertical stress vs. vertical and horizontal strains for wallette WS_3.	61
Figure 2.58 Vertical stress vs. vertical and horizontal strains for wallette WS_4.	62
Figure 2.59 Vertical stress vs. vertical and horizontal strains for wallette WS_5.	62
Figure 2.60 Vertical stress vs. vertical and horizontal strains for wallette WS_6.	63
Figure 2.61 Vertical stress vs. vertical strain and determination of the modulus of elasticity for wallette WS_1.	63
Figure 2.62 Vertical stress vs. vertical strain and determination of the modulus of elasticity for wallette WS_2.	64
Figure 2.63 Vertical stress vs. vertical strain and determination of the modulus of elasticity for wallette WS_3.	64
Figure 2.64 Vertical stress vs. vertical strain and determination of the modulus of elasticity for wallette WS_4.	65
Figure 2.65 Vertical stress vs. vertical strain and determination of the modulus of elasticity for wallette WS_5.	65
Figure 2.66 Vertical stress vs. vertical strain and determination of the modulus of elasticity for wallette WS_6.	66

x *Collapse Shaking Table Test on URM Cavity Wall Structure representative of a Dutch Terraced House*

Figure 2.67 Distribution of moduli of elasticity obtained for calcium silicate wallettes.	67
Figure 2.68 Application of force as a function of time applied to clay wallettes.	67
Figure 2.69 Clay brick wallette (WCL_6) subjected to test and after failure.	68
Figure 2.70 Vertical stress vs. vertical and horizontal strains for wallette WCL_1.	69
Figure 2.71 Vertical stress vs. vertical and horizontal strains for wallette WCL_2.	70
Figure 2.72 Vertical stress vs. vertical and horizontal strains for wallette WCL_3.	71
Figure 2.73 Vertical stress vs. vertical and horizontal strains for wallette WCL_4.	72
Figure 2.74 Vertical stress vs. vertical and horizontal strains for wallette WCL_5.	73
Figure 2.75 Vertical stress vs. vertical and horizontal strains for wallette WCL_6.	74
Figure 2.76 Vertical stress vs. vertical strain and determination of the modulus of elasticity for wallette WCL_1.	75
Figure 2.77 Vertical stress vs. vertical strain and determination of the modulus of elasticity for wallette WCL_2.	75
Figure 2.78 Vertical stress vs. vertical strain and determination of the modulus of elasticity for wallette WCL_3.	76
Figure 2.79 Vertical stress vs. vertical strain and determination of the modulus of elasticity for wallette WCL_4.	76
Figure 2.80 Vertical stress vs. vertical strain and determination of the modulus of elasticity for wallette WCL_5.	77
Figure 2.81 Vertical stress vs. vertical strain and determination of the modulus of elasticity for wallette WCL_6.	77
Figure 2.82 Distribution of moduli of elasticity obtained for clay wallettes.	78
Figure 2.83 Instrumentation placed on the calcium silicate triplets.	79
Figure 2.84 Instrumentation placed on the clay triplets.	79
Figure 2.85 Location of the instrumentation placed on the calcium silicate triplets (dimensions in mm).	79
Figure 2.86 Location of the instrumentation placed on the clay triplets (dimensions in mm).	80
Figure 2.87 Calibration of the complete test chain.	80
Figure 2.88 Test scheme for the determination of shear strength.	81
Figure 2.89 Final version of the shear strength test device.	81
Figure 2.90 Application of the pre-compression and shear stresses throughout the test starting with the lowest pre-compression level (TS_3).	82
Figure 2.91 Application of the pre-compression and shear stresses throughout the test initiated with the intermediate pre-compression level (TS_7).	82
Figure 2.92 Application of pre-compression and shear stresses throughout the test started at the highest pre-compression level (TS_11).	83
Figure 2.93 Theoretical determination of cohesion and angle of friction in the shear strength test.	84
Figure 2.94 Determination of cohesion and friction angle for specimen TS_3.	84
Figure 2.95 Acceptable collapse mechanisms for the shear strength test.	84
Figure 2.96 Completion of the test for the two types of triplets tested.	85
Figure 2.97 Example of one of the failure mechanisms obtained for each triplet in the shear strength test.	85

Figure 2.98 Shear strength, cohesion and internal friction angle for the calcium silicate triplets. ...	86
Figure 2.99 Shear strength, cohesion and internal friction angle for clay triplets.	87
Figure 2.100 Type of specimens subjected to bond strength test.	87
Figure 2.101 Example of a possible device for the test in accordance with EN 1052-5 (CEN, 2005).	88
Figure 2.102 Device used for the test.	88
Figure 2.103 Test of the two connections in calcium silicate blocks using the same test device.	89
Figure 2.104 Test of the two connections in clay bricks using the same test device.	89
Figure 2.105 Application of vertical force until bond failure.	90
Figure 2.106 Measure of the weight of the top unit, its adherent mortar and sand volume leading to failure.	90
Figure 2.107 Admissible failure mechanisms for the bond wrench test.	91
Figure 2.108 Example of failure mechanisms obtained for each triplet type in the bond wrench test.	92
Figure 3.1 Locations of the instrumentation: accelerometers (a) and displacement transducers (b) (letters indicate the component at which the transducers is attached to: SL = slab, RF = reference frame, IL = inner leaf, OL = outer leaf, FB = foundation beam, ST = shaking table, TP = timber plate and RB = roof ridge beam).	95
Figure 3.2 Pictures of the instrumentation.	100
Figure 4.1 Theoretical horizontal and vertical components of the adopted accelerograms.	105
Figure 4.2 Theoretical horizontal and vertical 5% damped acc. response spectra of the experimental inputs.	105
Figure 5.1 Input acceleration history for the impulsive loading (above) and average input (below).	110
Figure 5.2 Frequency response function from rectangular impulses in the horizontal direction. ...	110
Figure 5.3 Representation of the Singular Values matrix.	112
Figure 5.4 Frequency estimate (zero-crossings) and damping (logarithm decrement) of the impulse response estimate.	112
Figure 5.5 Joints filled with mortar.	113
Figure 5.6 Instrumented hammer and application of periodic excitation pulses.	114
Figure 5.7 Accelerometers at the centre of the load-bearing walls.	114
Figure 5.8 Frequency response function of East wall in decibel scale (left) and in linear scale (right), before removing the temporary support.	114
Figure 5.9 Frequency response function of East wall in decibel scale (left) and in linear scale (right), after removing the temporary support.	115
Figure 5.10 Frequency response function of West wall in decibel scale (left) and in linear scale (right), before removing the temporary support.	115
Figure 5.11 Frequency response function of West wall in decibel scale (left) and in linear scale (right), after removing the temporary support.	116
Figure 5.12 Frequency-domain decomposition results for dynamic identification on the laboratory floor.	117
Figure 5.13 Enhanced frequency-domain decomposition results for dynamic identification on the laboratory floor.	117

Figure 5.14 FDD mode shapes for dynamic identification on the laboratory floor.	118
Figure 5.15 EFDD mode shapes for dynamic identification on the laboratory floor.	118
Figure 5.16 Test specimen on the shaking table.	118
Figure 5.17 3D view of the accelerometers setup for dynamic identification.	119
Figure 5.18 FDD results for 1 st dynamic identification (Test 1).	119
Figure 5.19 EFDD results for 1 st dynamic identification (Test 1).	120
Figure 5.20 FDD mode shapes for 1 st dynamic identification (Test 1).	121
Figure 5.21 EFDD mode shapes for 1 st dynamic identification (Test 1).	122
Figure 5.22 FDD results for 2 nd dynamic identification (Test 3).	123
Figure 5.23 EFDD results for 2 nd dynamic identification (Test 3).	123
Figure 5.24 FDD mode shapes for 2 nd dynamic identification (Test 3).	124
Figure 5.25 EFDD mode shapes for 2 nd dynamic identification (Test 3).	125
Figure 5.26 FDD results for 7 th dynamic identification (Test 14).	126
Figure 5.27 EFDD results for 7 th dynamic identification (Test 14).	126
Figure 5.28 FDD mode shapes for 7 th dynamic identification (Test 14).	127
Figure 5.29 EFDD mode shapes for 7 th dynamic identification (Test 14).	128
Figure 5.30 FDD results for 8 th dynamic identification (Test 18).	129
Figure 5.31 EFDD results for 8 th dynamic identification (Test 18).	129
Figure 5.32 FDD mode shapes for 8 th dynamic identification (Test 18).	130
Figure 5.33 FDD mode shapes for 8 th dynamic identification (Test 18).	131
Figure 5.34 Specimen transportation to the shaking table.	132
Figure 5.35 Evolution of the crack pattern in the Inner CS walls: up to test FEQ2-150%.	134
Figure 5.36 Evolution of the crack pattern in the Inner CS walls: from test FEQ2-200% to test FEQ2-300%.	135
Figure 5.37 Evolution of the crack pattern in the outer clay veneer walls.	135
Figure 5.38 Snapshots of the FEQ2-300% test.	137
Figure 5.39 Pictures of the specimen at the end of the test FEQ-300%.	138
Figure 5.40 Pictures of the furniture before the testing sequence.	139
Figure 5.41 Pictures of the specimen at the end of test FEQ-300%.	139
Figure 5.42 FEQ1-50%: Theoretical-experimental 5% damped response spectra in both motion directions.	140
Figure 5.43 FEQ1-100%: Theoretical-experimental 5% damped response spectra.	141
Figure 5.44 FEQ1-150%: Theoretical-experimental 5% damped response spectra.	141
Figure 5.45 FEQ2-50%-COMP: Theoretical-experimental 5% damped response spectra.	142
Figure 5.46 FEQ2-50%: Theoretical-experimental 5% damped response spectra.	142
Figure 5.47 FEQ2-100%: Theoretical-experimental 5% damped response spectra.	142
Figure 5.48 FEQ2-150%: Theoretical-experimental 5% damped response spectra.	143
Figure 5.49 FEQ2-60%-COMP: Theoretical-experimental 5% damped response spectra.	143
Figure 5.50 FEQ2-120%-COMP: Theoretical-experimental 5% damped response spectra.	143

Figure 5.51 FEQ2-200%: Theoretical-experimental 5% damped response spectra.....	144
Figure 5.52 FEQ2-300%: Theoretical-experimental 5% damped response spectra.....	144
Figure 5.53 FEQ1-50%: Displacement and acceleration histories.....	145
Figure 5.54 FEQ1-100%: Displacement and acceleration histories.....	145
Figure 5.55 FEQ1-150%: Displacement and acceleration histories.....	146
Figure 5.56 FEQ1-50%-COMP: Displacement and acceleration histories.....	146
Figure 5.57 FEQ2-50%: Displacement and acceleration histories.....	147
Figure 5.58 FEQ2-100%: Displacement and acceleration histories.....	147
Figure 5.59 FEQ2-150%: Displacement and acceleration histories.....	148
Figure 5.60 FEQ2-60%-COMP: Displacement and acceleration histories.....	148
Figure 5.61 FEQ2-120%-COMP: Displacement and acceleration histories.....	149
Figure 5.62 FEQ2-200%: Displacement and acceleration histories.....	149
Figure 5.63 FEQ2-300%: Displacement and acceleration histories.....	150
Figure 5.64 FEQ1-50%: Longitudinal cross section deflected shape.....	151
Figure 5.65 FEQ1-100%: Longitudinal cross section deflected shape.....	151
Figure 5.66 FEQ1-150%: Longitudinal cross section deflected shape.....	151
Figure 5.67 FEQ1-150%: Longitudinal cross section deflected shape.....	152
Figure 5.68 FEQ2-50%-COMP: Longitudinal cross section deflected shape.....	152
Figure 5.69 FEQ2-100%: Longitudinal cross section deflected shape.....	152
Figure 5.70 FEQ2-150%: Longitudinal cross section deflected shape.....	153
Figure 5.71 FEQ2-60%-COMP: Longitudinal cross section deflected shape.....	153
Figure 5.72 FEQ2-120%-COMP: Longitudinal cross section deflected shape.....	153
Figure 5.73 FEQ2-200%: Longitudinal cross section deflected shape.....	154
Figure 5.74 Differential displacement recorded between the top of the CS longitudinal piers and the RC slab.....	155
Figure 5.75 Differential displacement recorded between the top of the longitudinal clay piers and the timber plate.....	155
Figure 5.76 Comparison between roof recorded and integrated absolute horizontal displacement histories.....	156
Figure 5.77 Comparison between roof recorded and integrated relative horizontal displacement histories.....	157
Figure 5.78 Comparison between floor recorded and integrated absolute horizontal displacement histories.....	157
Figure 5.79 Comparison between floor recorded and integrated relative horizontal displacement histories.....	158
Figure 5.80 Displacement and acceleration histories of the East wall during the attainment of the OOP collapse.....	159
Figure 5.81 Evolution of specimen hysteretic response.....	160
Figure 5.82 Evolution of specimen hysteretic response.....	161
Figure 5.83 Hysteretic response during the FEQ2-300%.....	161

xiv *Collapse Shaking Table Test on URM Cavity Wall Structure representative of a Dutch Terraced House*

Figure 5.84 Backbone capacity curve.	162
Figure 5.85 Evolution of the roof response.....	163
Figure 5.86 Roof response during FEQ2-300%.	164
Figure 5.87 Roof backbone curve.	164
Figure 5.88 Identification of the DLs on the building backbone curve.	166
Figure 5.89 Summary of the performance of the building specimen.	167

1 CONSTRUCTION OF THE BUILDING PROTOTYPE

The present experimental campaign aims at investigating the vulnerability of URM cavity-wall terraced houses of the late 1970s. This residential typology is characterised by wide openings on the front and back sides. The transverse walls, that separate units, are double-wythe cavity walls without any openings. Internal transverse walls are composed of a couple of load-bearing walls, carrying most of the vertical loads coming from the floors and roof and, therefore, they are capable of resisting significant in-plane lateral forces. Houses built with this common configuration are expected to be characterised by two very different seismic behaviours in the two principal directions. These structures are generally more flexible and vulnerable in the longitudinal direction. Figure 1.1 shows the front view of a classic terraced house and its plan view.

Adjacent units are generally structurally detached, and the discontinuous slabs rest only on the load-bearing walls of the individual units. Each unit is therefore completely self-supported by transverse walls and structurally independent from the other units. The only common walls are the outer veneer walls. For this reason, it was possible to test on the shaking table a representative sub-volume (one end-unit) of an entire terraced house (as shown in Figure 1.1). The first floor is generally made of a reinforced concrete (RC) slab, while the second floor is either a RC or timber diaphragm. The presence of a timber roof usually dominates over other typical roofing solutions for this building typology.

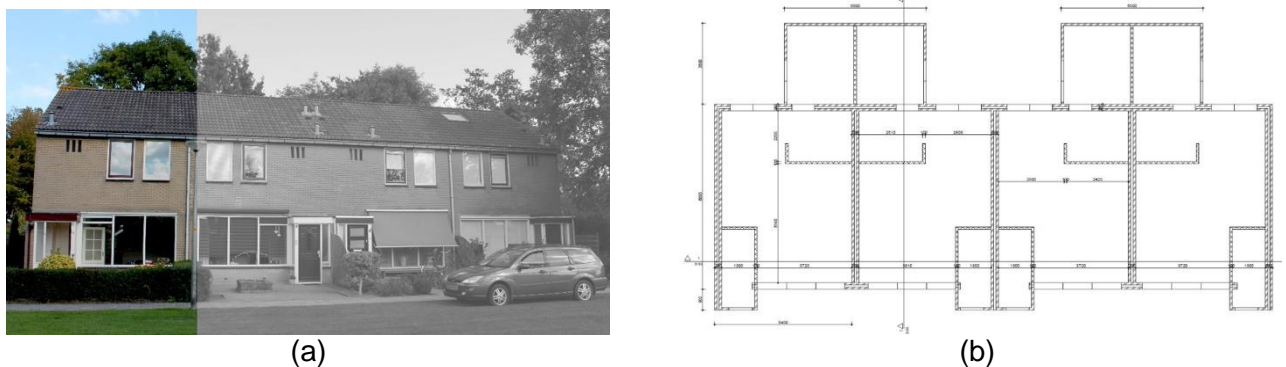


Figure 1.1 A typical terraced house in Groningen: (a) illustration of the front façade; (b) plan view.

1.1 Scope and motivation of the LNEC test

The test-house built in the EUCENTRE laboratory and tested in September 2015 (Graziotti et al. 2016a) was a full-scale two-storey building, with a timber roof and RC slabs, representing an end-unit of a typical terraced house. The testing campaign included in situ mechanical characterisation tests (Tondelli et al. 2015) and laboratory tests comprising: characterisation tests performed on brick units, mortar and small masonry assemblies; in-plane cyclic shear-compression and dynamic out-of-plane tests on full-scale masonry piers (Graziotti et al. 2016b). Another shaking table test was carried out on a full-scale building representing a typical Dutch detached house.

Having not reached collapse in the shaking table tests performed in Pavia, in order to avoid damage to the laboratory facilities, the main goal of the present test was initially studying large damage levels and assessing the failure mechanism leading to structural collapse of these houses. In particular, although the LNEC specimen represents a sub-volume of the EUCENTRE one, it will be interesting to observe if the structural collapse will be led by a soft-storey mechanism or by the overturning of the system gables and timber roof diaphragm. In this latter case, the LNEC first storey, after the roof overturning, could be (feasibility to be confirmed by the specimen damage evolution) further tested till the attainment of collapse by simulating the roof mass using appropriate additional masses connected to the RC slab.

16 Collapse Shaking Table Test on URM Cavity Wall Structure representative of a Dutch Terraced House

On the other hand, the experimental work carried out so far, supported by reliable numerical activities and risk models, suggested that the probability of structural collapse occurring in the Groningen region, according to the expected hazard, is rather low, representing only a limited fraction of the overall seismic risk. Therefore, while the construction and preparation of the LNEC test-house was done, the focus of the overall study shifted to understanding and evaluating the different damage levels experienced by these structural typologies. Emphasis is now placed on the study of the attainment of initial structural damage states and on the response of non-structural components, which in many cases govern the building performance in terms of economic losses and downtime.

Therefore, the proposal for the LNEC test shifted to performing incremental dynamic tests (matching the testing sequence carried out in Pavia) with particular attention to the occurrence of first damage states and their evolution; the evaluation of the building response subjected to low-intensity tests is therefore crucial to better characterise the seismic performance at different ground motion intensities. Moreover, a further idea was to equip the ground floor of the specimen (corresponding to the first-floor of the EUCENTRE specimen) with some building finishing such as a plaster layer and common furniture (e.g. bookshelves, paintings, tables etc.). The choice of applying a plaster layer on the inner side of the south CS wall and half of the East and West walls of the building prototype can help in individuating both the damage occurring to structural masonry piers and simply the one related to building finishing. This information is most valuable for a refined characterisation of the overall seismic risk.



Figure 1.2 Views of the full-scale specimen built in Eucentre, Pavia, Italy.

1.2 Geometry of the specimen

The test house built in the LNEC laboratory, in Lisbon, was a full-scale one-storey building, with a timber roof and RC slab, corresponding to the second floor and roof of the specimen built in the EUCENTRE laboratory. The LNEC building prototype is 5.82 m long, 5.46 m wide and 4.93 m high with a total mass M of 31.7 t. Table 1.1 specifies the masses associated to each structural element.

Table 1.1 Masses of the different structural elements characterising the specimen.

Side	CS Wall [t]	Clay Wall [t]	RC Slab [t]	Roof [t]
North	1.47	1.62	11.40	2.83
South	1.79	1.94		
West	3.39	3.82		
East	3.39	-		

The walls, supported by a steel-concrete composite foundation, consisted of two unreinforced masonry leaves. The inner load-bearing leaf was made of calcium silicate (CS) bricks whereas the external leaf was a clay brick veneer without any load-bearing function. The RC floor slab

covered the span between the two transverse (East and West) inner CS walls. The inner CS masonry was continuous along the entire perimeter of the house, while the outer clay brick leaf was not present in the East façade, simply because the specimen was meant to represent the end-unit of a system of terraced houses. The only geometric difference with respect to the specimen built in Pavia is represented by the door in the North elevation, which allowed an easy access to the inside of the prototype building. Pictures of the specimen after the end of the construction are shown in Figure 1.3. Figure 1.4 depicts the specimen's ground plan views and the horizontal direction of shaking.

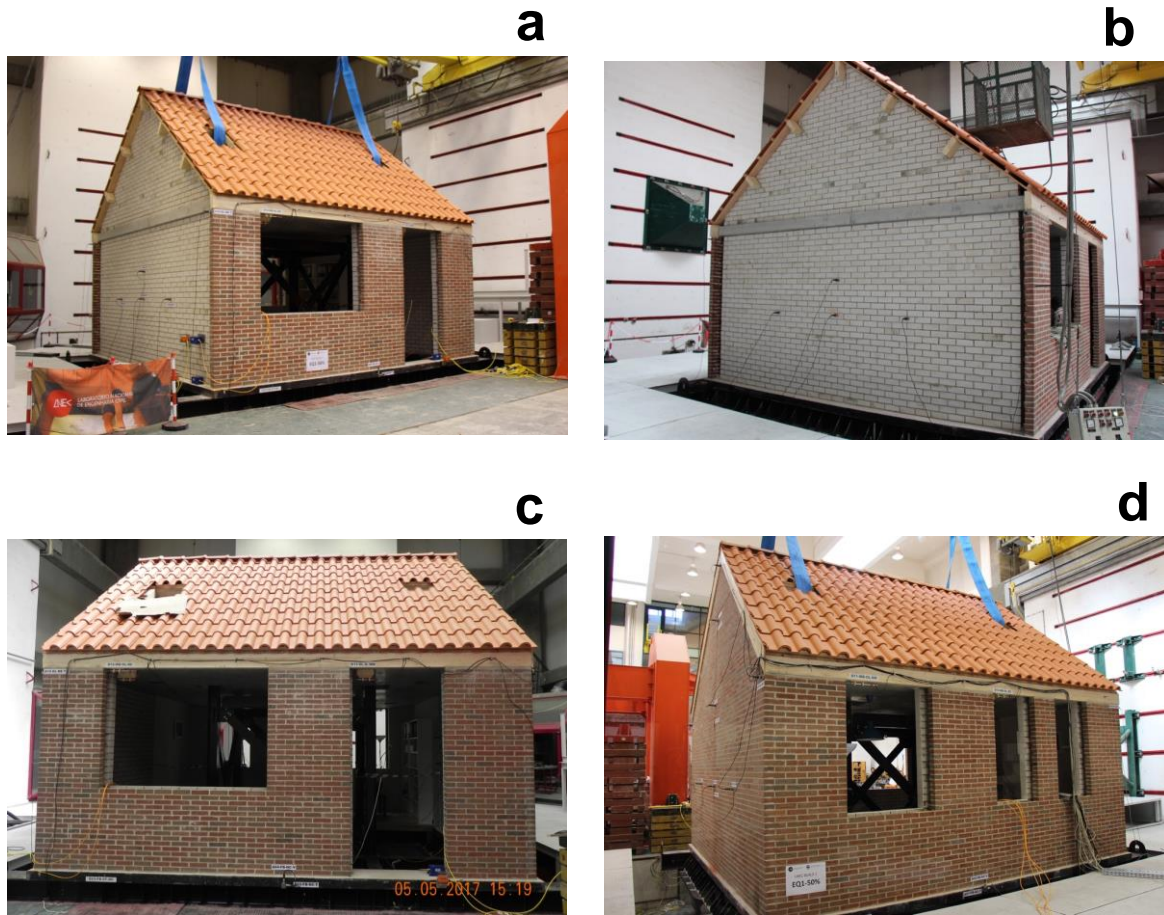
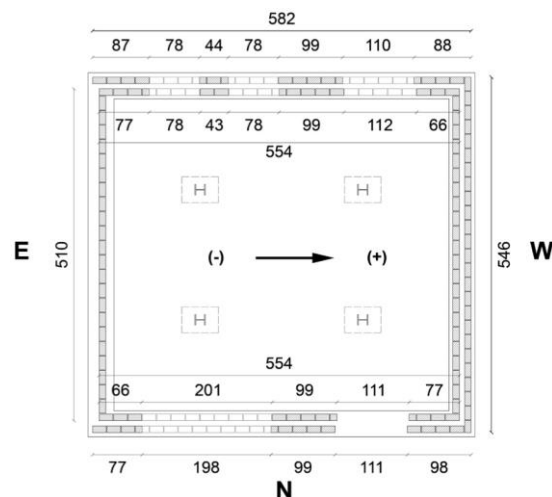


Figure 1.3 Views of the full-scale specimen built in LNEC, Lisbon, Portugal: (a) North-East elevation; (b) East elevation; (c) North elevation; (d) South-West elevation.



18 Collapse Shaking Table Test on URM Cavity Wall Structure representative of a Dutch Terraced House

Figure 1.4 Plan view of the ground floor. The arrow indicates the direction of the shaking table motion.

An air gap of 80 mm was left between the two leaves, as usually seen in common practice. L-shaped steel ties with a diameter of 3.1 mm and a length of 200 mm were inserted in the 10-mm-thick mortar bed-joints during the laying of the bricks, ensuring the connection between the two masonry leaves. They were placed as shown by the CS inner leaf walls elevation views in Figure 1.5. In particular, the L hook side was embedded in the inner CS walls for a length of 70 mm, while the “zig-zag” extremity was embedded in the clay masonry for a length of 50 mm. Two gable walls in the transverse façades (East and West) supported a 43° pitched timber roof. Figure 1.5 shows the elevation views of the specimen’s inner leaf walls. The blue dots indicate the location of the steel ties connecting the two leaves. Figure 1.6 shows, instead, the elevation views of the specimen’s outer leaves.

A rigid steel-frame will be installed in the interior of the test-house. This structure will be a rigid reference system for a direct measure of the floors, walls and roof displacements. A gap of 20 cm in both directions ensured no interference between the building prototype and the rigid frame.

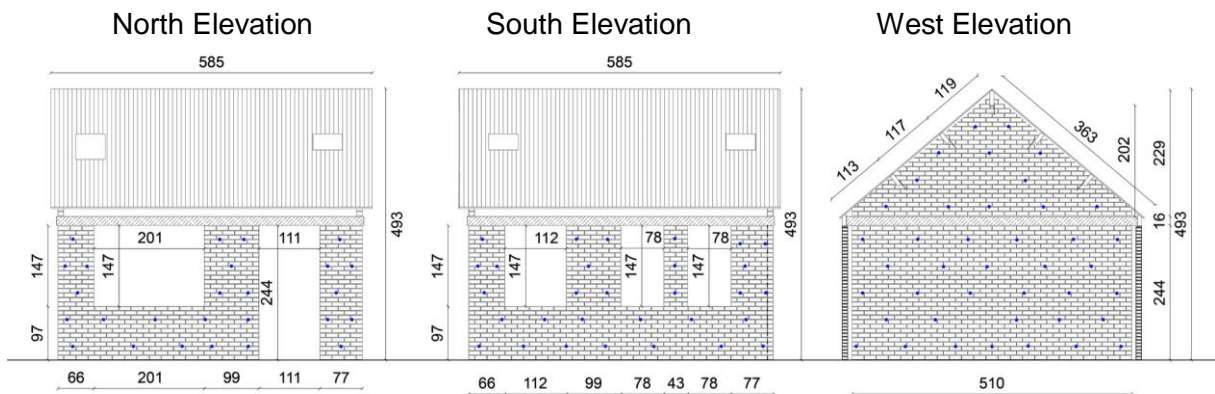


Figure 1.5 Elevation views of the specimen's CS inner leaf.

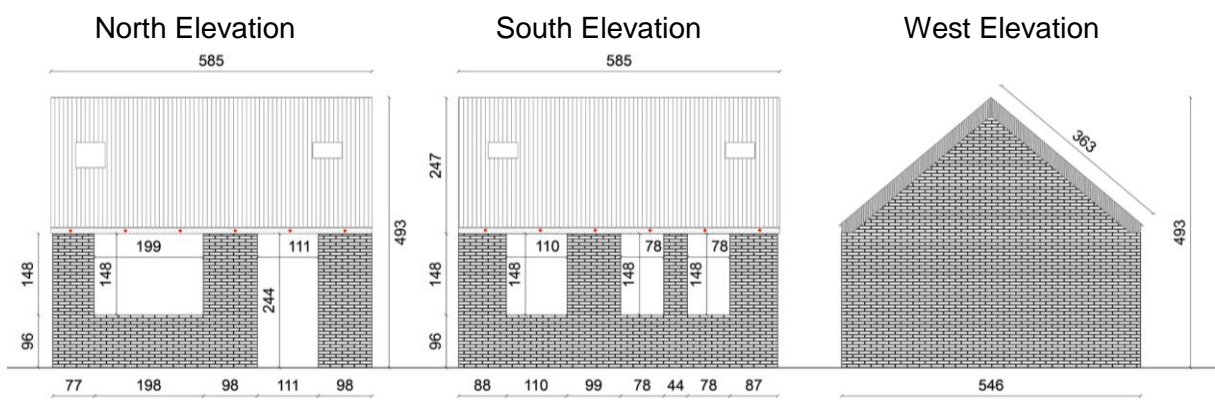


Figure 1.6 Elevation views of the specimen's clay outer leaf.

1.3 Building construction details

It is well known among the engineering community that construction details can significantly affect the seismic response of a structure, especially a URM building. Observation of damage caused by major earthquakes, as well as laboratory tests (Tomažević et al. 1991, Magenes et al. 2014) have shown that the role of the connections between horizontal and vertical structural elements is of primary importance for ensuring a good structural performance. The construction details of the specimen were representative of the Dutch common practice of the

1960s and 1970s. Figure 1.7 presents pictures captured during the construction phase of the specimen.

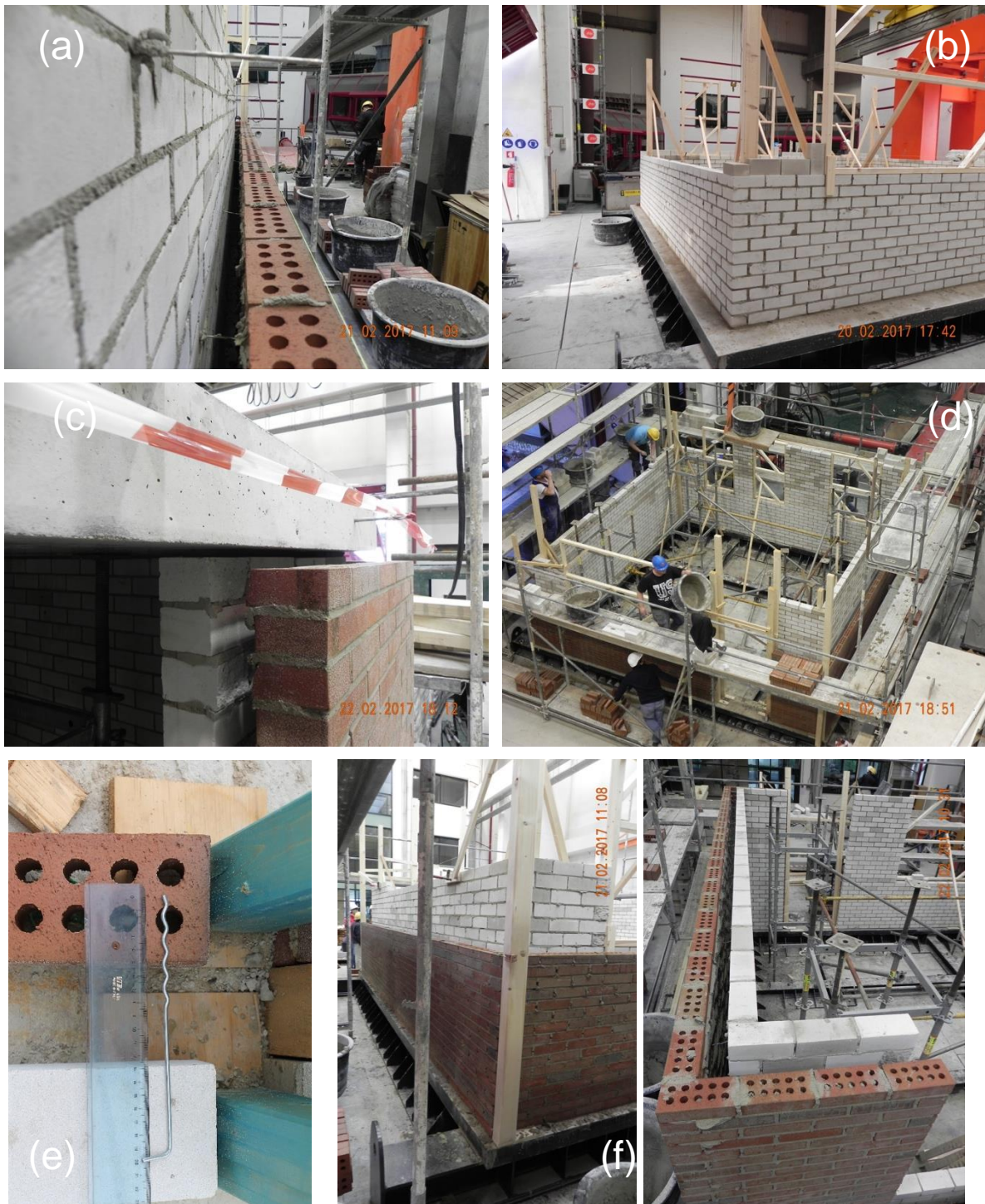


Figure 1.7 Construction details of the specimen: (a) positioning of cavity steel ties; (b) building phase of inner CS leaf; (c) laying of the first-floor slab; (d) construction of the first floor (e) geometry of steel tie; (f) construction of the first-floor level; (g) inner and outer leaves before the laying of the RC slab.

The slab was not directly supported by the longitudinal walls; the gap between the slab and the inner CS longitudinal walls was filled with mortar after the removal of the temporary supports and the attainment of the slab's deflection. Similarly, the timber beams were not in contact with the longitudinal clay walls, but they were attached to the edge of the first-floor slab

20 Collapse Shaking Table Test on URM Cavity Wall Structure representative of a Dutch Terraced House

by means of 100-cm-spaced 10-mm-diameter threaded bars cast to the RC slab, while the resulting gap between the beams and the top of the veneer was also filled with mortar afterwards. Such details were adopted in order to reproduce a load-bearing configuration common in the Dutch building stock. Figure 1.8 (a) illustrates a detail of the connection between the two longitudinal walls, the RC slab and the timber beam, while Figure 1.8 (b) shows a picture of the same detail taken during the specimen construction. Figure 1.8 (c) and (d) show instead the gap at the top of the longitudinal walls filled with mortar after the removal of the temporary support. This solution resulted in almost no vertical load being transmitted to the longitudinal walls under static conditions.

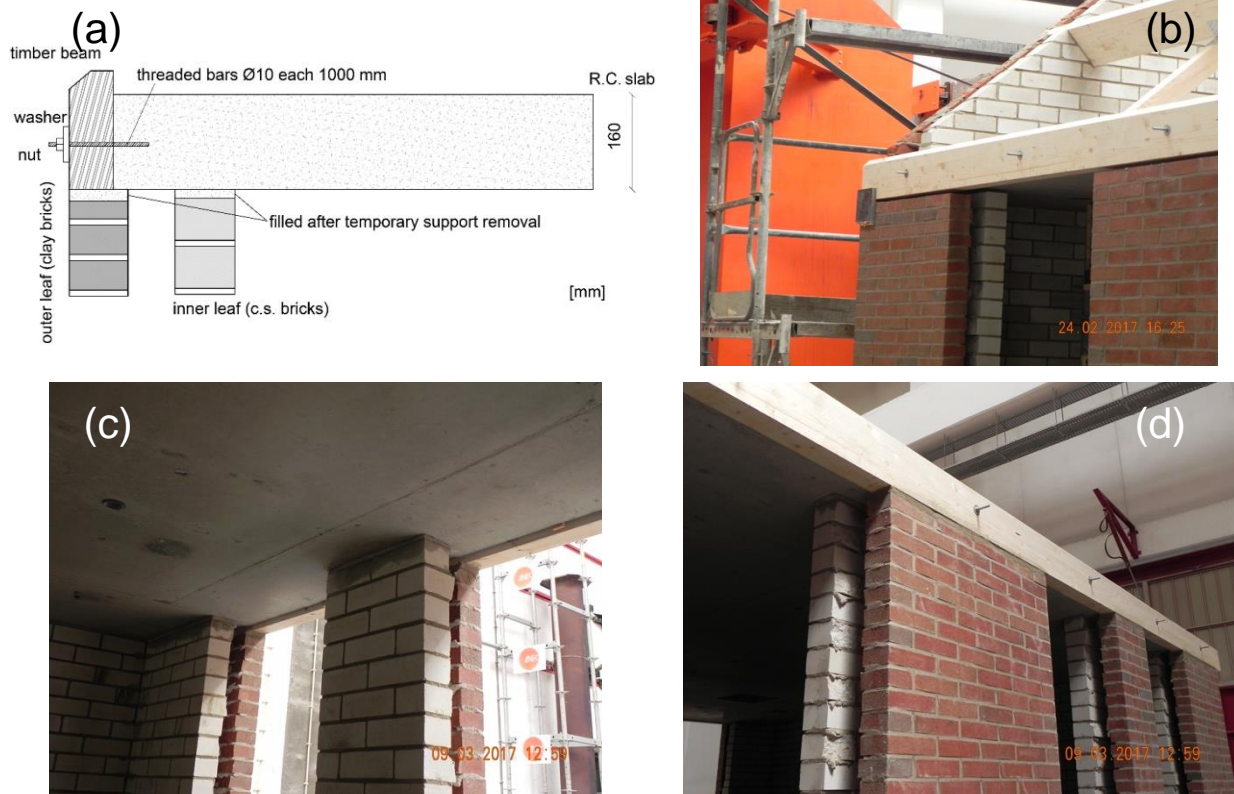


Figure 1.8 Details of the connections between the precast RC slabs and the longitudinal CS walls: (a,c) from the inside and (b,d) from the outside.

The timber roof is a simple structure consisting of one ridge beam, two timber plates on top of the longitudinal outer leaves of the walls and two girders per side between the ridge beam and the timber plates, at approximately 1.2 m of distance. Tongue and groove planks, with a width equal to 182 mm and a thickness of 18 mm, will be nailed on top by means of two 60x2 mm nails at each intersection (Figure 1.9 (a)). The planks did not cover the entire inclined length of the roof. Figure 1.9 (a) shows also the detail of their lay and connection with the timber beams. The timber beams of the roof are supported by the transverse inner CS leaves (West and East gables), whereas this connection was further reinforced by the presence of L-shaped steel anchors, as shown in Figure 1.9 (b). The roof diaphragm is characterised by four openings (three with dimension 54x45 cm, one 54x72 cm large) allowing, by means of a cable system, to sustain the RC slab in case of need and preventing a global collapse on the shaking table. The opening in the North-East corner is larger, granting access to the first floor (see Figure 1.10).

The in-plane stiffness of the timber diaphragm is essentially provided by the nailed connections between beams and planks, as well as by the effectiveness of the tongue and groove joints. The roof has been completed by the installation of clay tiles.

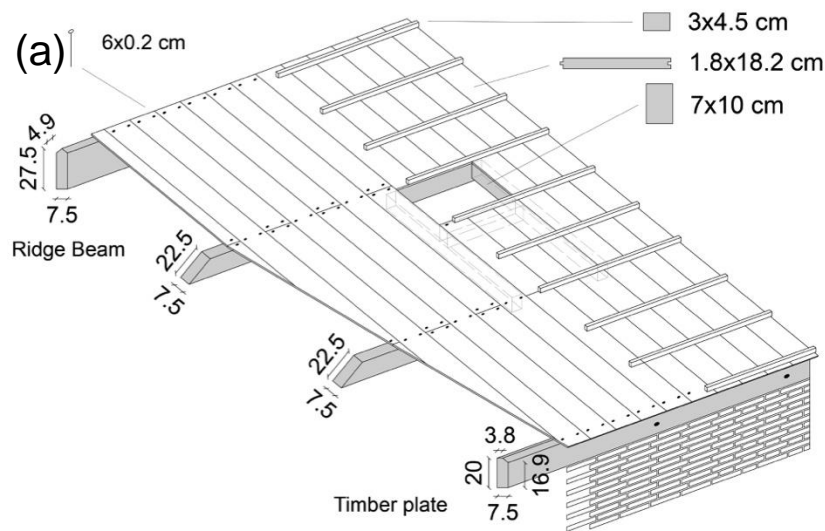


Figure 1.9 Details of the roof structure: (a) geometry of the timber diaphragm; (b) connection between the timber beams and the West gable.

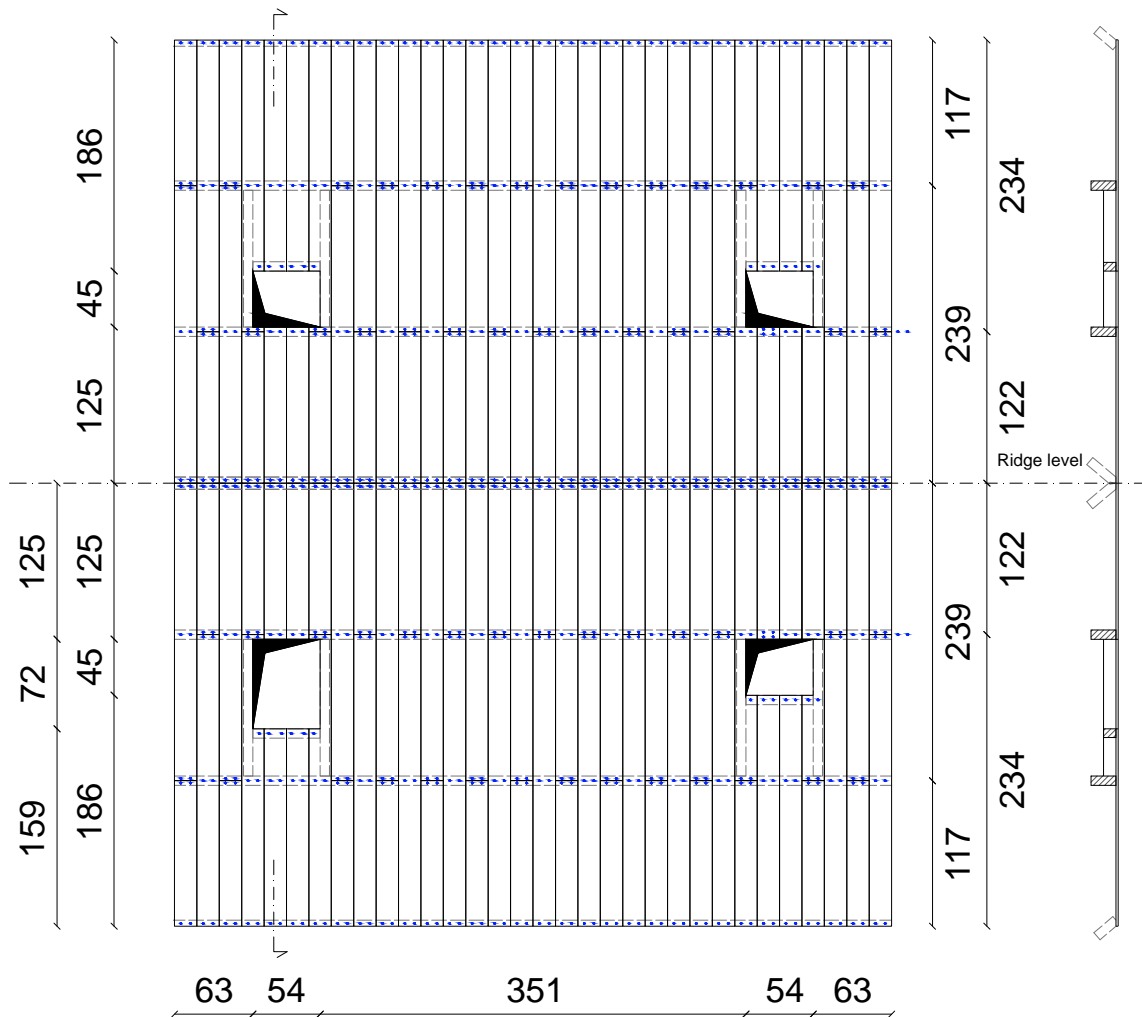


Figure 1.10 Plan view of the roof structure: geometry of the openings; the blue dots indicate the location of the nails connecting the planks with the beams.

22 Collapse Shaking Table Test on URM Cavity Wall Structure representative of a Dutch Terraced House

Table 1.2 indicates the masses of the different elements characterising the roof structure, while Figure 1.11 shows pictures of the roof construction and views of the specimen with the roof completed with the laying of the tiles.



Figure 1.11 Construction of the roof and views of specimen after the laying of the tiles.

Table 1.2 Masses of the different elements characterising the roof of the specimen.

Element	Mass [t]
Wooden planks	0.442
Horizontal profiles (for the positioning of tiles)	0.096
Wood elements around the holes	0.029
Beams (including ridge beam and timber plates)	0.295
Tiles	1.970
Total	2.835

1.4 Building prototype finishing

In order to study the performance of non-structural components the building inside the ground floor has been decorated with a layer of plaster and some common furnitures. Referring to Figure 1.12 the numbers indicate the different equipment inserted in the building prototype: (1) bookshelf anchored to the wall, (2) bookshelf not anchored to the wall, (3) ground lamp, (4) chair/sofa, (5) table with flowerpot and table lamp, (6) table with TV, (7) painting on the out-of-plane wall, (8,9) paintings on the in-plane walls, (10) chandelier.

2 MATERIALS CHARACTERISATION

This part of the experimental campaign allowed the mechanical properties of the building materials employed for the construction of the specimen to be determined, similarly to the campaign carried out in Pavia (Graziotti et al. 2015). It comprised strength tests on mortar samples, as well as tests on small masonry assemblages, such as compression tests, bond wrench tests and shear tests on triplets. The dimensions of the CS units were 212×102×71 mm. The clay bricks were perforated with ten vertical holes, they had a void ratio of 17% and dimensions of 211×100×50 mm. The flexural and compressive strength of the mortar were determined according to the prescriptions of EN 1015-11 (1999). Six masonry wallettes made of CS and four made of clay bricks were tested in compression in the direction perpendicular to the horizontal bed-joints, according to EN 1052-1 (1998). These tests allowed the determination of the compressive strength of masonry (f_m), as well as the secant elastic modulus of masonry at 33% of the compressive strength (E_1). Bond wrench tests on CS and clay masonry triplets were performed in order to determine the bond strength of masonry, according to EN 1052-5 (1998). Specimens of both types of masonry were also subjected to shear tests for the determination of the initial shear strength (f_{v0}) and friction coefficient (μ), according to the guidelines given by EN 1052-3 (1998).

Tests performed at the Delft University of Technology (TU Delft) allowed the determination of the tensile load capacity of the steel ties connecting the two masonry leaves (Messali et al. 2016). They found that the pull-in and pull-out strengths of the “zigzag” tie extremity embedded in clay masonry specimens, considering an overburden pressure of 0.3 MPa, was higher than the strengths associated with the hook extremity embedded in CS specimens and subjected to the same imposed pressure. The average pull-out and push-in strengths recorded for CS specimens were approximately 1.46 kN and 1.09 kN, respectively. Moreover, the tensile ultimate capacity of the steel anchors was approximately 4.3 kN. In Table 2.1 the green sections represent mechanical properties obtained from previously performed tests, while the remaining properties were determined during this experimental campaign.

26 Collapse Shaking Table Test on URM Cavity Wall Structure representative of a Dutch Terraced House

Table 2.1 Masonry mechanical properties.

Material properties	Symbol	UM	Calcium Silicate		Clay	
			Average	C.o.V.	Average	C.o.V.
Density of masonry	ρ	[kg/m ³]	1800	0.01	1839	0.01
Compressive strength of masonry unit	f_b	[MPa]	16.3	0.13	32.45	0.13
Tensile strength of masonry unit	f_{bt}	[MPa]	2.74	0.06	4.78	0.20
Elastic modulus of unit	E_{bt}	[MPa]	8990	0.36	7211	0.53
Compressive strength of mortar	f_c	[MPa]	6.20 ^H 8.45 ^C	0.06 ^H 0.35 ^C	8.34 ^H 8.67 ^C	0.11 ^H 0.18 ^C
Flexural strength of mortar	f_t	[MPa]	2.87 ^H 4.21 ^C	0.03 ^H 0.14 ^C	3.03 ^H 3.23 ^C	0.03 ^H 0.03 ^C
Compressive strength of masonry in the direction perpendicular to bed joints	f_m	[MPa]	9.80	0.10	19.19	0.05
Elastic modulus of masonry in the direction perpendicular to bed joints (33% f_m)	E_m	[MPa]	7955	0.18	12798	0.13
Flexural bond strength	f_w	[MPa]	0.36	0.20	0.19	0.47
Masonry (bed joint) initial shear strength	f_{v0}	[MPa]	0.45	-	0.41	-
Masonry (bed joint) shear friction coefficient	μ	[-]	0.48	-	0.75	-

^H = referred to house specimen

^C = referred to characterisation tests specimens

2.1 Mortar characterisation tests

2.1.1 Characterisation and identification of samples before hardening

The bedding mortar used in the masonry with calcium silicate blocks is different from the one used in the masonry with clay bricks. Both mortars are pre-dosed with cement and hydraulic lime, with the references of the products used in the two bedding mortars shown in Figure 2.1.



Product used in bedding mortar
for calcium silicate blocks
ref.:150102 t.h.t.



Product used in bedding mortar
for clay bricks
ref.: 1401151030 t.h.t.

Figure 2.1 Types of product used in each bedding mortar.

Since there are two types of products for manufacturing the mortars, the amount of water used for each one is different. Table 2.2 shows the adopted percentage of water for each mortar. These values were measured by Dutch construction professionals that prepared the mortars and are presented in Table 2.2.

Table 2.2 Adopted amount of water for each type of mortar.

Type of mortar	Water [kg]	Product [kg]	Water / product ratio [%]
Bedding mortar for calcium silicate blocks	2.9	25 (1 bag)	12
Bedding mortar for clay bricks	3.75	25 (1 bag)	15

The mortar samples were collected by LNEC technicians during the construction of the full-scale model and during the construction of the specimens for characterisation tests (*wallettes* and *triplets*). Figure 2.2 illustrates the construction of the full-scale model in one of the phases in which the mortar samples were collected. Figure 2.3 illustrates the construction of masonry characterisation specimens.



Figure 2.2 Construction of the full scale model at the time of collection of mortar samples.

28 Collapse Shaking Table Test on URM Cavity Wall Structure representative of a Dutch Terraced House



Figure 2.3 Construction of characterisation specimens at the time of mortar sampling.

The mortar samples were collected directly from the *in situ* mortar mix and then molded into standard molds measuring 160 x 40 x 40 mm, as shown in Figure 2.4.

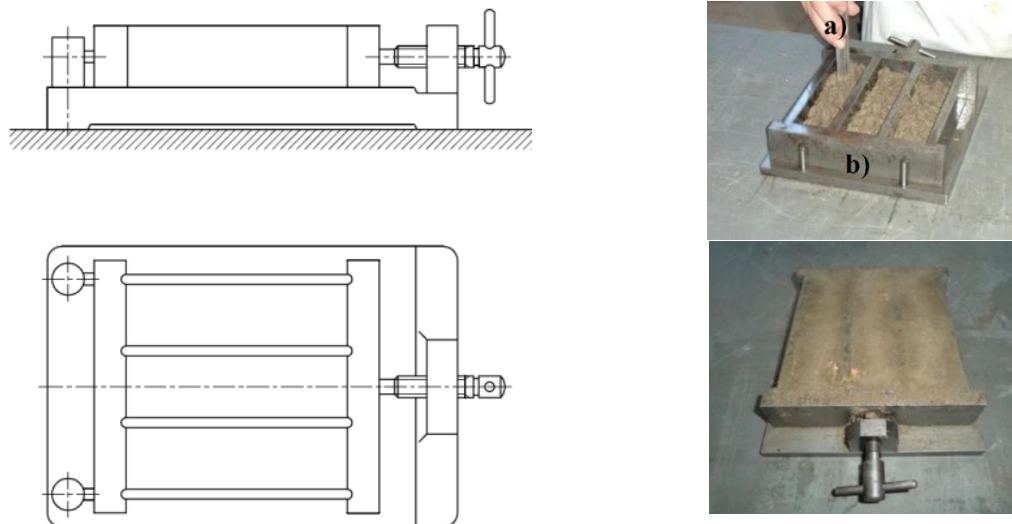


Figure 2.4 Molding of masonry specimens: (a) pestle and (b) mold.

The designation of the mortar samples is conformant with the following description:

- | | |
|--------|---|
| MX_1_1 | First collection of mortar for masonry X removed from the walls of the first floor of the full-scale model. |
| MX_1_2 | Second mortar collection for masonry X removed from the walls of the first floor of the full-scale model. |
| MX_C_1 | First collection of mortar for the masonry X removed from the characterisation specimens. |
| MX_C_2 | Second collection of mortar for masonry X removed from the characterisation specimens. |
| MX_2_1 | Collection of mortar for masonry X removed from the walls of the second floor of the full-scale model. |

The first letter of the designation corresponds to the type of sample "mortar", the "X" corresponds to the type of blocks used in each masonry wall: "S" stands for calcium silicate blocks and "CL" for the clay bricks. The character after the first underscore corresponds to the sample removal zone and the number after the second underscore corresponds to the number of collections made.

For each mortar collection the respective mortar mix was observed and all its constituents were measured. Table 2.3 shows the date and the water / product ratio for each batch corresponding to the collection of the respective samples.

Table 2.3 Determination of the water / product ratio for each corresponding mortar mix collection of samples.

Identification of the sample	Date of collection	Product [kg]	Water [kg]	Water / product ratio [%]
MS_1_1	2017-02-20	25	2.830	11.3
MS_1_2	2017-02-20	25	2.830	11.3
MS_C_1	2017-02-22	25	2.830	11.3
MS_C_2	2017-02-22	25	2.830	11.3
MS_2_1	2017-02-21	25	2.830	11.3
MCL_1_1	2017-02-20	25	3.670	14.7
MCL_C_1	2017-02-22	25	3.670	14.7
MCL_C_2	2017-02-22	25	3.670	14.7
MCL_2_1	2017-02-21	25	3.670	14.7

The tests considered adequate for characterising these samples were:

- Tests for the determination of the bulk density of fresh mortar;
- Tests for the determination of the consistence of fresh mortar (by flow table).

2.1.2 Tests for the determination of the bulk density of fresh mortar

The bulk density was determined by the quotient between the sample mass and its volume, for standard compaction conditions. The adopted methodology for this test is described in the standard EN 1015-6 "Methods of test for mortar for masonry - Part 6: Determination of bulk density of fresh mortar" (1998). The test starts by the pre-determination of the mass of the container (cylindrical cup), thus obtaining m_1 . Then, using a spatula, the cylindrical cup is filled with a first layer up to approximately half of its capacity. The contents are then compacted with 10 strokes carried out from the oscillation of the container on alternate sides. The process continues by filling the container a little over its capacity, and repeating the same compaction process as described above. Finally, the surface is leveled with the aid of a spatula by removing the excess mortar so that the surface becomes flat and coincident with the upper edge of the container. The outer surface of the container is conveniently cleaned to remove any residual mortar and the assembly is weighed (thus obtaining m_2).

Considering that the mortar mass is given by the difference between the mass of the set m_2 and the mass of the empty container m_1 , the bulk density of the mortar can be determined by the following equation.

$$D = \frac{m_2 - m_1}{V} \quad (1)$$

where:

D is the bulk density [kg/m³]

m_2 is the mass of the container with mortar [kg];

m_1 is the mass of the container [kg];

V is the volume of the container [m³].

30 Collapse Shaking Table Test on URM Cavity Wall Structure representative of a Dutch Terraced House

Figure 2.5 shows some phases of the test being performed, while the results obtained for the collected mortar are given in Table 2.4.



Figure 2.5 Carrying out the determination of bulk density of fresh mortar.

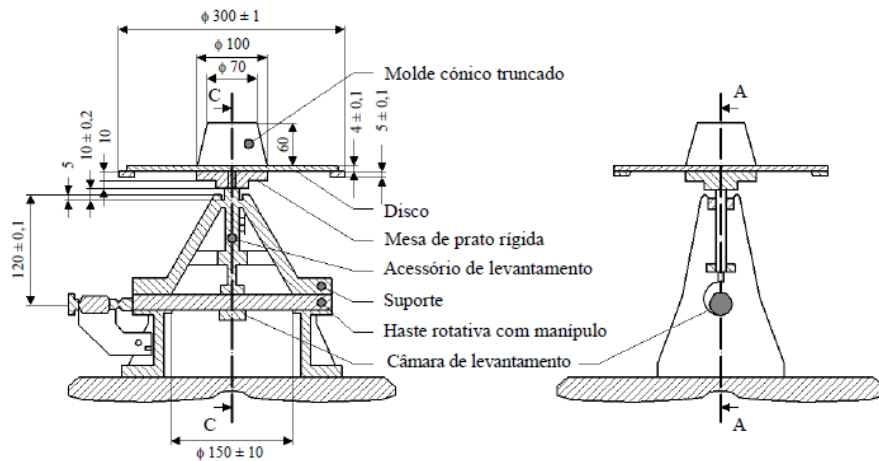
Table 2.4 Results obtained for the determination of bulk density of all mortars.

c	m ₁ [kg]	m ₂ [kg]	Bulk density [kg/m ³]
MS_1_1	0.463	2.136	1673
MS_1_2	0.464	2.108	1645
MS_C_1	0.463	2.146	1683
MS_C_2	0.464	2.183	1720
MS_2_1	0.464	2.134	1670
Average MS			1678
Standard deviation MS			27.23
MCL_1_1	0.464	2.385	1922
MCL_C_1	0.464	2.361	1898
MCL_C_2	0.464	2.345	1881
MCL_2_1	0.463	2.415	1951
Average MCL			1913
Standard deviation MCL			30.41

2.1.3 Tests for the determination of the consistence of fresh mortar (by flow table)

The purpose of this test is to determine the consistency of the mortar in its fresh state. The consistency is a measure of the fluidity of the fresh mortar, measuring the deformation of the mortar when subjected to external forces. The methodology adopted for this test is described in the standard EN 1015-3 "Methods of test for mortar for masonry - Part 3: Determination of consistency of fresh mortar (by flow table)" (1999). The test begins by moistening the table and the mold after ensuring that they are properly cleaned, then the mold is placed centered on the table and the mortar is introduced in two equal layers. Both layers are compacted with 25 strokes with the compaction bar, making sure that each stroke reaches the full thickness of the layer to ensure uniform filling of the mold. The excess mortar is then extracted with the spatula, removing it and wiping with a cloth to leave the table dry and clean. Approximately 15 seconds later, the mold is raised slowly and 25 strokes are applied at a rate of 0.5 strokes per second in order to spread the mortar. The diameter (in millimeters) of the scattering is measured in two orthogonal directions (d_1 , and d_2). The mortar spreading is expressed in millimeters and is the result of the average values d_1 and d_2 .

Figure 2.6 (a) presents a schematic representation of the spreading table and in Figure 2.6 (b) some phases of the tests performed are illustrated. The results obtained for all mortar samples collected are given in Table 2.5.



(a)



(b)

Figure 2.6 Determination of consistence of fresh mortar by scattering: (a) schematic representation of equipment; (b) test run.

Table 2.5 Results obtained in the determination of the consistency of fresh mortar for all samples collected.

Identification of the sample	d_1 [mm]	d_2 [mm]	Consistency [mm]
MS_1_1	147	141	144
MS_1_2	143	148	146
MS_C_1	154	151	153
MS_C_2	-	-	(*)
MS_2_1	150	156	153
Average MS			149
Standard deviation MS			4.69
MCL_1_1	164	161	163
MCL_C_1	153	154	154
MCL_C_2	122	121	122
MCL_2_1	154	157	156
Average MCL			149
Standard deviation MCL			18.25

(*) It was not possible to perform this test because the mortar was already quite dry

2.1.4 Characterisation and identification of specimens (hardened mortar)

After the samples were collected, they were used in the construction of the specimens to perform the physical and mechanical tests at three different ages: 10 days, 20 days and 28 days, as shown in Figure 2.7. These tests consist on determining the dynamic modulus of elasticity and determining the bending and compressive strengths. The storage of the specimens in a controlled environment followed the requirements of standard EN 1015-11

32 Collapse Shaking Table Test on URM Cavity Wall Structure representative of a Dutch Terraced House

"Methods of test for masonry - Part 11: Determination of flexural and compressive strength of hardened mortar" (1999) which correspond to placing the mold in a plastic bag of polyethylene for 2 days, ensuring a relative humidity of $95 \pm 5\%$, in a room wrapped at $20 \pm 2^\circ\text{C}$ and a relative humidity of $65 \pm 5\%$. Subsequently, the specimens were demoulded and kept under the aforementioned curing conditions for 5 days, after which the specimens were removed from the bag and remained in the same room (at $20 \pm 2^\circ\text{C}$ and at a relative humidity of $65 \pm 5\%$) until the date of the test. Figure 2.8 illustrates the reported curing conditions of some of the specimens.



Figure 2.7 Part of mortar specimens.



Figure 2.8 Curing conditions of mortar specimens.

The designation of the specimens is the same used in the samples, but with an underscore and a number identifying each specimen. The 10 days-old characteristics of the various specimens of the two types of mortar are presented in Annex II.

Since the tests for the determination of the dynamic modulus of elasticity are non-destructive, the same specimens were also used for the bending and compression strength tests.

The selected tests for these samples were, thus:

- Tests to determine the dynamic modulus of elasticity;
- Tests for determination of flexural and compression strengths.

2.1.5 Tests for the determination of dynamic modulus of elasticity

The modulus of elasticity of a coating mortar is a property that translates its ability to absorb stresses and thus deformations. Thus, the quality and durability of a mortar coating are directly related to its modulus of elasticity. The dynamic modulus of elasticity was determined by the procedure described in standard NP EN 14146 "Test methods for natural stone. Determination of dynamic modulus of elasticity (by measuring fundamental resonance frequency)" (2006). This is a non-destructive test which consists in determining the resonance frequency of prismatic specimens through a vibration induced longitudinally to the test specimen. The specimen is attached to the measuring apparatus through its central part and is subsequently induced to vibrate at one of its extremities, with such vibration being received by a sensor placed at the other end of the specimen after having passed its entire length. In a frequency spectrum, we can observe the highest peak corresponding to the frequency of the specimen itself. Figure 2.9 shows one of the test specimens as well as the type of plot obtained.

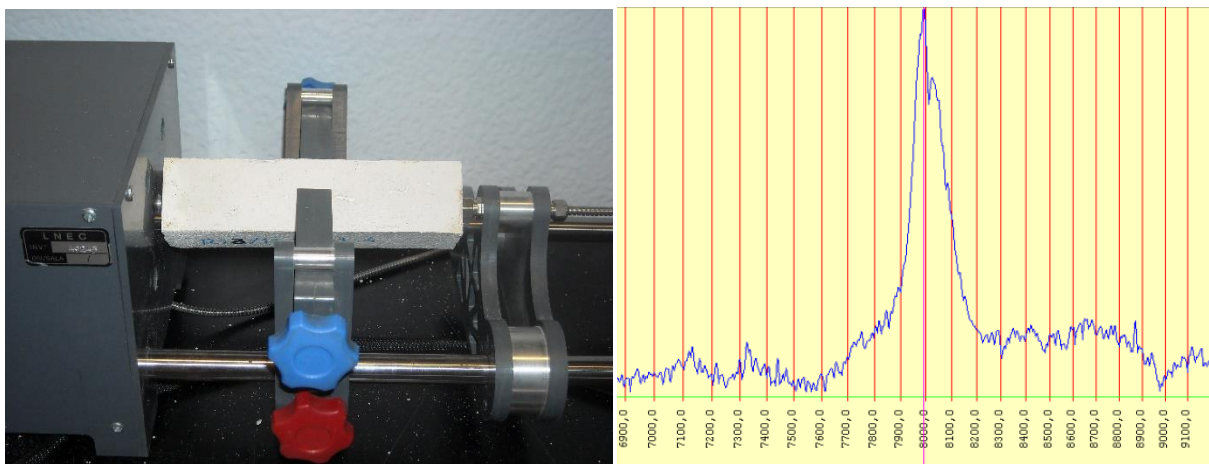


Figure 2.9 Carrying out the test to determine the dynamic modulus of elasticity and plot obtained.

From the observation of the frequency plot associated with each specimen it is possible to determine the fundamental resonance frequency (F) for each of them, which corresponds to the lowest frequency at which a maximum oscillation amplitude is obtained. After the specimens have been measured and weighed, and their resonance frequency determined, the dynamic modulus of elasticity was calculated using the following formula:

$$E_d = 4L^2 \times F^2 \times \rho \times 10^{-6} \quad (2)$$

where:

E_d is the dynamic modulus of elasticity [MPa];

L is the length of the specimen [m];

F is the longitudinal frequency of resonance [Hz];

ρ is the bulk density [kg/m^3].

In order to establish a relation between the days of maturation and the mechanical properties of the mortar, the results of the tests for the determination of the dynamic modulus of elasticity of the bedding mortar for calcium silicate blocks specimens (MS) for 10 days, 20 days and 28 days of age are presented in detail in Annex II and shown in Figure 2.10 to Figure 2.12.

34 Collapse Shaking Table Test on URM Cavity Wall Structure representative of a Dutch Terraced House

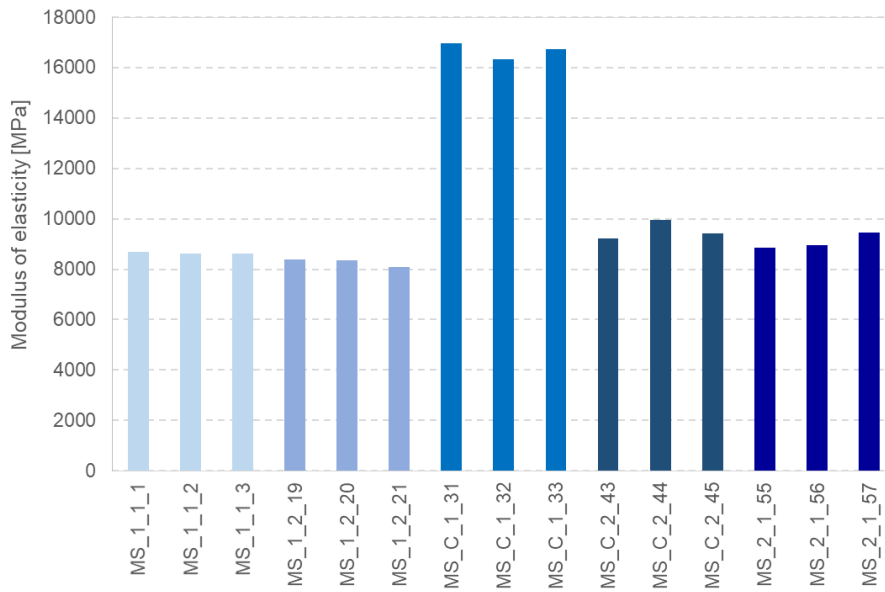


Figure 2.10 Test results for the determination of the dynamic modulus of elasticity of bedding mortar for the calcium silicate blocks (MS) after 10 days of age.

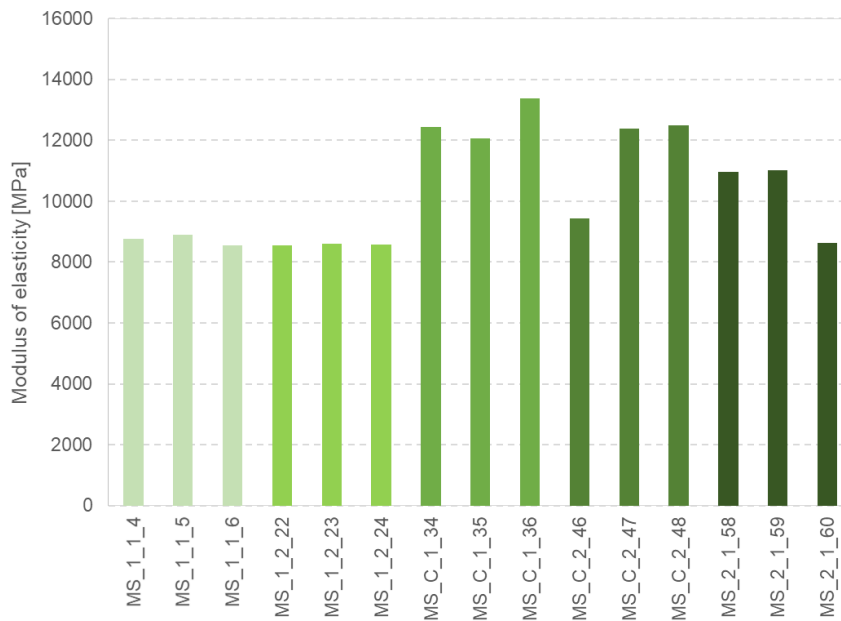


Figure 2.11 Test results for the determination of the dynamic modulus of elasticity of bedding mortar for the calcium silicate blocks (MS) after 20 days of age.

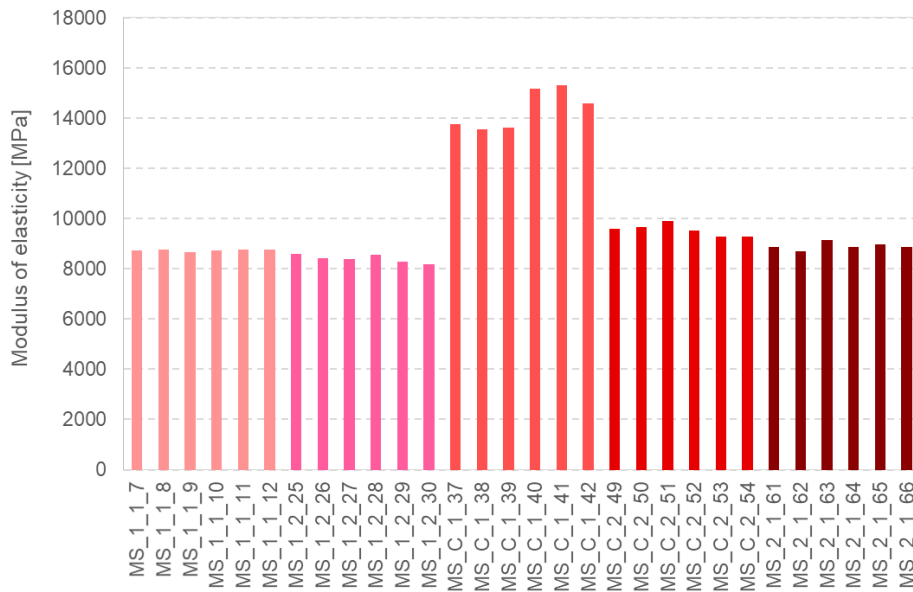


Figure 2.12 Test results for the determination of the dynamic modulus of elasticity of bedding mortar for the calcium silicate blocks (MS) after 28 days of age.

A similar analysis can be performed for the bedding mortar of clay bricks specimens (MCL). Results for 10 days, 20 days and 28 days of age are presented in detail in Annex II and shown in Figure 2.13 to Figure 2.15.

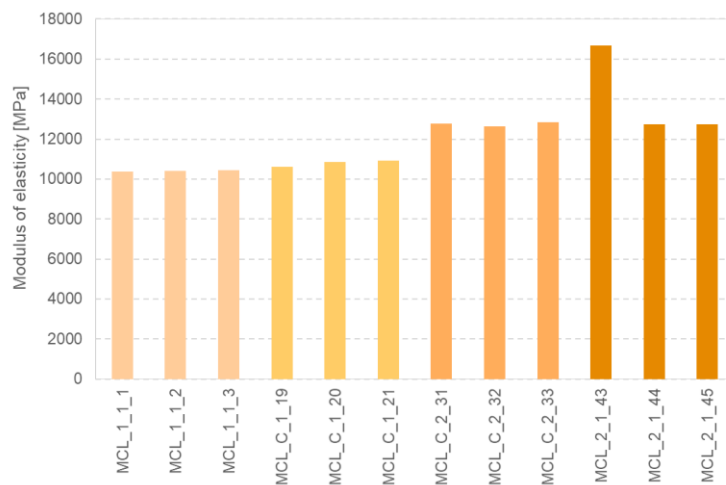


Figure 2.13 Test results for the determination of the dynamic modulus of elasticity of bedding mortar for the clay bricks (MCL) after 10 days of age.

36 Collapse Shaking Table Test on URM Cavity Wall Structure representative of a Dutch Terraced House

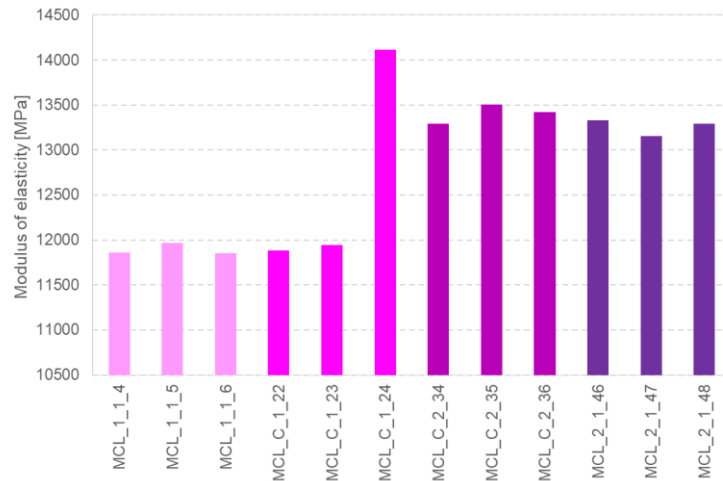


Figure 2.14 Test results for the determination of the dynamic modulus of elasticity of bedding mortar for the clay bricks (MCL) after 20 days of age.

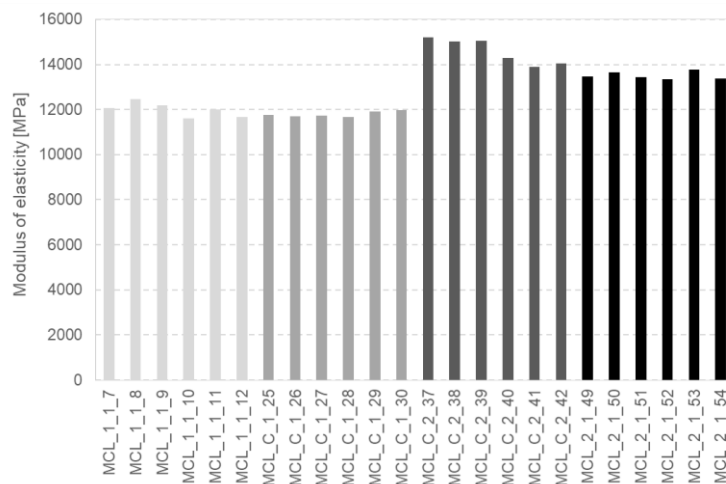


Figure 2.15 Test results for the determination of the dynamic modulus of elasticity of bedding mortar for the clay bricks (MCL) after 28 days of age.

Table 2.6 and Table 2.7 present a summary of the average dynamic modulus of elasticity obtained for the two types of bedding mortars collected directly from the full-scale model and the characterisation specimens, respectively.

Table 2.6 Summary of the average dynamic modulus of elasticity obtained for the two types of bedding mortar collected directly from the full-scale model for the different ages.

Specimens collected directly from the full scale model	Age of mortar	Dynamic modulus of elasticity of bedding mortar specimens for calcium silicate blocks			Dynamic modulus of elasticity of bedding mortar specimens for clay bricks		
		Average [MPa]	Standard deviation [MPa]	Coefficient of variation [-]	Average [MPa]	Standard deviation [MPa]	Coefficient of variation [-]
	10 days	8665	413	0.05	12231	2580	0.21
20 days	9174	902	0.10	12576	968	0.08	
28 days	8685	250	0.03	12755	1068	0.08	

Table 2.7 Summary of the average dynamic modulus of elasticity obtained for the two types of bedding mortar collected directly from the characterisation specimens for the different ages.

Specimens collected directly from characterisation specimens	Age of mortar	Dynamic modulus of elasticity of bedding mortar specimens for calcium silicate blocks			Dynamic modulus of elasticity of bedding mortar specimens for clay bricks		
		Average [MPa]	Standard deviation [MPa]	Coefficient of variation [-]	Average [MPa]	Standard deviation [MPa]	Coefficient of variation [-]
	10 days	13872	980	0.07	13405	919	0.07
	20 days	12033	435	0.04	13026	539	0.04
	28 days	11941	685	0.06	13188	1970	0.15

The plot of Figure 2.16 shows the relation of the dynamic moduli of elasticity of the two types of bedding mortar as a function of maturation time. The dashed lines refer to the modulus of elasticity of the bedding mortars for the calcium silicate blocks and the clay bricks (MS and MCL) taken from the characterisation test specimens. The continuous lines refer to the dynamic moduli of elasticity of the bedding mortars for the calcium silicate blocks and the clay bricks taken from the real-scale model.

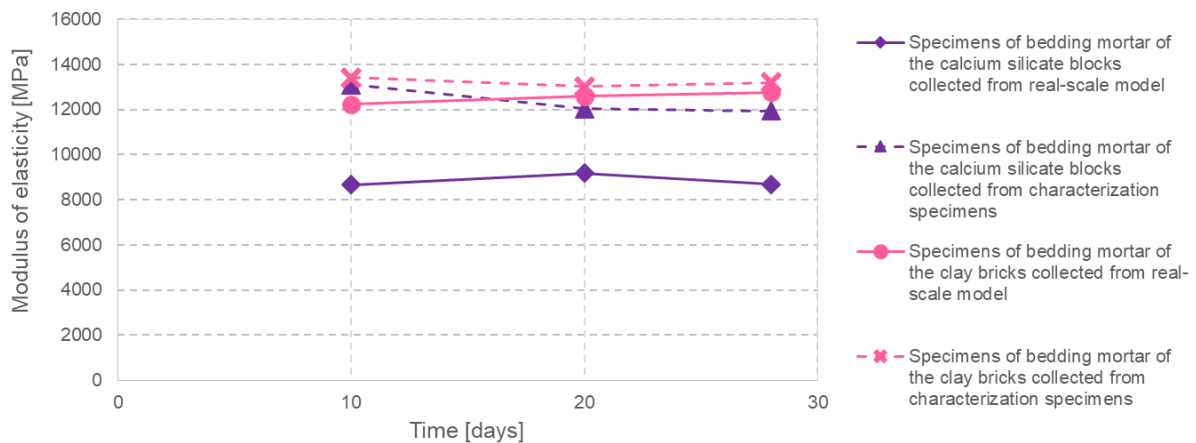


Figure 2.16 Relation between dynamic moduli of elasticity and maturation time for the two bedding mortars removed from the full scale model and the characterization test specimens.

2.1.6 Tests for the determination of flexural and compressive strengths

Test for the determination of flexural strength

The test to determine the flexural strength was performed in accordance with the standard EN 1015-11 (1999). The purpose of this test is to obtain the flexural strength of the mortar (hardened mortar), by applying a half-span load to a simply supported prismatic specimen as depicted in Figure 2.17 (a). The specimen is placed on the test machine and is centered with the longitudinal axis perpendicular to the two supports, ensuring that one of the side molding faces stays fixed on the supports. The load is applied at mid-span through an upper bearing point, and imposing a gradual force and increasing continuously, between 10 and 50 N/s, forcing the failure to occur in a range of time between 30 and 90 seconds. The maximum force supported by the specimen is recorded until failure and the flexural strength of the specimen then calculated. In Figure 2.17 (b) one of the test specimens is shown.

38 Collapse Shaking Table Test on URM Cavity Wall Structure representative of a Dutch Terraced House

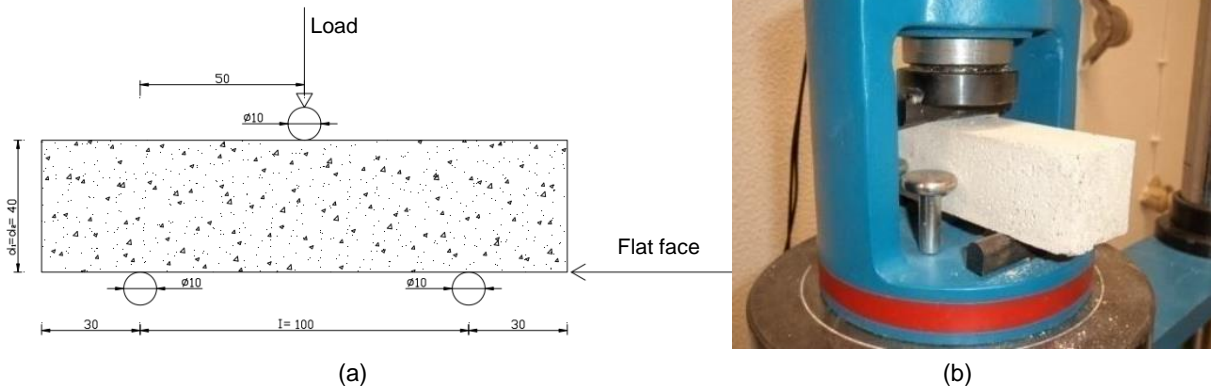


Figure 2.17 Test for determination of flexural strength: (a) scheme of positioning of the specimen and (b) specimen being tested.

The flexural strength is given by the following equation:

$$f_t = 1.5 \times \frac{F_f \times l^2}{b \times d} \quad (4)$$

where:

f_t is the flexural strength [MPa];

F_f is the maximum flexural force applied to the specimen at the moment of rupture [N];

l is the distance between the bottom rollers [mm];

b is the width of the test specimen [mm];

d is the height of the test specimen [mm].

Test for the determination of compressive strength

The test to determine the compressive strength was performed in accordance with the standard EN 1015-11 (1999). This test allows the determination of the compressive strength of mortar specimens (hardened mortar). This test is performed immediately after the flexural test, and on the prisms resulting therefrom, by applying a load until failure.

The specimen is placed centered on the lower plate of the machine test with the flat face in contact to the lower plate. The upper plate of the machine is lowered until it contacts the upper face of the specimen, as shown in Figure 2.18 (a). An increasing force is then applied gradually and without shock, in order to obtain the failure between 30 and 90 seconds until the failure of the specimen. The compressive strength values determined by this method are designated by f_c . The calculation is to the following formula:

$$f_c = \frac{F_c}{A_c} \quad (5)$$

where:

f_c is the compressive strength [MPa];

F_c is the maximum compressive force applied to the specimen at the moment of failure [N];

A_c is the area of the specimen in contact with the plates of the machine test [mm²].

Figure 2.18 (b) depicts one of the specimens being tested.

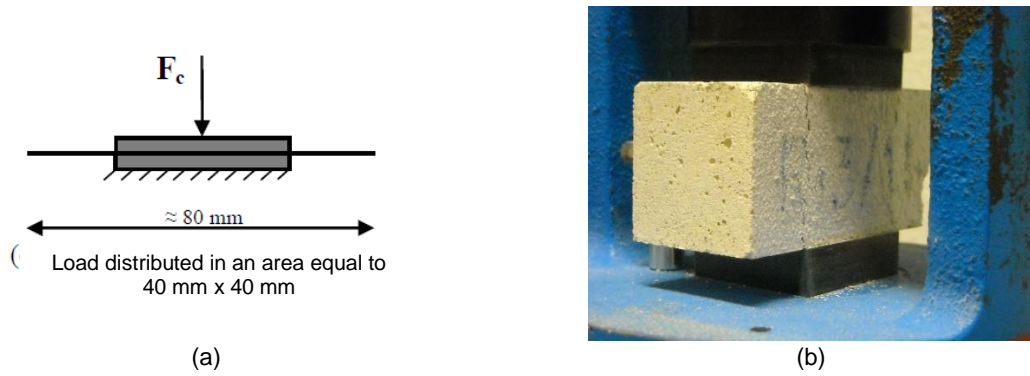


Figure 2.18 Test for compressive strength: (a) test scheme and (b) specimen being tested.

In order to obtain a relation between the maturation time and the mechanical properties of the mortars, Figure 2.19 to Figure 2.24 show the test results on flexural and compressive strengths of bedding mortar specimens for the calcium silicate blocks (MS) after 10 days, 20 days and 28 days of age. Additional results are given in Annex II. In the plots of Figure 2.22 to Figure 2.24, the compressive strength is represented with bars and the value of the modulus of elasticity for the corresponding specimens is represented by a line.

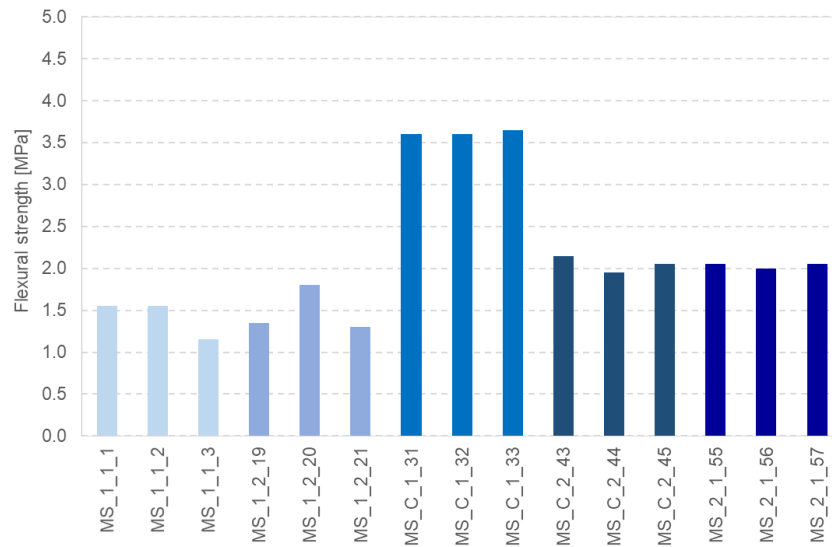


Figure 2.19 Flexural strength test results for bedding mortar specimens used with calcium silicate blocks (MS) after 10 days of age.

40 Collapse Shaking Table Test on URM Cavity Wall Structure representative of a Dutch Terraced House

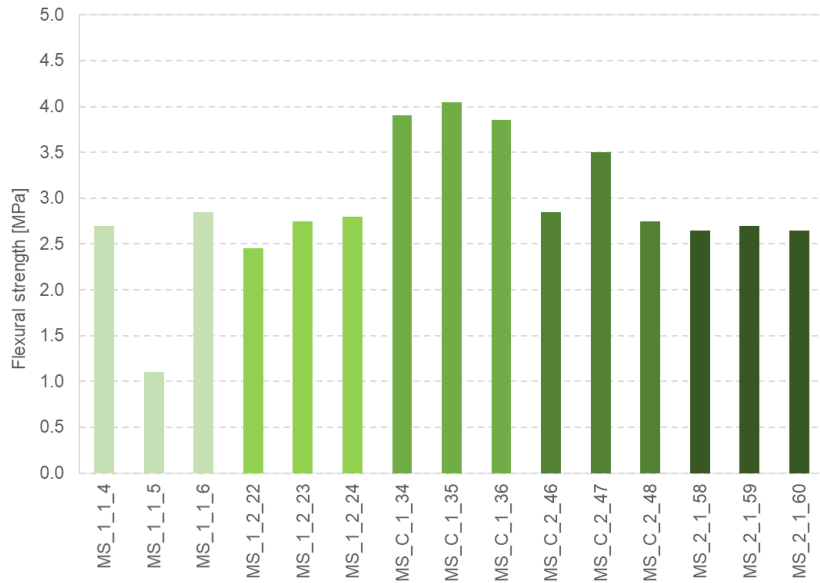


Figure 2.20 Flexural strength test results for bedding mortar specimens used with calcium silicate blocks (MS) after 20 days of age.

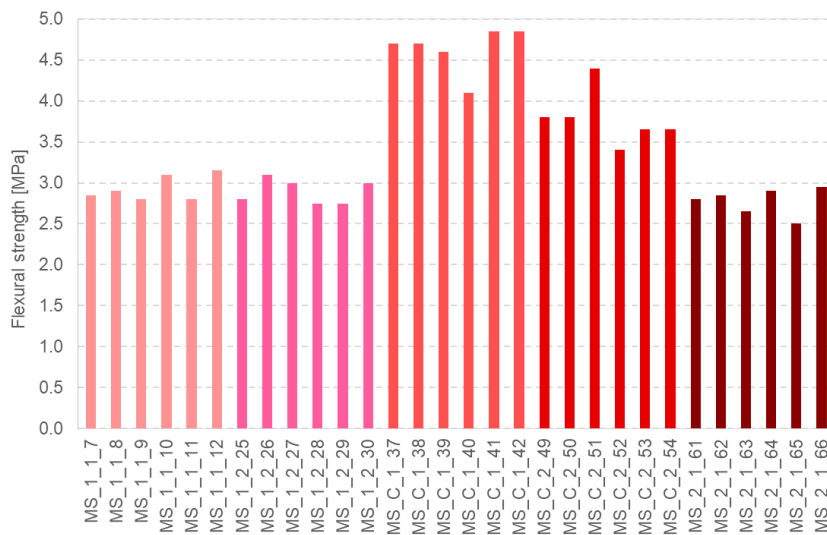


Figure 2.21 Flexural strength test results for bedding mortar specimens used with calcium silicate blocks (MS) after 28 days of age.

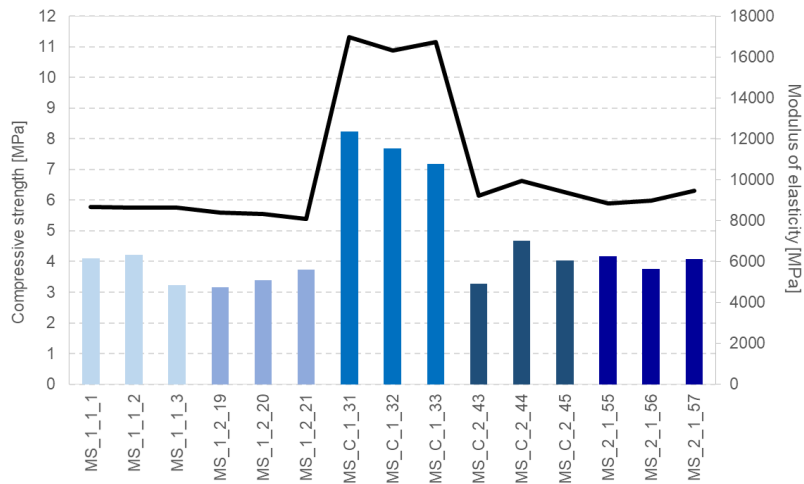


Figure 2.22 Compressive strength and modulus of elasticity test results for bedding mortar specimens used with calcium silicate blocks (MS) after 10 days of age.

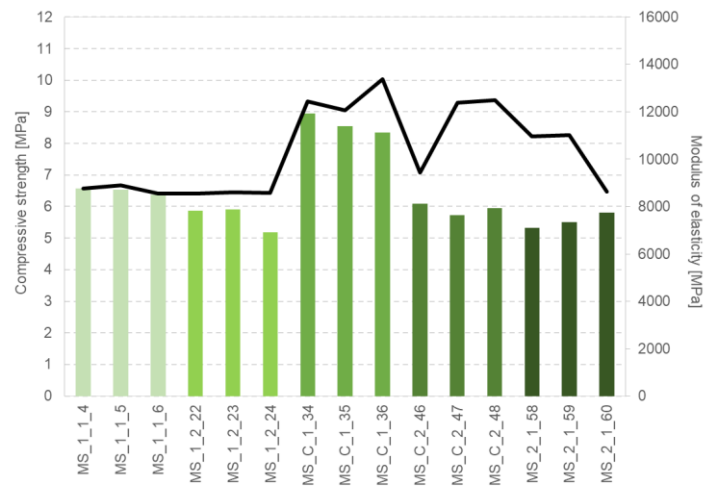


Figure 2.23 Compressive strength and modulus of elasticity test results for bedding mortar specimens used with calcium silicate blocks (MS) after 20 days of age.

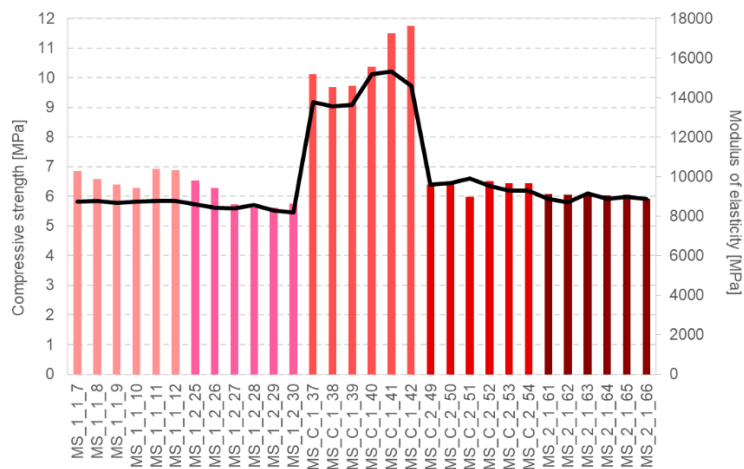


Figure 2.24 Compressive strength and modulus of elasticity test results for bedding mortar specimens used with calcium silicate blocks (MS) after 28 days of age.

42 Collapse Shaking Table Test on URM Cavity Wall Structure representative of a Dutch Terraced House

Figure 2.25 presents the distribution of the flexural and compressive strengths of bedding mortars for the calcium silicate blocks (MS) after 28 days of age.

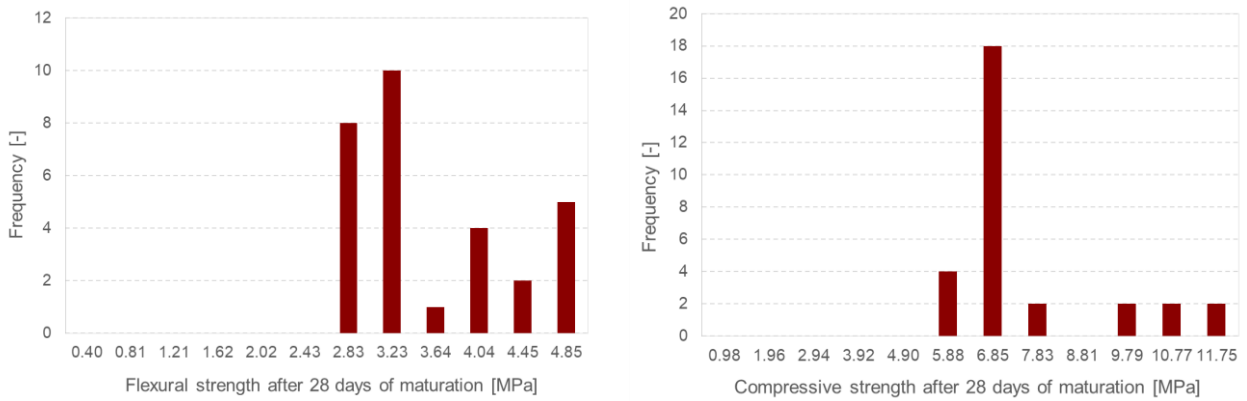


Figure 2.25 Distribution of the flexural and compressive strength of bedding mortars used with calcium silicate bricks (MS) after 28 days of age.

In order to obtain a relation between the maturation time and the mechanical properties of the mortars, Figure 2.26 to Figure 2.31 show the test results for the determination of flexural and compressive strengths of bedding mortar specimens for the clay bricks (MCL) after 10 days, 20 days and 28 days of age. Additional results are shown in Annex II. In the plots of Figure 2.29 to Figure 2.31, the compressive strength is represented with bars and the value of the modulus of elasticity for the corresponding specimens is represented by a line.

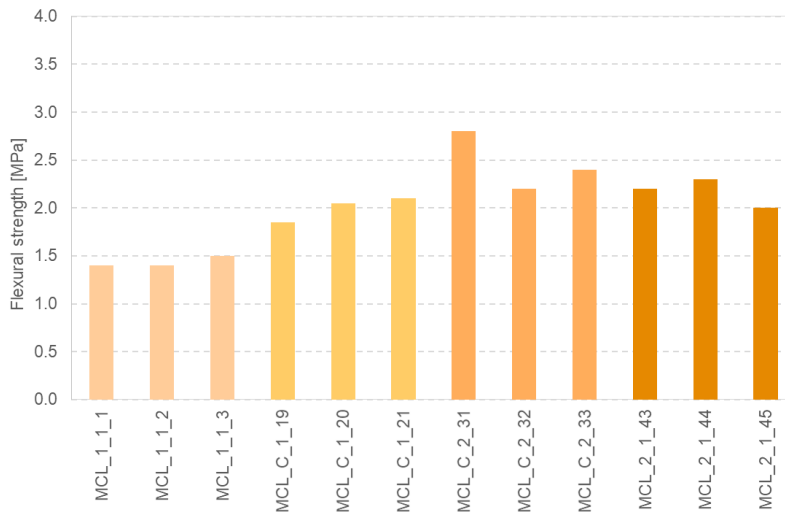


Figure 2.26 Flexural strength test results for bedding mortar specimens used with clay bricks (MCL) after 10 days of age.



Figure 2.27 Flexural strength test results for bedding mortar specimens used with clay bricks (MCL) after 20 days of age.

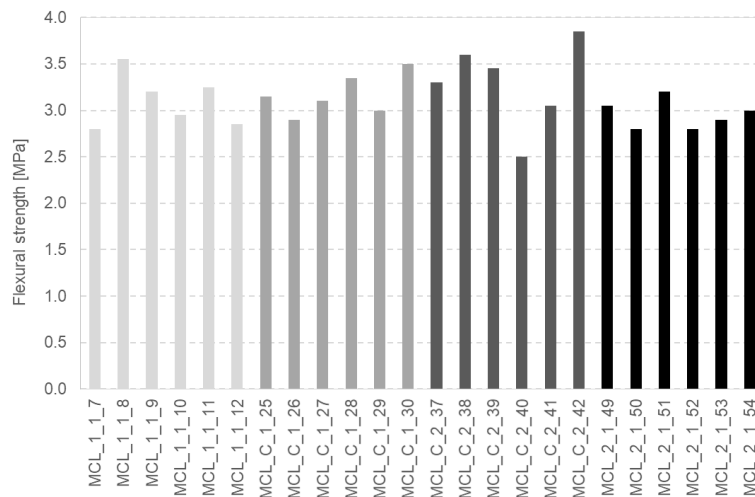


Figure 2.28 Flexural strength test results for bedding mortar specimens used with clay bricks (MCL) after 28 days of age.

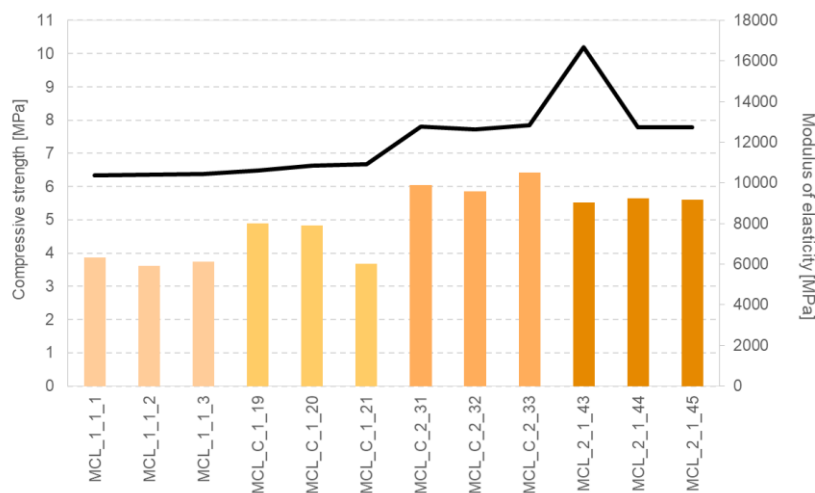


Figure 2.29 Compressive strength and modulus of elasticity test results for bedding mortar specimens used with clay bricks (MCL) after 10 days of age.

44 Collapse Shaking Table Test on URM Cavity Wall Structure representative of a Dutch Terraced House

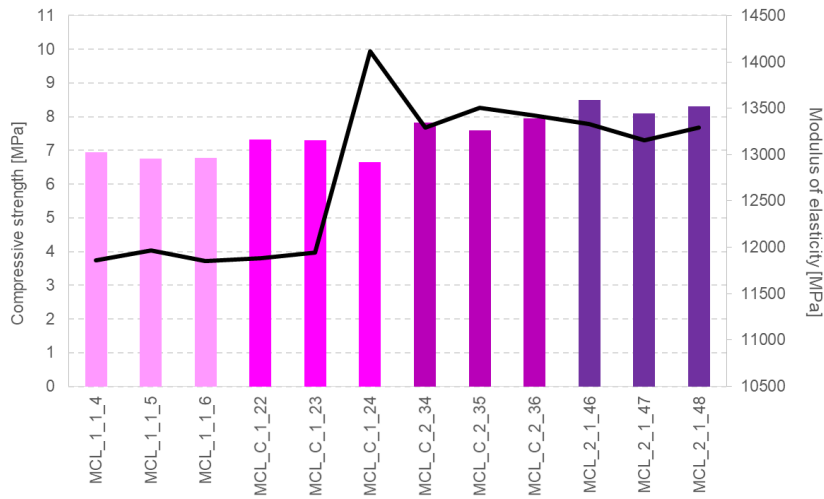


Figure 2.30 Compressive strength and modulus of elasticity test results for bedding mortar specimens used with clay bricks (MCL) after 20 days of age.

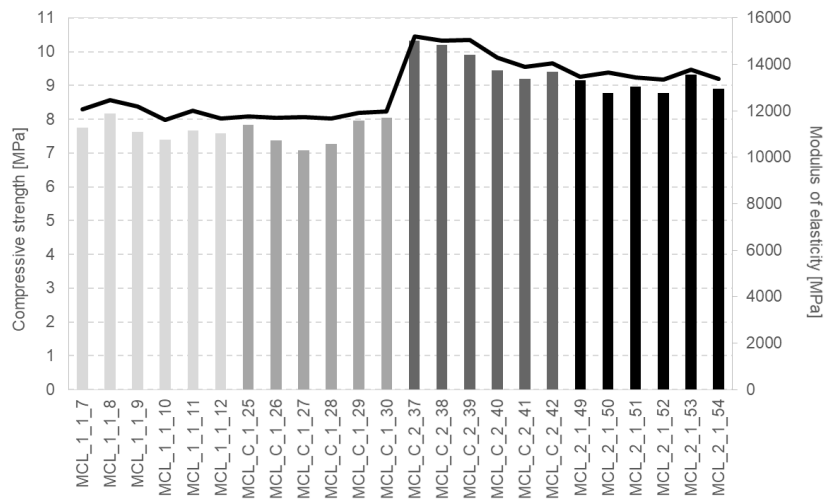


Figure 2.31 Compressive strength and modulus of elasticity test results for bedding mortar specimens used with clay bricks (MCL) after 28 days of age.

Figure 2.32 presents the distribution of the flexural and compressive strengths of bedding mortars for the clay bricks (MCL) after 28 days of age.

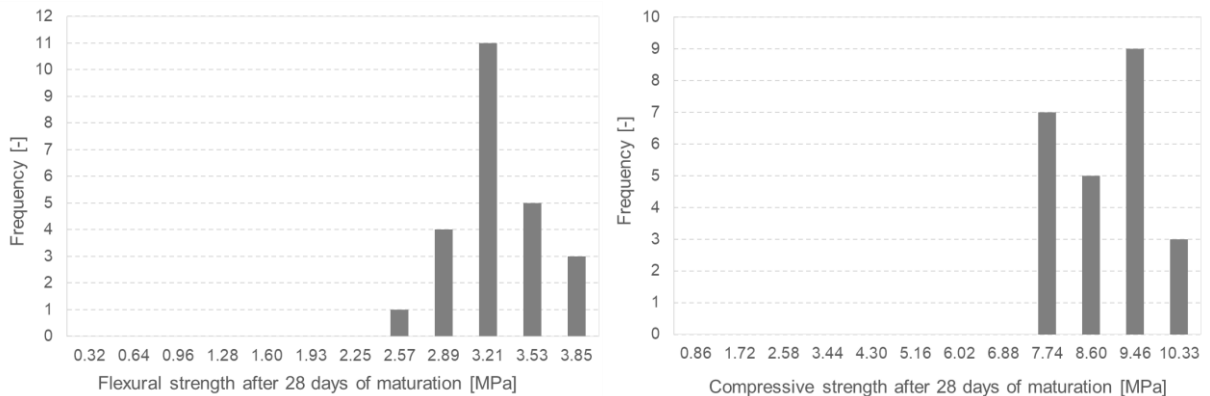


Figure 2.32 Distribution of the flexural and compressive strengths of bedding mortars for the clay bricks (MCL) after 28 days of age.

Table 2.8 and Table 2.9 show the summary of the averages of compressive and flexural strength obtained for the two types of bedding mortars collected directly from the full-scale model and the characterisation specimens, respectively.

Table 2.8 Summary of the compressive and flexural strength averages obtained for the two types of bedding mortars collected directly from the full-scale model for different ages.

Specimens collected directly from the full scale model	Type of mortar	Age of mortar	Compressive strength			Flexural strength		
			Average [MPa]	Standard deviation [MPa]	Coefficient of variation [-]	Average [MPa]	Standard deviation [MPa]	Coefficient of variation [-]
	MS	10 days	3.76	0.30	0.08	1.75	0.34	0.20
		20 days	5.89	0.52	0.09	2.52	0.26	0.10
		28 days	6.20	0.39	0.06	2.87	0.08	0.03
	MCL	10 days	4.67	1.30	0.28	1.80	0.52	0.29
		20 days	7.56	1.04	0.14	2.37	0.40	0.17
		28 days	8.34	0.91	0.11	3.03	0.10	0.03

Table 2.9 .Summary of the compressive and flexural strength averages obtained for the two types of bedding mortars collected directly from characterisation specimens for different ages.

Specimens collected directly from characterisation specimens	Type of mortar	Age of mortar	Compressive strength			Flexural strength		
			Average [MPa]	Standard deviation [MPa]	Coefficient of variation [-]	Average [MPa]	Standard deviation [MPa]	Coefficient of variation [-]
	MS	10 days	5.84	2.62	0.45	2.83	1.11	0.39
		20 days	7.27	1.90	0.26	3.48	0.64	0.18
		28 days	8.45	2.93	0.35	4.21	0.60	0.14
	MCL	10 days	5.29	1.16	0.22	2.23	0.33	0.15
		20 days	7.44	0.49	0.07	2.20	0.07	0.03
		28 days	8.67	1.52	0.18	3.23	0.09	0.03

The plots of Figure 2.33 and Figure 2.34 show the relation of the compressive and flexural strength as a function of maturation time for the two types of bedding mortar. The dashed line refers to the flexural and compressive strength of the bedding mortars taken from the characterisation test specimens. The continuous line refers to the flexural and compressive strengths of the bedding mortars taken from the full-scale model.

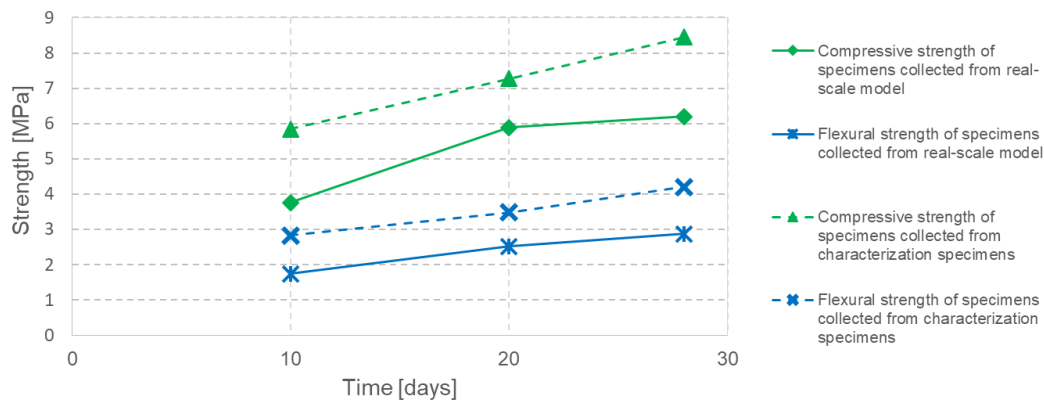


Figure 2.33 Relation between flexural and compressive strengths and maturation time of bedding mortars for the calcium silicate blocks (MS) removed from the full-scale model and the characterisation test specimens.

46 Collapse Shaking Table Test on URM Cavity Wall Structure representative of a Dutch Terraced House

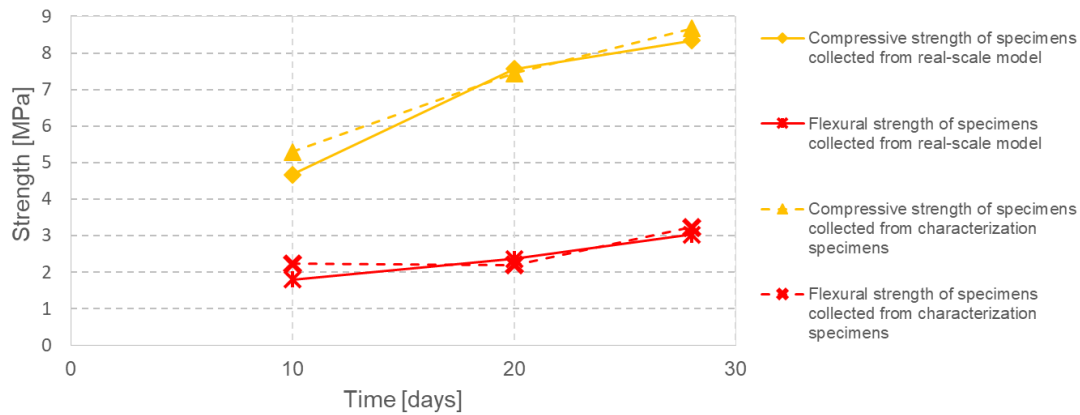


Figure 2.34 Relation between flexural and compressive strength and maturation time of bedding mortars for the clay bricks (MCL) removed from the full-scale model and the characterisation test specimens.

2.2 Block characterisation tests

2.2.1 Characterisation and identification of specimens

As previously mentioned, there are two types of masonry with corresponding two types of blocks. The inner load-bearing walls are composed of calcium silicate blocks and the outer walls are composed of perforated clay bricks. Figure 2.35 shows the two types of blocks that were tested.

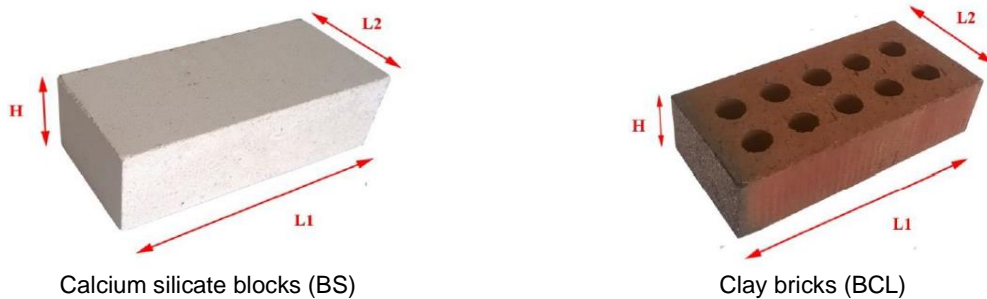


Figure 2.35 Blocks used and indication of their dimensions.

Several specimens of each type of block were collected and selected from the material used for the construction of the full-scale model and the characterisation samples (Figure 2.36 and Figure 2.37). The specimens collected were more than 30 days inside the premises of the laboratory units without specific packaging until the date of the test.



Calcium silicate blocks (BS)



Clay bricks (BCL)

Figure 2.36 Collection of test pieces.



Calcium silicate blocks (BS)



Clay bricks (BCL)

Figure 2.37 Blocks units.

The designation of the blocks is in accordance with the following:

- Calcium silicate blocks (BS);
- Clay bricks (BCL).

The drilling percentage of the perforated clay bricks is 17% (Graziotti F. et al.; 2015). In Table 2.10 the characteristics of the various specimens of the two types of blocks selected for the tests are presented, with additional details provided in Annex III.

Table 2.10 Characteristics of the two types of blocks selected for the tests.

Type of specimen	Average Mass [kg]	Average Length (L1) [mm]	Average Width (L2) [mm]	Average Height (H) [mm]
BS	2.894	212.7	103.0	70.7
BCL	1.704	211.2	100.9	50.0

The bulk density average values for the calcium silicate and clay blocks are given in Table 2.11, with additional details provided in Annex III.

48 Collapse Shaking Table Test on URM Cavity Wall Structure representative of a Dutch Terraced House

Table 2.11 Bulk density for calcium silicate and clay blocks.

Specimen	Average bulk density	Standard deviation	C.o.V.
	[kg/m ³]	[kg/m ³]	[-]
BS	1867.94	44.95	0.02
BCL	1597.96	25.50	0.02

The selected tests for these specimens were:

- Test for determination of moisture content;
- Test for the determination of water absorption capillarity coefficient.

2.2.2 Test for the determination of moisture content

The test for determination of the moisture content was carried out on six specimens of each type based on the procedures described in EN 772-10 "Methods of test for masonry units Part 10: Determination of moisture content of calcium silicate and autoclaved aerated Concrete units" (1999), in NP EN 1097-5 "Tests of the mechanical and physical properties of the aggregates. Part 5: Determination of the water content by drying in a ventilated oven" (2011), and in the procedure of LNEC FE Pa 47 (2015). This test has as its main objective to determine the moisture content by the thermogravimetric method.

To carry out this test, six calcium silicate block specimens were selected with the designation BS_11 to BS_16 and six clay brick specimen with the designation BCL_11 to BCL_16. After the selection of the specimens, they were individually weighed and placed in a ventilated oven at a constant temperature of 105 ± 5 ° C, as shown in Figure 2.38, and weighed every 24 hours. This procedure must be carried out until a constant weight is obtained, i.e. until two consecutive weighings correspond to a mass loss of less than 0,2% of the total mass. After the specimens had reached a constant mass, the test pieces were again weighed, according to Figure 2.39.

The moisture content is determined according to the following formula:

$$w_s = \frac{m_{0,s} - m_{dry,s}}{m_{dry,s}} \times 100 \quad (6)$$

where:

w_s is the percentage moisture content [%];

$m_{0,s}$ is the mass of the specimen before drying [g];

$m_{dry,s}$ is the mass of the specimen after drying [g].

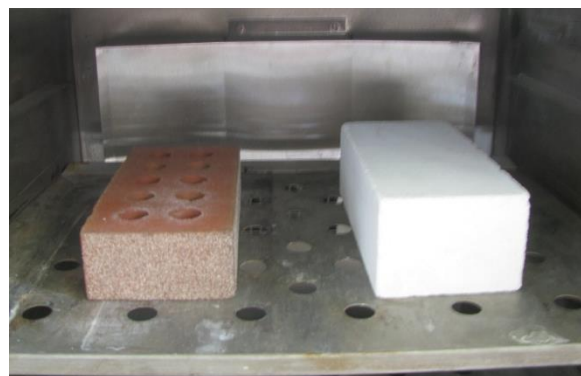
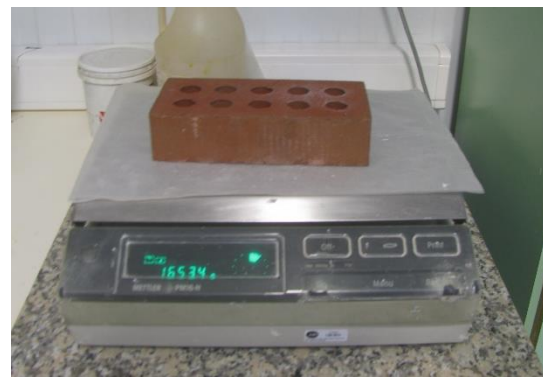


Figure 2.38 Drying the blocks in a ventilated oven.



Calcium silicate blocks (BS)



Clay bricks (BCL)

Figure 2.39 Weighing of blocks.

Table 2.12 shows the weighings carried out until a constant mass of 0.2% is reached for the calcium silicate blocks, while Table 2.13 presents the results for the clay bricks.

Table 2.12 Weighing until constant mass is reached for the calcium silicate blocks.

Date	BS_11		BS_12		BS_13		BS_14		BS_15		BS_16	
	Mass [g]	Checking stopping criterion (0,2%)										
05/04/2017	2747	-	2895	-	2808	-	2743	-	2893	-	2805	-
06/04/2017	2723	Continue	2868	Continue	2783	Continue	2719	Continue	2865	Continue	2778	Continue
07/04/2017	2726	Stop	2868	Stop	2782	Stop	2718	Stop	2863	Stop	2773	Continue
10/04/2017	-	-	-	-	-	-	-	-	-	-	2774	Stop

Table 2.13 Weighing until constant mass is reached for the clay bricks.

Data	BCL_11		BCL_12		BCL_13		BCL_14		BCL_15		BCL_16	
	Mass [g]	Checking stopping criterion (0,2%)										
05/04/2017	1727	-	1728	-	1733	-	1736	-	1728	-	1729	-
06/04/2017	1726	Continue	1727	Continue	1730	Continue	1735	Continue	1727	Stop	1729	Continue
07/04/2017	1721	Continue	1726	Continue	1733	Continue	1733	Continue	-	-	1730	Continue
10/04/2017	1725	Continue	1728	Continue	1731	Continue	1736	Continue	-	-	1729	Continue
11/04/2017	1725	Stop	1726	Continue	1731	Stop	1733	Continue	-	-	1730	Continue
12/04/2017	-	-	1726	Stop	-	-	1735	Stop	-	-	1726	Continue
13/04/2017	-	-	-	-	-	-	-	-	-	-	1728	Stop

Table 2.14 summarises the percentages of moisture content of the two types of blocks.

50 Collapse Shaking Table Test on URM Cavity Wall Structure representative of a Dutch Terraced House

Table 2.14 Percentage of moisture content of the two types of blocks.

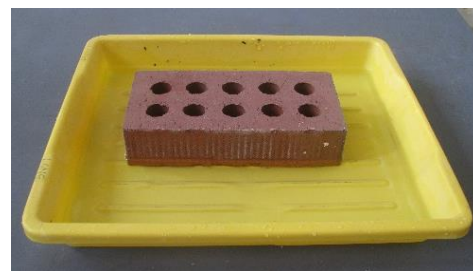
Specimen	W _s [%]	Average [%]	Standard deviation [%]	Coefficient of variation [%]
BS_11	0.77	0.96	0.12	0.13
BS_12	0.94			
BS_13	0.93			
BS_14	0.92			
BS_15	1.05			
BS_16	1.12			
BCL_11	0.12	0.09	0.03	0.37
BCL_12	0.12			
BCL_13	0.12			
BCL_14	0.06			
BCL_15	0.06			
BCL_16	0.06			

2.2.3 Test for determination of the water absorption capillarity coefficient

The test for determination of the capillarity coefficient was performed on six specimens of each type of block by the procedures described in EN 772-11 "Methods of test for masonry units Part 11: Determination of water absorption of aggregate concrete, autoclaved aerated concrete" (2011) and in the LNEC PE / Sup-01 test procedure (2006). The results of this work are presented in Table 2.15. To perform this test the specimens were initially dried at 105 ± 5 ° C until 0.1% of constant mass was obtained. After cooling, the faces that were immersed in water (2 measurements per dimension, near the edges) are measured and the area that is in contact with the water is determined. Subsequently the initial mass of the specimen was measured and the blocks inserted in a tray with elements that allow the passage of water under them, with the face to be submerged downwards, immersed in water up to 5 ± 1 mm, as shown in Figure 2.40. After the specified period for the material concerned, which in this case is 60 ± 2 s, the specimen is removed and the surface water is removed with absorbent paper and the specimens are weighed.



Calcium silicate blocks (BS)



Clay bricks (BCL)

Figure 2.40 Determination of the water absorption coefficient by capillarity of the carrier.

The water absorption coefficient by capillarity determined by this method is designated by C. The calculation is done according to the following formula:

$$C = \frac{M_i - M_0}{A \times \sqrt{t_i}} \quad (7)$$

where:

C is the water absorption coefficient by capillarity [kg/m².min^{0.5}];

M_i is the mass of the dry specimen [kg];

M_f is the mass of the specimen after immersion in water for 60 seconds [kg];

A is the area of the specimen in contact with water [m^2];

t_i is the immersion time of the specimen in water (60 seconds in this specific case) [s].

This test was performed on the calcium silicate blocks test pieces designated by BS_11 to BS_16 and on the clay brick specimens designated BCL_11 to BCL_16. Table 2.15 shows the results of the water absorption coefficient by capillarity of the blocks.

Table 2.15 Results for the determination of the water absorption coefficient by capillarity for the two types of blocks.

Specimen	Area [m^2]	Initial Mass [g]	Final Mass [g]	Immersion time [s]	Coefficient of water absorption [$\text{g}/(\text{m}^2 \cdot \text{s}^{1/2})$]	Average [$\text{g}/(\text{m}^2 \cdot \text{s}^{1/2})$]	Average [$\text{kg}/(\text{m}^2 \cdot \text{min}^{1/2})$]
BS_11	0.021738	2742.79	2762.72	60	118.36	111.02	0.9
BS_12	0.021831	2886.69	2901.90		117.86		
BS_13	0.021752	2801.93	2818.88		100.60		
BS_14	0.021735	2738.05	2757.80		117.31		
BS_15	0.021767	2885.60	2900.11		86.06 (*)		
BS_16	0.021725	2798.30	2815.29		100.96		
BCL_11	0.021400	1727.15	1746.12	60	114.44	128.57	1.0
BCL_12	0.021441	1727.67	1752.20		114.22		
BCL_13	0.021585	1733.21	1757.73		146.65		
BCL_14	0.021364	1735.84	1757.76		132.46		
BCL_15	0.021431	1727.88	1748.36		123.37		
BCL_16	0.021440	1729.51	1752.81		140.30		

(*)This value was not counted for the average because it departed more than 25% from the mean value

2.3 Masonry characterisation tests

2.3.1 Characterisation and identification of specimens

For the two types of existing masonry (masonry consisting of calcium silicate blocks and masonry consisting of clay bricks), fourteen small walls were constructed, which are called *wallettes*, with six layers for calcium silicate blocks *wallets* with dimensions approximately 433 x 102 x 475 mm, and seven layers for clay brick wallets with dimensions of approximately 430 x 100 x 410 mm. This dimensions are according to the provisions of norm NP EN 1052-1 (2002). Thirty-six specimens with three blocks, which were designated as *triplets*, were dimensioned with approximately 236 x 212 x 101 mm for the calcium silicate *triplets* and 170 x 210 x 100 mm for the clay *triplets*. Figure 2.41 shows the two *wallettes* and *triplets* types that were constructed for the tests.

52 Collapse Shaking Table Test on URM Cavity Wall Structure representative of a Dutch Terraced House



Calcium silicate *wallettes* (WS)



Clay *wallettes* (WCL)



Calcium silicate *triplets* (TS e BWS)



Clay *triplets* (TCL e BWCL)

Figure 2.41 Types of masonry specimens (wallettes and triplets) built for testing.

The construction of the specimens for the characterisation tests (*wallettes* and *triplets*) took place in February 2017 during the construction of the full-scale model and was carried out by construction professionals from the Netherlands, as shown in Figure 2.42.



Wallettes



Triplets

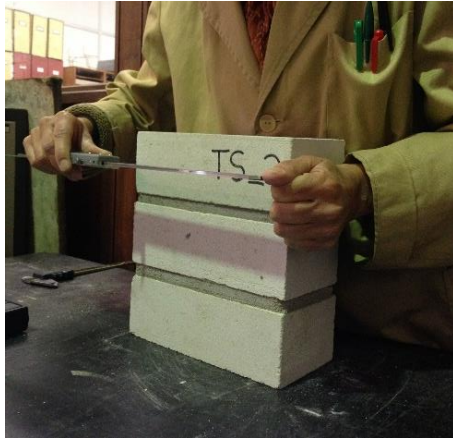
Figure 2.42 Construction of wallettes and triplets.

The designation of the specimens is in accordance with the following descriptions:
WS – Calcium silicate *wallettes* for the compression strength tests;
WCL – Clay *wallettes* for the compression strength tests;
TS – Calcium silicate *triplets* for the shear strength tests;
TCL – Clay *triplets* for the shear strength tests;
BWS – Calcium silicate *triplets* for the bond strength tests;
BWCL – Clay *triplets* for the bond strength tests.

The selected tests for these specimens were:

- Compression strength tests (W##);
- Shear strength tests (T##);
- Bond wrench tests (BW##).

All of the specimens were measured with a caliper and weighed on a digital weighing-machine, as shown in Figure 2.43.



Wallettes



Triplets

Figure 2.43 Example of characterisation (measure and weight) of all specimens.

Figure 2.44 presents a schematic view with the various parameters measured in the test specimens, while in Table 2.16 the dimensions and mass of the two types of *wallettes* constructed for the compression strength tests are summarised, with additional details provided in Annex IV.

Table 2.16 Dimensions and masses of the two types of *wallettes* constructed for the compression strength tests.

Specimen	Average Length [mm]	Average Width [mm]	Average Height [mm]	Average Mass [kg]
WS	433.7	102.8	474.9	38.119
WCL	430.0	100.5	410.4	32.631

54 Collapse Shaking Table Test on URM Cavity Wall Structure representative of a Dutch Terraced House

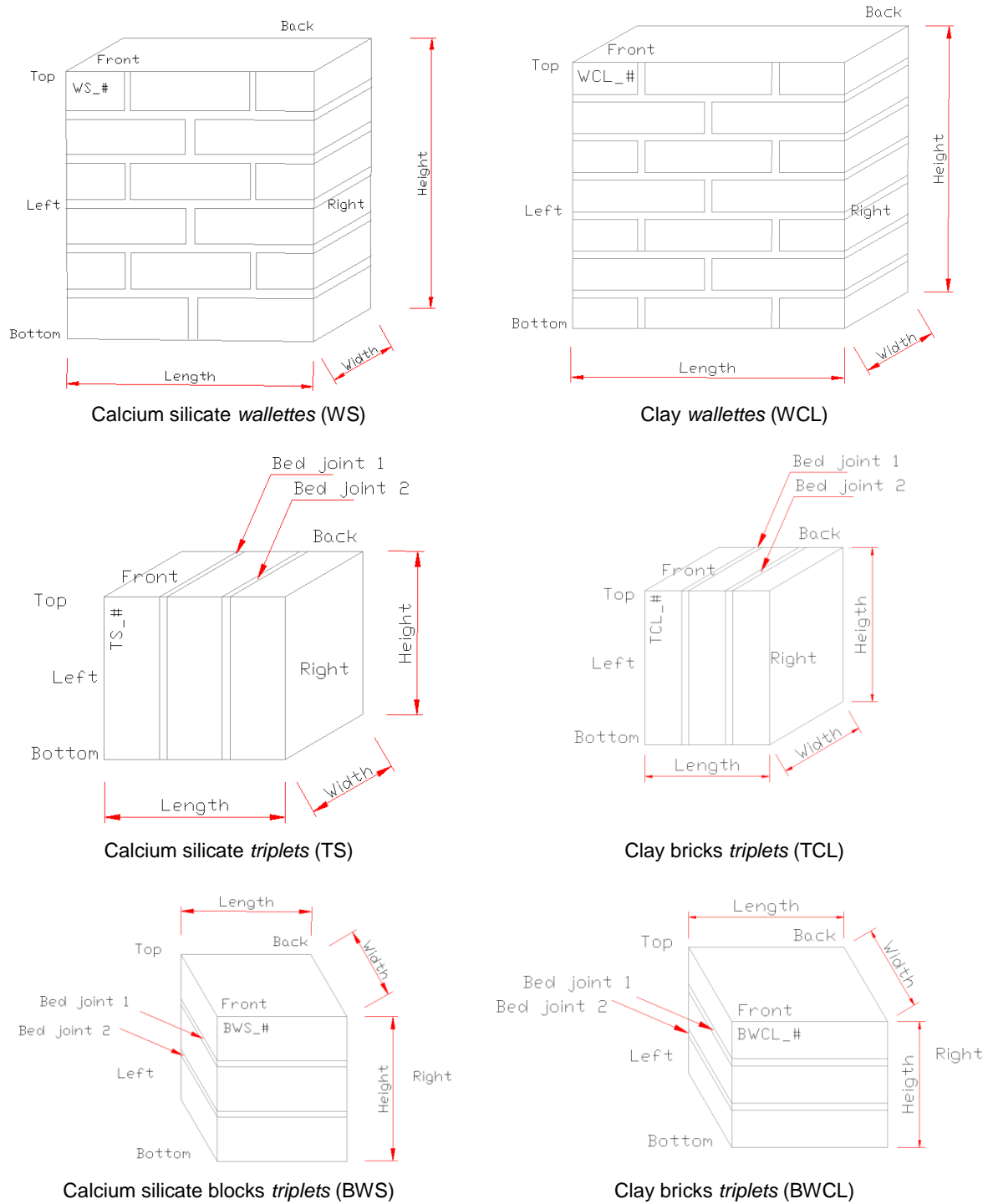


Figure 2.44 Schematic with the identification of the parameters measured in the various specimens.

In Table 2.17, the dimensions and masses of the two types of *triplets* built for the shear strength tests are presented, while in Table 2.18, the dimensions and masses of the two types of *triplets* built for the bond strength tests are shown. Additional details are provided in Annex IV.

Table 2.17 Dimensions and masses of calcium silicate and clay triplets for the shear strength tests.

Specimen	Average Height [mm]	Average Width [mm]	Average Length [mm]	Average Mass [kg]
TS	212.7	102.8	235.1	9.406
TCL	210.3	100.8	171.3	6.635

Table 2.18 Dimensions and masses of the two types of wallettes built for the bond wrench tests.

Specimen	Average Height [mm]	Average Width [mm]	Average Length [mm]	Average Mass [kg]
BWS	236.08	102.33	213.33	9.376
BWCL	172.86	100.49	210.49	6.565

The bulk density values for the calcium silicate block and clay brick *wallettes* and *triplets* are summarised in Table 2.19, with additional results presented in Annex IV.

Table 2.19 Summary of the results of the bulk density for the two types of specimens.

Specimen type	Bulk density		
	Average [kg/m ³]	Standard deviation [kg/m ³]	Coefficient of variation [-]
Calcium silicate <i>wallettes</i> and <i>triplets</i>	1819.02	21.17	0.01
Clay <i>wallettes</i> and <i>triplets</i>	1813.60	21.22	0.01

2.3.2 Test for the determination of compressive strength

The test to determine the compressive strength was performed according to an adaptation of the standard method described in the portuguese standard NP EN 1052-1 (2002). The principle of this test is the determination of the compressive strength of masonry specimens and possible determination of the respective modulus of elasticity and *Poisson* coefficient.

This test was carried out in the abovementioned *wallettes*. Due to the small irregularities of the lower and upper faces of the specimens (areas that would be in contact with the plates of the press), these faces were regularised with a thin layer of gypsum, as shown in Figure 2.45. After this regularisation a very fine layer of gypsum is placed on both sides already with the specimen on top of the testing machine, which are leveled by the plates of the press, as shown in Figure 2.46.

56 Collapse Shaking Table Test on URM Cavity Wall Structure representative of a Dutch Terraced House



Preparation



After being regularised



Verification of the adjustments of *wallettes* faces



Figure 2.45 Regularisation of the *wallettes* faces.



Figure 2.46 Final regularisation of the *wallettes* faces on top of the testing machine.

Wallettes were not perfectly tiled at the time of construction, as shown in Figure 2.47



Figure 2.47 Lack of verticality in wallettes.

Subsequently, the specimens were instrumented with four displacement transducers on each face, as shown in Figure 2.48. The vertical displacement transducers are of type W20 (with a measuring range of ± 20 mm) and measure strains for the determination of the modulus of elasticity (1,2,5 and 6) and two horizontal displacement transducers of type W10 (with a measuring range of ± 10 mm, since smaller deformations are expected) that measure deformations in the direction perpendicular to the force in order to provide an evaluation of *Poisson's* coefficient (3, 4, 7 and 8). The instrumentation was placed in the central area of the specimen so that the measurements are carried out in an area that is not affected by the boundary conditions, as illustrated in the schemes of Figure 2.49 and Figure 2.50 (the schematics with the instrumentation locations for all tested *wallettes* are shown in Annex IV). Additionally, two displacement transducers were placed that measure the deformation of the plates of the press so that the deformation of the specimen up to failure may be recorded. For example, Figure 2.51 and Figure 2.52 shows the instrumentation performed on each face of two types of *wallettes*. The displacement transducers and the testing machine were duly calibrated immediately prior to the start of the trials with the collaboration of the Metrological Quality Unit of the LNEC Scientific Instrumentation Centre.

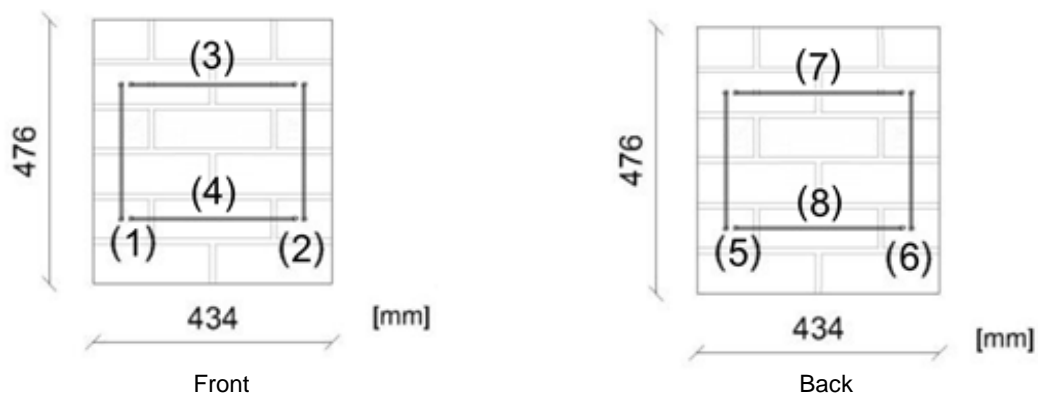


Figure 2.48 – Scheme and numbering of the transducers placed on each face of the two types of the wallettes.

58 Collapse Shaking Table Test on URM Cavity Wall Structure representative of a Dutch Terraced House

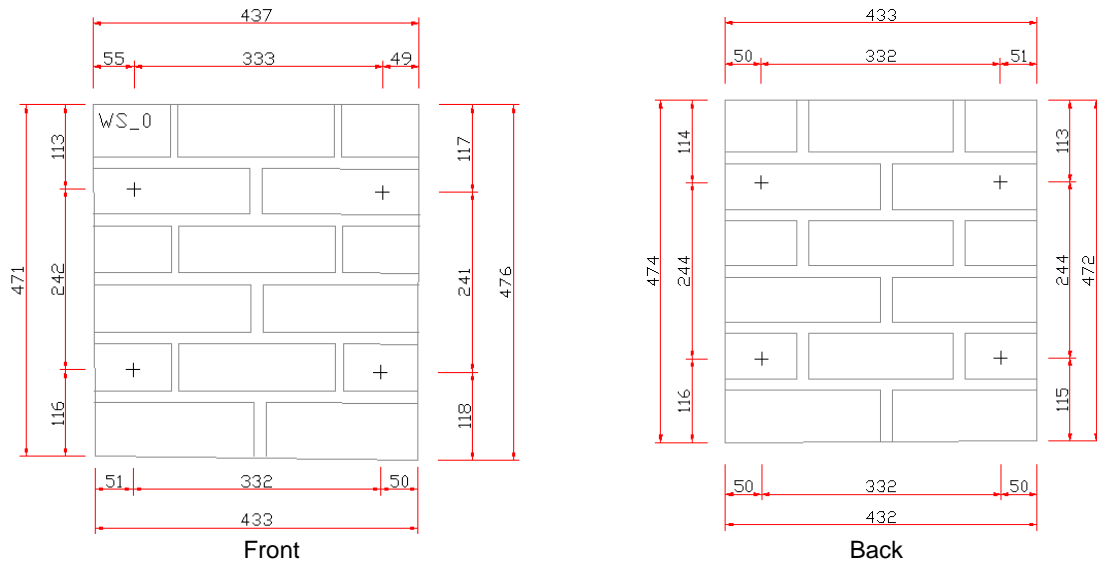


Figure 2.49 Scheme with the location of the transducers placed on each face of the calcium silicate wallettes.

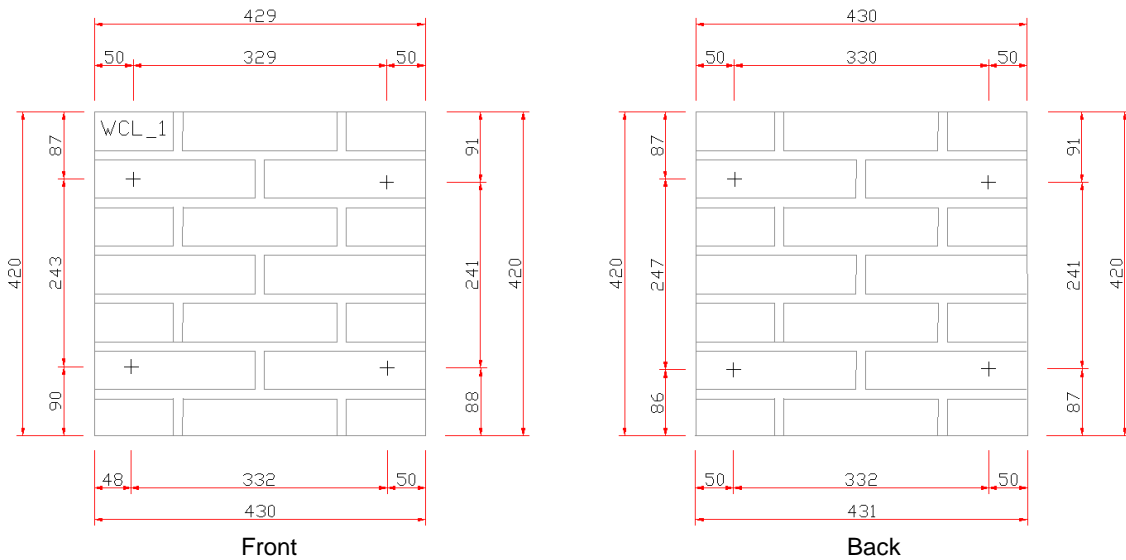


Figure 2.50 Scheme with the location of the transducers placed on each face of the clay wallettes.



Figure 2.51 Instrumentation placed on each face of the calcium silicate wallettes.

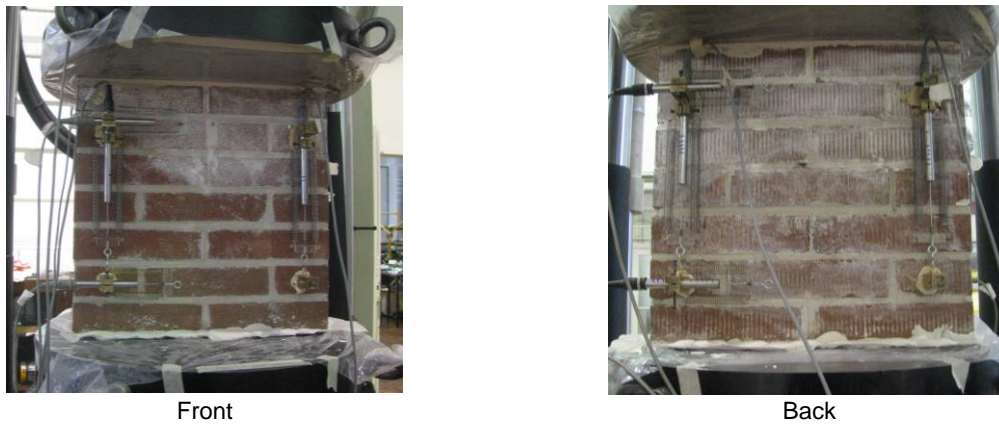


Figure 2.52 Instrumentation placed on each face of the clay wallettes.

The test procedure for the calcium silicate *wallettes* consists essentially in placing the specimen in the test machine for load application without shock, i.e. in a gradual way and at a controlled speed until the failure of the specimen. Several increasing cycles of loading and unloading were carried out, with increments of 74 kN and starting at 74 kN (at each load level three cycles were performed), as illustrated in the plot of Figure 2.53 which shows the force as a function of time. The test was performed on a machine with a capacity of 1000 kN, with a control in force and with a test speed of 1.1 kN/s. A sampling frequency of 5 Hz was used, each run lasting approximately 75 minutes. The load application was performed vertically to the specimen.

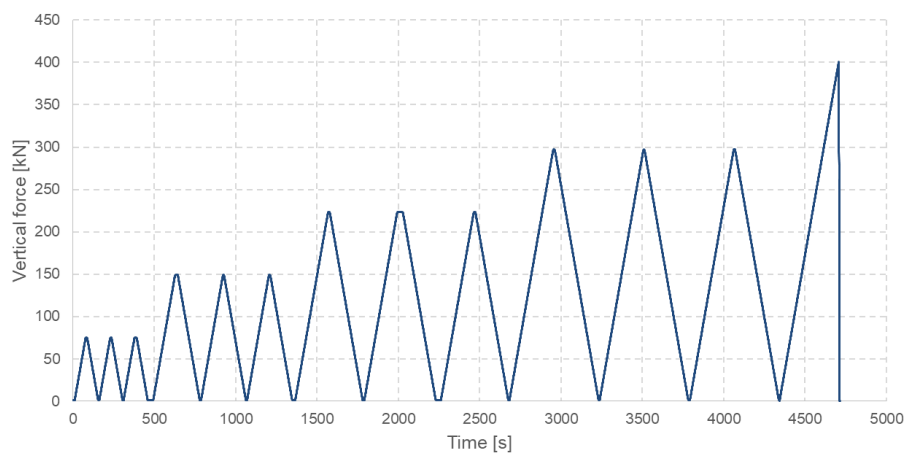


Figure 2.53 Application of force as a function of time applied to calcium silicate wallettes.

For the sake of safeguarding the equipment, the instrumentation was maintained up to the third load level, of 296 kN, and after the last cycle at this load level the final loading was started until the specimen failure. For this final loading, the deformation until failure was measured using the transducers installed in the press plate. The WS_0 *wallette* was used to evaluate the compressive strength of the test specimens in order to define the loading threshold from which the instrumentation should be removed.

Figure 2.54 and Figure 2.55 present two calcium silicate *wallettes* during the test and after their failure, while in Annex V the figures with the obtained fractures are presented for all specimens.

60 Collapse Shaking Table Test on URM Cavity Wall Structure representative of a Dutch Terraced House



Figure 2.54 Calcium silicate block walette (WS_1) during the test and after failure.



Figure 2.55 Calcium silicate block walette (WS_2) during the test and after failure.

The results of the compressive strength obtained in the calcium silicate *wallettes* are summarised in Table 2.20. In order to determine the modulus of elasticity of the *wallettes*, the average of the vertical deformations recorded by the displacement transducers 1, 2, 5 and 6 was computed and the modulus of elasticity (E_1), given by the secant line from the origin up to 33% of the failure load, was derived.

Table 2.20 Summary of the compressive strength for the calcium silicate *wallettes*.

Specimen	Date of test	Average gross area [mm ²]	Maximum force [kN]	Compressive strength [MPa]
WS_1	15/05/2017	44424	402.80	9.07
WS_2	16/05/2017	44635	462.76	10.37
WS_3	18/05/2017	45096	490.16	10.87
WS_4	19/05/2017	44667	420.52	9.41
WS_5	19/05/2017	44590	378.76	8.49
WS_6	22/05/2017	44611	471.24	10.56
Average		44670	437.71	9.80
Standard deviation		225	43.57	0.94
Coefficient of variation [-]		0.01	0.10	0.10

Figure 2.56 to Figure 2.60 shows the plots that relate the vertical and horizontal deformations to the vertical load measured for each specimen.

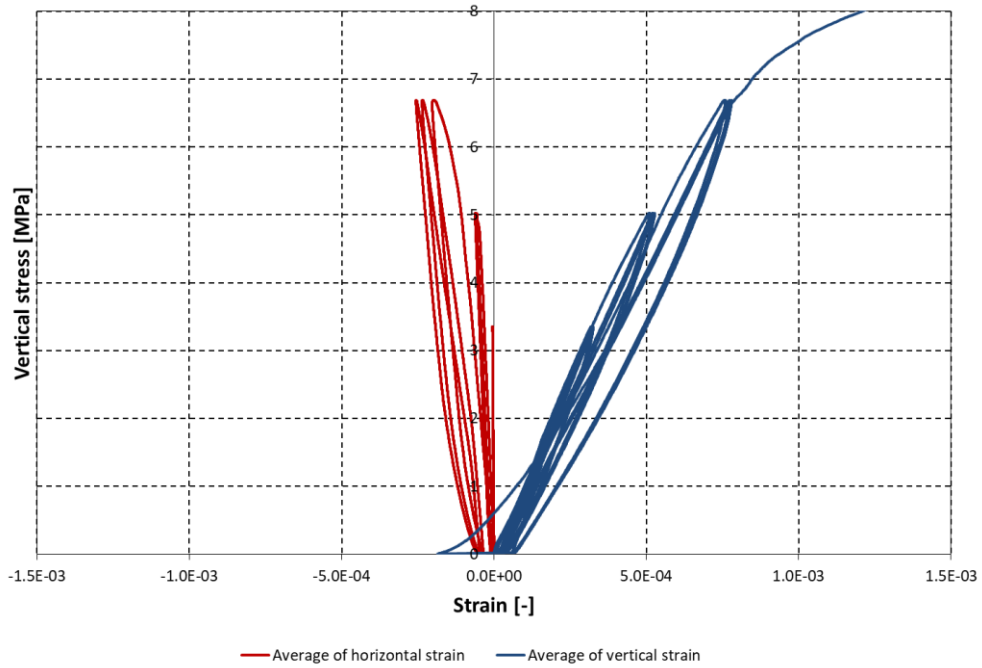


Figure 2.56 Vertical stress vs. vertical and horizontal strains for wallette WS_1.

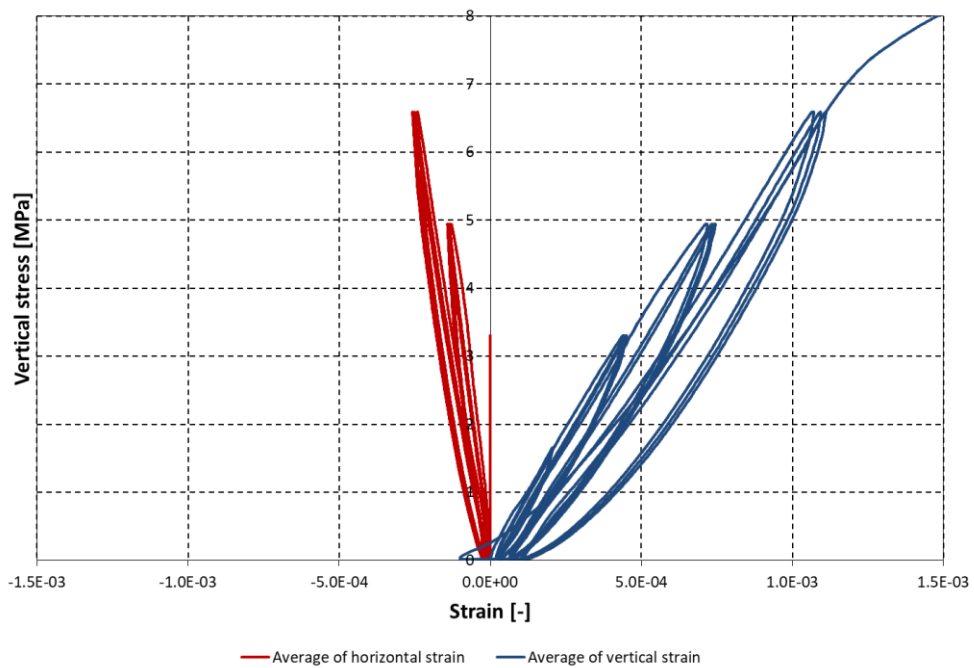


Figure 2.57 Vertical stress vs. vertical and horizontal strains for wallette WS_3.

62 Collapse Shaking Table Test on URM Cavity Wall Structure representative of a Dutch Terraced House

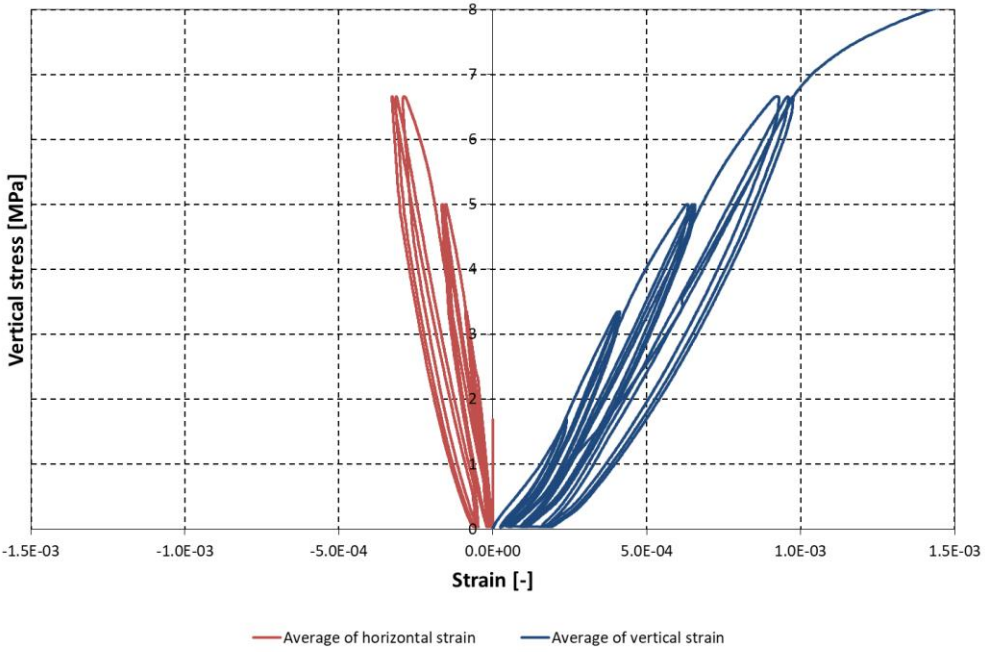


Figure 2.58 Vertical stress vs. vertical and horizontal strains for wallette WS_4.

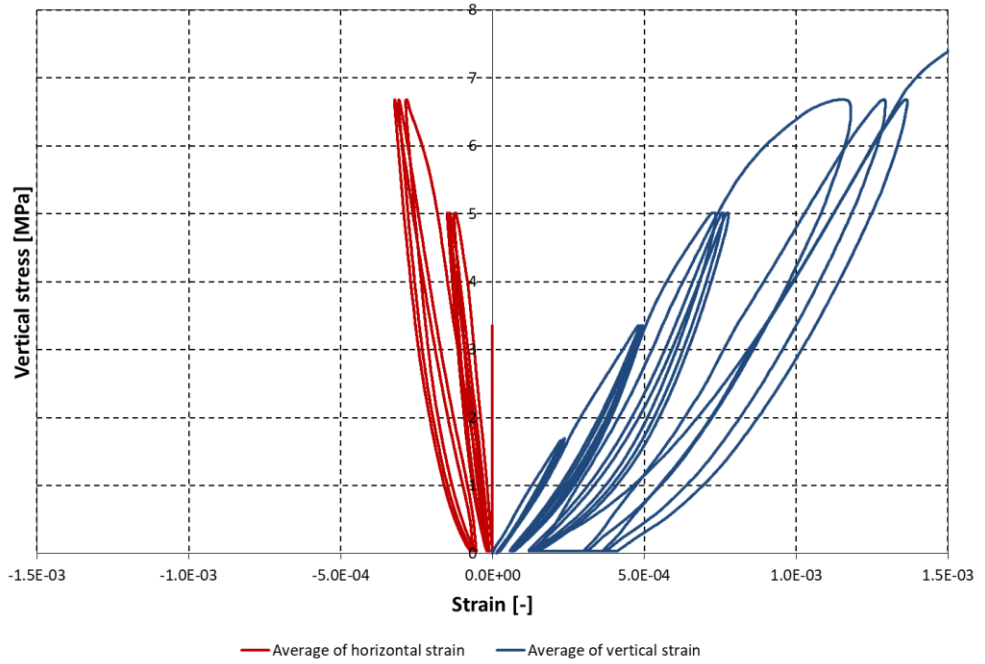


Figure 2.59 Vertical stress vs. vertical and horizontal strains for wallette WS_5.

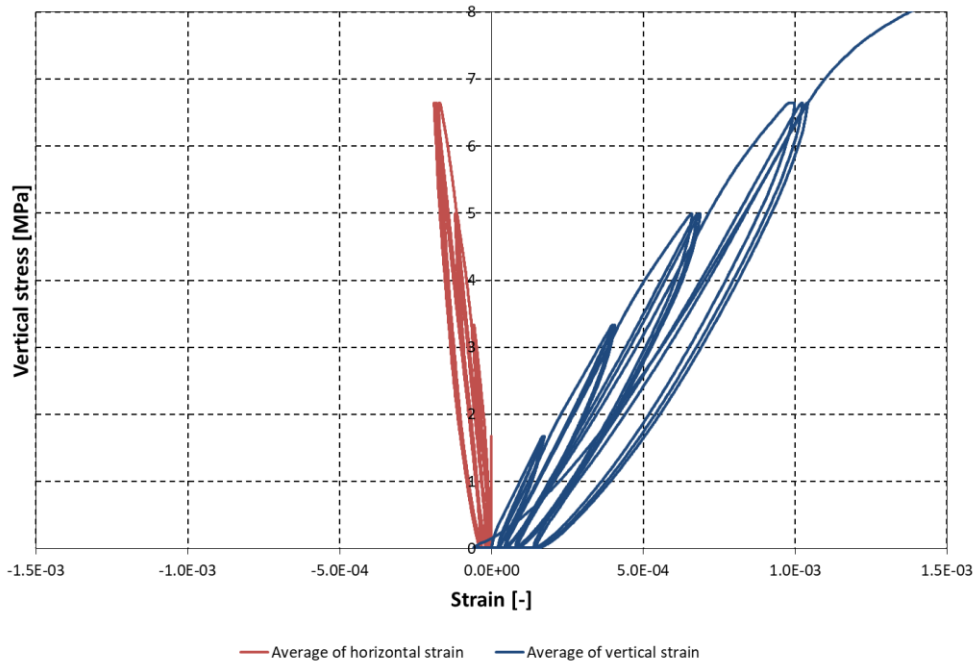


Figure 2.60 Vertical stress vs. vertical and horizontal strains for wallette WS_6.

Figure 2.61 to Figure 2.66 show the plots relating the vertical stress with the vertical strain measured for the CS wallettes, as well as the corresponding modulus of elasticity.

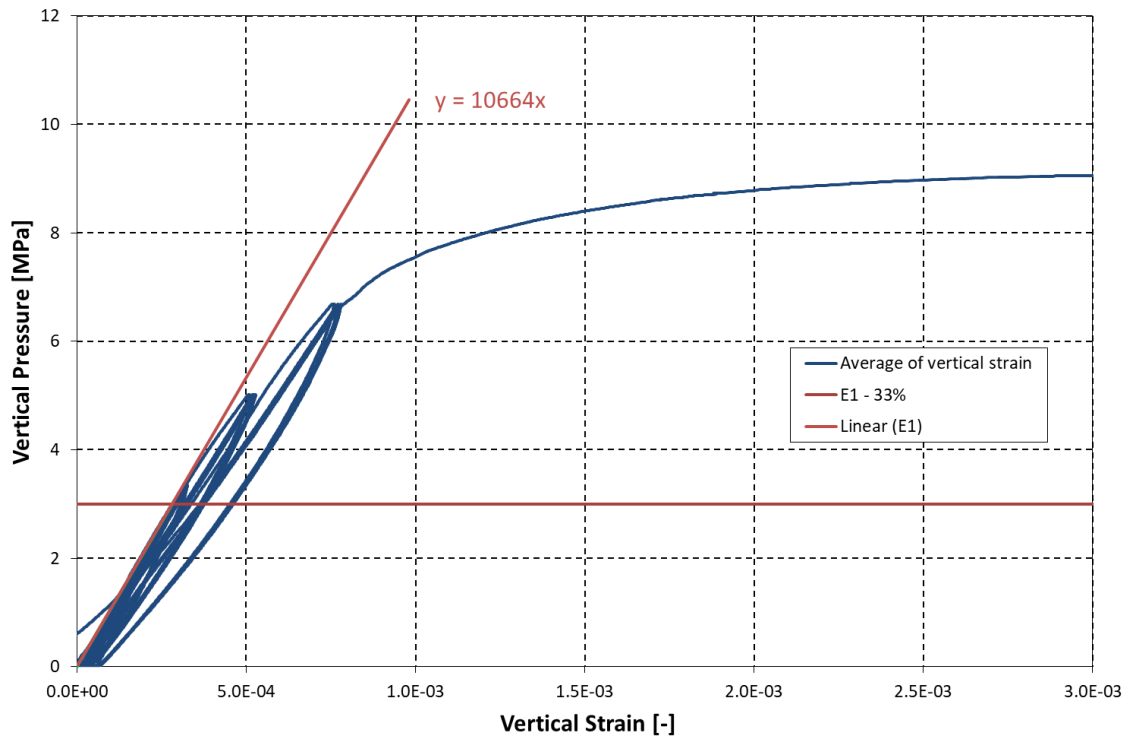


Figure 2.61 Vertical stress vs. vertical strain and determination of the modulus of elasticity for wallette WS_1.

64 Collapse Shaking Table Test on URM Cavity Wall Structure representative of a Dutch Terraced House

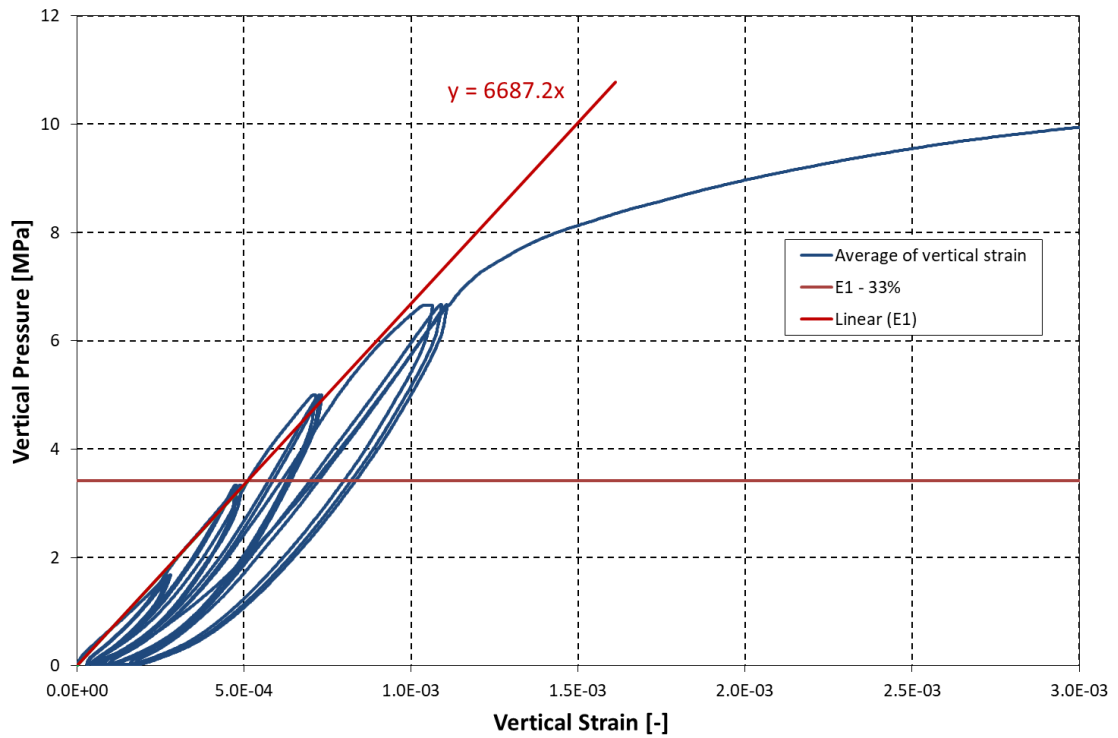


Figure 2.62 Vertical stress vs. vertical strain and determination of the modulus of elasticity for wallette WS_2.

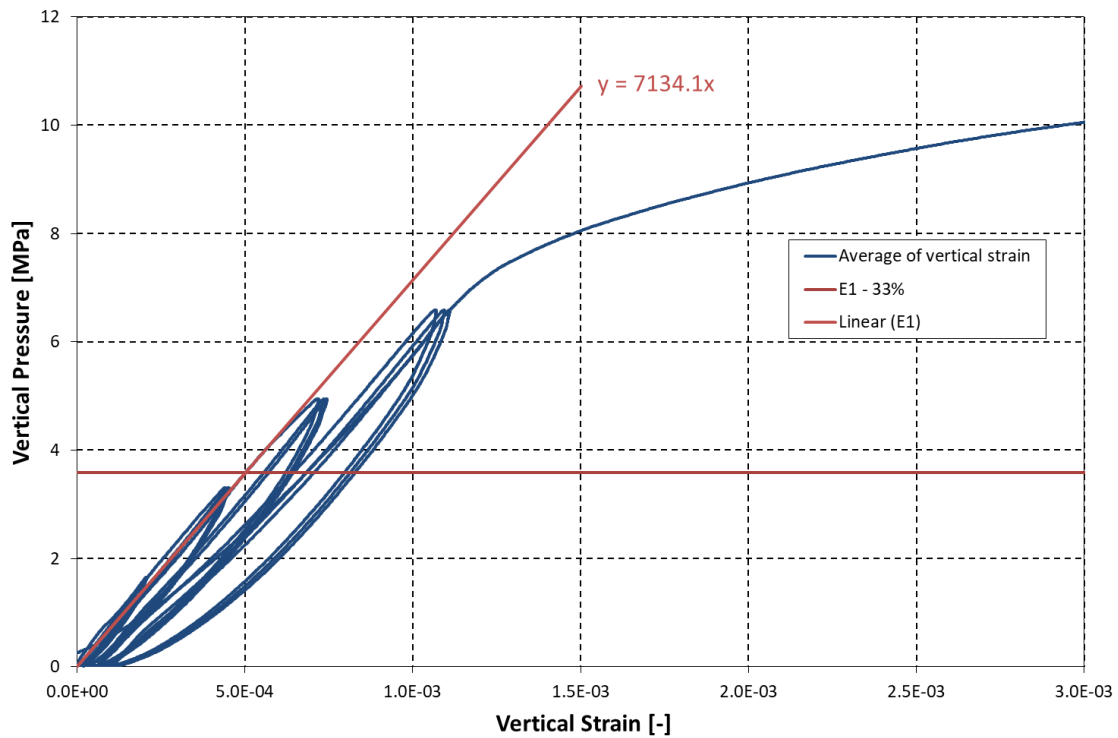


Figure 2.63 Vertical stress vs. vertical strain and determination of the modulus of elasticity for wallette WS_3.

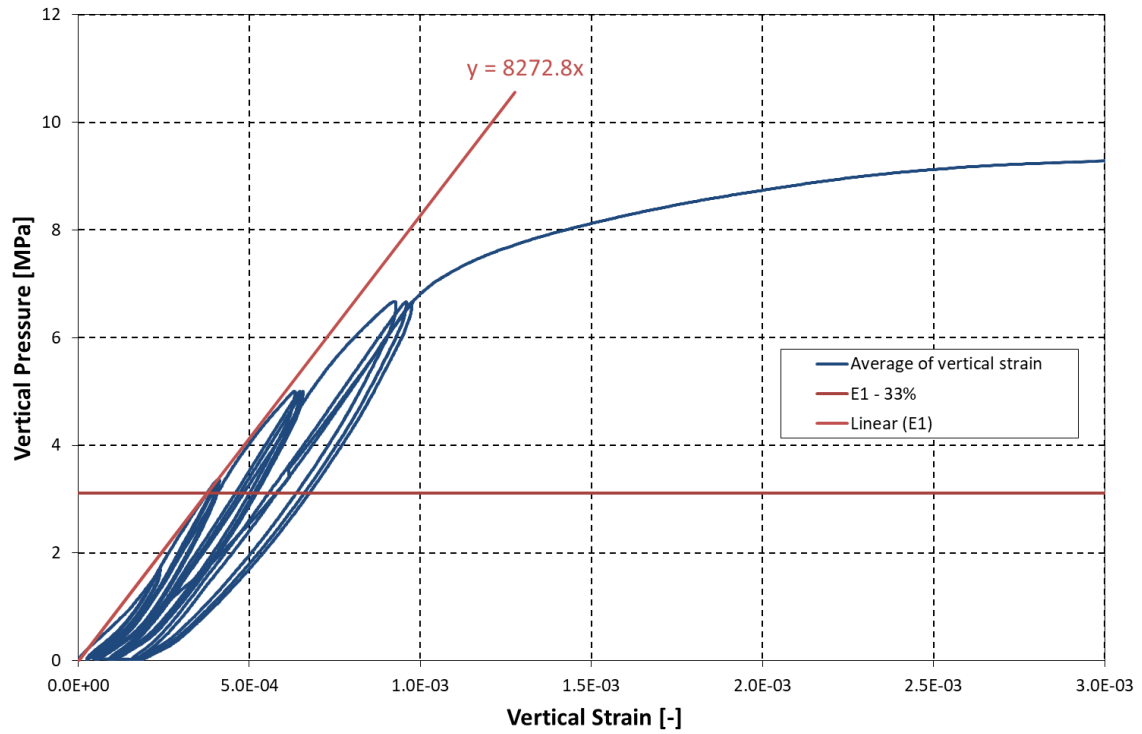


Figure 2.64 Vertical stress vs. vertical strain and determination of the modulus of elasticity for wallette WS_4.

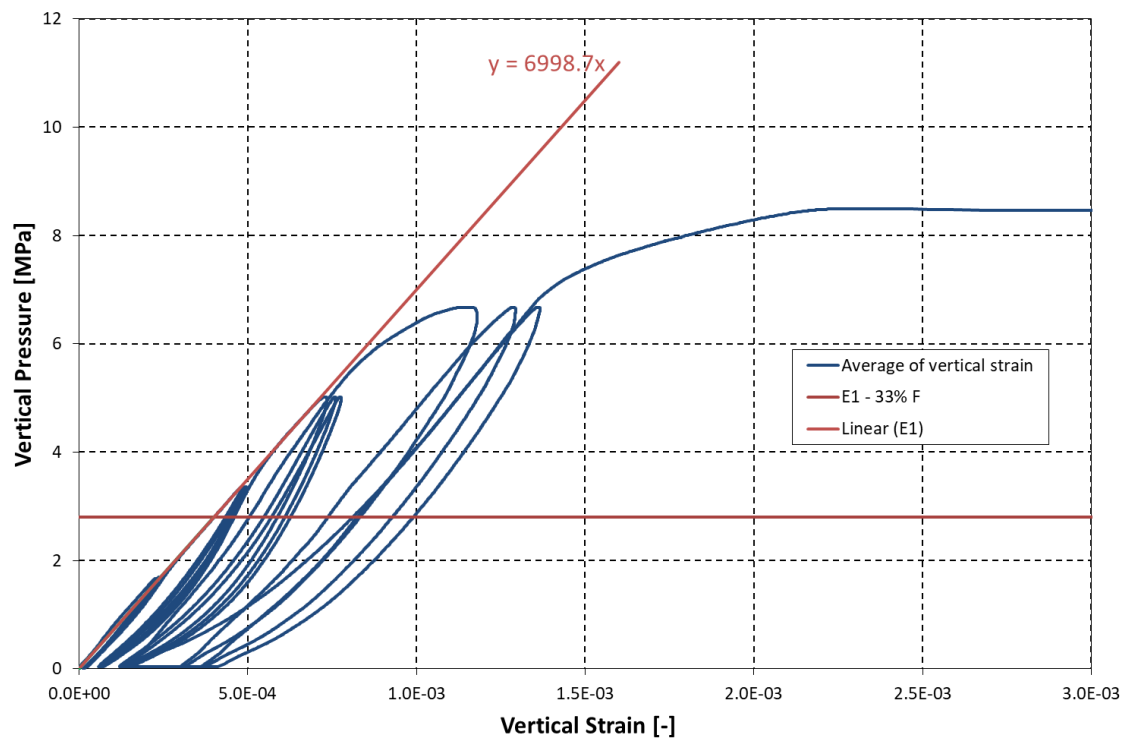


Figure 2.65 Vertical stress vs. vertical strain and determination of the modulus of elasticity for wallette WS_5.

66 Collapse Shaking Table Test on URM Cavity Wall Structure representative of a Dutch Terraced House

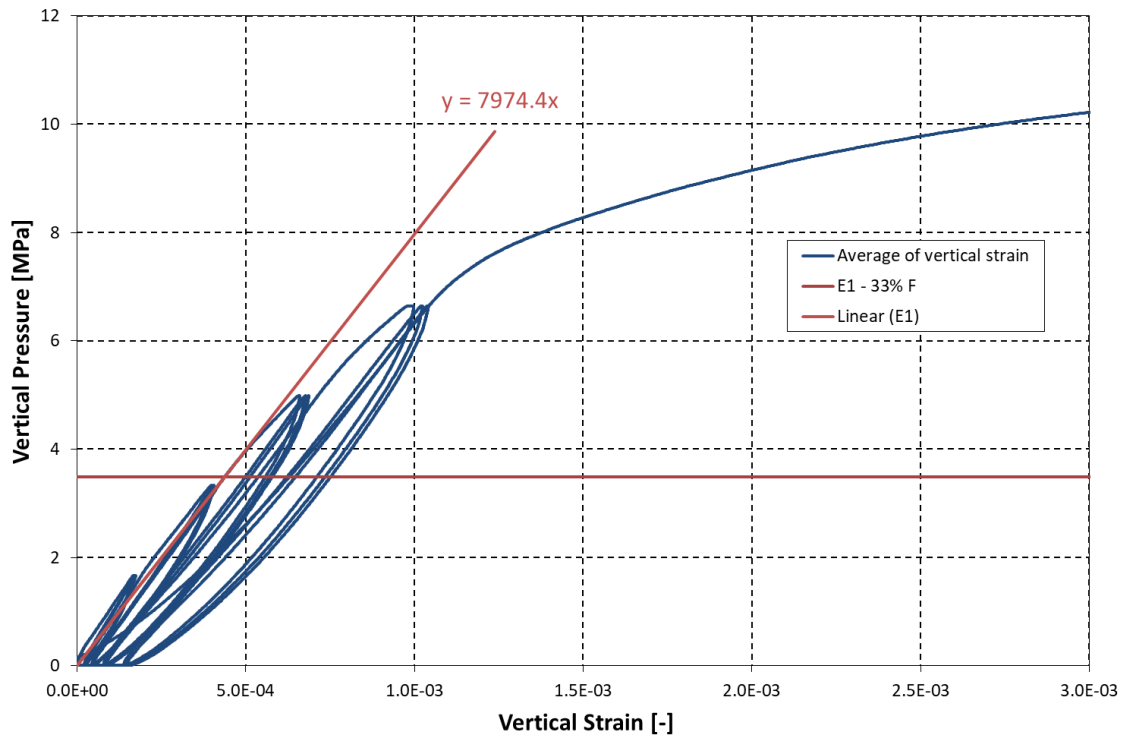


Figure 2.66 Vertical stress vs. vertical strain and determination of the modulus of elasticity for walette WS_6.

The results obtained for the modulus of elasticity E_1 for each walette are summarised in Table 2.21 for the calcium silicate walleets, while Figure 2.67 shows the distribution of moduli of elasticity obtained for the calcium silicate walleets.

Table 2.21 Summary of the modulus of elasticity for calcium silicate walleets.

Specimen	Compression strength [MPa]	E_1 (33% F_{max}) [MPa]
WS_1	9.07	10664
WS_2	10.37	6687
WS_3	10.87	7134
WS_4	9.41	8273
WS_5	8.49	6999
WS_6	10.56	7974
Average [MPa]	9.80	7955
Standard deviation [MPa]	0.94	1458
Coefficient of variation [-]	0.10	0.18

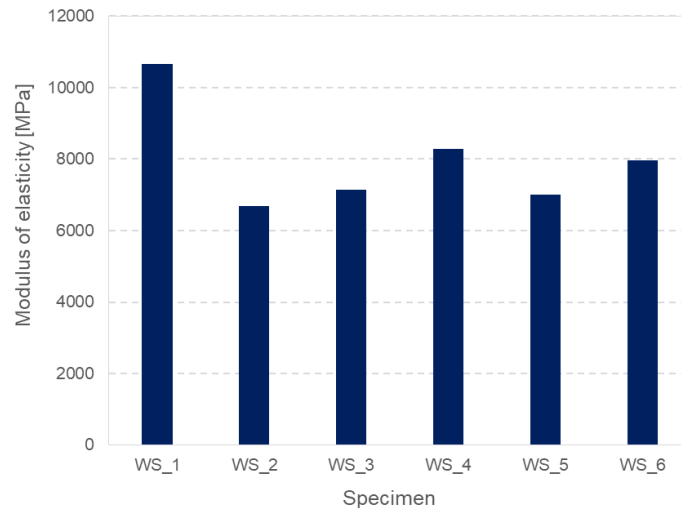


Figure 2.67 Distribution of moduli of elasticity obtained for calcium silicate wallettes.

For clay *wallettes* several increasing cycles of loading and unloading were carried out, with increments of 175 kN and starting at 175 kN (at each load level three cycles were performed), as illustrated in the plot of Figure 2.68 which shows the force as a function of time. The test was again performed on a machine with a capacity of 1000 kN, with a control in force in the cycles up to 500 kN of load level and in displacement-control for cycles reaching load levels above 500 kN. The test speed while in force control was of 3.5 kN/s and while in displacement control was of 0.01 mm/s. A sampling frequency of 5 Hz was used, each run lasting approximately 60 minutes. The load application was performed vertically to the specimen.

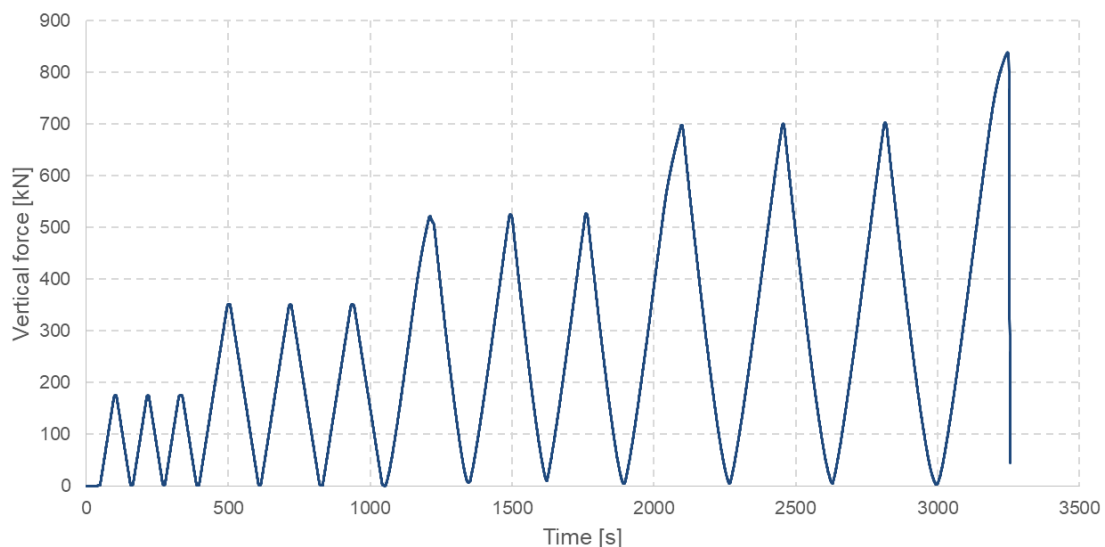


Figure 2.68 Application of force as a function of time applied to clay wallettes.

Figure 2.69 presents a clay *wallette* during the test and after its failure. In Annex V the figures with the obtained fractures are presented for all specimens.

68 Collapse Shaking Table Test on URM Cavity Wall Structure representative of a Dutch Terraced House

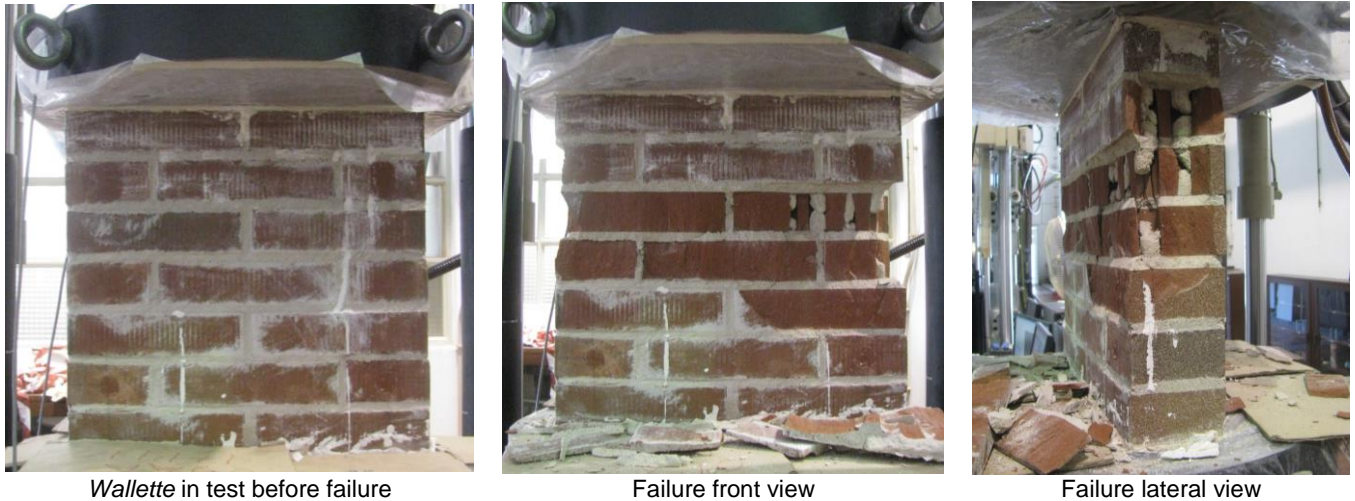


Figure 2.69 Clay brick walette (WCL_6) subjected to test and after failure.

The results of the compressive strength obtained for the clay *wallettes* are summarised in Table 2.22. Figure 2.70 to Figure 2.75 shows the plots that relate the vertical and horizontal deformations to the vertical load measured for each specimen.

Table 2.22 Summary of the compressive strength for the clay *wallettes*.

Specimen	Date of test	Average gross area [mm ²]	Maximum force [kN]	Compressive strength [MPa]
WCL_1	29-06-2017	43429	913.90	21.04
WCL_2	04-07-2017	42726	777.30	18.19
WCL_3	21-07-2017	43073	823.60	19.12
WCL_4	20-07-2017	43586	804.50	18.46
WCL_5	30-06-2017	43530	827.80	19.02
WCL_6	04-07-2017	43431	838.80	19.31
Average		43296	830.69	19.19
Standard deviation		331	45.95	1.00
Coefficient of variation [-]		0.01	0.06	0.05

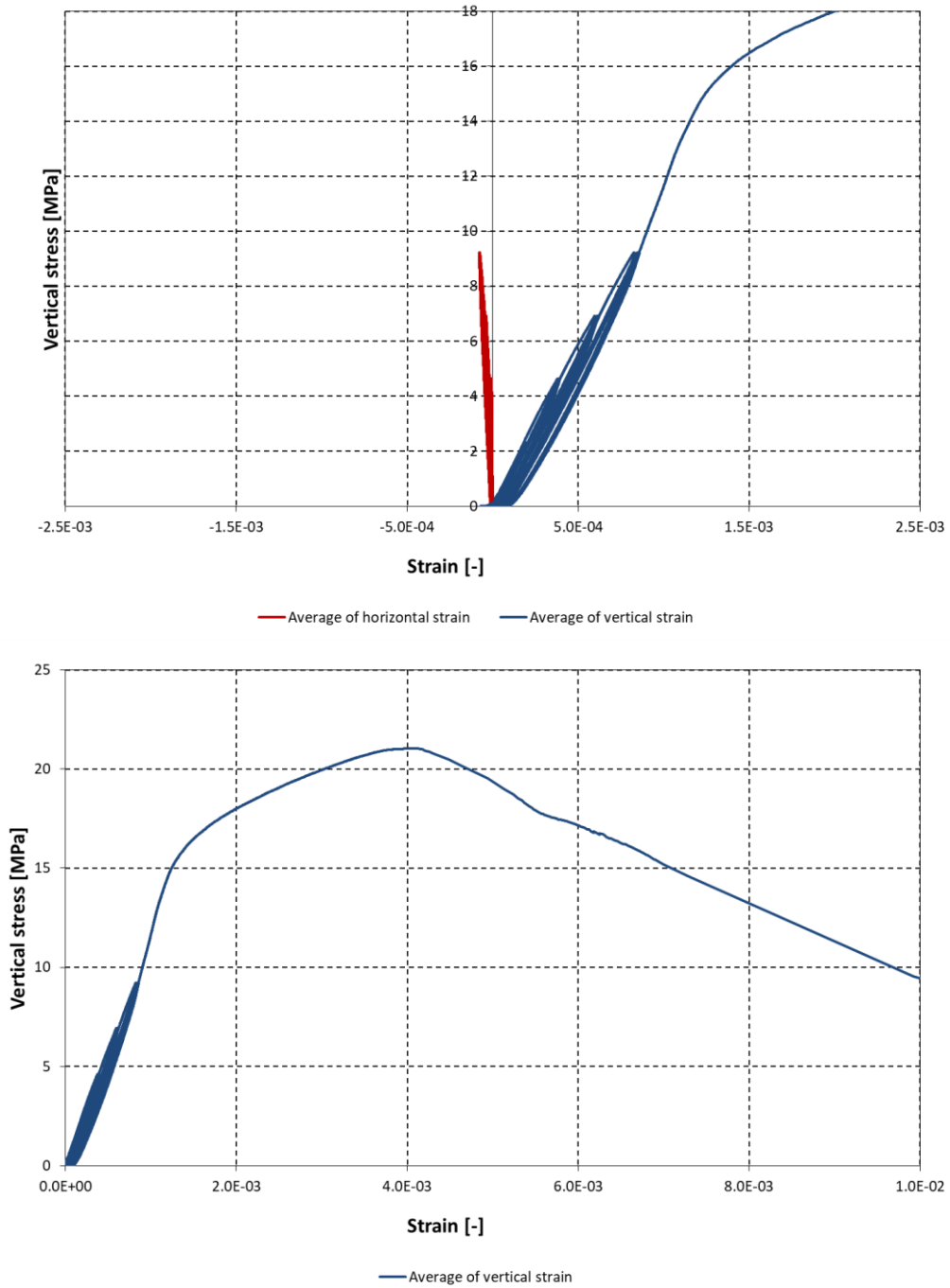


Figure 2.70 Vertical stress vs. vertical and horizontal strains for wallette WCL_1.

70 Collapse Shaking Table Test on URM Cavity Wall Structure representative of a Dutch Terraced House

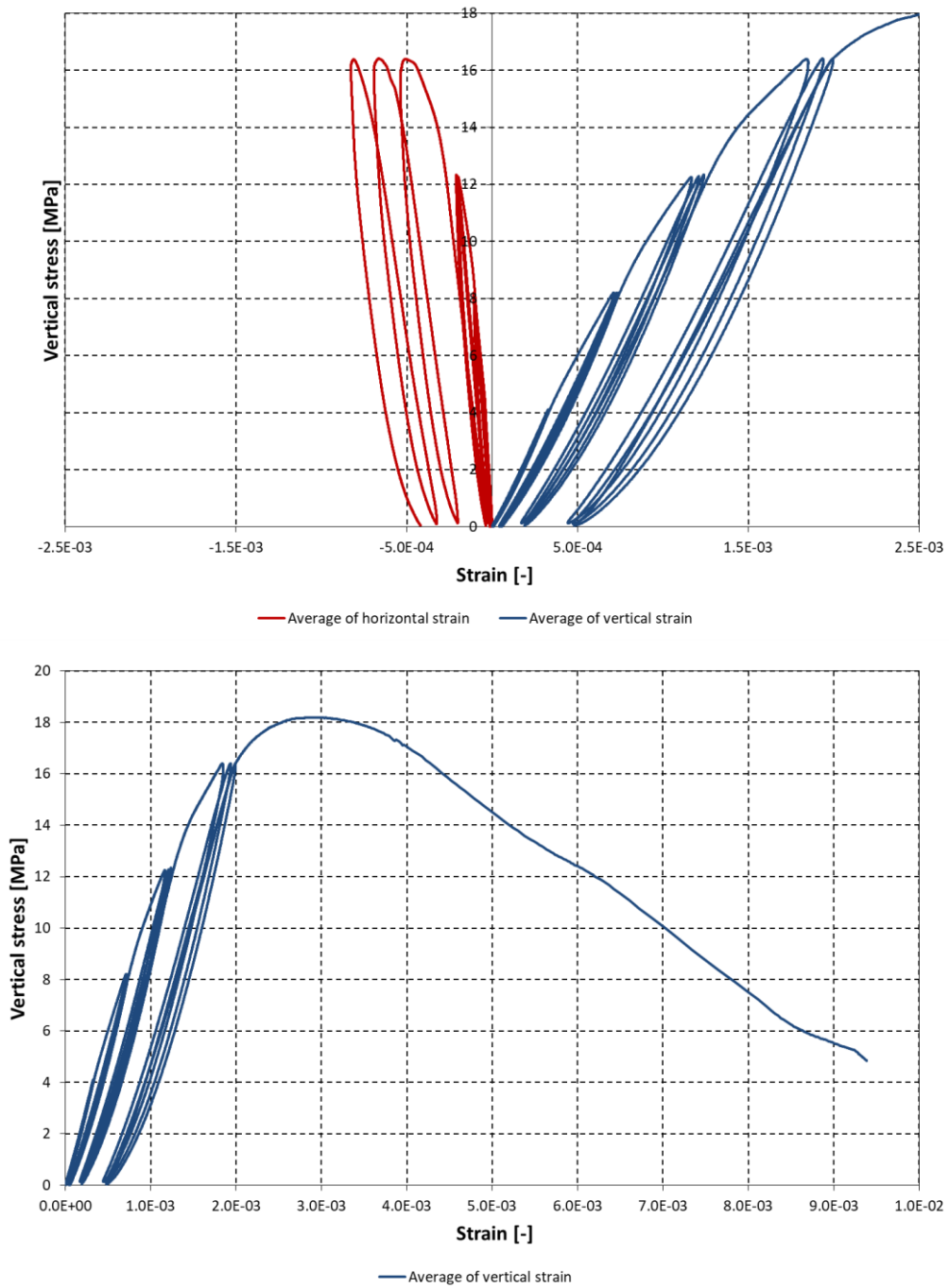


Figure 2.71 Vertical stress vs. vertical and horizontal strains for walette WCL_2.

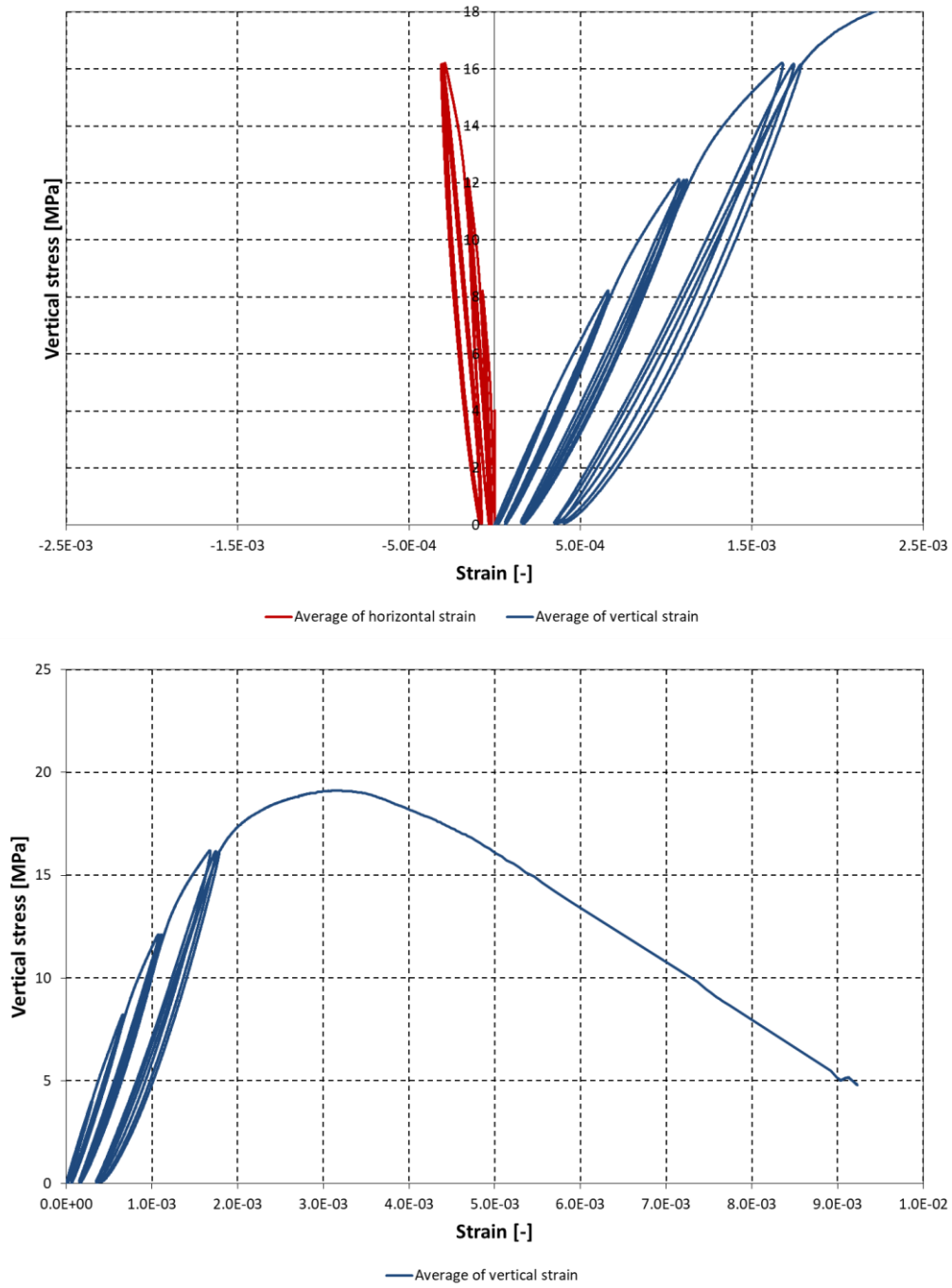


Figure 2.72 Vertical stress vs. vertical and horizontal strains for wallette WCL_3.

72 Collapse Shaking Table Test on URM Cavity Wall Structure representative of a Dutch Terraced House

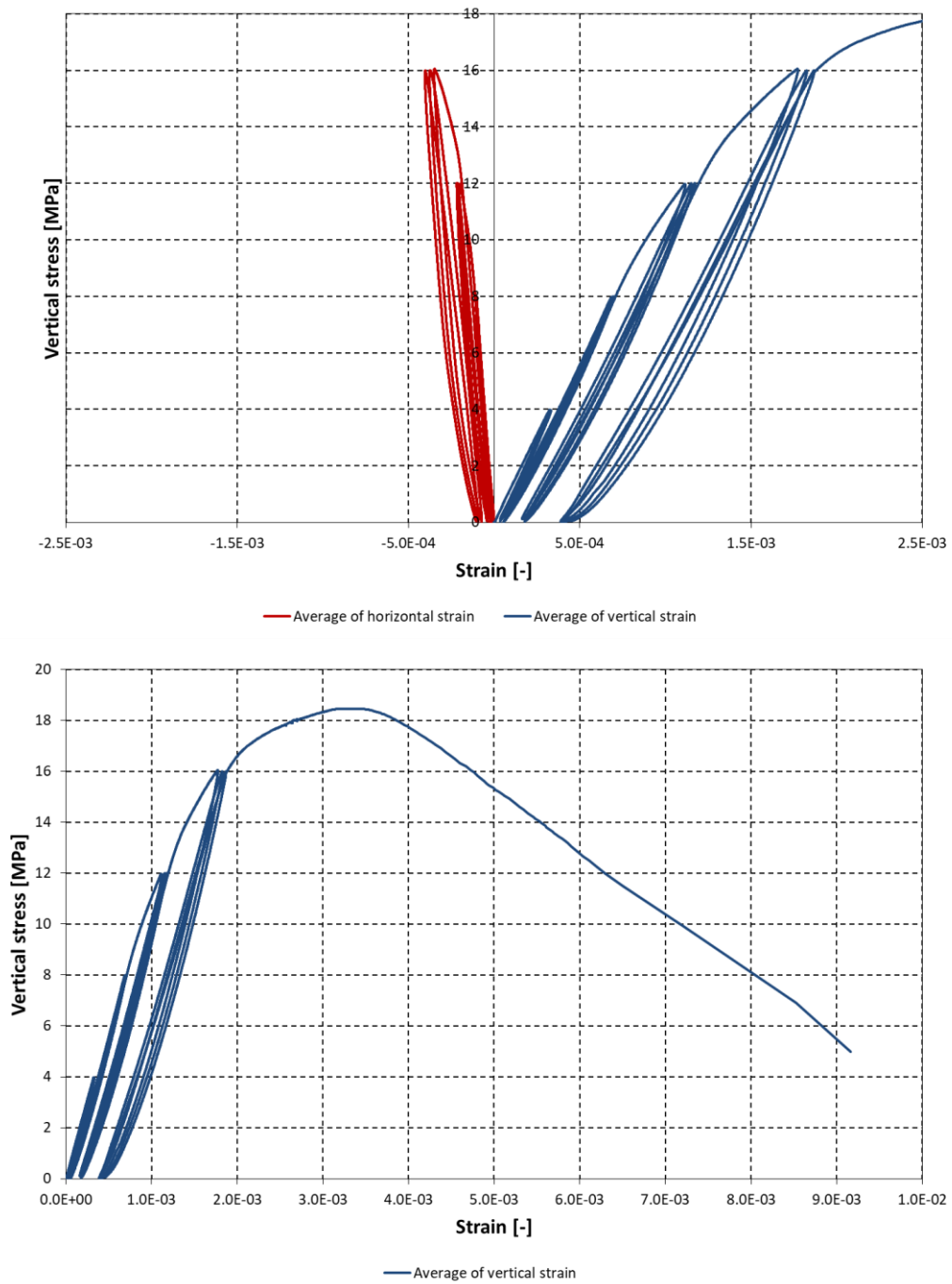


Figure 2.73 Vertical stress vs. vertical and horizontal strains for wallette WCL_4.

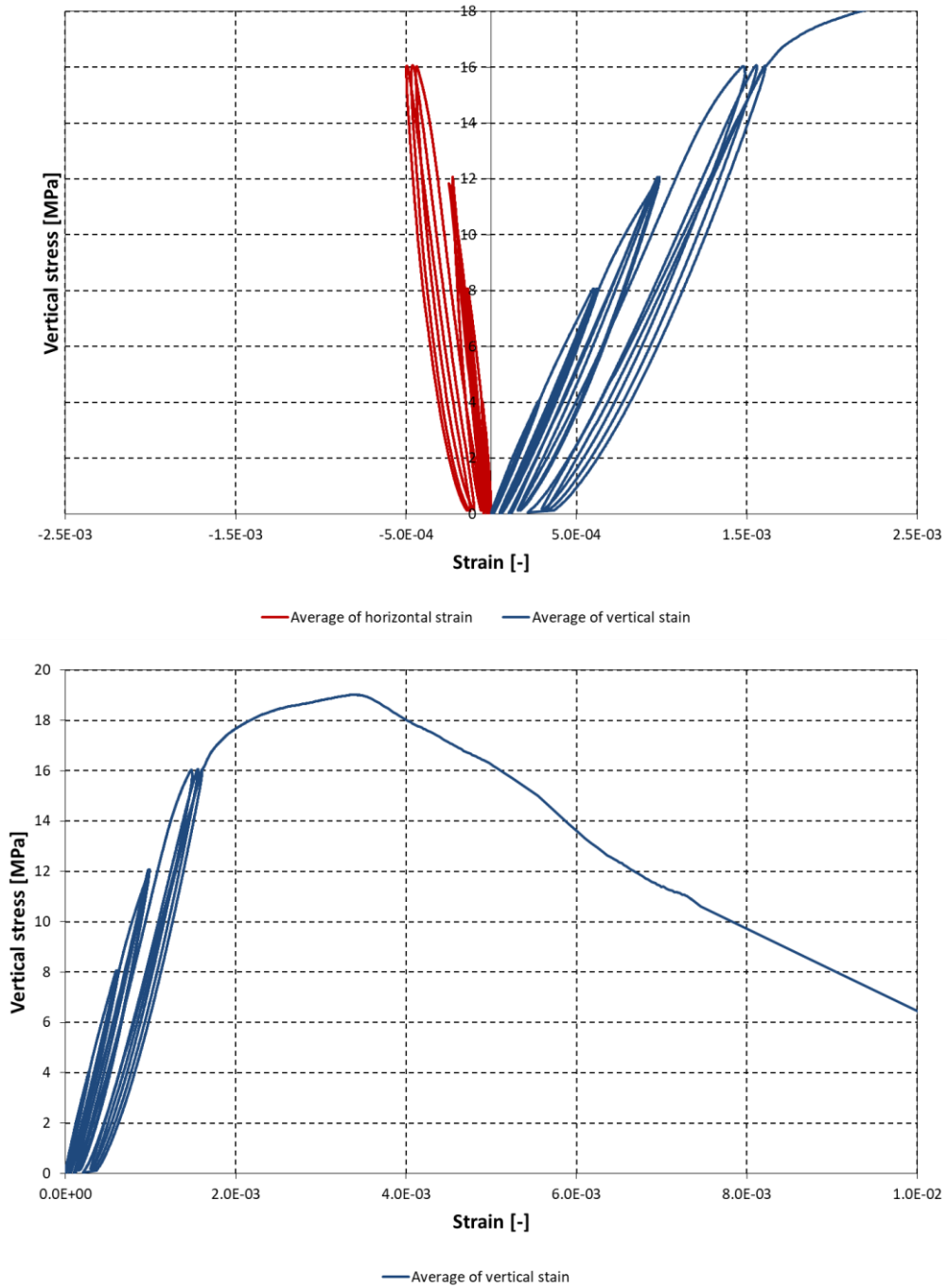


Figure 2.74 Vertical stress vs. vertical and horizontal strains for wallette WCL_5.

74 Collapse Shaking Table Test on URM Cavity Wall Structure representative of a Dutch Terraced House

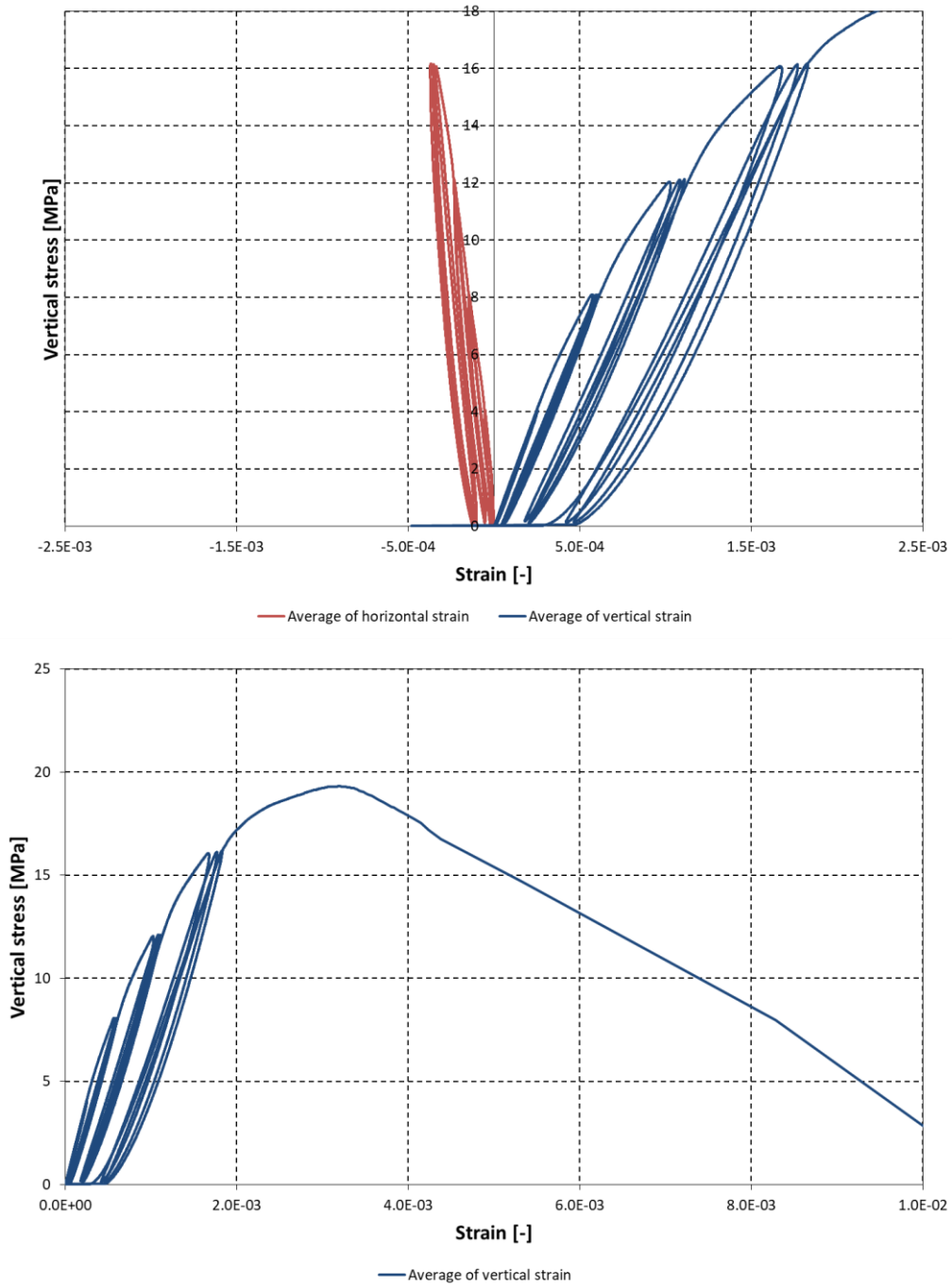


Figure 2.75 Vertical stress vs. vertical and horizontal strains for wallette WCL_6.

Figure 2.76 to Figure 2.81 show the plots relating the vertical stress with the vertical strain measured for the clay *wallettes*, as well as the corresponding modulus of elasticity.

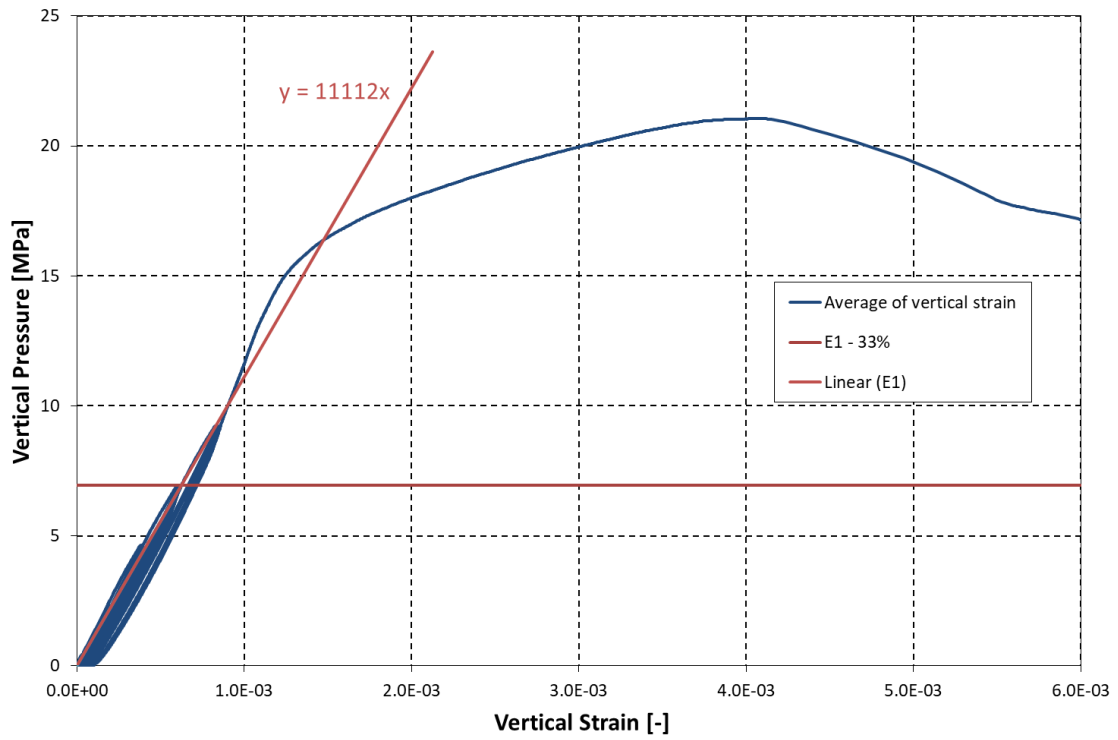


Figure 2.76 Vertical stress vs. vertical strain and determination of the modulus of elasticity for wallette WCL_1.

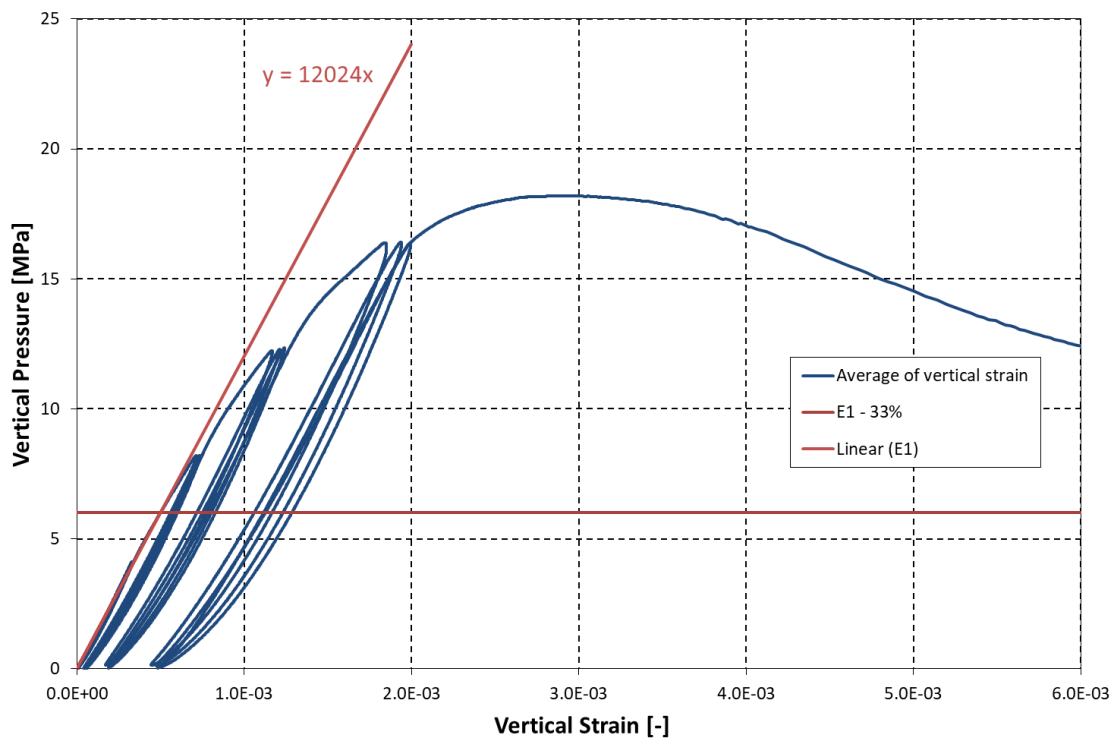


Figure 2.77 Vertical stress vs. vertical strain and determination of the modulus of elasticity for wallette WCL_2.

76 Collapse Shaking Table Test on URM Cavity Wall Structure representative of a Dutch Terraced House

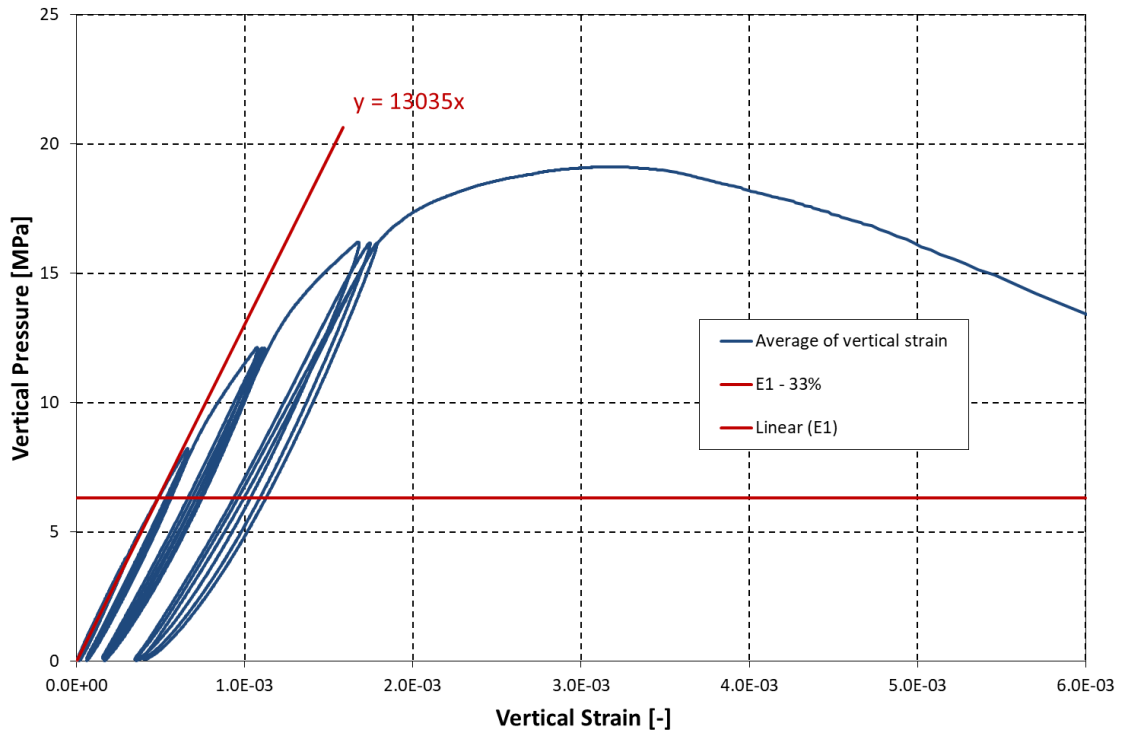


Figure 2.78 Vertical stress vs. vertical strain and determination of the modulus of elasticity for wallette WCL_3.

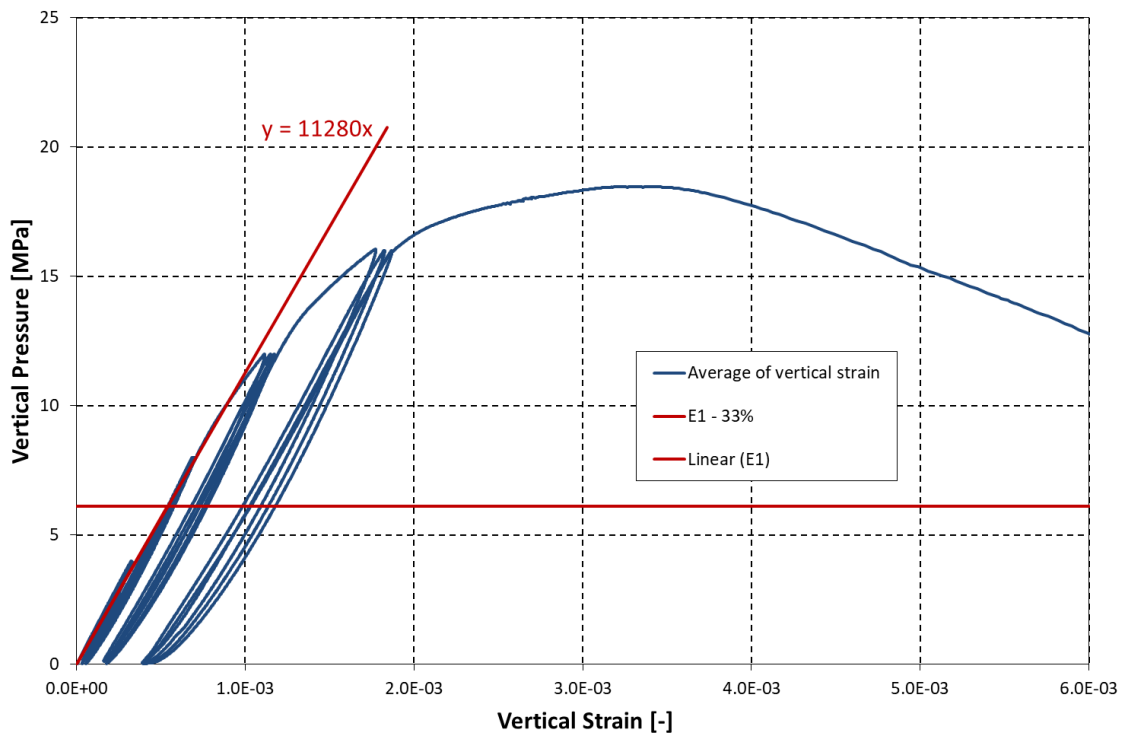


Figure 2.79 Vertical stress vs. vertical strain and determination of the modulus of elasticity for wallette WCL_4.

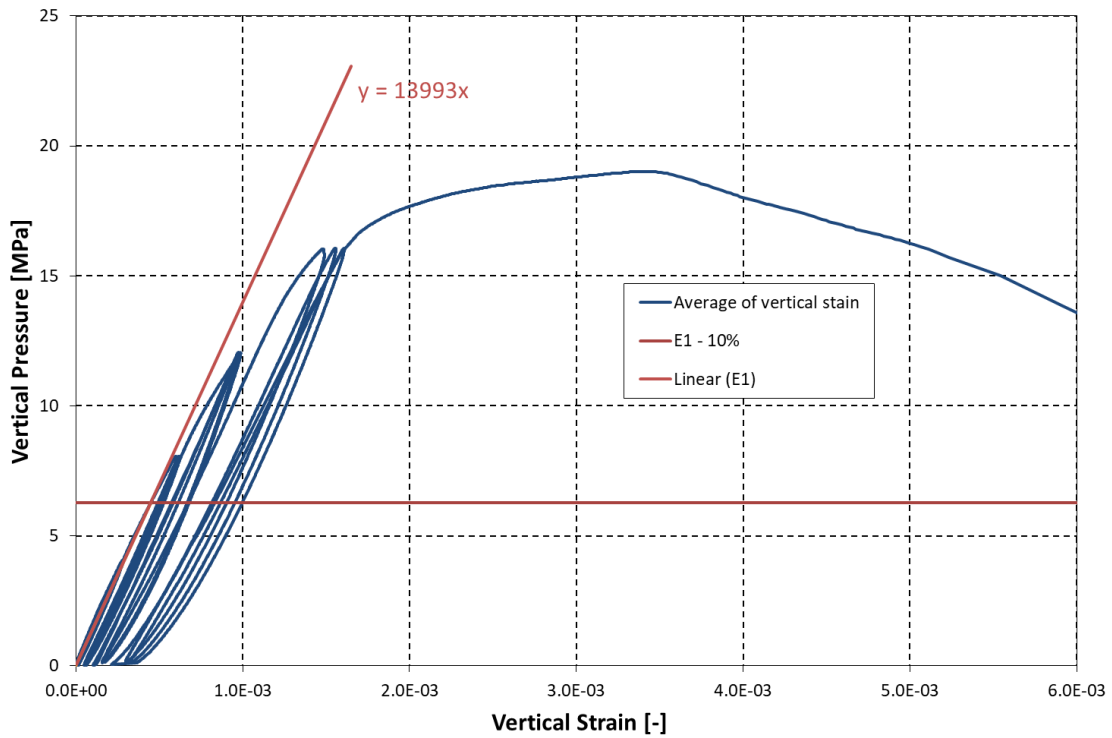


Figure 2.80 Vertical stress vs. vertical strain and determination of the modulus of elasticity for wallette WCL_5.

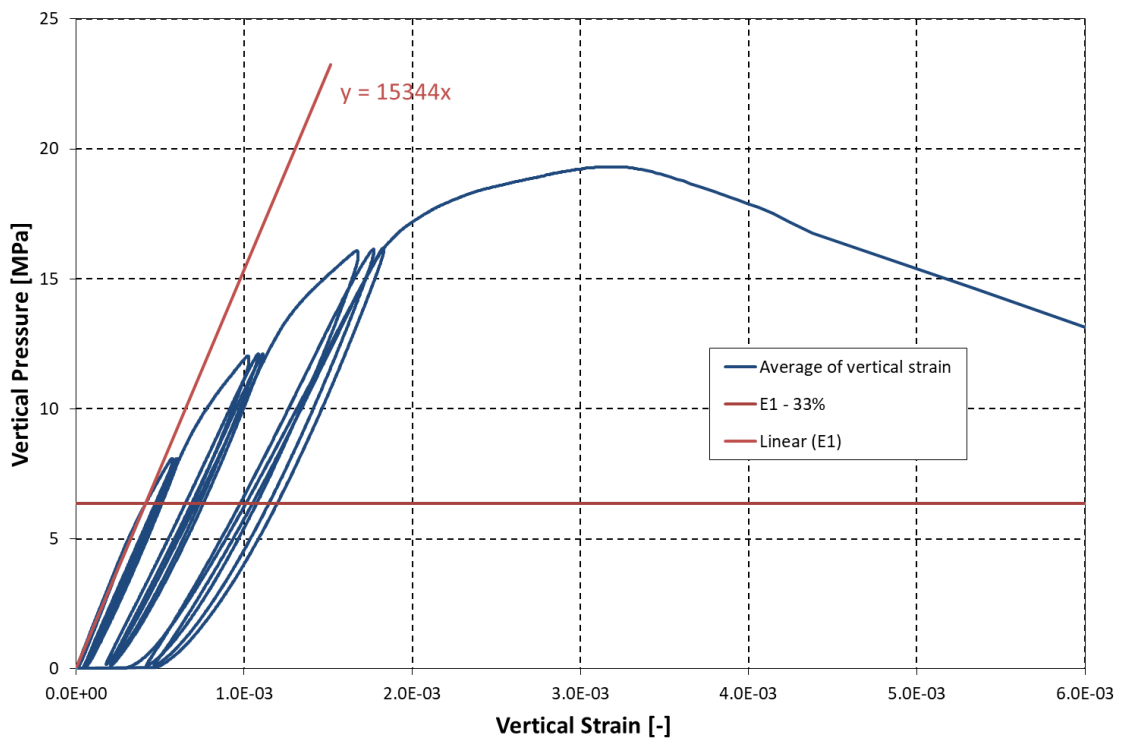


Figure 2.81 Vertical stress vs. vertical strain and determination of the modulus of elasticity for wallette WCL_6.

The results obtained for the modulus of elasticity E_1 for each *wallette* are summarised in Table 2.23 for the clay *wallettes*, while Figure 2.82 shows the distribution of moduli of elasticity obtained for the clay *wallettes*.

78 Collapse Shaking Table Test on URM Cavity Wall Structure representative of a Dutch Terraced House

Table 2.23 Summary of the modulus of elasticity for clay walleets.

Specimen	Compression strength [MPa]	E_1 (33% F_{max}) [MPa]
WCL_1	21.04	11112
WCL_2	18.19	12024
WCL_3	19.12	13035
WCL_4	18.46	11280
WCL_5	19.02	13993
WCL_6	19.31	15344
Average [MPa]	19.19	12798
Standard deviation [MPa]	1.00	1656
Coefficient of variation [-]	0.05	0.13

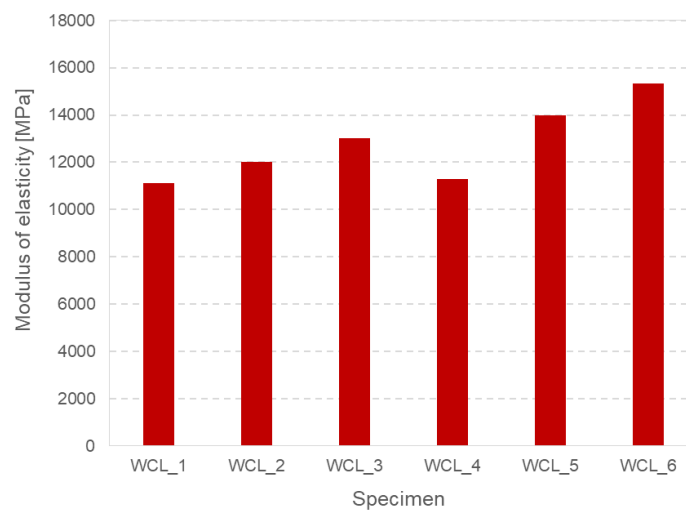


Figure 2.82 Distribution of moduli of elasticity obtained for clay walleets.

2.3.3 Test for the determination of shear strength

The test for determination of shear strength was performed according to an adaptation of the standard method described in the standard NP EN 1052-3 "Métodos de ensaio de alvenaria; Parte 3: Determinação da resistência inicial ao corte" (2005). The principle of this test is the determination of the initial shear strength in the plane of the horizontal joints, the characteristic value of the cohesion and the coefficient of friction.

This test was carried out on the two types of *triplets* already mentioned (calcium silicate *triplets* and clay *triplets*). With the objective of recording the evolution of the displacements in the specimens during the tests, two displacement transducers were used on one side with the purpose of analyzing the behavior of the block / mortar interface, thus registering the vertical displacement differential between rows. This displacement ratio was defined by a small plate, fixed to the central block, thus allowing to determine the displacements in the end blocks relative to the central block. Two deformeters (1 and 2) were also placed on each side of the joint to measure the horizontal displacements in these joints, thus allowing them to be measured during the test. Figure 2.83 presents the instrumentation placed on calcium silicate *triplets* and Figure 2.84 presents the instrumentation placed on clay *triplets*. An example of the location of the instrumentation on both types of specimens is shown in Figure 2.85 and Figure 2.86 (the schematics with the instrumentation locations for all tested *triplets* are given in Annex IV).

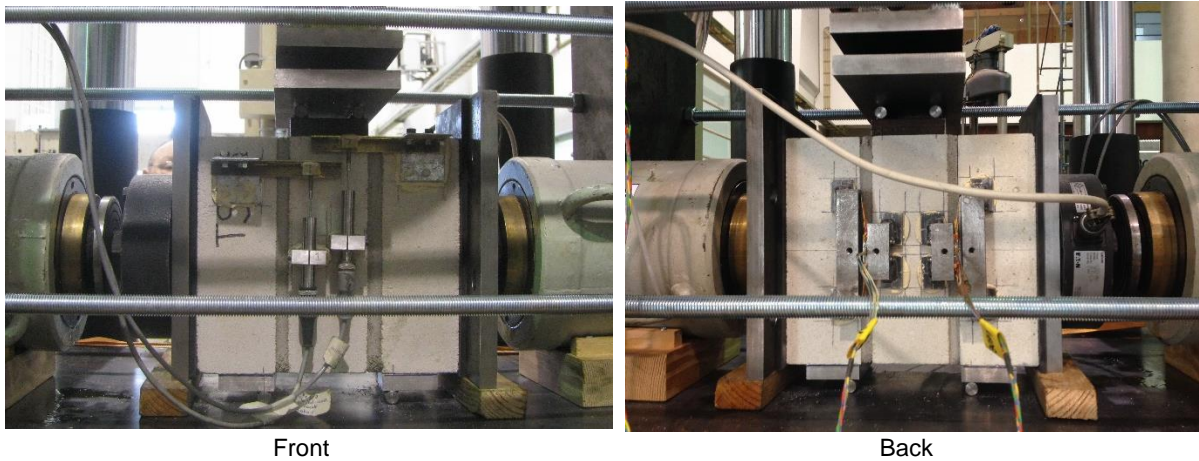


Figure 2.83 Instrumentation placed on the calcium silicate triplets.

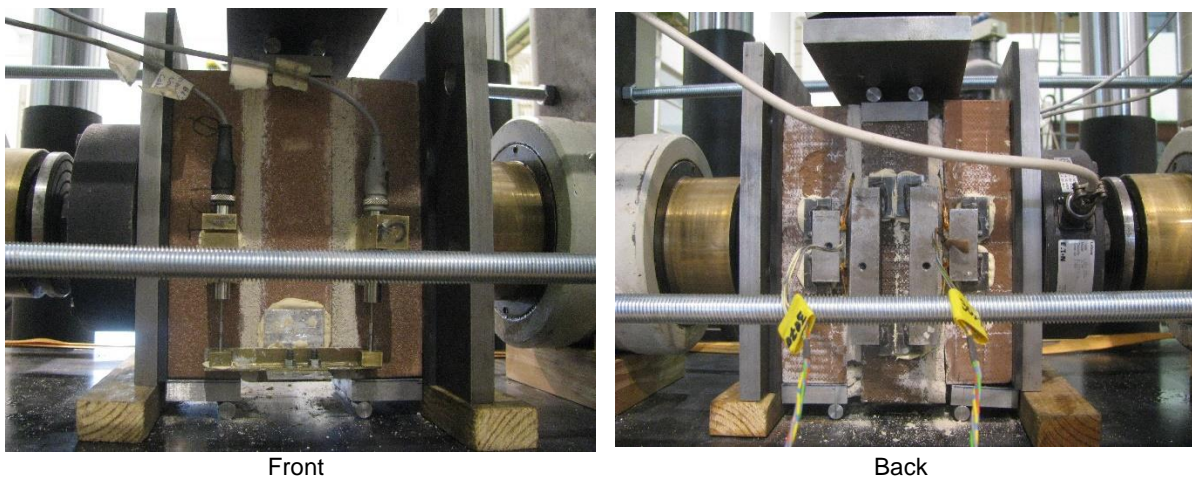


Figure 2.84 Instrumentation placed on the clay triplets.

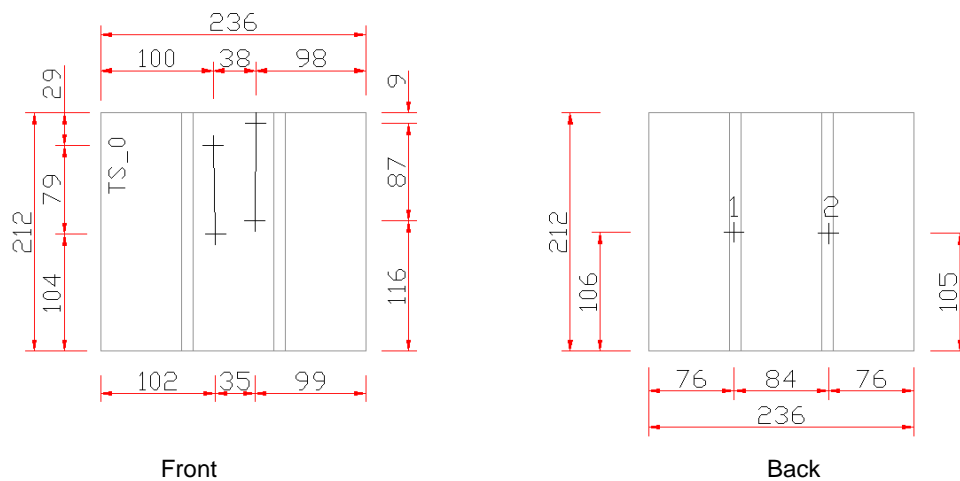


Figure 2.85 Location of the instrumentation placed on the calcium silicate triplets (dimensions in mm).

80 Collapse Shaking Table Test on URM Cavity Wall Structure representative of a Dutch Terraced House

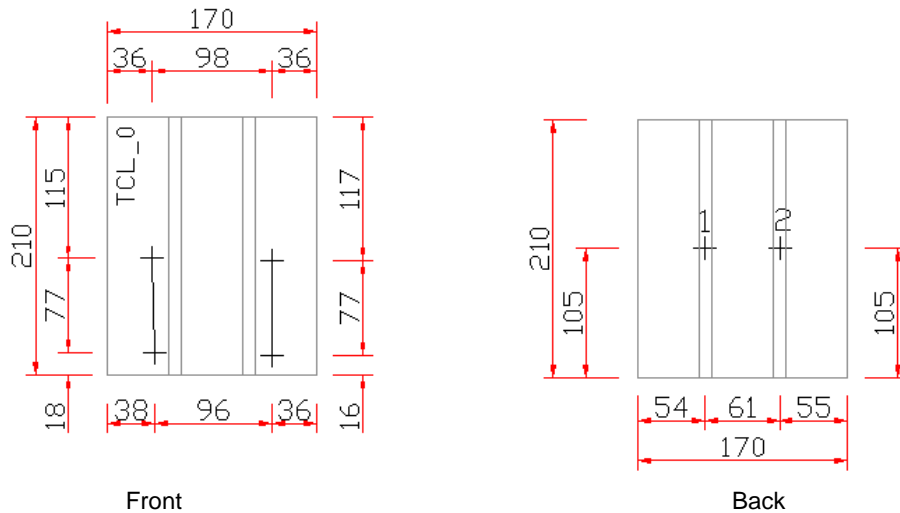


Figure 2.86 Location of the instrumentation placed on the clay triplets (dimensions in mm).

Since the blocks present a strength greater than 10 N/mm^2 , the pre-compression stress F_{pi} to be applied on the specimens should be $0,2 \text{ N/mm}^2$, $0,6 \text{ N/mm}^2$ and $1,0 \text{ N/mm}^2$. The pre-compression force should be uniform and well distributed on the faces of the specimen.

The compression force was read by a load cell with a capacity of 25 kN while the shear force was measured by the load cell of the actuator of the testing machine itself, with a maximum capacity of 1000 kN. The use of an auxiliary pumping system with an accumulator ensured that the various pre-compression levels remained constant during the test, even though some dilatancy is to be expected.

The hydraulic jacks, load cell and acquisition equipment, i.e. the complete test chain, were duly calibrated immediately prior to the start of the tests with the collaboration of the Metrological Quality Unit of the LNEC Scientific Instrumentation Centre, as shown in Figure 2.87. Given the existence of small irregularities on the lateral sides of the triplets (areas to be pre-compressed) a neoprene rubber was placed between the specimen and the plates of the hydraulic jacks that apply the pre-compression.

The shear strength test consisted on the application of a vertical force in the central block, a shear force, and an horizontal force applied to the geometric center of the specimen, a pre-compression force. The shear force was applied with displacement-control at a speed of 0.01 mm/s and a sampling frequency of 25 Hz. The test scheme is shown in Figure 2.88.



Figure 2.87 Calibration of the complete test chain.

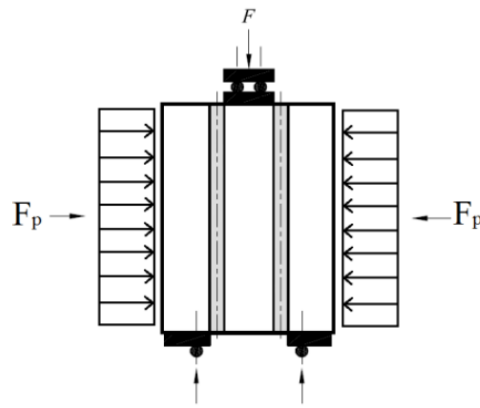


Figure 2.88 Test scheme for the determination of shear strength.

A device was initially created to perform this test, which was modified over several iterations until the definitive version that was actually used. Figure 2.89 shows the final device. The details of these elements can be found in Annex VI.

The initial shear strength of the masonry was determined with a shear action defined by three points of application of load parallel to the horizontal joints and with the simultaneous application of a pre-compression force perpendicular to the horizontal joints. The tests were carried out, recording the load and deformation values, identifying the representative values upon failure, and the test was finalised after confirmation of the significant reduction of the shear force and measurement of the deformation for the various pre-compression levels.

Cohesion and shear stress were determined on at least three specimens at each pre-compression level ($0,2 \text{ N/mm}^2$, $0,6 \text{ N/mm}^2$ and $1,0 \text{ N/mm}^2$). The friction was then determined for the two remaining pre-compression levels different from the initial one, as exemplified in the plots of Figure 2.90, Figure 2.91 and Figure 2.92 for the case of calcium silicate *triplets*.



Figure 2.89 Final version of the shear strength test device.

82 Collapse Shaking Table Test on URM Cavity Wall Structure representative of a Dutch Terraced House

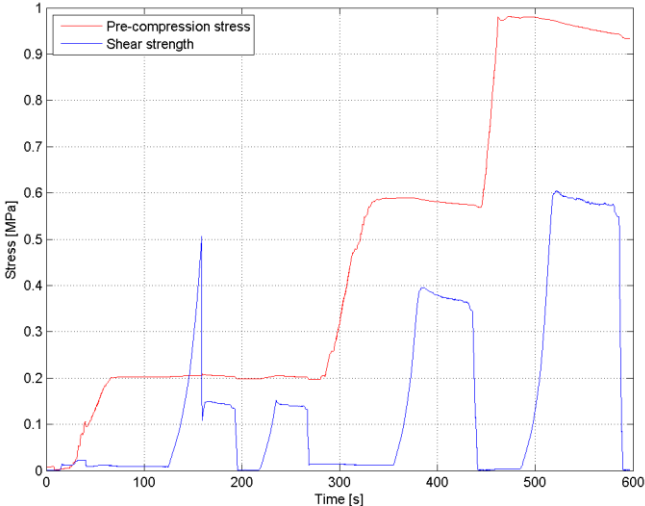


Figure 2.90 Application of the pre-compression and shear stresses throughout the test starting with the lowest pre-compression level (TS_3).

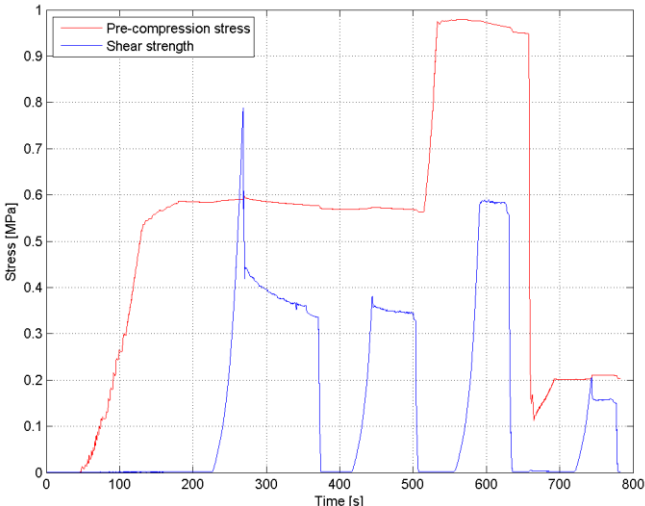


Figure 2.91 Application of the pre-compression and shear stresses throughout the test initiated with the intermediate pre-compression level (TS_7).

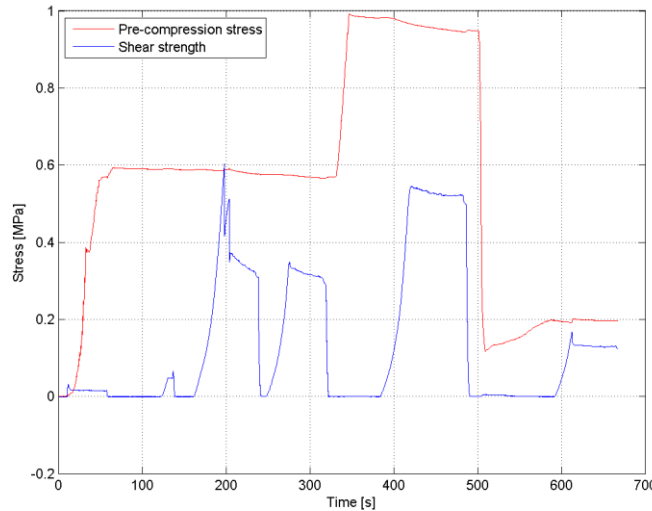


Figure 2.92 Application of pre-compression and shear stresses throughout the test started at the highest pre-compression level (TS_11).

For each specimen the pre-compression stress and the shearing stress were calculated according to the following formulas:

$$f_{pi} = \frac{F_{pi}}{A_{ei}} \quad (9)$$

$$f_{vi} = \frac{F_{i,m\acute{a}x.}}{2 \times A_{ei}} \quad (10)$$

where:

- f_{pi} is the pre-compression stress [MPa];
- F_{pi} is the pre-compression force [N];
- A_{ei} is the effective area of contact [mm²];
- f_{vi} is the shear failure stress [MPa];
- $F_{i,m\acute{a}x.}$ is the shear failure force [N].

For each pair of values (f_{pi} , f_{vi}) it is possible to obtain a plot like the one shown in Figure 2.93. Coulomb's law is the most representative of the results. The shear strength of the bedding mortar of the specimens (f_v) depends on three parameters: cohesion, coefficient of friction and transversal compression. Cohesion contributes to the force only if the bedding mortar is not cracked, while the frictional force also acts after cracking, as long as there is contact between the two materials. The shear strength (f_v), according to Coulomb's law, is linearly depending on the pre-compression stress (f_p):

$$f_v = f_{v0} + \mu \times f_p \quad (11)$$

where:

- f_{v0} is the cohesion [MPa];
- μ is the angle of friction with dimensionless units [-].

For each specimen, the cohesion and internal friction angle were calculated, as shown in the plot of Figure 2.94.

84 Collapse Shaking Table Test on URM Cavity Wall Structure representative of a Dutch Terraced House

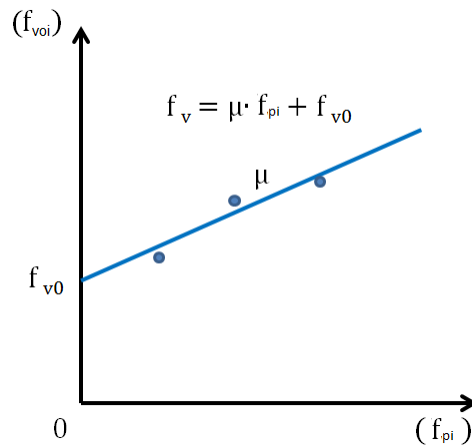


Figure 2.93 Theoretical determination of cohesion and angle of friction in the shear strength test.

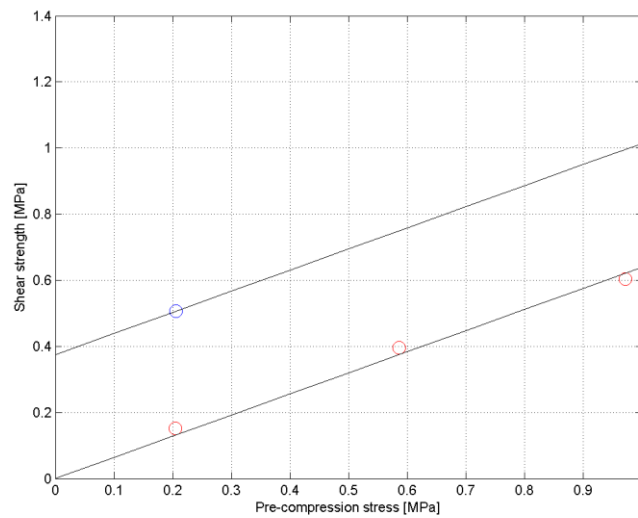


Figure 2.94 Determination of cohesion and friction angle for specimen TS_3.

The acceptable collapse mechanisms for the test to be considered valid are shown in Figure 2.95.

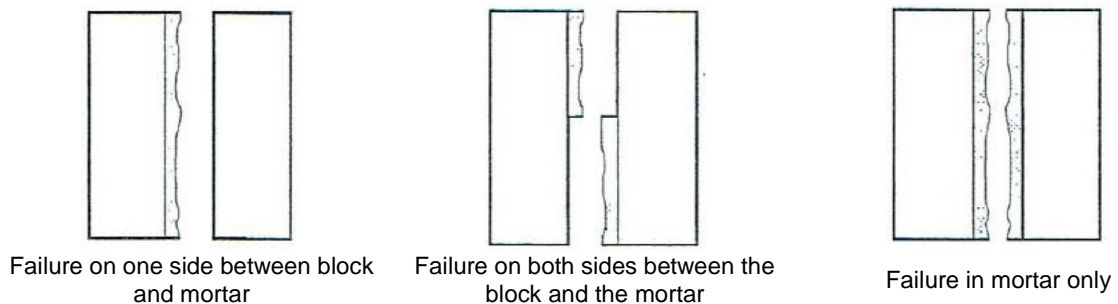
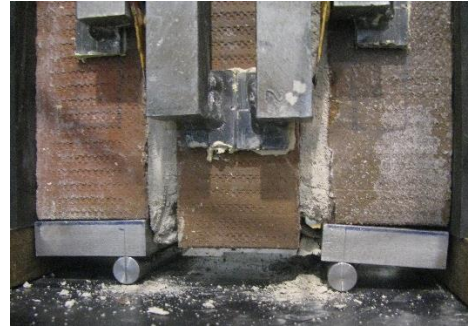


Figure 2.95 Acceptable collapse mechanisms for the shear strength test.

The test is finished upon the measurement of the friction after fracture formations, while there is contact between the two materials, as shown in Figure 2.96



Calcium silicate triplet



Clay triplet

Figure 2.96 Completion of the test for the two types of triplets tested.

The type of failure mechanisms obtained in the various tests are as exemplified in Figure 2.97. Annex V presents further details on the obtained fractures for all the specimens tested.



Calcium silicate triplet



Clay triplet

Figure 2.97 Example of one of the failure mechanisms obtained for each triplet in the shear strength test.

The shear strength results obtained in the tests for the two types of specimens are summarised in Table 2.24.

Table 2.24 Summary of the shear strength obtained for the calcium silicate triplets.

Specimen	Date of test	Contact area A_{ei} [mm ²]	Pre-compression stress f_{pi} [MPa]	Shear strength f_{vi} [MPa]
TS_0	24-05-2017	21915	0.19 (*)	0.67 (*)
TS_1	25-05-2017	21863	0.20	0.48
TS_2	26-05-2017	21893	0.22	0.58
TS_3	29-05-2017	21838	0.21	0.51
TS_4	29-05-2017	21703	0.20	0.51
TS_5	29-05-2017	21752	0.21	0.58
TS_6	29-05-2017	21795	0.99	0.96
TS_7	30-05-2017	21935	0.59	0.79
TS_8	30-05-2017	21864	0.98	0.97
TS_9	30-05-2017	21872	0.59	0.80
TS_10	30-05-2017	21909	0.97	0.85
TS_11	30-05-2017	21893	0.59	0.60

(*)The specimen TS_0 was tested in force control; it was only possible to obtain values for the first level of pre-compression

86 Collapse Shaking Table Test on URM Cavity Wall Structure representative of a Dutch Terraced House

Table 2.25 Summary of the shear strength obtained for the clay triplets.

Specimen	Date of test	Average gross area [mm ²]	Effective contact area A _{ei} [mm ²]	Pre-compression stress f _{pi} [MPa]	Shear strength f _{vi} [MPa]
TCL_0	01-06-2017	21335	17708	0.21	0.46
TCL_1	-	21129	17537	-	(*)
TCL_2	02-06-2017	21334	17707	0.22	0.57
TCL_3	02-06-2017	21180	17579	0.22	0.58
TCL_4	02-06-2017	21300	17679	0.60	1.04
TCL_5	05-06-2017	21210	17604	0.62	0.82
TCL_6	05-06-2017	21160	17563	0.62	0.95
TCL_7	05-06-2017	21212	17606	0.98	1.12
TCL_8	05-06-2017	21080	17496	1.00	1.11
TCL_9	05-06-2017	21002	17432	1.00	1.12

(*)specimen damaged before the start of the test

The plots in Figure 2.98 and Figure 2.99 relate the individual value of the failure stress to the shear strength and the individual pre-compression stress value of each *triplet* of each type of masonry, according to the point 10 of standard NP EN 1052-3 (IPQ, 2005). The plots for all specimens are given in Annex VII.

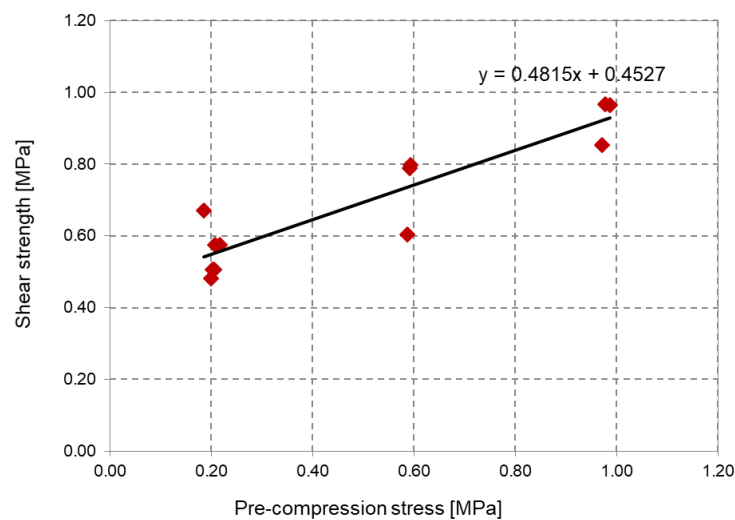


Figure 2.98 Shear strength, cohesion and internal friction angle for the calcium silicate triplets.

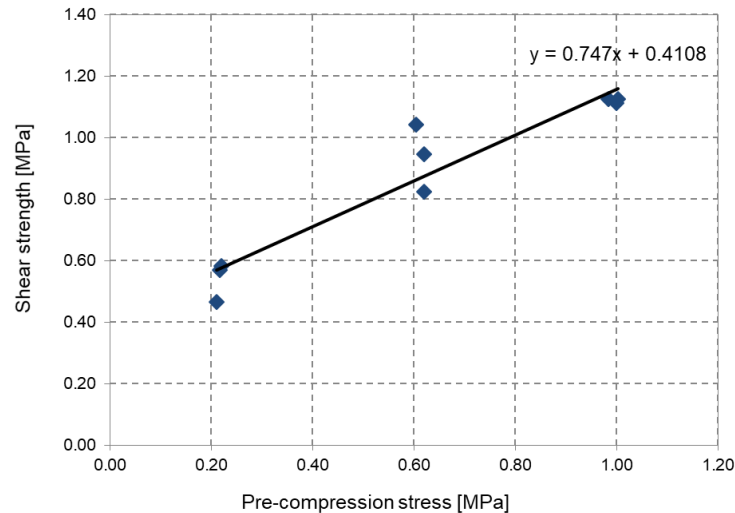


Figure 2.99 Shear strength, cohesion and internal friction angle for clay triplets.

By plotting a line of linear regression with all points and through the equation that translates this line we can derive the mean values of cohesion (f_{v0}) and angle of internal friction (μ), presented in Table 2.26 for the two types of triplets.

Table 2.26 Summary of average cohesion values and internal friction angles for the two types of triplets.

Specimen	f_{v0} [MPa]	μ [-]
Calcium silicate triplets	0.45	0.48
Clay triplets	0.41	0.75

2.3.4 Tests for the determination of bond strength

The purpose of this section is to describe the complementary destructive tests that were carried out on several samples for each type of masonry to determinate the bond strength of horizontal bed joints in masonry using the bond wrench method described in the standard EN 1052-5 "Methods of test for masonry - Part 5: Determination of bond strength by the bond wrench method" (2005).

The test was carried out on the two types of triplets already mentioned in the previous section (calcium silicate triplets and clay triplets), as shown in Figure 2.100.

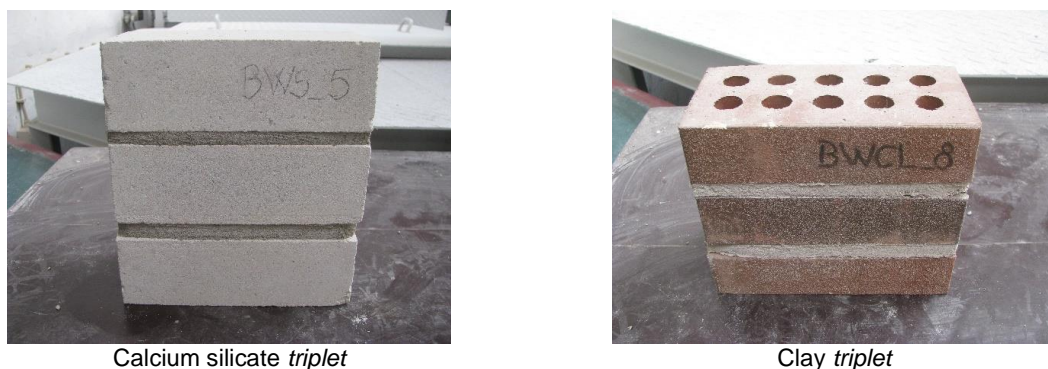


Figure 2.100 Type of specimens subjected to bond strength test.

88 Collapse Shaking Table Test on URM Cavity Wall Structure representative of a Dutch Terraced House

The main idea of the test is to keep the specimen rigidly held while a clamp is applied to the top unit, see Figure 2.101. A bending moment is applied to the clamp by a lever until the top unit is torn from the remaining part of the specimen. From the stresses achieved by the specimen, the bond strength of the masonry can be evaluated.

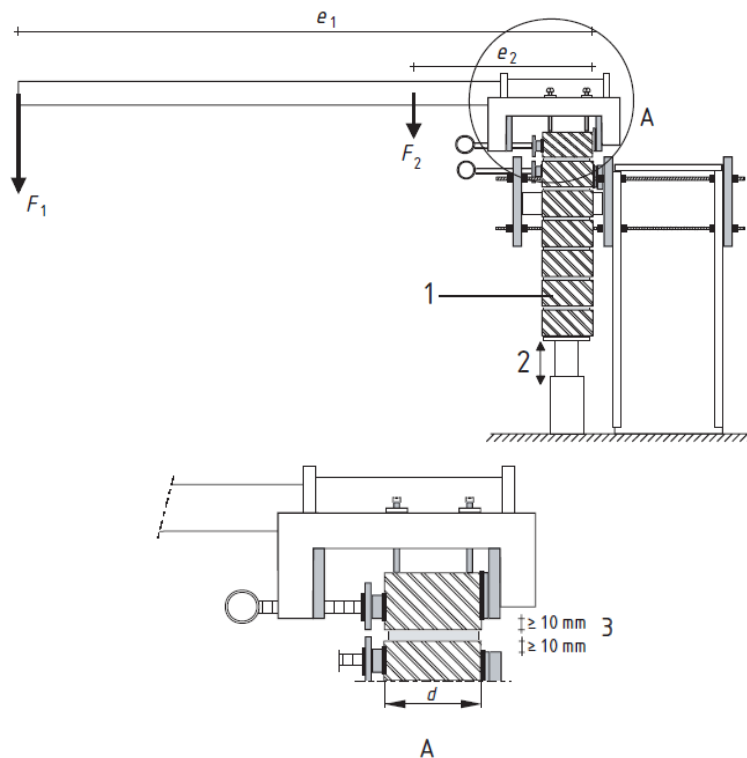


Figure 2.101 Example of a possible device for the test in accordance with EN 1052-5 (CEN, 2005).

A device was created to carry out this test. It was modified during the test campaign, since initially a torque wrench with a memory needle for moment recording was planned to be used but in the end a horizontal bar was used instead. Figure 2.102 shows the final device, whose details can be found in Annex VI.



Figure 2.102 Device used for the test.

The equipment has two independent steel frame structures: a lower support frame with two side plates, reinforced with gussets, and welded to a base plate, which holds in place the unit beneath the top bed joint of the specimen without applying any significant bending moment to any lower units; the upper structure is a lever with a clamp at one end, made up of three welded plates and a horizontal level steel rebar, which can be applied to the top unit of the *triplet*.

The test procedure was as follows:

1. The lower frame was attached to a rigid plate and a position for the *triplet* was defined, according with the standard. The screws were clamping approximately with equal torque (it was used a ratchet torque wrench). Bricks and small pieces of timber were used with the thickness of the joints to ensure the same fixing height as defined in the standard. This was envisaged for two reasons: i) since the lower structure is common to the two types of *triplets* that have different heights; and ii) so that after the first failure of the connection the specimen could be raised to the required height, allowing the second connection to be tested, as shown in Figure 2.103 and Figure 2.104;



Figure 2.103 Test of the two connections in calcium silicate blocks using the same test device.



Figure 2.104 Test of the two connections in clay bricks using the same test device.

2. The *triplet* was securely clamped in the retaining frame such that the second from top unit had a reasonable degree of restraint against rotation but the joint to be tested remained between 10 and 15 mm clear of the lower clamp. The clamp was intertwined with thin layers of a material such as plywood to ensure an even grip;
3. Fix the upper clamp with lever arm on the upper block to be tested, respecting the tightening location indicated by the standard (a distance equal to or greater than 10 mm from the test joint) and ensuring that the lever is horizontal;
4. Apply the vertical force on the lever end that should be approximately 1 meter long as per indication of the standard. Sand pouring on a bucket was used for applying the vertical force up to a bond failure, as shown in Figure 2.105;
5. Weighing of the top unit, the adherent mortar and the sand volume (including the container) leading to a bond failure, as shown in Figure 2.106.



Figure 2.105 Application of vertical force until bond failure.



Figure 2.106 Measure of the weight of the top unit, its adherent mortar and sand volume leading to failure.

For each valid failure the bond strength was calculated using the following expression, which includes the effects of both applied bending moment and compression:

$$f_{wi} = \frac{F_1 e_1 + F_2 e_2 - \frac{2}{3} d (F_1 + F_2 + W/4)}{\frac{bd^2}{6}} \quad (12)$$

where:

f_{wi} bond strength in masonry [MPa];

b width of the bed joint tested [mm];

d depth of the specimen [mm];

e_1 distance from the applied load (F_1) to the tension face of the specimen [mm];

e_2 distance from the center of gravity of the lower and upper clamp (F_2) from the tension face of the specimen [mm];

F_1 applied load [N];

F_2 weight of the bond wrench [N];

W weight of the masonry unit pulled off the specimen and any adherent mortar [N].

The modes of failure represented in Figure 2.107 were considered valid to calculate the bond strength, according to EN 1052-5 (2005). The type of bond failure mechanisms obtained in the tests are those exemplified by Figure 2.108. In Annex V, the pictures for all tested specimens are presented.

The bond strength values obtained from the tests for the two types of specimens are presented in Table 2.27 and Table 2.28, while their average values are shown in Table 2.29.

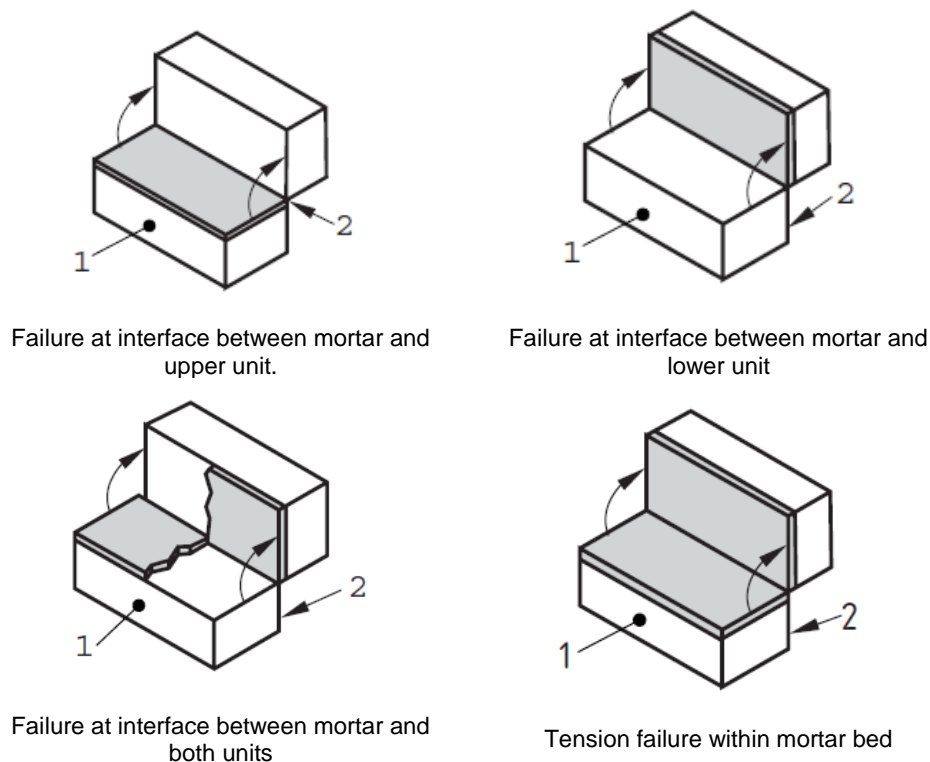


Figure 2.107 Admissible failure mechanisms for the bond wrench test.

92 Collapse Shaking Table Test on URM Cavity Wall Structure representative of a Dutch Terraced House



Calcium silicate triplets



Clay triplets

Figure 2.108 Example of failure mechanisms obtained for each triplet type in the bond wrench test.

Table 2.27 Bond strength for the calcium silicate triplets.

Specimen	<i>b</i>	<i>d</i>	<i>Z</i>	<i>e</i> ₁	<i>e</i> ₂	<i>F</i> ₁	<i>F</i> ₂	<i>W</i>	<i>M</i> ₁	<i>M</i> ₂	<i>f</i> _{wi}
	[mm]	[mm]	[mm ³]	[mm]	[mm]	[N]	[N]	[N]	[N.mm]	[N.mm]	[MPa]
BWS_0	213.5	102.3	372172	945	205	166.51	100.68	30.86	157347	20639	0,43
BWS_0	213.5	102.3	372172	945	205	126.52	100.68	26.85	119561	20639	0,33
BWS_1	213.0	102.7	374283	945	205	160.06	100.68	28.83	151257	20639	0.41
BWS_1	213.0	102.7	374283	945	205	159.98	100.68	30.85	151183	20639	0.41
BWS_2	212.5	102.6	372532	945	205	173.07	100.68	32.56	163549	20639	0.44
BWS_2	212.5	102.6	372532	945	205	153.05	100.68	31.25	144628	20639	0.40
BWS_3	213.0	102.2	371010	945	205	174.40	100.68	32.32	164810	20639	0.45
BWS_3	213.0	102.2	371010	945	205	134.19	100.68	31.24	126810	20639	0.35
BWS_4	215.0	102.2	373907	945	205	84.28	100.68	28.60	79642	20639	0.23
BWS_4	215.0	102.2	373907	945	205	96.93	100.68	36.24	91601	20639	0.26
BWS_5	213.0	102.1	370067	945	205	121.64	100.68	29.14	114954	20639	0.32
BWS_5	213.5	102.3	372172	945	205	103.67	100.68	28.39	97970	20639	0.28

Table 2.28 Bond strength for the clay triplets

Specimen	<i>b</i>	<i>d</i>	<i>Z</i>	<i>e</i> ₁	<i>e</i> ₂	<i>F</i> ₁	<i>F</i> ₂	<i>W</i>	<i>M</i> ₁	<i>M</i> ₂	<i>f</i> _{wi}
	[mm]	[mm]	[mm ³]	[mm]	[mm]	[N]	[N]	[N]	[N.mm]	[N.mm]	[MPa]
BWCL_1	213.5	102.3	372172	945	205	84.29	100.68	23.30	79652	20639	0.23
BWCL_2	213.0	102.7	374283	945	205	88.10	100.68	17.61	83258	20639	0.24
BWCL_3	212.5	102.6	372532	945	205	24.56	100.68	22.40	23213	20639	0.09
BWCL_4	213.0	102.2	371010	945	205	31.64	100.68	17.20	29897	20639	0.11
BWCL_4	213.0	102.2	371010	945	205	60.89	100.68	23.43	57542	20639	0.18
BWCL_5	215.0	102.2	373907	945	205	127.42	100.68	17.16	120414	20639	0.33
BWCL_5	215.0	102.2	373907	945	205	22.40	100.68	27.91	21164	20639	0.09
BWCL_6	213.0	102.1	370067	945	205	127.13	100.68	22.00	120136	20639	0.34
BWCL_6	213.0	102.1	370067	945	205	75.79	100.68	19.01	71623	20639	0.22
BWCL_7	213.0	102.1	370067	945	205	63.78	100.68	22.11	60276	20639	0.19
BWCL_7	213.0	102.1	370067	945	205	63.41	100.68	18.52	59924	20639	0.19
BWCL_8	213.0	102.1	370067	945	205	27.83	100.68	22.37	26300	20639	0.10

Table 2.29 Summary of bond strength in the two types of tested specimens.

Type of specimen	Bond strength		
	Average [MPa]	Standard deviation [MPa]	Coefficient of variation [-]
Calcium silicate <i>triplets</i>	0.36	0.07	0.20
Clay <i>triplets</i>	0.19	0.09	0.47

2.4 Analysis of the materials characterisation results

The main objective of this section of the work consisted on an in-depth characterisation of the various constituent materials of masonry cavity walls that were used in a real-scale model subjected to seismic tests until its collapse. These tests enabled us to obtain relevant data to the interpretation of the tests carried out on the full-scale model, as well as to the validation of the representativeness of the experimental results, using numerical models, regarding the properties of masonry in real buildings in the Groningen region.

Regarding the properties to be obtained, it was concluded that the devices created for this purpose, based on the normative documents, proved to be quite suitable for the tests carried out. On the other hand, the type and location of instrumentation provided with the desired quality all the necessary quantities for the correct analysis and interpretation of the experimental results obtained.

Although the experimental tests carried out are based on normative documents, since this is a research report, some of the parameters recommended by these documents were modified to accomplish the intended objectives of this work. On the other hand, in several tests more parameters were determined than the ones foreseen in the normative documents, which also implied some adjustments of the devices and the test methods.

The construction of the models and test specimens proved to be quite representative of the typology in study: the imperfections carried out in the work were also reproduced in these models and specimens, more specifically in the *wallettes* built for the tests for the determination of the compressive strength where the modulus of elasticity was also determined. In this context, given the irregularity of the face of the specimens and the lack of verticality of the *wallettes*, it was necessary and very important to correct these imperfections by placing a thin layer of regularisation so that the load was applied evenly (gypsum was chosen due to its fast curing time).

Concerning the bedding mortars that were analysed, in addition to the values obtained being consistent with the reference bibliography, a good ratio between the modulus of elasticity and the compressive strength obtained experimentally for the different ages was verified. On the other hand, it was verified that the representativeness of the bedding mortars studied in the characterisation test specimens versus the real-scale model was closer in the masonry composed of clay bricks.

With respect to the masonry *wallettes*, it was found that, in terms of strength, the load-bearing masonry composed of blocks of calcium silicate, has a compressive strength substantially lower than the masonry composed of clay bricks, which is relegated to aesthetic and insulation functions.

In the case of the shear strength of the masonry *triplets*, it was also verified that the values of shear strength and of the angle of internal friction are higher in the case of masonry composed of clay bricks when compared to the calcium silicate *triplets*. However, the bond strength obtained was significantly larger for the calcium silicate *triplets*.

3 INSTRUMENTATION OF THE SPECIMEN

In order to detect and monitor the structural response under different levels of input motion, several kinematic measuring instruments were installed on the building. The location and typology of the instruments was determined based on the identification of the critical zones and on the physical quantity to be recorded. The instrumentation consisted of 40 accelerometers and 24 displacement transducers. Figure 3.1 (a) shows the ID number and the locations of the accelerometers installed on both inner and outer leaves, as well as on the floor and on the ridge beam of the roof.

Figure 3.1 (b) shows, instead, the displacement transducers installed on the specimen: 8 wire potentiometers and 16 linear variable displacement transducers (LVDTs). The displacements measured between the specimen and the rigid reference frame were considered equivalent to the relative displacements with respect to the shaking table surface. In particular, wire potentiometers were installed in order to record the out-of-plane response of the East and West façades at the mid-height of the first storey and the gable. The LVDTs were used to monitor directly the longitudinal and transverse displacement of the slab with respect to the reference steel frame. LVDTs were also installed to monitor the eventual slippage between the base of the walls and the steel foundation beam, between the RC slab and the top of the CS longitudinal walls and the differential displacement between the RC slab and the outer leaf observed in Graziotti et al. 2015.

Table 3.1 and Table 3.2 list the accelerometers and the displacement transducers, respectively describing their location in the specimen and the column (Col.#) identifying the recorded histories in the .txt files containing the test experimental data. The data is organised in matrix form and named in accordance to Table 4.1. The data acquisition time step is 0.005 s, columns 35 to 74 contain the acceleration time-histories recorded by the accelerometers mounted on the structure. The displacement histories recorded by wire potentiometers are listed in columns 9 to 16, while those recorded by traditional potentiometers are found in columns 17 to 32. Columns 1 to 8 contain the actuators read-out data, in terms of longitudinal (x direction), transverse (y direction) and vertical (z direction) displacements and accelerations. Columns 33 and 35 contain the actuators longitudinal and vertical forces. The last columns (75 to 90) contain quantities that were not directly measured, such as average floor displacements, total base-shear force and the inter-storey drift ratio time-histories. In general, the authors suggest to use these last sets of data (especially for the FEQ-300% when many instruments saturated). Table 3.1 specifies also the lumped mass associated to each instrument in computing the inertial forces. Table 3.3 specifies the content of all the remaining columns of the .txt files.

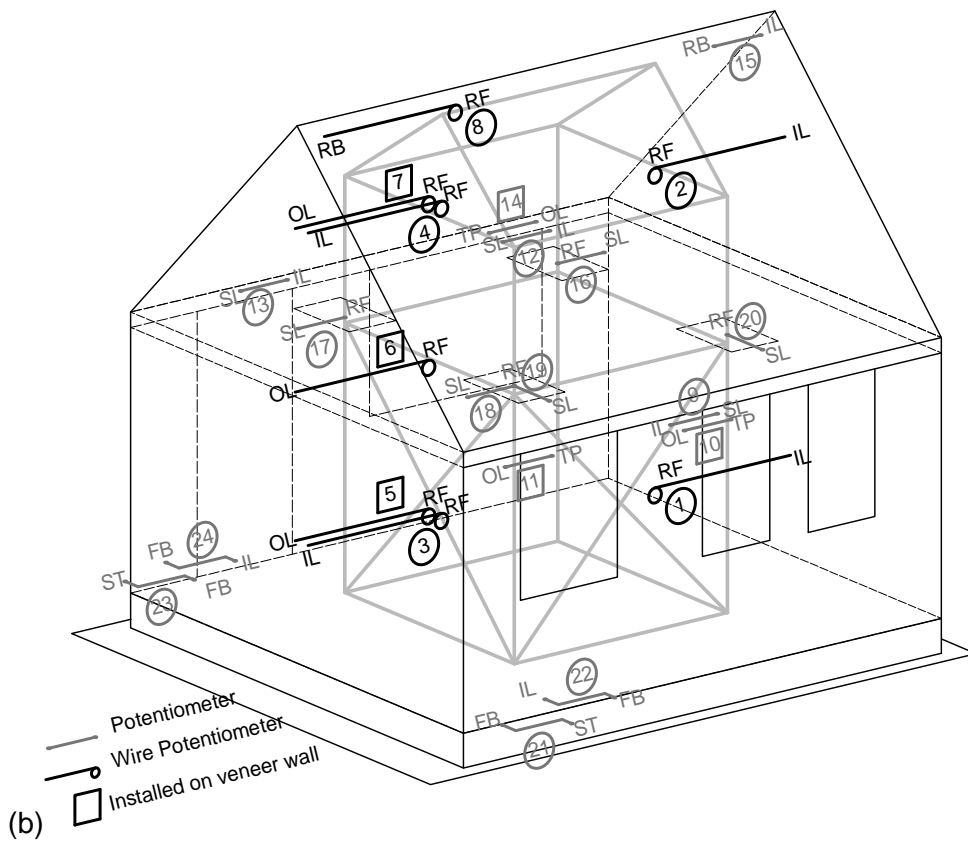
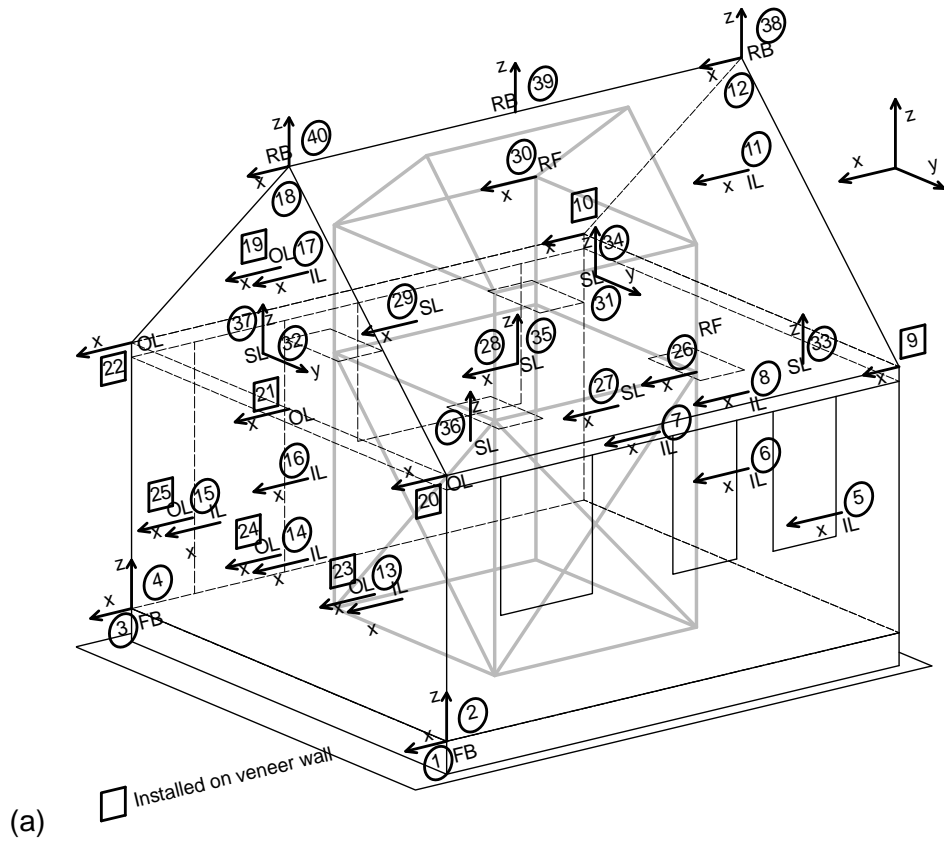


Figure 3.1 Locations of the instrumentation: accelerometers (a) and displacement transducers (b) (letters indicate the component at which the transducers is attached to: SL = slab, RF = reference frame, IL = inner leaf, OL = outer leaf, FB = foundation beam, ST = shaking table, TP = timber plate and RB = roof ridge beam).

Table 3.1 Summary of the accelerometers and their location.

Instr. #	Col. #	UM	Mass [kg]	Location of the instrument
1	35	[g]	3421.5	installed on the foundation beam on the South side and is used to record the accelerations in the x direction at the foundation level
2	36	[g]	0.0	installed on the foundation beam on the South side and is used to record the accelerations in the z direction at the foundation level
3	37	[g]	2976.2	installed on the foundation beam on the North side and is used to record the accelerations in the x direction at the foundation level
4	38	[g]	0.0	installed on the foundation beam on the North side and is used to record the accelerations in the z direction at the foundation level
5	39	[g]	226.5	installed at mid-height (15 th brick layer) of the inner East CS OOP wall (145 cm from the South-East corner) recording the accelerations in the x direction
6	40	[g]	172.2	installed at mid-height (15 th brick layer) of the inner East CS OOP wall (mid-length of the wall) recording the accelerations in the x direction
7	41	[g]	226.5	installed at mid-height (15 th brick layer) of the inner East CS OOP wall (145 cm from the North-East corner) recording the accelerations in the x direction
8	42	[g]	400.5	installed at 2/3 height (21 st brick layer) of the inner East CS OOP wall (mid-length of the wall) recording the accelerations in the x direction
9	43	[g]	527.7	installed at the top of the outer South clay veneer (South-East corner of the wall) recording the accelerations in the x direction
10	44	[g]	404.4	installed at the top of the outer North clay veneer (North-East corner of the wall) recording the accelerations in the x direction
11	45	[g]	606.4	installed at the mid-height (14 th brick layer) of the inner CS gable wall (East side) recording the accelerations in the x direction
12	46	[g]	825.8	installed at the roof ridge beam (East side) recording the accelerations in the x direction
13	47	[g]	226.5	installed at mid-height (15 th brick layer) of the inner West CS OOP wall (145 cm from the South-West corner) recording the accelerations in the x direction
14	48	[g]	172.2	installed at mid-height (15 th brick layer) of the inner West CS OOP wall (mid-length of the wall) recording the accelerations in the x direction
15	49	[g]	226.5	installed at mid-height (15 th brick layer) of the inner West CS OOP wall (145 cm from the North-West corner) recording the accelerations in the x direction
16	50	[g]	400.5	installed at 2/3 height (21 st brick layer) of the inner West CS OOP wall (mid-length of the wall) recording the accelerations in the x direction
17	51	[g]	606.4	installed at the mid-height of the inner CS gable wall (West side) recording the accelerations in the x direction
18	52	[g]	938.1	installed at the roof ridge beam (West side) recording the accelerations in the x direction
19	53	[g]	683.9	installed at the mid-height (63 rd brick layer) of the outer clay gable wall (West side) recording the accelerations in the x direction
20	54	[g]	579.1	installed at the floor level of the outer West clay veneer (South-West corner of the wall) recording the accelerations in the x direction
21	55	[g]	621.0	installed at the floor level of the outer West OOP clay veneer (centre of the wall) recording the accelerations in the x direction
22	56	[g]	603.9	installed at the floor level of the outer West clay veneer (North-West corner of the wall) recording the accelerations in the x direction

23	57	[g]	295.3	installed at mid-height (15 th brick layer) of the outer West OOP clay veneer (143 cm from the South-West corner) recording the accelerations in the x direction
24	58	[g]	293.4	installed at mid-height (15 th brick layer) of the outer West OOP clay veneer (mid-length of the wall) recording the accelerations in the x direction
25	59	[g]	295.3	installed at mid-height (15 th brick layer) of the outer West OOP clay veneer (143 cm from the North-West corner) recording the accelerations in the x direction
26	60	[g]	0.0	installed at the floor level of the steel frame recording the accelerations in the x direction
27	61	[g]	6160.1	installed on the slab (South side) to record the accelerations in the x direction
28	62	[g]	3808.0	installed on the slab (centre) to record the accelerations in the x direction
29	63	[g]	6062.8	installed on the slab (North side) to record the accelerations in the x direction
30	64	[g]	0.0	installed at the second level of the steel frame recording the accelerations in the x direction
31	65	[g]	0.0	installed on the slab on the North-East corner to record the accelerations in the y direction
32	66	[g]	0.0	installed on the slab on the North-West corner to record the accelerations in the y direction
33	67	[g]	0.0	installed on the slab on the South-East side to record the accelerations in the z direction
34	68	[g]	0.0	installed on the slab on the North-East side to record the accelerations in the z direction
35	69	[g]	0.0	installed on the centre of the slab to record the accelerations in the z direction
36	70	[g]	0.0	installed on the slab on the South-West corner to record the accelerations in the z direction
37	71	[g]	0.0	installed on the slab on the North-West side to record the accelerations in the z direction
38	72	[g]	0.0	installed at the roof ridge beam (East side) recording the accelerations in the z direction
39	73	[g]	0.0	installed at the mid-span of the roof ridge beam recording the accelerations in the z direction
40	74	[g]	0.0	installed at the roof ridge beam (West side) recording the accelerations in the z direction

98 Collapse Shaking Table Test on URM Cavity Wall Structure representative of a Dutch Terraced House

Table 3.2 Summary of the displacement transducers and their location.

Instr. #	Column #	UM	Location of the instrument
1	9	[mm]	installed at the mid-height of the inner CS OOP wall (East side) recording its horizontal displacement; +1.15 m
2	10	[mm]	installed at the mid-height of the CS gable wall (East side) recording its horizontal displacement; +3.71 m
3	11	[mm]	installed at the mid-height of the inner CS OOP wall (West side) recording its horizontal displacement; +1.18 m
4	12	[mm]	installed at the mid-height of the inner CS gable wall (West side) recording its horizontal displacement; +3.71 m
5	13	[mm]	installed at the mid-height of the outer clay OOP veneer (West side) recording its horizontal displacement; 1.15 m
6	14	[mm]	installed at the base of the outer clay gable (West side) recording its horizontal displacement; +2.18 m
7	15	[mm]	installed at the mid-height of the outer clay gable (West side) recording its horizontal displacement; +3.71 m
8	16	[mm]	installed to record the horizontal displacement of the roof ridge beam
9	17	[mm]	installed to record eventual sliding of CS inner leaf with respect to the slab (South side, Top of Pier 5)
10	18	[mm]	installed to record eventual sliding of outer South clay veneer with respect to the timber plate (small opening, Top of Pier 5)
11	19	[mm]	installed to record eventual sliding of outer South clay veneer with respect to the timber plate (large opening, Top of Pier 4)
12	20	[mm]	installed to record eventual sliding of North CS inner leaf with respect to the slab (window, Top of Pier 1)
13	21	[mm]	installed to record eventual sliding of North CS inner leaf with respect to the slab (door, Top of Pier 2)
14	22	[mm]	installed to record eventual sliding of North outer clay veneer with respect to the timber plate (window, Top of Pier 1)
15	23	[mm]	installed to record eventual sliding of the ridge Beam with respect to the CS gable wall (East side)
16	24	[mm]	installed on the slab (North-East corner) to record displacements in the x direction of the slab level
17	25	[mm]	installed on the slab (North-West corner) to record displacements in the x direction of the slab level
18	26	[mm]	installed on the slab (South-West corner) to record displacements in the x direction of the slab level
19	27	[mm]	installed on the slab (South-West corner) to record displacements in the y direction of the slab level
20	28	[mm]	installed on the slab (South-East corner) to record displacements in the y direction of the slab level
21	29	[mm]	installed to record eventual sliding of the foundation beam with respect to the shaking table (South side)
22	30	[mm]	installed to record eventual sliding of CS inner leaf with respect to the foundation beam (South side)
23	31	[mm]	installed to record eventual sliding of the foundation beam with respect to the shaking table (North side)
24	32	[mm]	installed to record eventual sliding of CS inner leaf with respect to the foundation beam (North side)

Table 3.3 Summary of the content of the remaining columns of the experimental data matrices.

Column #	UM	Location of the instrument
1	[mm]	Shaking Table Longitudinal Displacement
2	[mm]	Shaking Table Vertical Displacement
3	[g]	Shaking Table Longitudinal Acceleration
4	[g]	Shaking Table Transverse Acceleration
5	[g]	Shaking Table Vertical Acceleration
6	-	-
7	-	-
8	-	-
75	[g]	Average Horizontal Acceleration at the Foundation Beam Level (col 35-col 37)
76	[g]	Average Vertical Acceleration at the Foundation Beam Level (col 36-col 38)
77	[g]	Average Floor Horizontal Acceleration (col 61-col 62 –col 63)
78	[g]	Average Ridge-Beam Horizontal Acceleration (col 46–col 52)
79	[mm]	Average Floor Horizontal Displacement (col 24-col 25 –col 26)
80	[mm]	Ridge Horizontal Displacement (col 16)
81	[kN]	Base Shear computed according to lumped mass distribution presented above
82	[kN]	Simplified Base Shear with the following Mass distribution: 7092 kg at the foundation beam level, 22410 kg at the floor level and 2218 kg at the roof level.
83	[mm]	Ridge Relative Displacement
84	[mm]	Average Floor Horizontal Acceleration neglecting residual displacements
85	[mm]	Ridge Horizontal Displacement neglecting residual displacements (col 16)
86	[%]	Floor Drift (considered length=2520 mm)
87	[%]	Roof Drift (considered length=3500 mm)
88	[kN]	Base Shear computed according to a second lumped mass distribution representative of the inertial forces in the FEQ2-300% test
89	[kN]	Roof Force assuming a mass equal to 2600 kg (1/3 of the gable mass, ½ of the roof mass)
90	[mm]	Ridge relative displacement neglecting the residual displacements

Figure 3.2 shows pictures of the instrumentation installed on the specimen. The ID numbers shown in the pictures refers to the instrument number listed in Table 3.1 and Table 3.2.

100 Collapse Shaking Table Test on URM Cavity Wall Structure representative of a Dutch Terraced House



Figure 3.2 Pictures of the instrumentation.



Figure 3.2 (continued) Pictures of the instrumentation.

102 Collapse Shaking Table Test on URM Cavity Wall Structure representative of a Dutch Terraced House



Figure 3.2 (continued) Pictures of the instrumentation.



Figure 3.2 (continued) Pictures of the instrumentation.

4 TEST PROCEDURE

The building specimen was subjected to a sequence of incremental dynamic tests. A series of shaking table motions of increasing intensity were applied with the aim of assessing the ultimate capacity and the failure mechanism leading to the specimen collapse. Since the specimen constitutes a reduced version of EUCBUILD-1 (i.e. only the second floor and the roof have been built), the first-floor accelerations recorded in the test carried out by Graziotti et al. 2015 have been adopted as input at the base of the new building. Therefore, the actual horizontal longitudinal inputs were floor accelerograms of the EUCBUILD-1 subjected to incremental dynamic tests with two records: EQ1 and EQ2 representative of the dynamic characteristics of induced seismicity ground motions. The two original inputs correspond to two main scenarios with different return periods (scenario 1 and scenario 2), identified after a detailed study on the seismic hazard characteristics of the region (see Appendix B2 of Technical Report EUC318/2015U). In addition, the specimen prototype has been subjected also to combined horizontal and vertical motions. For this reason, two vertical components of the original records used for the EUCBUILD-1 (corresponding to scenario 1 and scenario 2), have been generated and compared with the vertical ground motions recorded in the Groningen field (see note “Selection of Vertical Acceleration Time-Series for Shake Table Testing of Groningen Masonry Building at LNEC”).

4.1 Shaking Table Input Sequence

The specimen has been subjected to two different types of base motion: i) dynamic identification tests using a sequence of impulsive responses of both the shaking table and the specimen by applying a displacement square wave, with 1 mm peak-to-peak amplitude and 0.1 Hz and ii) two-component earthquake records. As mentioned above, the horizontal components of the records were floor accelerograms recorded on the first floor of the specimen EUCBUILD-1; for practicality and to allow a better control of the shaking table performance, only the floor accelerograms produced by EQ1-100%, EQ1-150%, EQ2-100%, EQ2-150% and EQ2-200% were adopted as horizontal input components. These five floor accelerograms have been considered well representative of the progressive damage evolution occurring in the EUCBUILD-1 specimen allowing for a realistic comparison between the two tests; the selected vertical components, instead, were directly the EQ1 and EQ2 vertical motions scaled linearly at the considered level of intensity, assuming, hence, the first floor of the EUCBUILD-1 specimen as rigid in the vertical direction. Figure 4.1 presents the horizontal and vertical component acceleration histories of the adopted accelerograms.

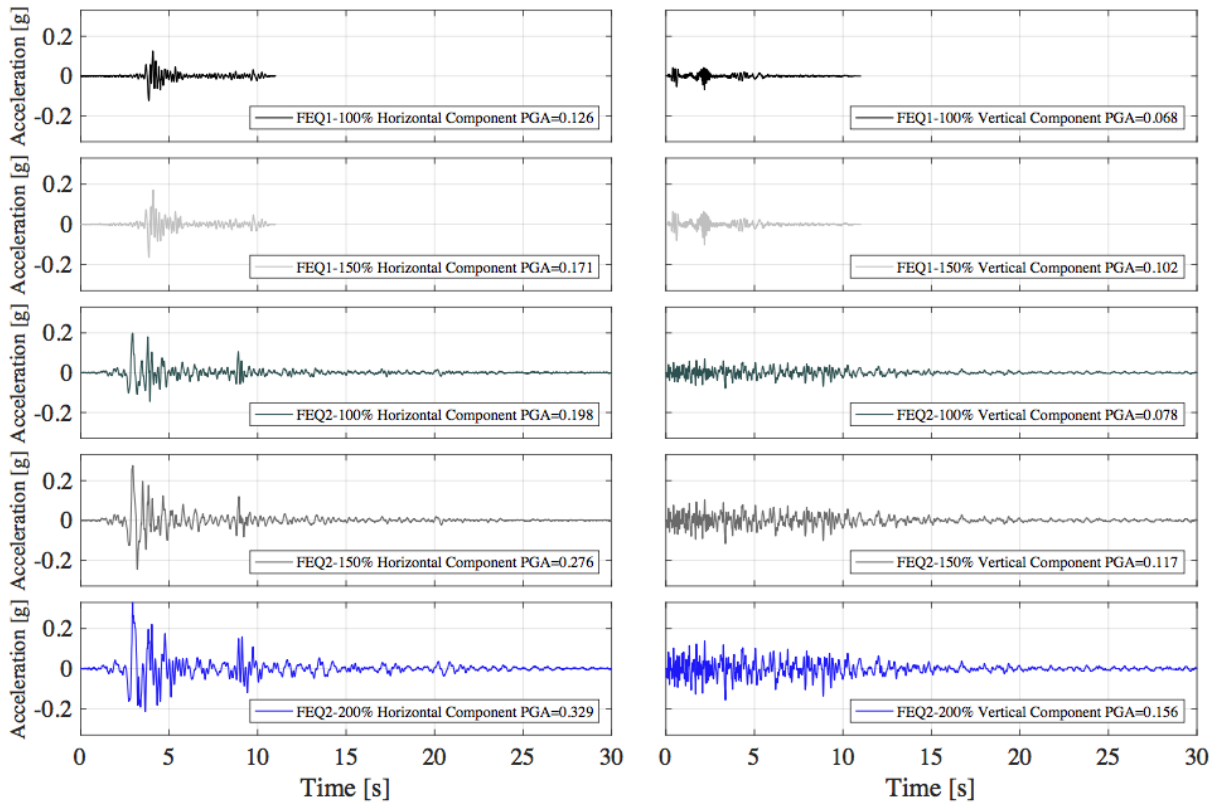


Figure 4.1 Theoretical horizontal and vertical components of the adopted accelerograms.

Figure 4.2 shows the 5% damped acceleration response spectrum of the selected experimental inputs, which reflect the induced seismicity input already filtered by the dynamics of the EUCBUILD-1 specimen and of the shaking table system of EUCENTRE.

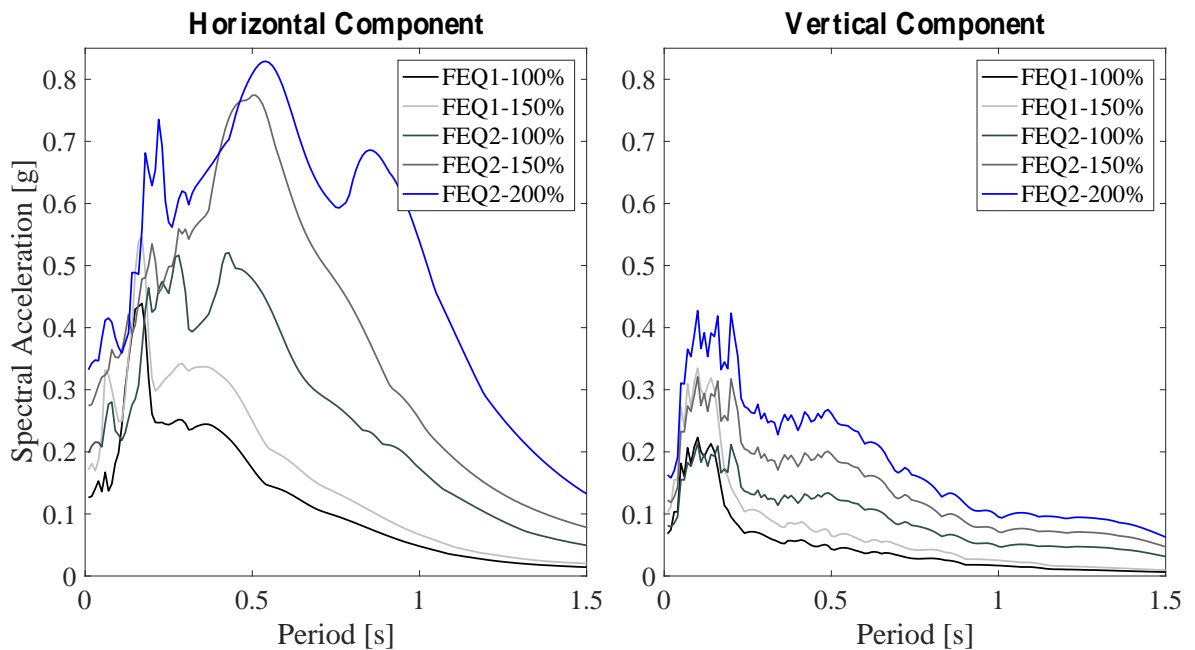


Figure 4.2 Theoretical horizontal and vertical 5% damped acc. response spectra of the experimental inputs.

The sequence of incremental tests followed strictly the one performed for EUCBUILD-1, increasing gradually the intensity of the ground motions and applying first FEQ1, followed by FEQ2. Table 4.1 presents the applied testing sequence specifying the input typology and the scaling factor characterising both motion components. Each test with increasing intensity was alternated by sequences of impulsive responses induced in the specimen (DPULSE), which, by means of a dynamic identification procedure, allowed the changes in the dynamic properties of the structure to be detected as the damage level increased. The incremental testing sequence stopped at test FEQ2-300% with the collapse of the East CS wall which failed out-of-plane.

Table 4.1 Applied testing sequence.

Test #	Test Name	Horizontal Input Component	Scaling Factor	Vertical Input Component	Scaling Factor
1	DPULSE-2.0	2.0 mm peak-to-peak displacement square wave	-	-	-
2	FEQ1-50%	1 st Floor Acc. of EUCBUILD-1 subjected to EQ1-100%	50%	EQ1-100% Vertical	50%
3	DPULSE-1.0	1.0 mm peak-to-peak displacement square wave	-	-	-
4	FEQ1-100%	1 st Floor Acc. of EUCBUILD-1 subjected to EQ1-100%	100%	EQ1-100% Vertical	100%
5	DPULSE-1.0	1.0 mm peak-to-peak displacement square wave	-	-	-
6	FEQ1-150%	1 st Floor Acc. of EUCBUILD-1 subjected to EQ1-150%	100%	EQ1-100% Vertical	150%
7	DPULSE-1.0	1.0 mm peak-to-peak displacement square wave	-	-	-
8	FEQ2-50%-COMP	1 st Floor Acc. of EUCBUILD-1 subjected to EQ2-100%	50%	EQ2-100% Vertical	50%
9	DPULSE-1.0	1.0 mm peak-to-peak displacement square wave	-	-	-
10	FEQ2-50%	1 st Floor Acc. of EUCBUILD-1 subjected to EQ2-100%	50%	EQ2-100% Vertical	50%
11	FEQ2-100%	1 st Floor Acc. of EUCBUILD-1 subjected to EQ2-100%	100%	EQ2-100% Vertical	100%
12	DPULSE-1.0	1.0 mm peak-to-peak displacement square wave	-	-	-
13	FEQ2-150%	1 st Floor Acc. of EUCBUILD-1 subjected to EQ2-150%	100%	EQ2-100% Vertical	150%
14	DPULSE-1.0	1.0 mm peak-to-peak displacement square wave	-	-	-
15	FEQ2-60%-COMP	1 st Floor Acc. of EUCBUILD-1 subjected to EQ2-200%	30%	EQ2-100% Vertical	60%
16	FEQ2-120%-COMP	1 st Floor Acc. of EUCBUILD-1 subjected to EQ2-200%	60%	EQ2-100% Vertical	120%
17	FEQ2-200%	1 st Floor Acc. of EUCBUILD-1 subjected to EQ2-200%	100%	EQ2-100% Vertical	200%
18	DPULSE-1.0	1.0 mm peak-to-peak displacement square wave	-	-	-
19	FEQ2-300%	1 st Floor Acc. of EUCBUILD-1 subjected to EQ2-200%	150%	EQ2-100% Vertical	300%

4.2 Characterisation of the induced ground motion tests

Table 4.2 presents the applied testing sequence specifying the floor motions and the following quantities:

- Nominal horizontal PGA;
- Nominal vertical PGA;
- Nominal horiz. spectral acceleration (5% damping) at the fundamental period, $Sa(T_1)$;
- Recorded horizontal PGA;
- Recorded vertical PGA;
- Calculated spectral acceleration (5% damping) at the fundamental period, $Sa(T_1)$;
- Recorded horizontal PGD;
- Recorded vertical PGD;
- Calculated horizontal PGV;
- Calculated vertical PGV.

Table 4.2 Summary of the floor motion testing sequence dynamic characteristics.

Test#-Test Name	Nom. H-PGA [g]	Nom. V-PGA [g]	Nom. Sa(T1) [g]	H-PGA [g]	V-PGA [g]	Sa(T1) [g]	H-PGD [mm]	V-PGD [mm]	H-PGV [mm/s]	V-PGV [mm/s]
2-FEQ1-50%	0.063	0.034	0.130	0.056	0.036	0.113	2.9	1.1	33.0	8.50
4-FEQ1-100%	0.126	0.068	0.261	0.119	0.075	0.249	5.5	2.2	66.3	26.6
6-FEQ1-150%	0.171	0.102	0.318	0.146	0.122	0.317	7.9	3.4	86.3	28.9
8-FEQ2-50%-C	0.099	0.039	0.213	0.137	0.054	0.280	10.7	3.8	73.5	22.9
10-FEQ2-50%	0.099	0.039	0.213	0.095	0.071	0.232	9.3	4.1	78.6	29.9
11-FEQ2-100%	0.198	0.078	0.425	0.218	0.100	0.540	20.7	7.8	141.4	45.3
13-FEQ2-150%	0.276	0.117	0.535	0.380	0.214	0.903	26.8	11.3	200.6	55.8
15-FEQ2-60%-C	0.099	0.047	0.189	0.129	0.045	0.232	12.2	4.5	88.7	24.3
16-FEQ2-120%-C	0.198	0.094	0.377	0.295	0.128	0.572	26.7	10.0	190.2	40.0
17-FEQ2-200%	0.330	0.156	0.629	0.393	0.184	0.736	40.1	14.2	272.7	66.5
19-FEQ2-300%	0.495	0.234	0.943	0.630	0.343	1.312	60.9	21.3	419.6	85.3

Further intensity measures characterising the input sequence are listed in Table 4.3:

- Calculated average spectral acceleration (5% damping) between the fundamental period one ($Sa(T_1)$, $T_1=0.20$ s) and the damaged period ($Sa(T_1)$, $T_1=0.25$ s), Sa_{av} ;
- Housner Intensity: defined as the integral of the pseudo-velocity elastic response spectrum between a structural period of 0.1 and 2.5 s:

$$HI(5\%) = \int_{0.1}^{2.5} PSV(5\%, T) dT \quad (13)$$

- Modified Housner Intensity: defined as the integral of the pseudo-velocity elastic response spectrum between a structural period of 0.1 and 0.5 s (which corresponds to the range of periods of interest for the tested specimen):

$$mHI(5\%) = \int_{0.1}^{0.5} PSV(5\%, T) dT \quad (14)$$

- Arias Intensity;
- Cumulative absolute velocity;
- Significant duration (5-95%);
- Significant duration (5-75%).

108 Collapse Shaking Table Test on URM Cavity Wall Structure representative of a Dutch Terraced House

Table 4.3 Summary of the floor motion dynamic characteristics.

Test#-Test Name	S _{av} [g]	HI [mm]	mHI [mm]	IA [mm/s]	CAV [mm/s]	SD _{5-75%} [s]	SD _{5-95%} [s]
2-FEQ1-50%	0.124	70.0	21.4	10.9	424.8	0.60	5.04
4-FEQ1-100%	0.260	132.0	42.2	46.3	859.4	0.59	5.00
6-FEQ1-150%	0.328	186.2	56.9	83.5	1218.5	0.81	5.92
8-FEQ2-50%-C	0.276	196.1	46.1	70.4	1608.6	1.74	6.67
10-FEQ2-50%	0.237	188.4	41.7	66.4	1834.6	3.3	10.16
11-FEQ2-100%	0.559	379.9	85.9	272	3308.5	2.09	7.55
13-FEQ2-150%	0.629	590.6	120.6	587.3	4307.2	1.57	6.32
15-FEQ2-60%-C	0.212	273.8	39.1	73.8	1881.4	2.21	10.59
16-FEQ2-120%-C	0.496	601.6	87.3	382.6	4147.5	2.46	9.02
17-FEQ2-200%	0.639	881.8	121.5	782	6185.3	2.67	10.54
19-FEQ2-300%	1.019	1345.3	185.1	1948.8	9777.4	3.76	10.45

5 TEST RESULTS

5.1 Specimen dynamic identification

5.1.1 Introduction and methodology

Many signals are appropriate for use in experimental modal analysis, such as random white noise vibration or impulsive signals. In the estimation of frequency response functions, the choice depends upon the characteristics of the system, the theory underlying the parameter estimation and the expected utilization of the data. Different types of excitation signals have their own characteristics and some are more suited for some goals than others.

In the LNEC shaking table test, deterministic step signals (rectangular pulses) are usually adopted for estimating the frequency response functions (FRFs) based on input-output relationships, since they provide a good coherence between input and output signals in a range from 0.1 Hz up to 40 Hz. Those signals are used either for characterisation of the entire test system (shaking table + specimen) used in the adaptive tuning process of the desired target signals to be imposed in the shaking table, or for a dynamic identification of the specimen (on the shaking table). In this last case, the FRFs are used to quantify the specimen dynamic characteristics along the testing stages as a means to assess its damage evolution (decrease of natural frequencies and increase of modal damping).

The properties of the step signals that are used in the LNEC shaking table for characterisation of the dynamic properties of the entire system are the following:

- Amplitude: 0.5 mm to 5 mm, depending on the type of structure and the quality of the digital signals assessed by the signal-to-noise ratio (SNR);
- Number of pulses: 36;
- Time before the first impulse: 5 seconds;
- Time interval between pulses: 10 seconds;
- Total duration: 360 seconds.

The dynamic identification through the impulsive responses is obtained from the acceleration histories shown in Figure 5.1. The FRFs are computed by LNEC-SPA (Mendes and Campos Costa 2007) taking into account the single-input / multi-output relations (SIMO) between the acquired signals. Figure 5.2 represents one of those functions obtained from the impulsive tests in the horizontal direction and for one output channel.

From the point of view of damage assessment, measured through the changes in the FRFs along the entire test protocol, it is important to use always the same type and amplitude of the input signals in order to be able to compare compatible results.

The estimation of the complex FRF $H_i(f)$ is done, according to the method described in Bendat et al. (2010), by the following formula:

$$H_i(f) = \frac{G_{xy_i}(f)}{G_{xx}(f)} \quad (15)$$

where x stands for shaking table input acceleration in each direction independently, y_i a given response acceleration at any location and direction on the structure, $G_{xy_i}(f)$ is the cross spectral density estimate between input and output signals and $G_{xx}(f)$ is the auto spectrum density estimate of the input signal.

The coherency function, which measures the quality of the transfer function, is computed as:

$$\gamma_{xy_i}^2(f) = \frac{|G_{xy_i}(f)|^2}{G_{xx}(f)G_{y_iy_i}(f)} \quad (16)$$

110 Collapse Shaking Table Test on URM Cavity Wall Structure representative of a Dutch Terraced House

where $G_{y_i y_i}(f)$ is the auto spectrum density estimate of the output signal. For a given frequency f , the closest the coherency function is to one the more related is the input to the output signals.

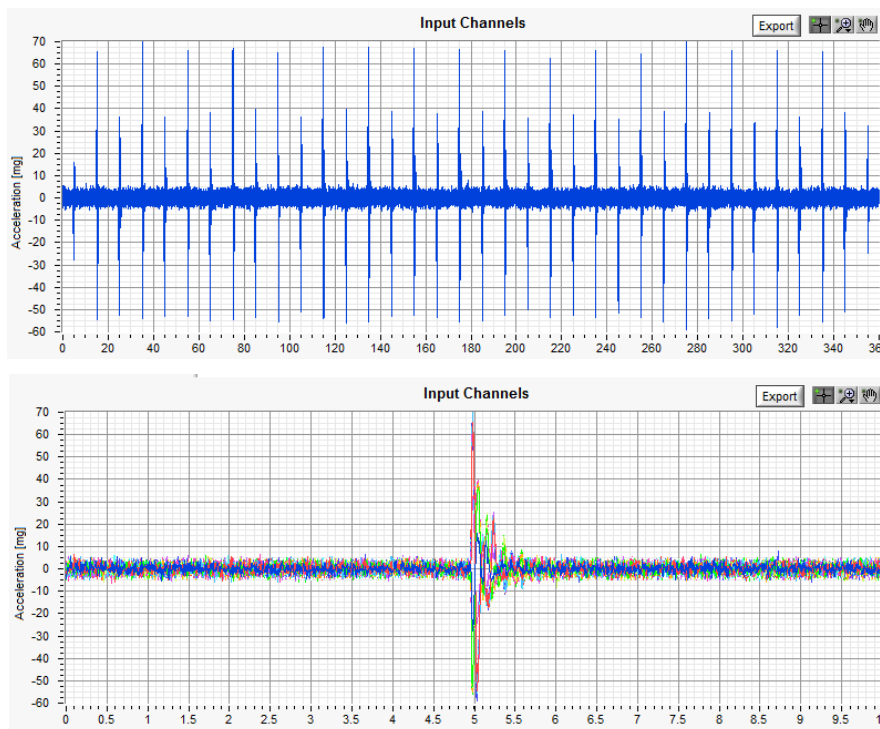


Figure 5.1 Input acceleration history for the impulsive loading (above) and average input (below).

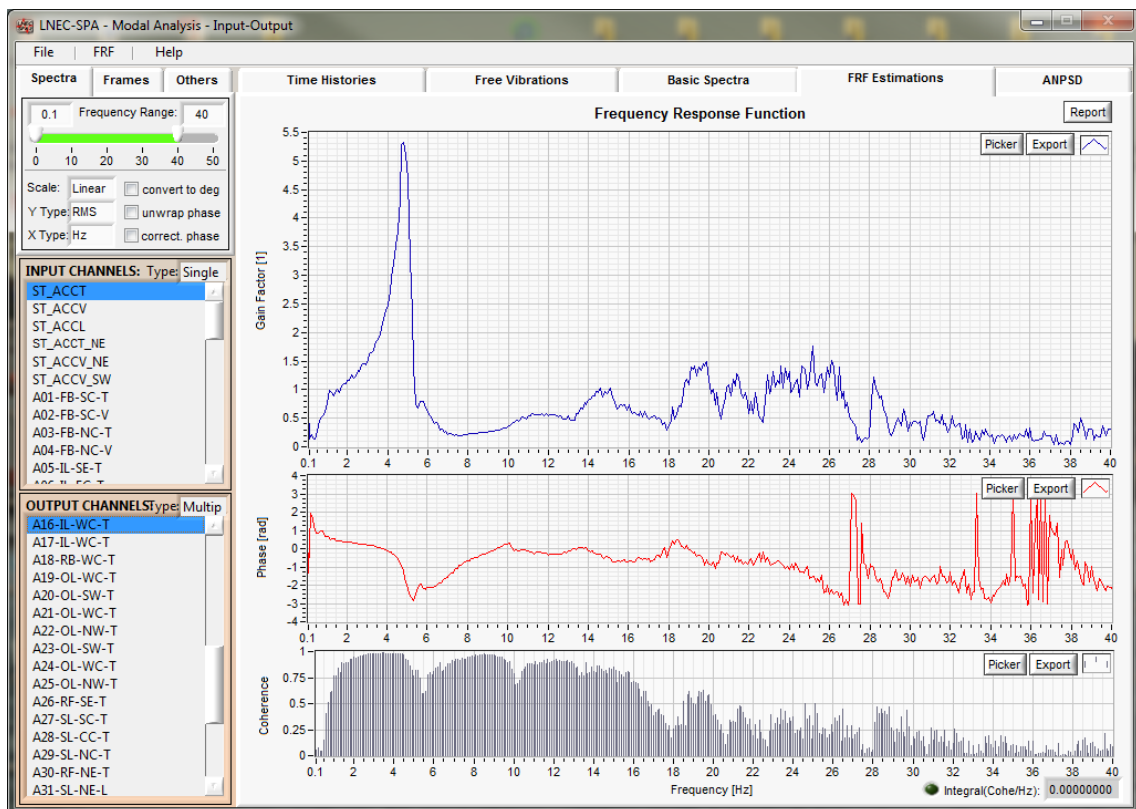


Figure 5.2 Frequency response function from rectangular impulses in the horizontal direction.

In the following sections, the methods used to estimate the natural frequencies, modal damping values and mode shapes are briefly introduced.

5.1.1.1 Frequency-Domain Decomposition method (FDD)

The FDD method is based on the diagonalization of the spectral response density matrices, in order to decompose them into the modal contributions at each frequency. The diagonalization can be done through the Singular Value Decomposition (SVD) of each of the datasets. This decomposition corresponds to a single degree of freedom identification of the system for each singular value. This method can be described as:

- i. The structural response can be defined in modal coordinates and obtained from the sum of the contributions of the modes of vibration, through:

$$y(t) = \Phi q(t) \quad (17)$$

where Φ is the matrix containing the configuration of the vibration modes, ordered by columns, and q is the vector of modal coordinates;

- ii. The matrix of auto-correlation response functions can be calculated using:

$$C_{yy}(\tau) = E\{y(t + \tau)y(t)^T\} \quad (18)$$

- iii. Introducing (1) in the previous equation:

$$C_{yy}(\tau) = E\{\Phi q(t + \tau)q(t)^H \Phi^H\} = \Phi C_{qq}(\tau) \Phi^H \quad (19)$$

where $(.)^H$ represents the conjugate transposed operator for Hermitian matrices. The previous equation indicates that the matrix of the vibration modes' configurations allows to relate the matrices of the auto-correlation functions of the response and the auto-correlation functions, written in modal coordinates;

- iv. Applying the Fourier transform to the previous equation in the frequency domain yields:

$$G_{yy}(f) = \Phi G_{qq}(f) \Phi^H; \quad (20)$$

For uncorrelated modal coordinates, G_{qq} is a diagonal matrix and the modes of vibration present in the columns of Φ are orthogonal, concluding that the previous expression is similar to the one resulting from the decomposition into singular values:

$$SVD(A) = U(f) S U(f)^H = [\{u_i(f)\}, \dots] \begin{bmatrix} \ddots & & \\ & S_i & \\ & & \ddots \end{bmatrix} [\{u_i(f)\}, \dots]^H \quad (21)$$

where the matrix S is a diagonal real matrix with the singular values in descending order and has a representation along the various frequencies of the type indicated in Figure 5.3. It presents peaks coincident with the vibration modes and other dynamic phenomena that may introduce concentrated vibrations in a given frequency, for example rotary machines. The matrix U is of the complex type and contains in its columns the orthogonal vectors which are estimates of the modal configurations for each mode of vibration identified. It should be noted that when using the SVD algorithm, the matrix U depends on the frequency due to the rearrangement of the singular values involved in the algorithm.

112 Collapse Shaking Table Test on URM Cavity Wall Structure representative of a Dutch Terraced House

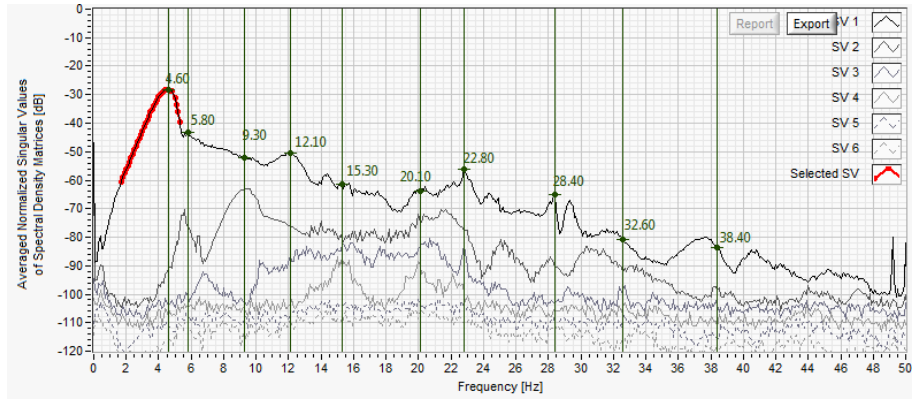


Figure 5.3 Representation of the Singular Values matrix.

5.1.1.2 Enhanced Frequency-Domain Decomposition method (EFDD)

The Enhanced Frequency-Domain Decomposition method (EFDD), proposed by Brincker et al. 2001, which provides estimates of modal damping and better estimates of vibration frequencies than the FDD method, was also used. This method consists of making an adjustment to the auto-correlation functions of a single degree of freedom, obtained from the functions of spectral density, selecting through a chosen criterion and weighing a set of points in the vicinity of each resonance, and finally applying the inverse of the Fourier transform. The criteria used in this method consists in defining a limit value of the MAC coefficient (Modal Assurance Criterion) which takes values between 0 and 1, obtaining the unit value when the vibration modes have the same configuration and null value when they are orthogonal.

This method allows more accurate estimates of the vibration frequencies, since it is based on the adjustment to the zero-crossings of the auto-correlation function and not only on a peak value, which can be influenced by several factors such as frequency resolution. The modal damping can be obtained from the logarithmic decrement of the impulse response function, as shown in Figure 5.4.

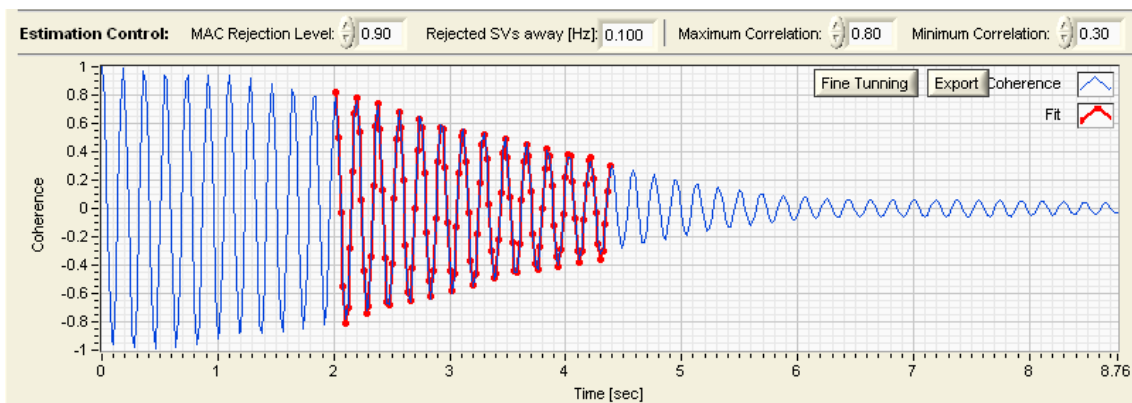


Figure 5.4 Frequency estimate (zero-crossings) and damping (logarithm decrement) of the impulse response estimate.

The numerical correlation of the mode shape vectors of the undamaged state of the model and the subsequent damaged states can also be obtained by computing the abovementioned MAC coefficient as shown in the equation below.

$$MAC_{u,d} = \frac{|\sum_{i=1}^n \varphi_i^u \varphi_i^d|^2}{\sum_{i=1}^n (\varphi_i^u)^2 \sum_{i=1}^n (\varphi_i^d)^2} \quad (22)$$

where φ^u is the mode shape vector corresponding to the undamaged condition of the model, φ^d is the mode shape vector corresponding to the damaged condition of the model and n is the number of estimated degrees of freedom (Allemang et al. 1982). The result of this expression is a scalar value in the range of 0 and 1 and indicates the extent of correlation between the two cases.

5.1.2 Dynamic identification results

Previously to moving the specimen onto the shaking table, there were two occasions when dynamic identification tests were performed: upon the removal of the temporary support of the slab and before lifting the model. The dynamic identification results of these two occasions are presented in the following two sections, while the dynamic identification for impulsive responses on the shaking table are presented afterwards.

5.1.2.1 Removal of slab temporary support

Two weeks after placing the reinforced concrete slab on the load bearing walls, its temporary support was removed and the bed joint at the top of the walls with openings was filled with fresh mortar, as depicted in Figure 5.5.



Figure 5.5 Joints filled with mortar.

As mentioned before, the weight of the slab is intended to be supported by the CS walls without openings only. When the temporary support of the slab was removed, the mortar layers at the connection of the slab to the blind walls had already hardened, but no additional vertical loads were applied to those walls other than their dead weight.

A simple dynamic characterisation test was performed during this operation in order to understand the influence of the vertical stresses due to the weight of the slab on the out-of-plane stiffness of the blind walls. A hammer instrumented with an accelerometer was used to input periodic excitation pulses at mid-height of the East and West blind walls and at about one-third of their horizontal span, as shown in Figure 5.6. The output of this excitation was measured by accelerometers positioned at the centre of the load-bearing walls, see Figure 5.7.

Regarding the East side, where only a CS brick wall exists, Figure 5.8 exhibits the FRF before the removal of the temporary support in both decibel and linear scales and indicates a frequency of vibration for the first out-of-plane mode of the wall around 27.4 Hz. This value should be compared with the one depicted in Figure 5.9, after the removal of the temporary support, which corresponds to 31.0 Hz.

114 Collapse Shaking Table Test on URM Cavity Wall Structure representative of a Dutch Terraced House



Figure 5.6 Instrumented hammer and application of periodic excitation pulses.



Figure 5.7 Accelerometers at the centre of the load-bearing walls.

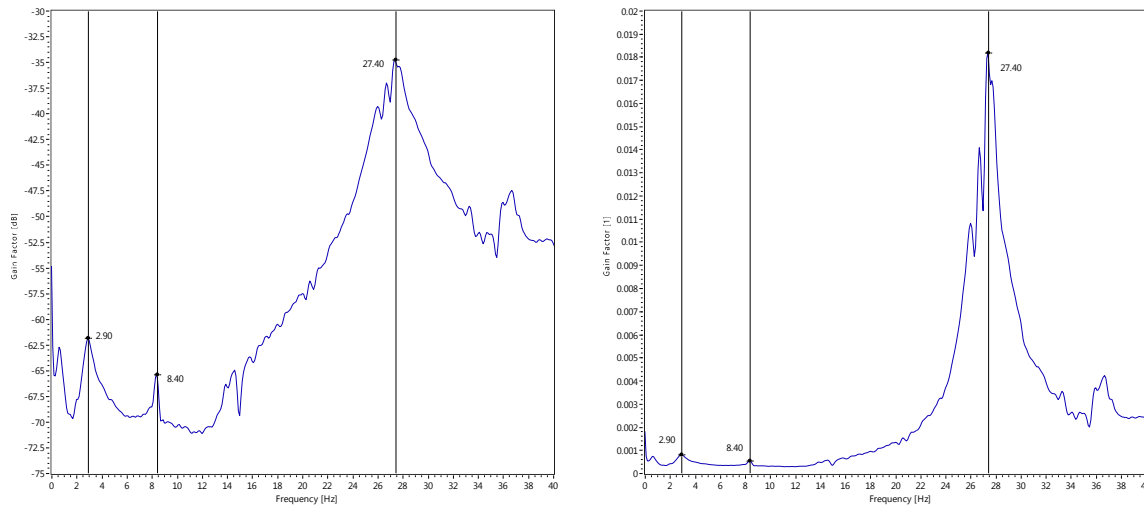


Figure 5.8 Frequency response function of East wall in decibel scale (left) and in linear scale (right), before removing the temporary support.

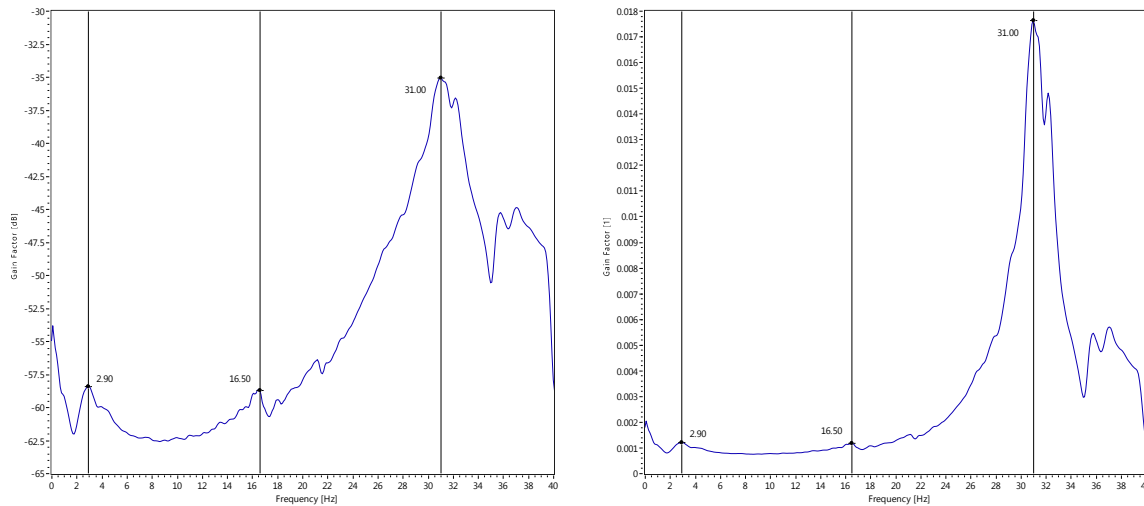


Figure 5.9 Frequency response function of East wall in decibel scale (left) and in linear scale (right), after removing the temporary support.

This increase of the eigen-frequency corresponds to an increased stiffness of the wall, regarding this out-of-plane mode, which should be attributed to the increased vertical stresses on the wall. These stresses increase the confinement of the wall and of any micro-cracks that may possibly exist. It should be noted that the added mass of the slab is not expected to be affecting this local out-of-plane mode of vibration of the East wall.

In what concerns the West wall, it should first be noted that the slab rests on the inner wall only and that this wall is connected to the veneer wall by steel ties – the density of which is about 2 ties/m². The initial characterisation, presented in Figure 5.10, points to an eigen-frequency of the first out-of-plane mode of vibration of the order of 25.9 Hz. A second mode of vibration, with a nodal point at the position of the accelerometer, is apparent at the anti-resonance value of 33.2 Hz.

The interpretation of the FRF after the temporary support removal, shown in Figure 5.11, is not as straightforward and would require the use of further measurement points to make it more assertive. In fact, the highest peak in the new FRF corresponds to a frequency of 48.9 Hz which is almost twice the one of the previous FRF. If it corresponded to the same mode of vibration of the wall, it would imply that a very significant stiffening effect took place.

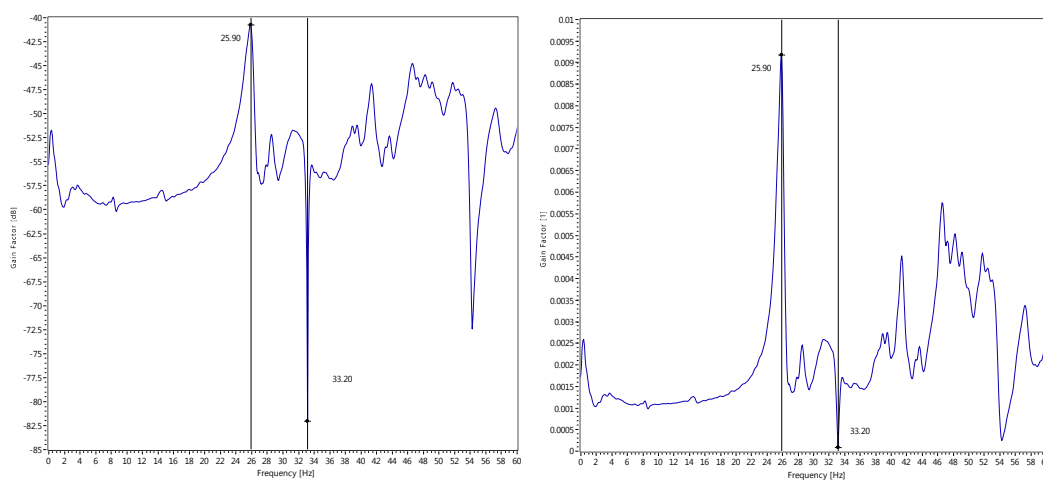


Figure 5.10 Frequency response function of West wall in decibel scale (left) and in linear scale (right), before removing the temporary support.

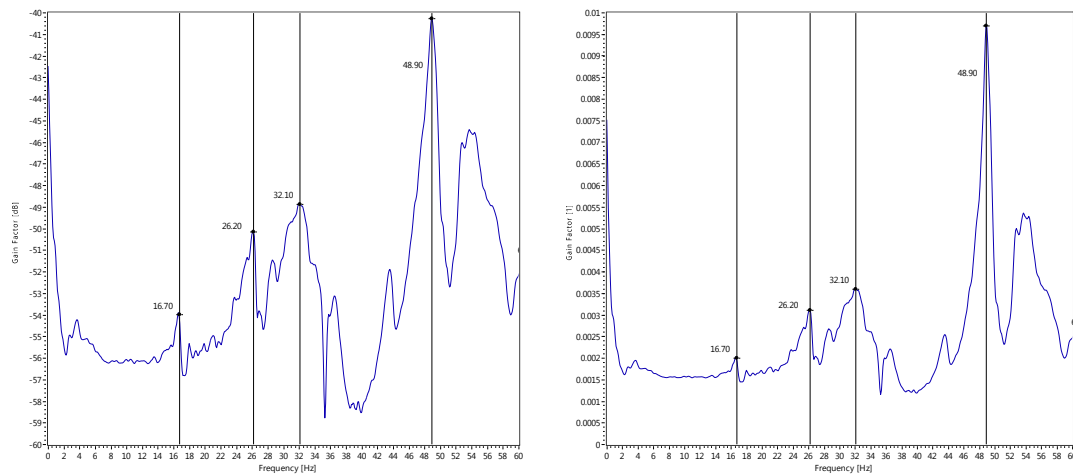


Figure 5.11 Frequency response function of West wall in decibel scale (left) and in linear scale (right), after removing the temporary support.

It is possible that the initial frequency represents a mode of vibration involving the load bearing wall only, with a small participation of the veneer wall due to a possible lack of transmission of forces through the steel ties – the frequency of 25.9 Hz is similar to the one of the East wall prior to removing the temporary support. It is also possible that, after removing the temporary support, the steel ties at the load bearing wall become more confined and force a composite behaviour of both the inner and outer walls. Additionally, from the tests performed on the wallettes, it was shown that the stiffness of the veneer walls is larger than that of the inner walls. But, with twice the mass involved in such mode shape, it would require an increase of the cavity wall stiffness by a factor of almost eight to justify the new frequency of 48.9 Hz, which seems too large an increase.

On the other hand, it is also possible that this new peak frequency corresponds to a higher mode of vibration and that the first mode of vibration of the cavity wall is the more highly damped one appearing around 32.1 Hz.

5.1.2.2 Ambient vibrations on the laboratory floor

Prior to moving the model to the shaking table, a dynamic identification was performed with a reduced set of accelerometers, based on ambient vibrations. These were assimilated to a broad frequency random noise, resulting in the FDD results depicted in Figure 5.12 and the EFDD results in Figure 5.13.

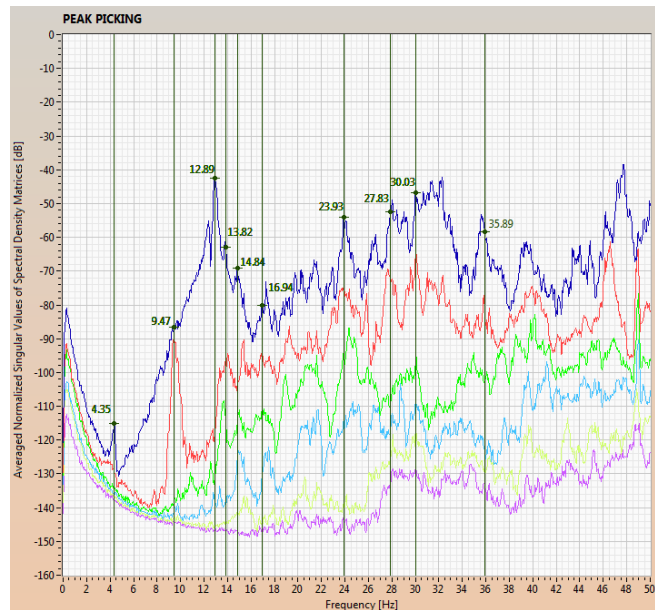


Figure 5.12 Frequency-domain decomposition results for dynamic identification on the laboratory floor.

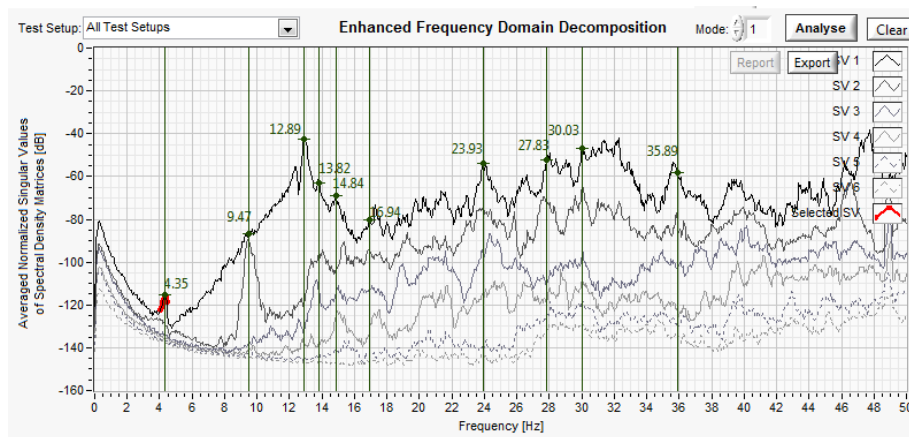


Figure 5.13 Enhanced frequency-domain decomposition results for dynamic identification on the laboratory floor.

The estimated frequency and damping values for the initial three modes of vibration are given in Table 5.1, with similar results for the two methodologies in terms of the eigen-frequencies. The EFDD also allows having a rough assessment of the modal damping values. It should be noted that these frequency and damping estimates correspond to very small amplitudes of vibration and are somewhat influenced by the fact that the laboratory floor where the model was built is not a foundation slab and is far from being a rigid one.

Table 5.1 Summary of vibration modes' characteristics for dynamic identification on the laboratory floor.

Mode	FDD Frequency [Hz]	EFDD Frequency [Hz]	Damping [%]
1	4.35	4.31	3.34
2	9.47	9.62	3.45
3	12.89	12.98	1.21

118 Collapse Shaking Table Test on URM Cavity Wall Structure representative of a Dutch Terraced House

The first mode shape for both methodologies is represented in Figure 5.14 and in Figure 5.15.

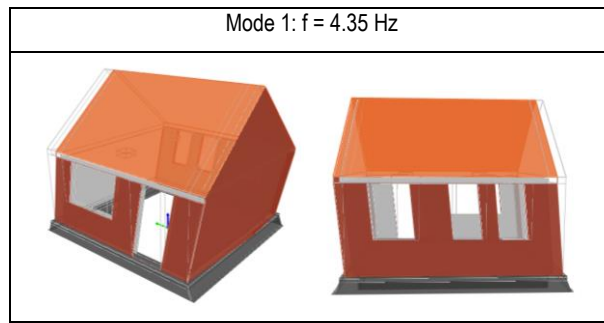


Figure 5.14 FDD mode shapes for dynamic identification on the laboratory floor.

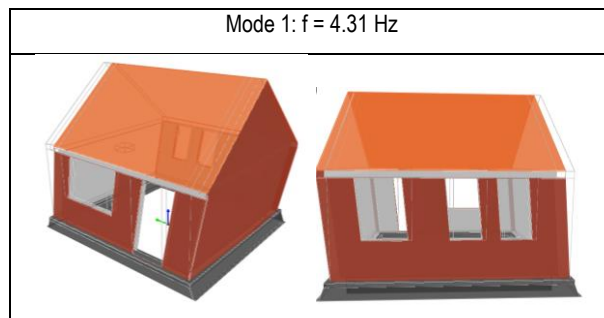


Figure 5.15 EFDD mode shapes for dynamic identification on the laboratory floor.

5.1.2.3 1st dynamic identification (Test 1)

After transportation and positioning of the model on the shaking table, Figure 5.16, a dynamic identification test was performed using the impulsive motion DPULSE-2.0. The accelerometer setup for modal animation of the vibration modes is depicted in Figure 5.17. The FDD results are shown in Figure 5.18, while the EFDD results are presented in Figure 5.19.



Figure 5.16 Test specimen on the shaking table.

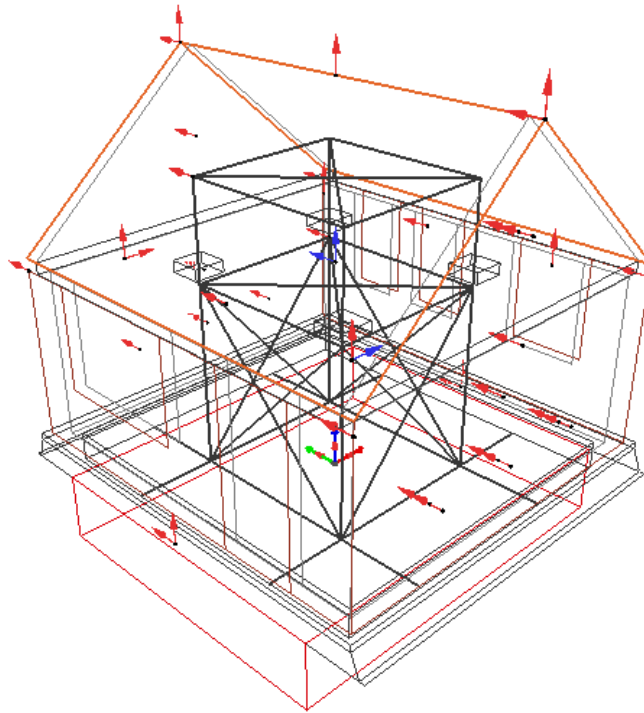


Figure 5.17 3D view of the accelerometers setup for dynamic identification.

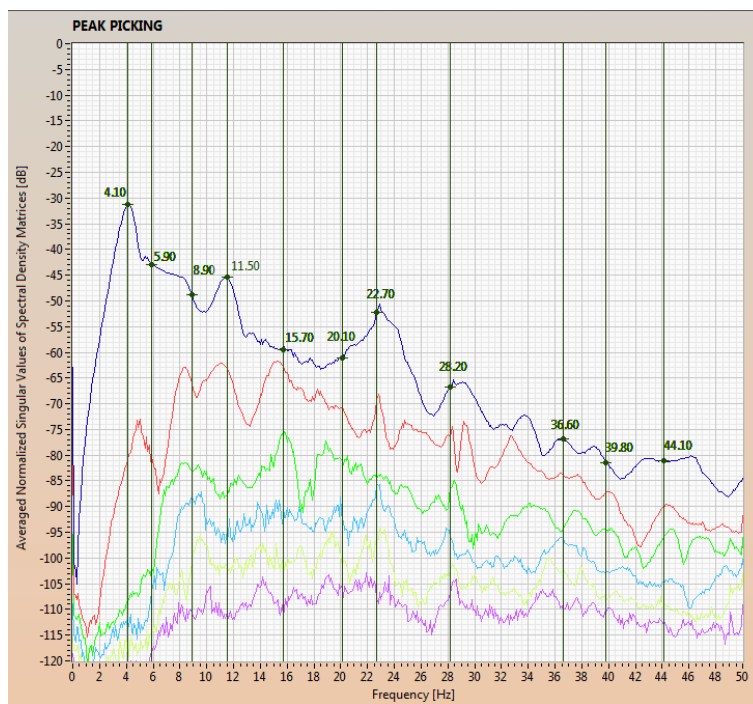


Figure 5.18 FDD results for 1st dynamic identification (Test 1).

120 Collapse Shaking Table Test on URM Cavity Wall Structure representative of a Dutch Terraced House

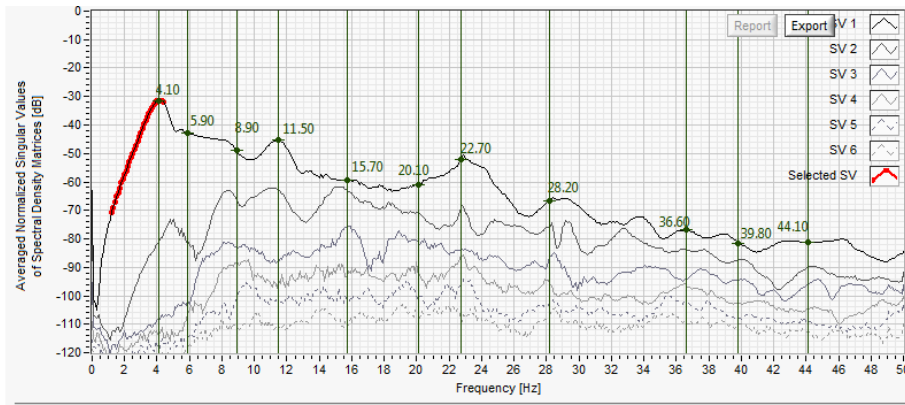


Figure 5.19 EFDD results for 1st dynamic identification (Test 1).

It is important to note that there is a new frequency appearing between the first and second ones detected in the ambient vibration modal identification. This is absolutely natural since the shaking table system is in itself a flexible system which affects the mode shapes, frequencies and damping values of the specimen, as summarised in Table 5.2 and in both Figure 5.20 and Figure 5.21. Hence, the system now presents a first mode of vibration where the shaking table is moving to one side and the model to the other side, while the second mode of vibration corresponds to both the model and the shaking table moving in the same direction. The MAC coefficients relating the mode shapes are presented in Table 5.3.

Despite the apparent decrease in the modal frequencies with respect to the ambient vibration dynamic identification, they should not be directly compared for two reasons. The first reason is that the impulsive response for motion DPULSE-2.0 is much larger than the one for ambient vibrations. In fact, the impulsive motion was reduced in subsequent dynamic identifications in order not to damage the model unnecessarily. The second reason was already mentioned and corresponds to a different dynamic of the specimen on the laboratory floor or on a dynamic system as the shaking table.

Table 5.2 Summary of vibration modes' characteristics for 1st dynamic identification (Test 1).

Mode	FDD Frequency [Hz]	EFDD Frequency [Hz]	Damping [%]
1	4.10	4.11	4.31
2	5.90	5.88	4.39
3	8.90	8.93	1.57
4	11.50	11.45	1.82
5	15.70	15.75	1.35

Table 5.3 MAC coefficients for 1st dynamic identification (Test 1).

MODE_i_j		MODE_01_01	MODE_02_01	MODE_03_01	MODE_04_01	MODE_05_01
	Frequency [Hz]	4.1	5.9	8.9	11.5	15.7
MODE_01_01	4.1	1.00	0.91	0.58	0.35	0.43
MODE_02_01	5.9	0.91	1.00	0.61	0.34	0.35
MODE_03_01	8.9	0.58	0.61	1.00	0.62	0.40
MODE_04_01	11.5	0.35	0.34	0.62	1.00	0.57
MODE_05_01	15.7	0.43	0.35	0.40	0.57	1.00

i Mode

j dynamic identification

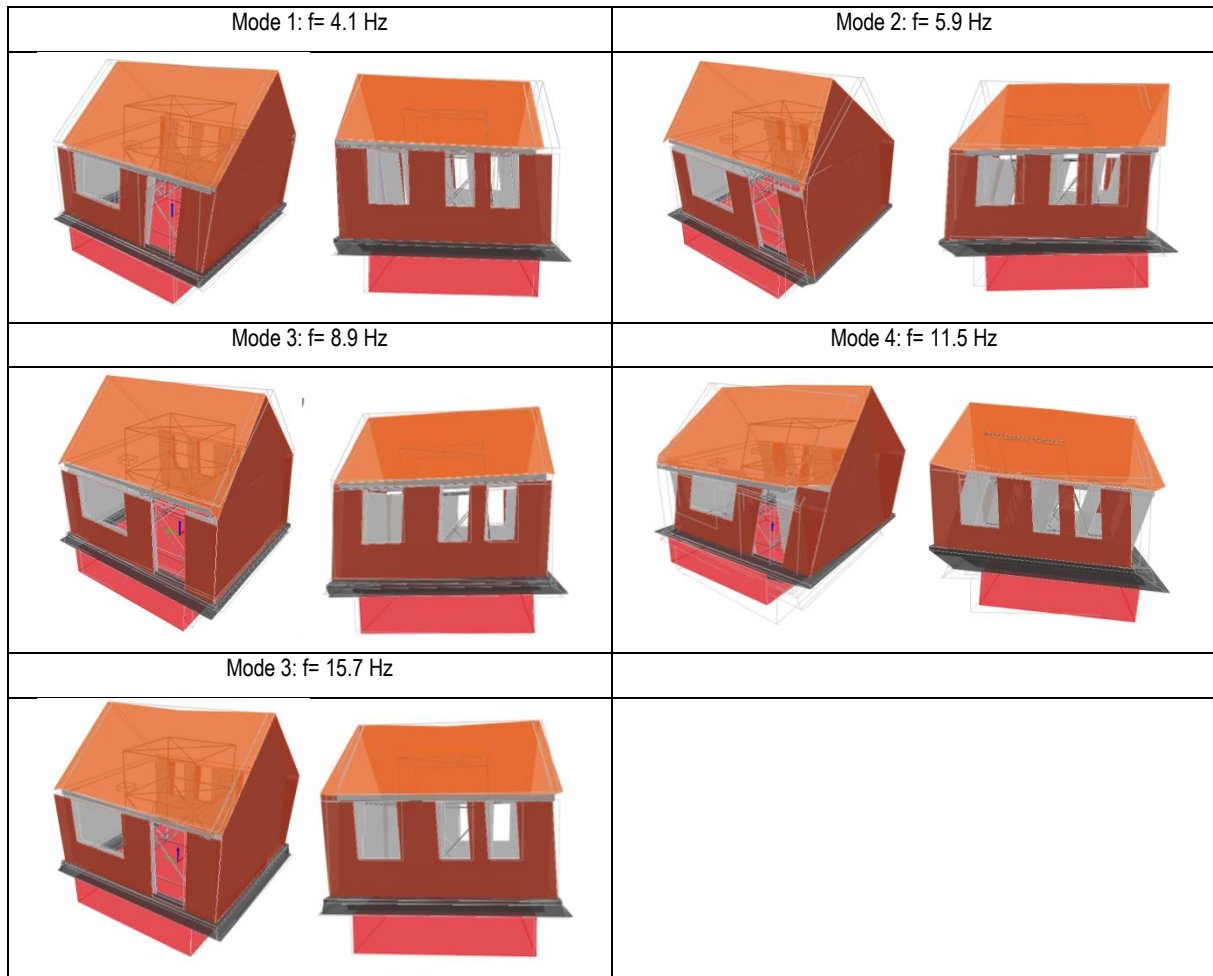


Figure 5.20 FDD mode shapes for 1st dynamic identification (Test 1).

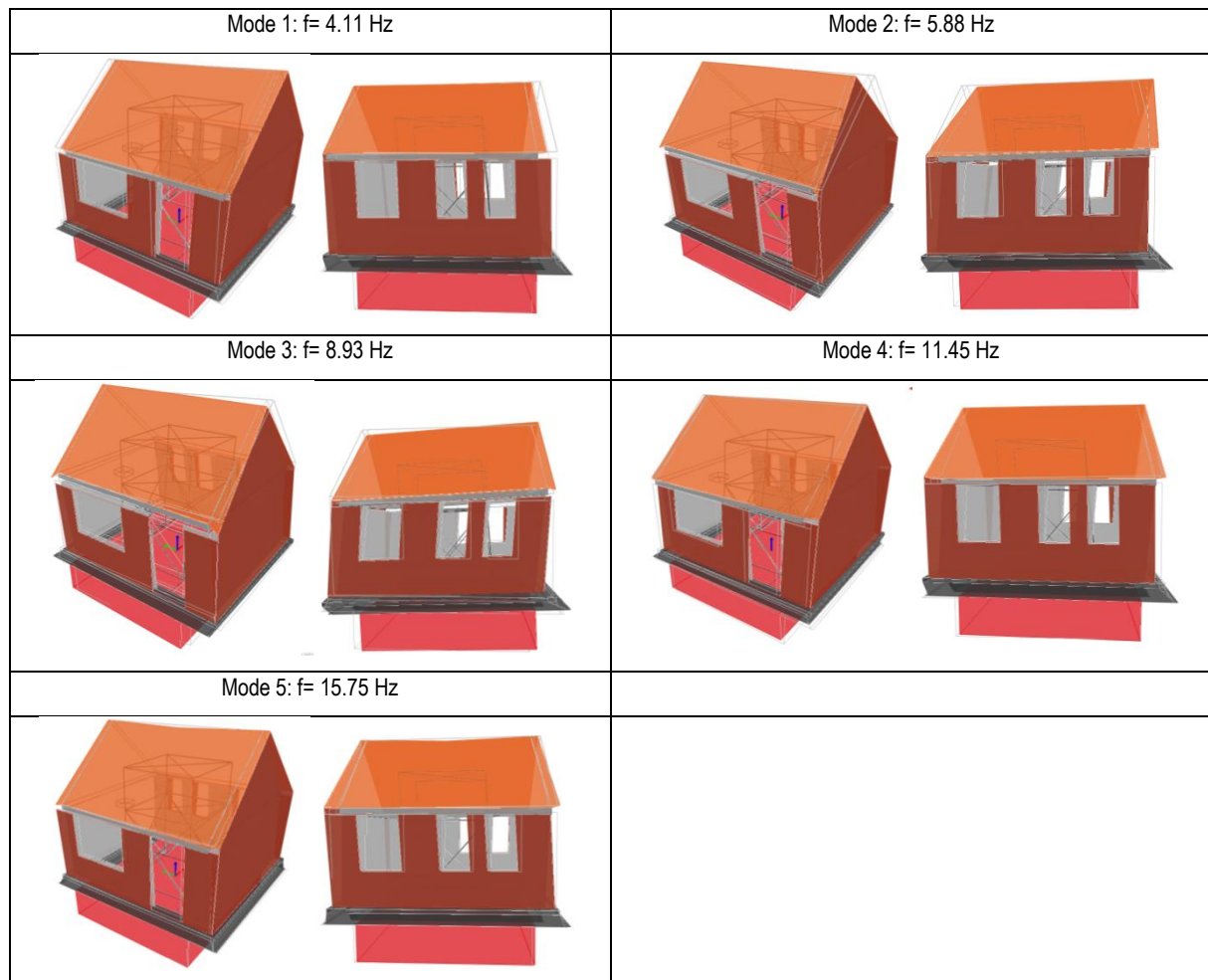


Figure 5.21 EFDD mode shapes for 1st dynamic identification (Test 1).

The first vibration mode presents a configuration where the model and the shaking table move in phase in the longitudinal direction, while the second mode shows an opposite phase motion between the top of the building specimen, going to one side, and the shaking table and base of the model, moving to the opposite side. The third mode is a longitudinal mode also involving some motion of the shaking table.

The fourth mode is essentially a longitudinal mode with a configuration where the outer walls move in opposite phase with respect to the inner walls. Finally, the fifth mode is again a longitudinal mode, but now involving some vertical motion at mid-span of the ridge beam.

5.1.2.4 2nd dynamic identification (Test 3)

This dynamic identification test, and all of the following, was performed using the impulsive motion DPULSE-1.0, with half the amplitude of the previous one. For a smaller amplitude, it is expected to have relatively larger values of the modal frequencies, as represented in Figure 5.22, Figure 5.23 and Table 5.4, since the secant stiffness of the specimen is slightly larger.

The value obtained for the fundamental mode of vibration shows that, although during the specimen transportation to the shaking table some small cracking appeared in the model, such damage is not reflected in its overall dynamic characteristics. Moreover, the first seismic test FEQ1-50% also did not introduce any visible damage on the structure.

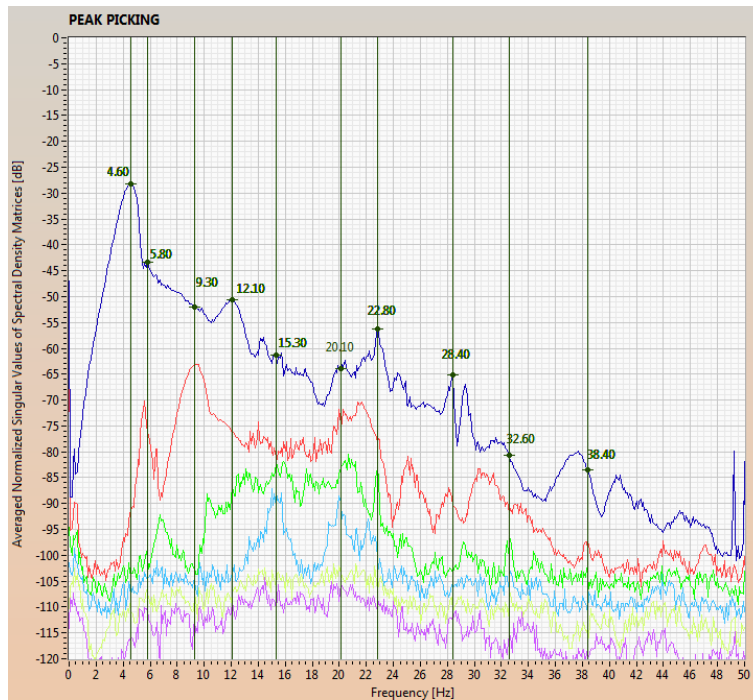


Figure 5.22 FDD results for 2nd dynamic identification (Test 3).

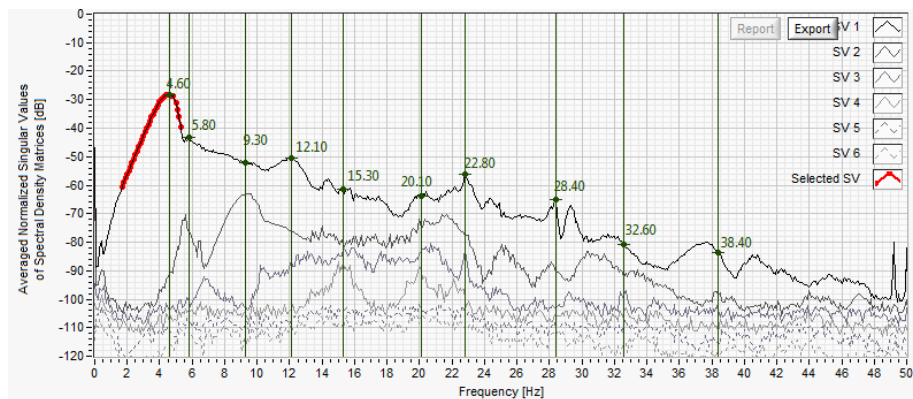


Figure 5.23 EFDD results for 2nd dynamic identification (Test 3).

Table 5.4 Summary of vibration modes' characteristics for 2nd dynamic identification (Test 3).

Mode	FDD Frequency [Hz]	EFDD Frequency [Hz]	Damping [%]
1	4.50	4.46	4.25
2	5.80	5.83	3.55
3	9.30	9.29	1.94
4	12.10	12.14	1.75
5	15.30	15.29	1.16

124 Collapse Shaking Table Test on URM Cavity Wall Structure representative of a Dutch Terraced House

The MAC coefficients relating the mode shapes between themselves for this second dynamic identification test are presented in Table 5.5. These mode shapes will be used from now on as the reference mode shapes for computing the evolution of the MAC coefficients in subsequent dynamic identification tests.

Table 5.5 MAC coefficients for 2nd dynamic identification (Test 3).

MODE i_j		MODE_01_02	MODE_02_02	MODE_03_02	MODE_04_02	MODE_05_02
	Frequency [Hz]	4.5	5.8	9.3	12.1	15.3
MODE_01_02	4.5	1.00	0.92	0.61	0.40	0.56
MODE_02_02	5.8	0.92	1.00	0.58	0.33	0.46
MODE_03_02	9.3	0.61	0.58	1.00	0.75	0.72
MODE_04_02	12.1	0.40	0.33	0.75	1.00	0.82
MODE_05_02	15.3	0.56	0.46	0.72	0.82	1.00

i Mode

j dynamic identification

The mode shapes obtained from FDD and EFDD are shown in Figure 5.24 and Figure 5.25, respectively.

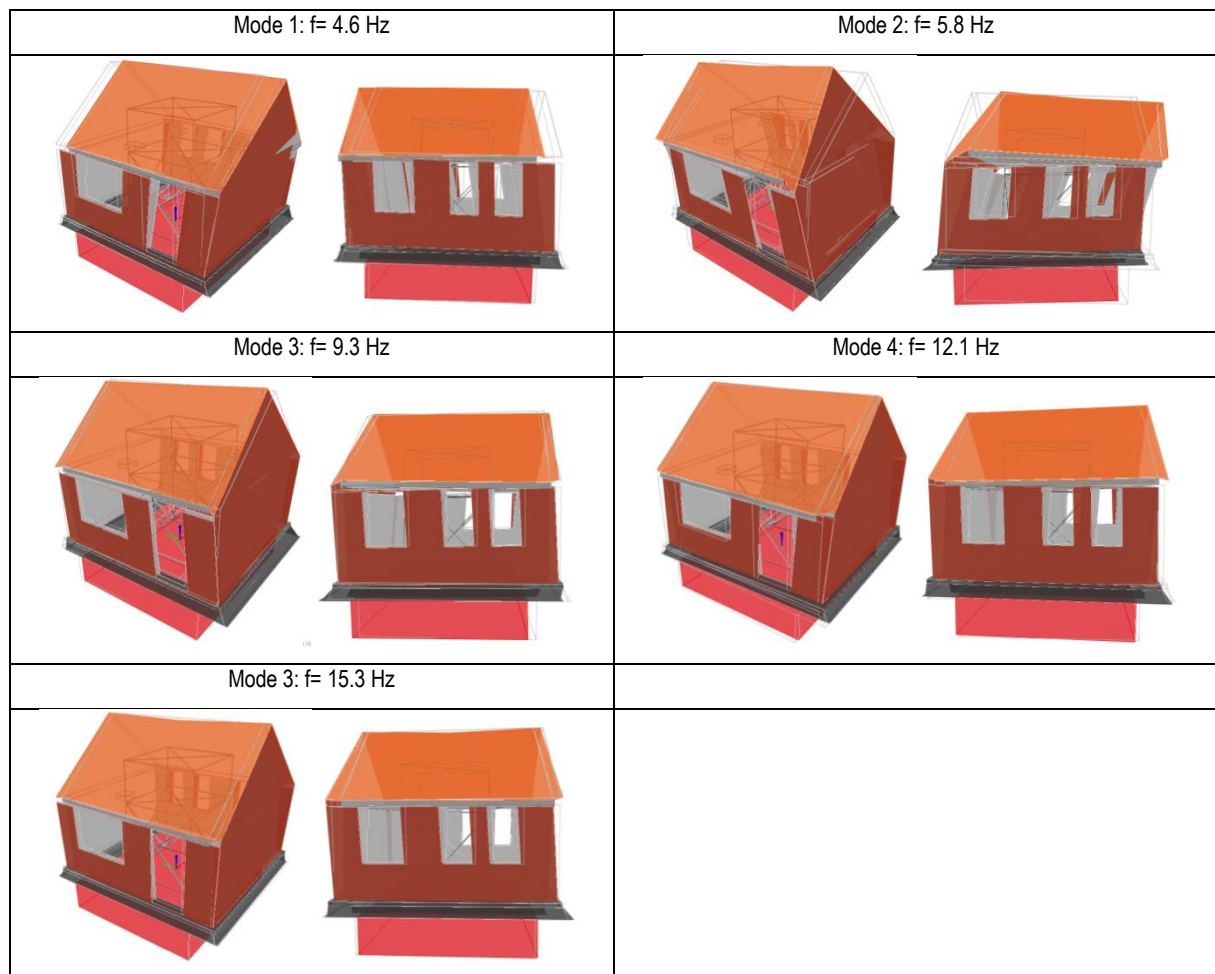


Figure 5.24 FDD mode shapes for 2nd dynamic identification (Test 3).

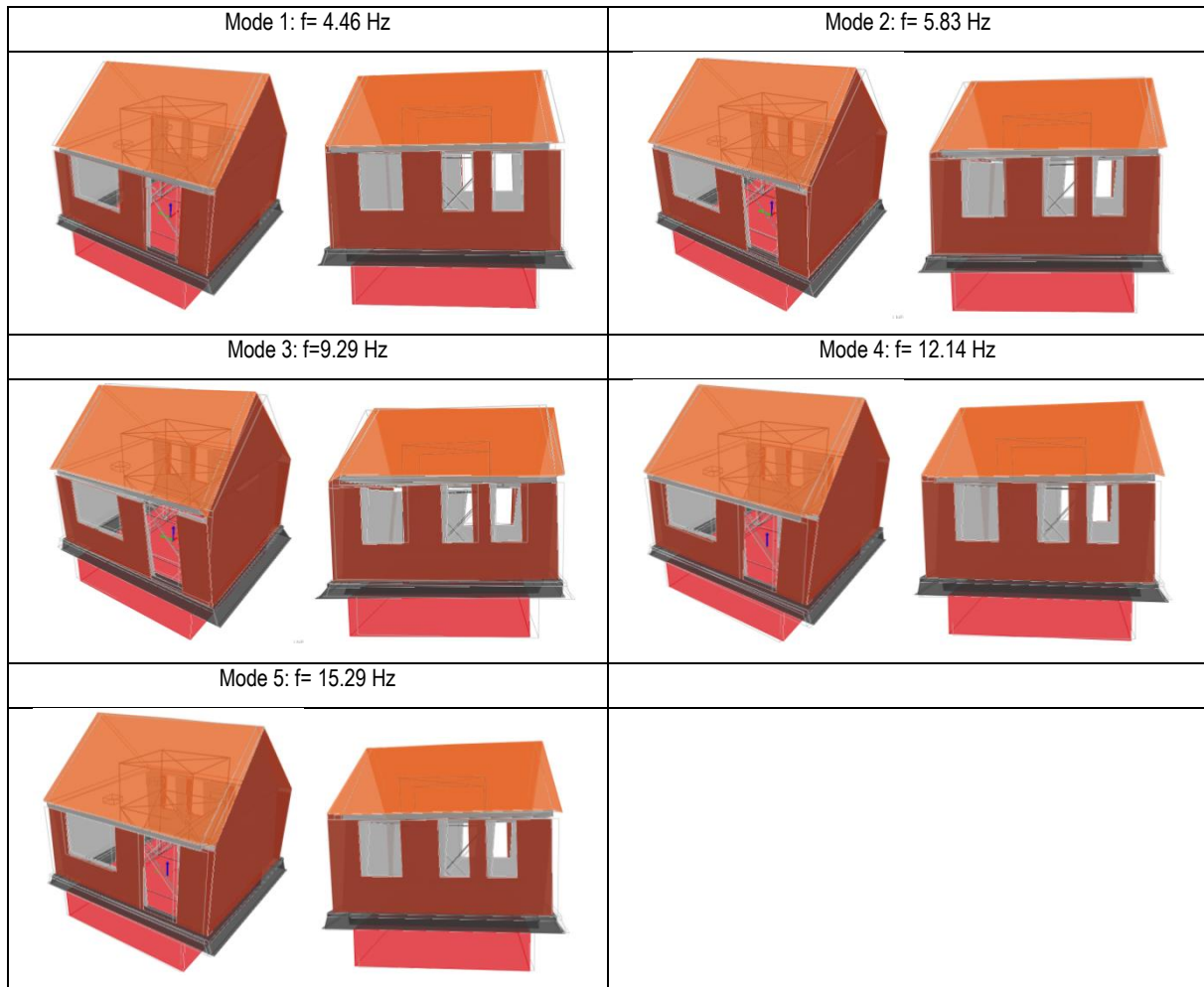


Figure 5.25 EFDD mode shapes for 2nd dynamic identification (Test 3).

Between the 3rd dynamic identification (Test 5) and the 6th dynamic identification (Test 12) there was no major evolution in the specimen's dynamic properties. Those results are presented in Annex I, following the same organisation of the previous one, with the only difference that the MAC coefficients now compare the mode shape evolution between the 2nd dynamic identification (Test 3) and the other ones.

5.1.2.5 7th dynamic identification (Test 14)

After the fundamental mode kept a constant frequency around 4.5 Hz in all previous dynamic identification tests, it reduced to around 4.2 Hz after the motion FEQ2-150%, as shown in the following figures and tables. Moreover, the modal damping of the first two modes has increased significantly, implying a larger energy dissipation in the existing cracks even for very small deformations. It is also apparent from the mode shapes that the inner walls are moving independently of the outer walls.

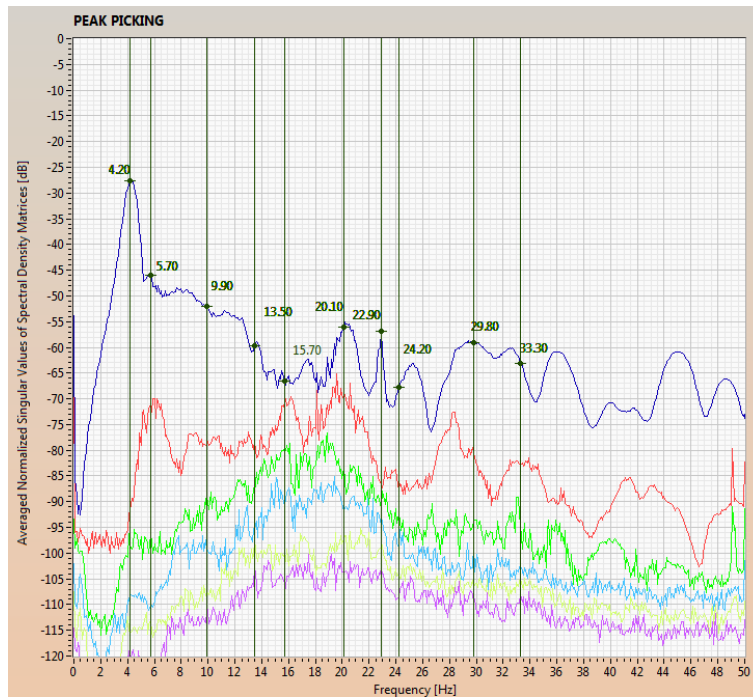


Figure 5.26 FDD results for 7th dynamic identification (Test 14).

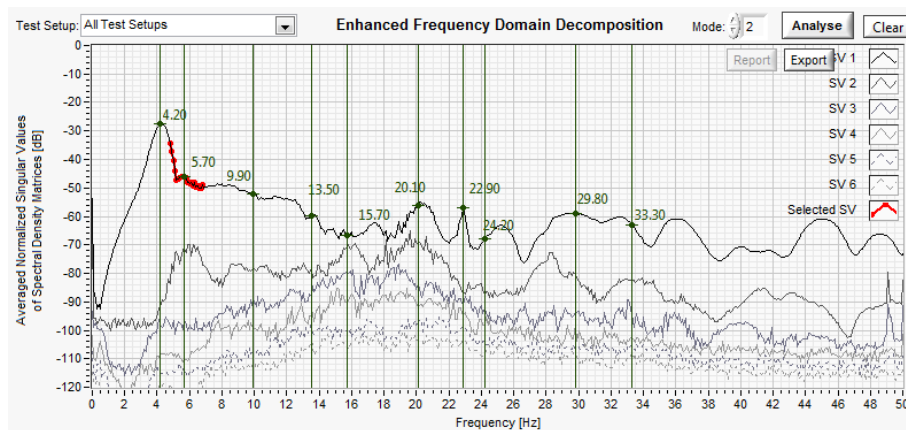


Figure 5.27 EFDD results for 7th dynamic identification (Test 14).

Table 5.6 Summary of vibration modes' characteristics for 7th dynamic identification (Test 14).

Mode	FDD Frequency [Hz]	EFDD Frequency [Hz]	Damping [%]
1	4.20	4.18	4.81
2	5.70	5.66	4.18
3	9.90	9.83	2.18
4	13.50	13.49	1.55
5	15.70	15.73	1.40

Table 5.7 MAC coefficients for 7th dynamic identification (Test 14).

MODE i_j		MODE_01_07	MODE_02_07	MODE_03_07	MODE_04_07	MODE_05_07
	Frequency [Hz]	4.1	5.7	9.9	13.5	15.7
MODE_01_02	4.5	0.98	0.90	0.63	0.57	0.45
MODE_02_02	5.8	0.90	0.98	0.58	0.45	0.33
MODE_03_02	9.3	0.60	0.51	0.89	0.78	0.65
MODE_04_02	12.1	0.40	0.27	0.75	0.88	0.78
MODE_05_02	15.3	0.60	0.44	0.76	0.92	0.88

i Mode

j dynamic identification

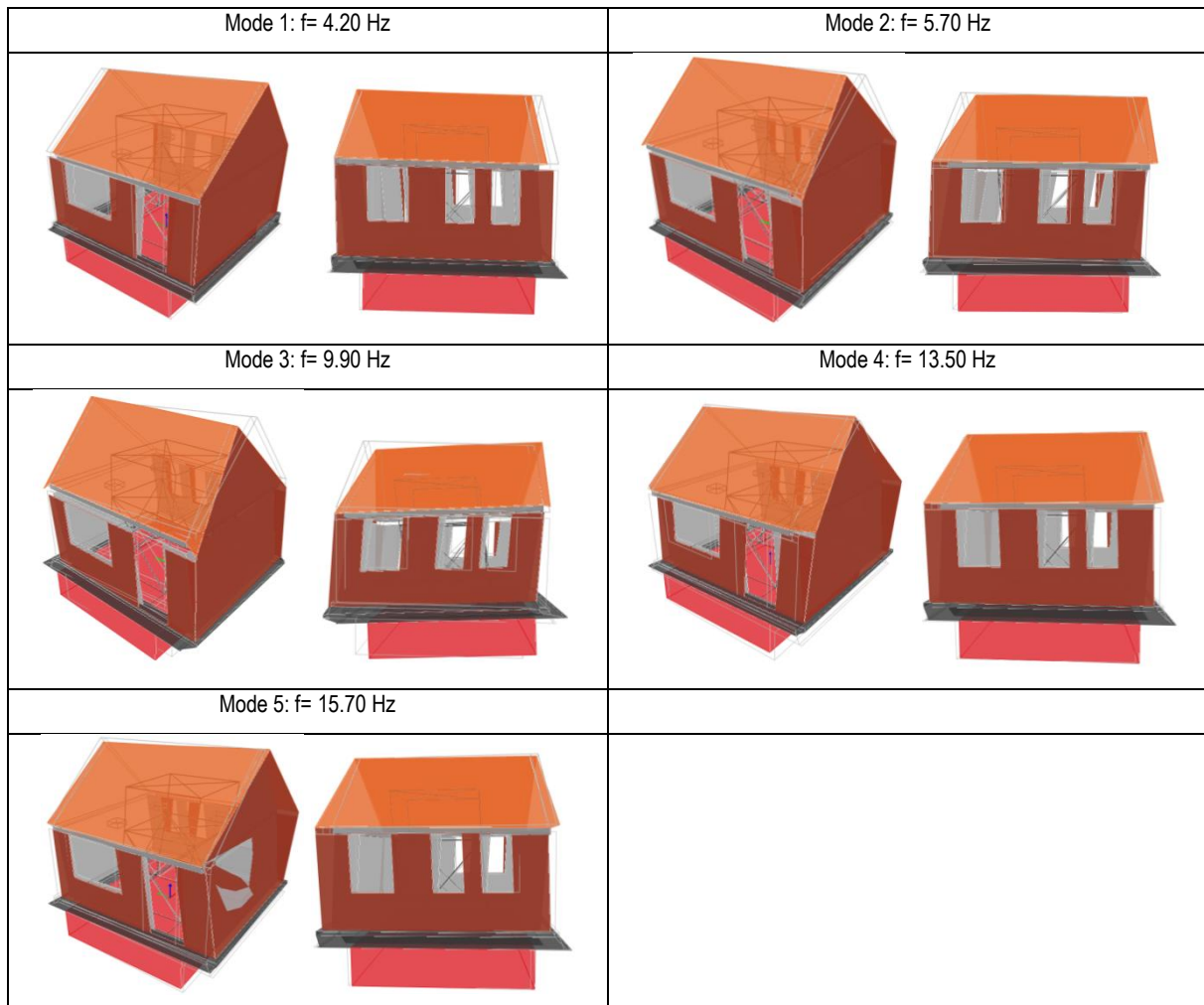


Figure 5.28 FDD mode shapes for 7th dynamic identification (Test 14).

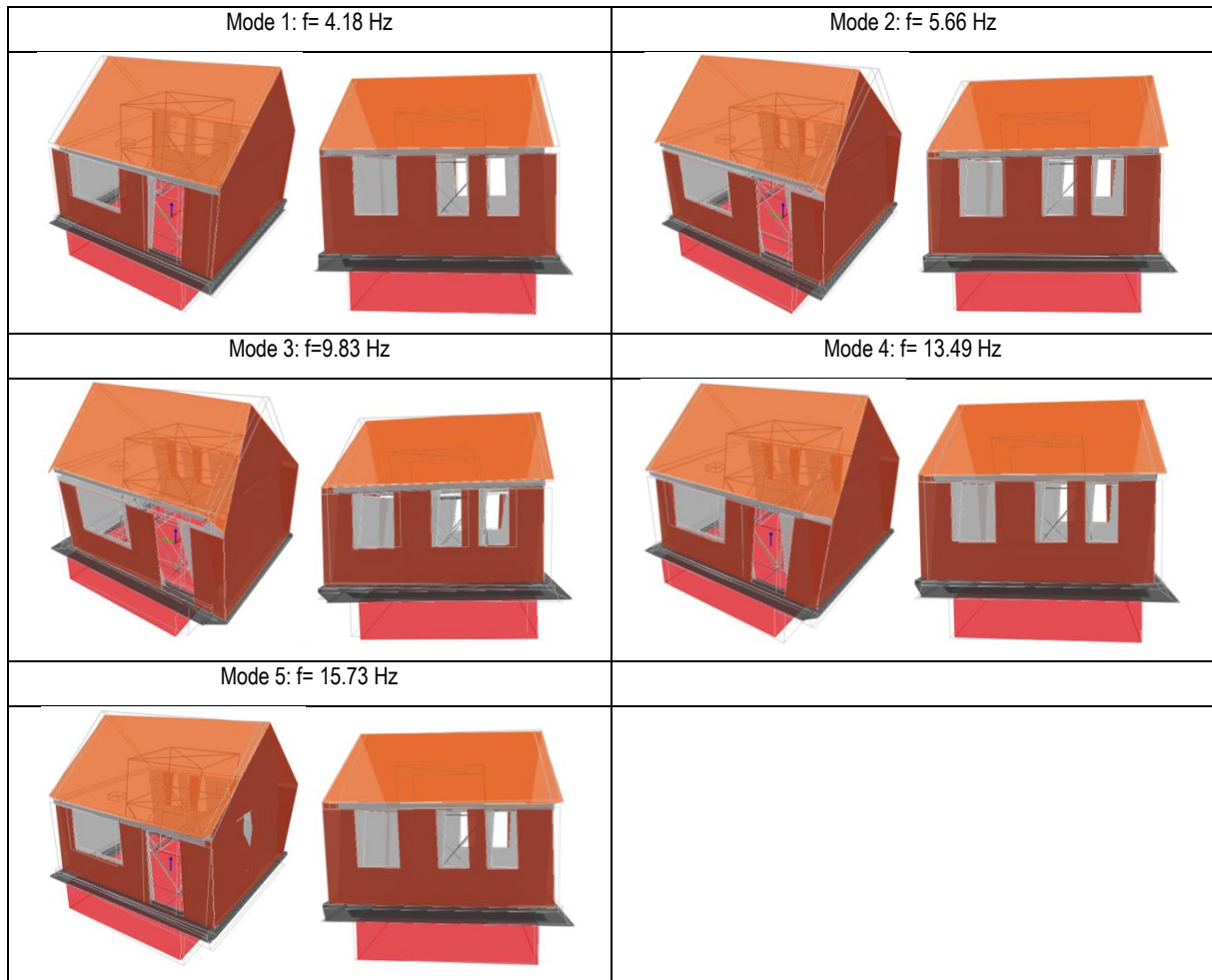


Figure 5.29 EFDD mode shapes for 7th dynamic identification (Test 14).

5.1.2.6 8th dynamic identification (Test 18)

After the motion FEQ2-200%, another important reduction in all initial frequencies was detected, as presented in the following figures and tables. The fundamental frequency is now reduced to around 3.8 Hz, corresponding to a stiffness reduction of about 30% with respect to the initial stiffness.

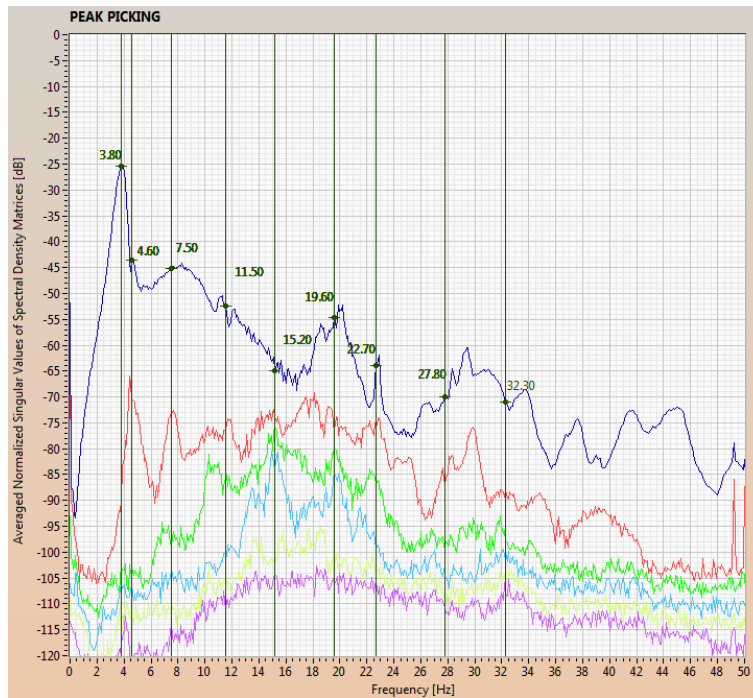


Figure 5.30 FDD results for 8th dynamic identification (Test 18).

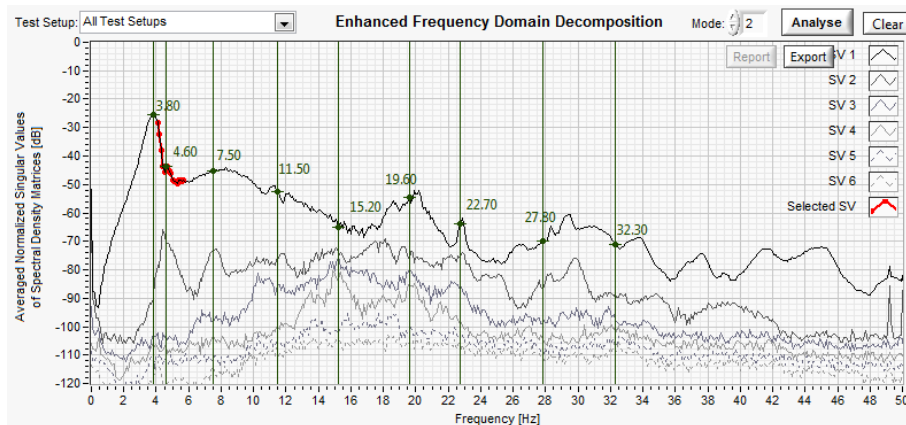


Figure 5.31 EFDD results for 8th dynamic identification (Test 18).

Table 5.8 Summary of vibration modes' characteristics for 8th dynamic identification (Test 18).

Mode	FDD Frequency [Hz]	EFDD Frequency [Hz]	Damping [%]
1	3.80	3.81	4.63
2	4.60	4.64	4.49
3	7.50	7.47	2.87
4	11.50	11.38	1.84
5	15.20	15.29	1.16

130 Collapse Shaking Table Test on URM Cavity Wall Structure representative of a Dutch Terraced House

Table 5.9 MAC coefficients for 8th dynamic identification (Test 18).

MODE i_j		MODE_01_08	MODE_02_08	MODE_03_08	MODE_04_08	MODE_05_08
	Frequency [Hz]	3.8	4.6	7.5	11.5	15.2
MODE_01_02	4.5	0.98	0.94	0.63	0.44	0.52
MODE_02_02	5.8	0.90	0.96	0.59	0.31	0.37
MODE_03_02	9.3	0.53	0.52	0.88	0.70	0.59
MODE_04_02	12.1	0.32	0.29	0.79	0.85	0.69
MODE_05_02	15.3	0.53	0.48	0.84	0.83	0.83

i Mode

j dynamic identification

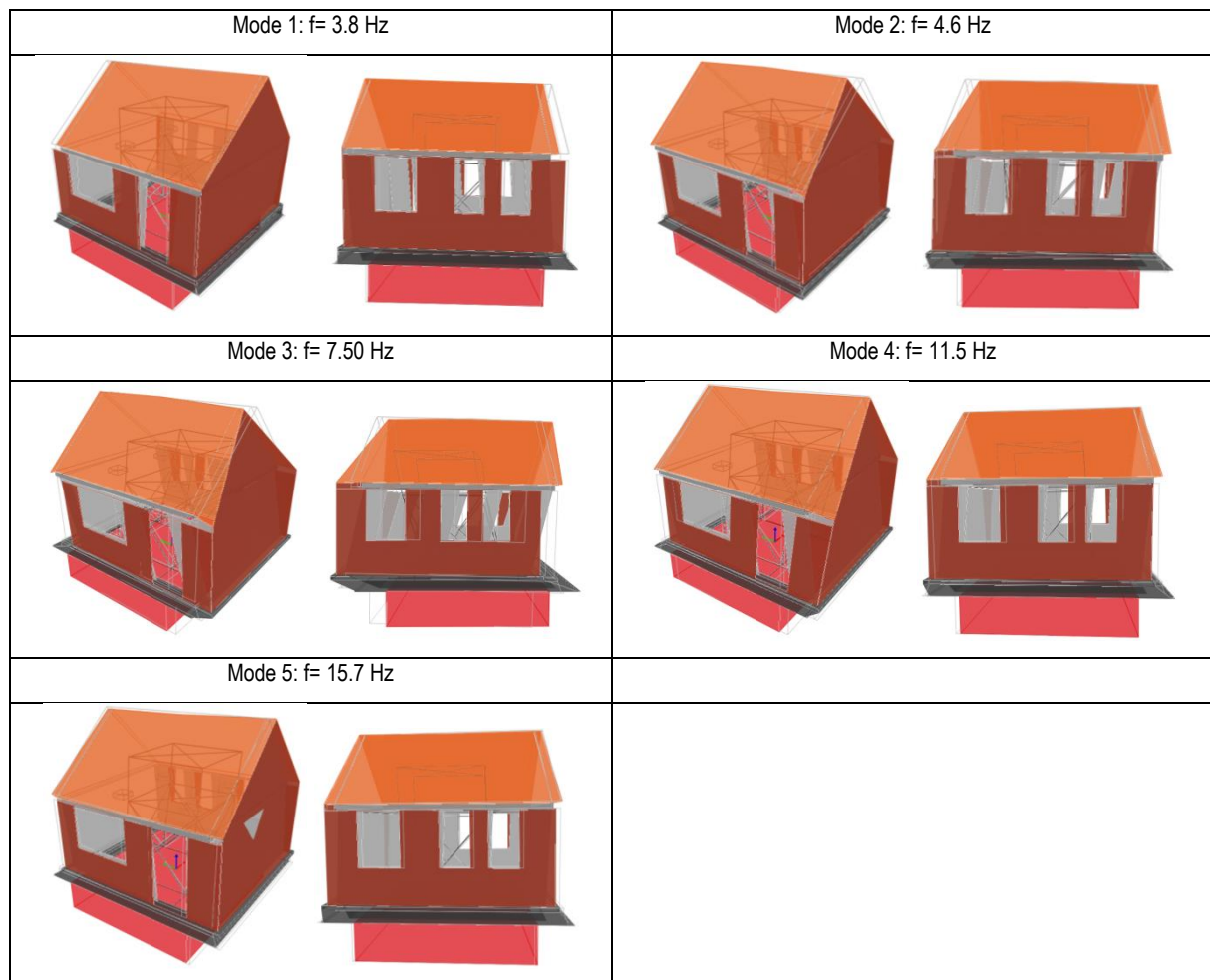


Figure 5.32 FDD mode shapes for 8th dynamic identification (Test 18).

The evolution of the fundamental frequency of vibration of the specimen and of the corresponding modal damping is summarised in Table 5.10. These results show that the dynamic characteristics of the specimen, in terms of its first mode of vibration, was basically unchanged throughout most of the test. A clear degradation of the specimen's dynamic properties only took place during the application of FEQ2-150%, FEQ2-200% and FEQ2-300%.

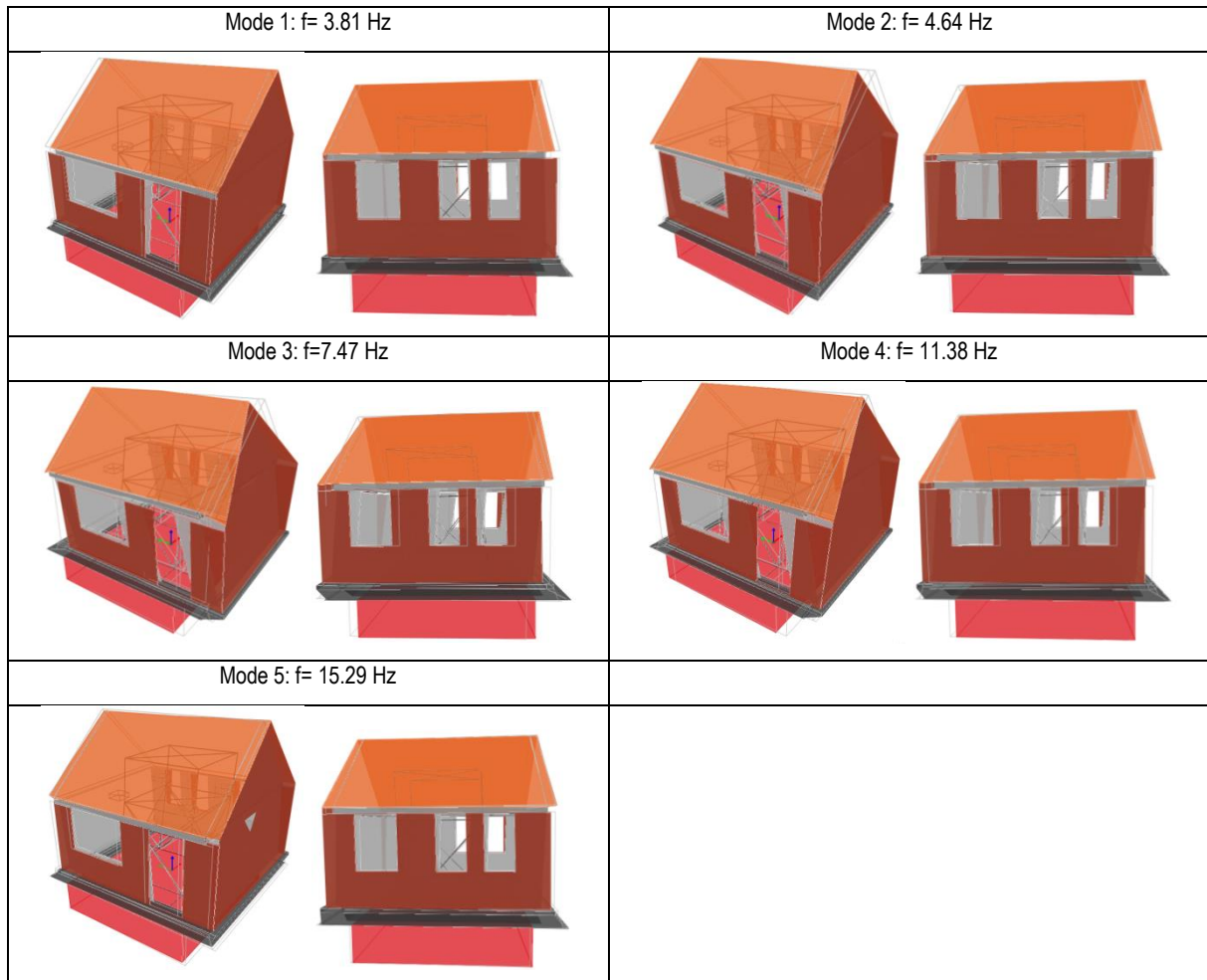


Figure 5.33 FDD mode shapes for 8th dynamic identification (Test 18).

Table 5.10 Evolution of the fundamental mode of vibration of the model during the shaking table test.

Dynamic ident. test	Frequency [Hz]	Damping [%]
1	4.11 (*)	4.31 (*)
2	4.46	4.25
3	4.46	4.28
4	4.45	4.29
5	4.48	4.28
6	4.47	4.36
7	4.18	4.81
8	3.81	4.63

(*)Test for higher excitation level

Besides the degradation of the dynamic properties, the mode shapes also show some significant changes. For instance, the second mode of vibration, whose frequency decreased from 5.83 Hz to 4.64 Hz, clearly presents a sliding motion of the slab with respect to the walls during the last dynamic identification test which is revealing of the damage state attained by the structure.

5.2 Damage evolution

The building prototype suffered slight damage during the transportation phase to the shaking table, due to a deflection of the mixed steel RC foundation beam and despite the vertical prestress applied to the walls for this operation. Cracks have been surveyed associated with the elongation of the fundamental period of vibration, as already discussed above. In particular, the most significant crack developed at the base of the CS central pier (Pier 2) of the North façade, starting from the bottom edge of the window. This damage appeared as a classical stepped crack with an average width of 1.5 mm. Other minor cracks have been observed on the plaster layer of the southern CS façade (spandrel between Pier 6 and Pier 7 and at the base of the Pier 5). Finally, horizontal cracks with the associated loss of the cohesion bond between the upper mortar bed-joint and the RC slab, appeared at the top of some of the CS piers, particularly visible in the walls with the plaster layer. The same horizontal cracks have been noticed on top of the outer clay longitudinal walls. Figure 5.34 shows a view of the specimen transportation to the shaking table.

Figure 5.35 and Figure 5.36 show the evolution of the damage surveyed on the CS walls through the entire testing sequence. At the end of each stage of the shaking table testing sequence, detailed surveys were carried out for reporting every possible evidence of damage having affected the structure. The walls covered with a plaster layer are shown in light grey. Figure 5.37 illustrates the damage evolution observed in the outer clay walls.



Figure 5.34 Specimen transportation to the shaking table.

The first damage (crack width of 0.2 mm) associated to a shaking table motion appeared on the plaster layer of the spandrel between Pier 5 and 6 in the south CS wall, during the test FEQ1-100% (PGA= 0.119g).

During test FEQ1-150% (PGA= 0.146g), two horizontal cracks with a negligible width developed at the base of the CS piers number 4 and 6, associated with the activation of a flexural/rocking behaviour. The crack at the base of Pier 4 continued horizontally, for a length of approximately 1 metre, in the transverse CS wall of the West side, probably due to a sort of flange effect. The observed damage did not change during the tests FEQ2-50%-COMP and FEQ2-50% (PGA=0.137 and 0.095g). A similar crack, due to a flexural/rocking behaviour, was surveyed at the base of Pier 1 of the North wall at the end of test FEQ2-100% (PGA=0.218g).

The FEQ2-150% test (PGA=0.380g) caused the development of new cracks and the elongation and widening of the pre-existing ones; a 1 mm stepped diagonal crack appeared on the spandrel between Piers 1 and 2 of the North CS wall; it is worth noticing that the diagonal cracks observed in the West CS transverse wall continued vertically in correspondence of the bookshelf anchored to the top of the wall.

A further worsening of the existing crack pattern has been noticed at the end of the test FEQ2-200% (PGA= 0.393g); new horizontal cracks with negligible thickness have been observed in the plaster of pier 5 and spandrel between piers 4 and 5 of the South CS wall. A slight detachment of the timber plate has been noticed in the South-West corner. Despite a clear rocking behaviour of the gable walls, evident from the displacement histories recorded by the installed displacement transducers, no visible cracks were detected on them. Moreover, the clay veneer walls did not suffer any significant visible damage up to the test FEQ2-200%.

The (partial) collapse of the specimen prototype was attained during the test FEQ2-300% (PGA=0.630g) exhibiting a rather fragile behaviour. The pronounced rocking mechanism developed by the slender longitudinal piers and the vertical input motion on the prototype led to an uplift of the RC slab causing a loss of restraint condition at the top of the East CS transverse wall, which failed out of plane. In addition to this local failure mode, a global severe damage in all longitudinal piers, associated with the expulsion of materials, was observed. Severe damage occurred also in the West CS transverse wall due to the interaction between the displacement drift imposed by the floor and the out-of-plane actions induced by the wall's inertial forces and the outer veneer wall (e.g. pushing and pulling the wall by means of the steel ties). Cracks have been observed on both East and West CS gable walls, in particular in the regions close to the L-shaped steel anchors.

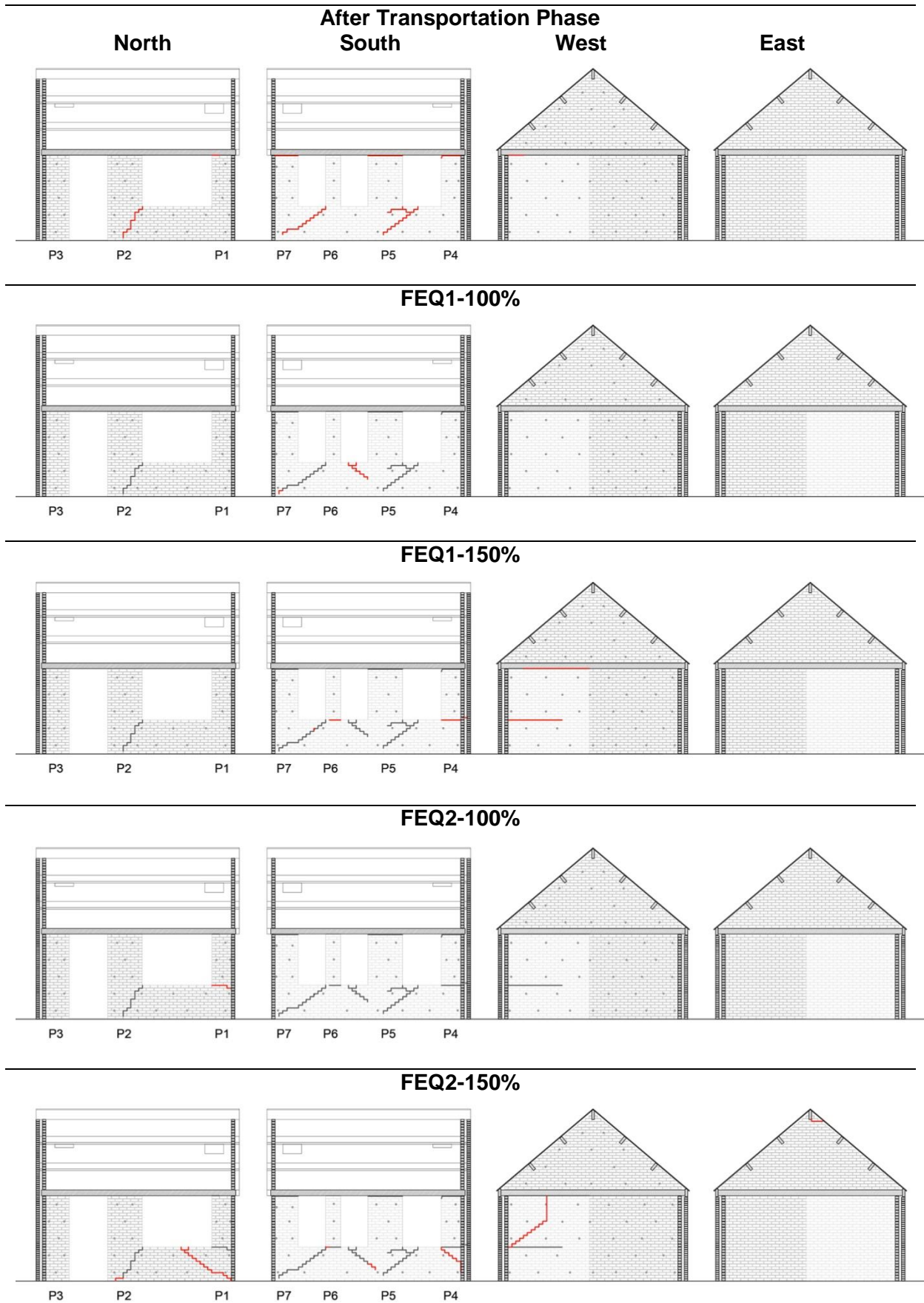


Figure 5.35 Evolution of the crack pattern in the Inner CS walls: up to test FEQ2-150%.

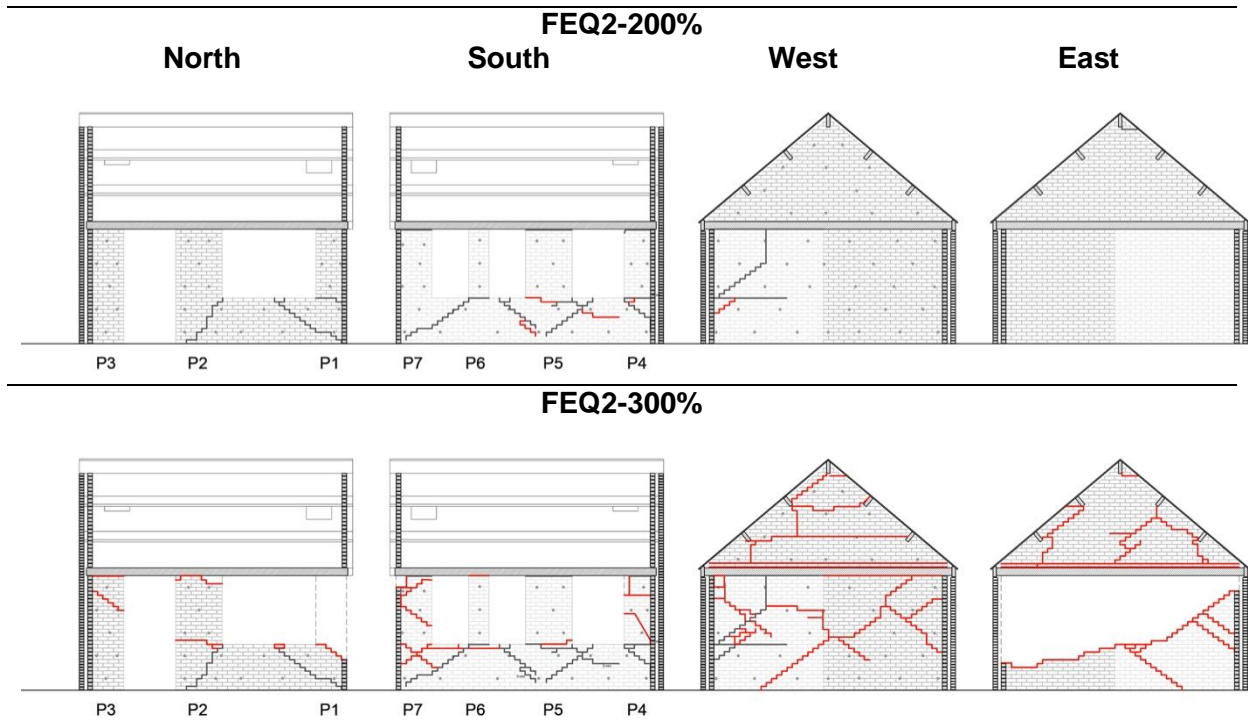


Figure 5.36 Evolution of the crack pattern in the Inner CS walls: from test FEQ2-200% to test FEQ2-300%.

Regarding the performance of the outer veneer wall, no significant damage has been observed up to test FEQ2-300%. In the test where the specimen reached a partial collapse, horizontal cracks have been surveyed at the base of all the longitudinal piers, a clear sign of rocking/sliding behaviour. The crack pattern surveyed on the West wall shows both the rocking mechanism of the system gable walls and roof and the triggering of a global pull-out/pull-in of the veneer wall which is not directly connected with the slab.

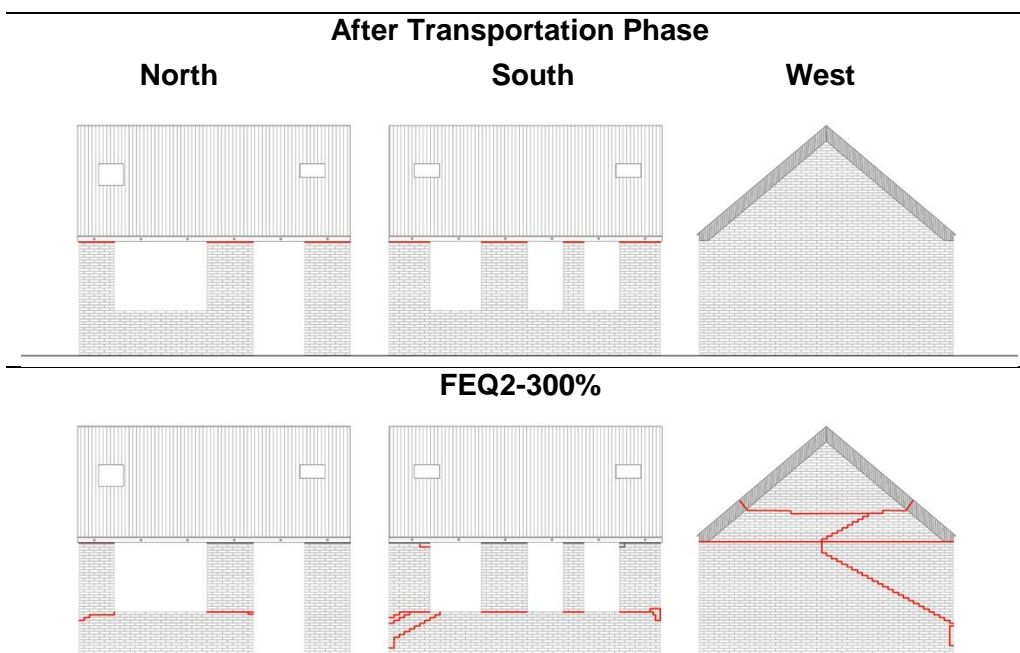


Figure 5.37 Evolution of the crack pattern in the outer clay veneer walls.

5.3 Description of the collapse mechanism

Figure 5.38 illustrates a sequence of frames of the video when the building prototype exhibited a local collapse of the East wall. The blue lines highlight the alignments of the structural elements during the response while the red lines draw attention to the opening of gaps between the different structural elements. Figure 5.38 (a), with the slab moving towards East, illustrates the pronounced rocking behaviour of Pier 3 (of both inner and outer leaves) causing the uplift of the RC slab and the opening of a gap on top of the east transverse wall. It is worth noticing also the different displacement profiles exhibited by the inner CS wall and the outer veneer wall, in particular regarding Pier 2 and Pier 7. This frame confirms the reduced contribution to the structure's overall response of the clay longitudinal walls which seemed not involved in the oscillation. A significant sliding of the upper portion of the CS Pier 3 is also visible.

Figure 5.38 (b) is a frame showing the structural response with the specimen displacing towards West with a clear rocking behaviour of all the longitudinal piers of the North veneer wall.

In the successive instants of response, the specimen displaced back towards East showing the closure of all the rocking gaps (see Figure 5.38 (c)) and again an evident rocking behaviour of the system RC slab and CS longitudinal piers leading to a reopening of the gap on top of the East transverse wall (Figure 5.38 (d) highlights the horizontal deformation at the wall top); the corners veneer longitudinal piers (Pier 1 and 7) after an initial rocking behaviour (Figure 5.38 (d)) continued moving towards East showing clear sliding of the entire piers (Figure 5.38 (e) and Figure 5.38 (f)); few instants later the reverse acceleration caused a global displacement of the structure towards East.

The lack of restraint at the CS East wall top in addition with the probable eccentric axial load transferred to the wall top by the slab moving towards East caused the out-of-plane failure of the wall upper portion (Figure 5.38 (e)) associated with the collapse of CS Pier 1 (Figure 5.38 (f)). With the collapse of the East load-bearing wall, the slab exhibited a large displacement in the longitudinal direction (East) and towards the South direction, resting at the end of the test on the outer veneer wall. Figure 5.39 presents some pictures of the specimen at the end of test FEQ-300%.

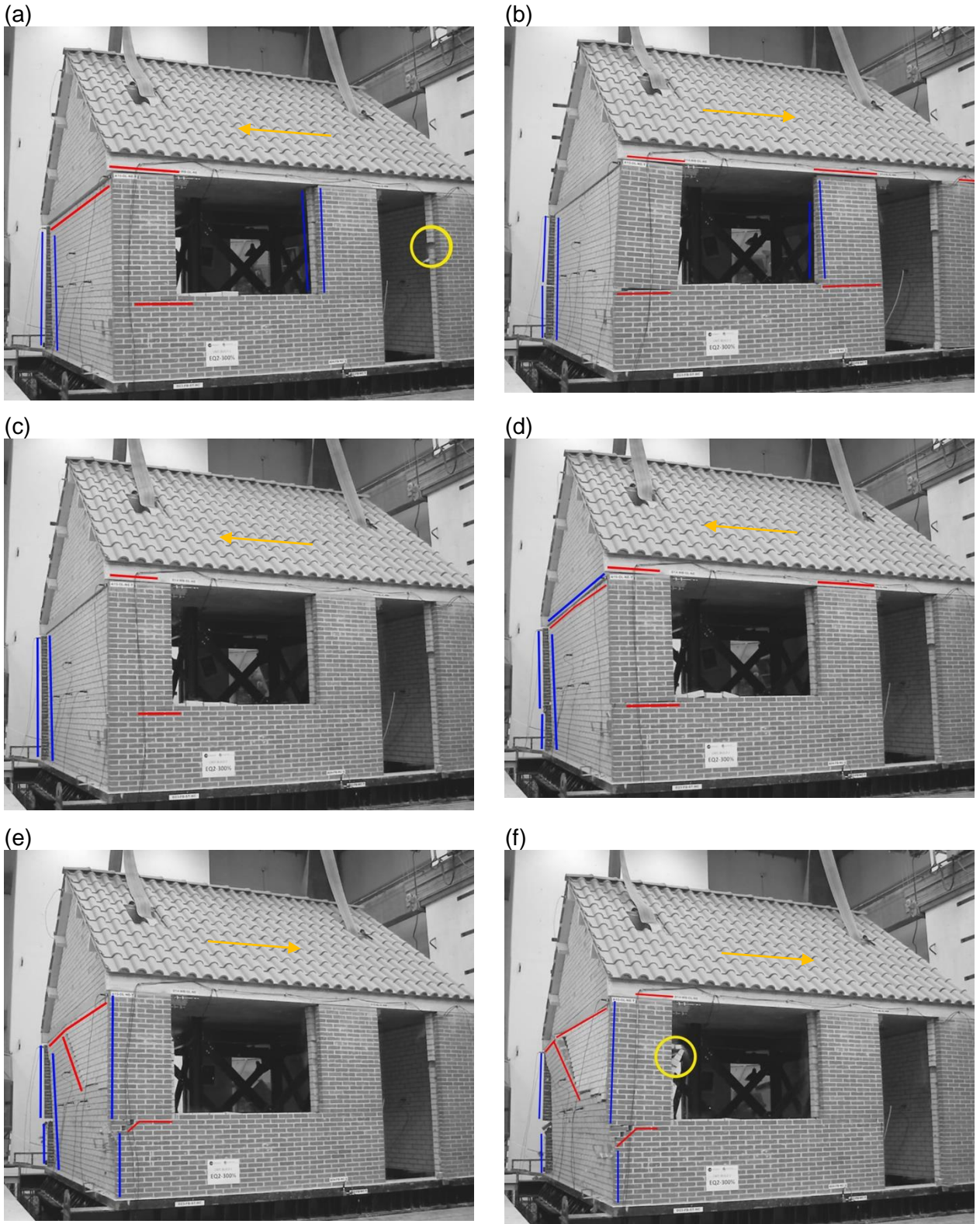


Figure 5.38 Snapshots of the FEQ2-300% test.



Figure 5.39 Pictures of the specimen at the end of the test FEQ-300%.

5.4 Furniture performance

Figure 5.40 shows pictures of the furniture placed in the building prototype at the beginning of the testing sequence. The furniture did not show any damage up to test FEQ2-200%. During test FEQ2-300% the bookshelf, not attached to the transverse wall, overturned hitting the table with the notebook. Figure 5.41 depicts the furniture after test FEQ2-300%.



Figure 5.40 Pictures of the furniture before the testing sequence.



Figure 5.41 Pictures of the specimen at the end of test FEQ-300%.

5.5 Shaking Table Performance

The target shaking table motions for this specimen were very demanding, since the shaking table should reproduce a floor motion observed on the building prototype tested in EUCENTRE. It must be noted that the motion attained in EUCENTRE, and in any shaking table system, is always affected by the dynamics of the specimen, its damage evolution and the shaking table dynamic characteristics and not always complies with the target motion. Therefore, the target floor motion to be applied at the LNEC shaking table, was already filtered by the EUCENTRE system and was intended to be reproduced in a different shaking table system, with more degrees of freedom, and with a specimen with different dynamic properties than the one tested in EUCENTRE. Nevertheless, the comparison between the theoretical response spectra (shown in Figure 4.2) and those obtained from the accelerations recorded on the specimen's foundation, shows a general good match.

A slight overshooting of low-period horizontal spectral ordinates was noticed in all FEQ2 tests. The vertical spectral ordinates overshooting was instead rather significant in the periods around 0.2 s. The FEQ2-150% test, in particular, presented a considerable overshooting around the period of 0.20 s in both vertical and horizontal directions. For this reason, a tuning procedure for the shaking table was followed before proceeding to the level FEQ2-200%, by performing two tuning iterations at smaller levels of excitation. From Figure 5.42 to Figure 5.52 the comparison between theoretical and experimental 5% damped acceleration response spectrum is proposed. It is possible to observe also, in those figures, the spectrum calculated with the floor average acceleration, highlighting test by test the change of the specimen's dynamic characteristics.

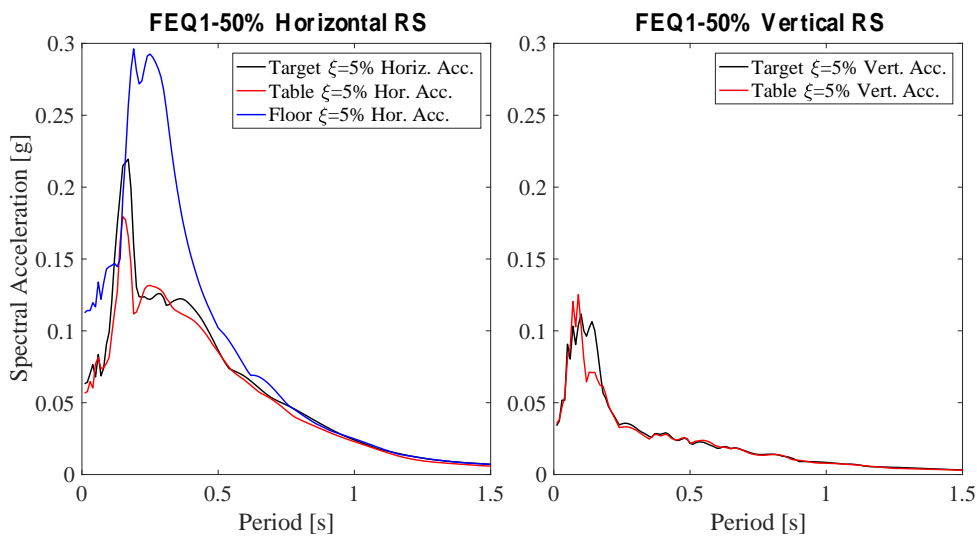


Figure 5.42 FEQ1-50%: Theoretical-experimental 5% damped response spectra in both motion directions.

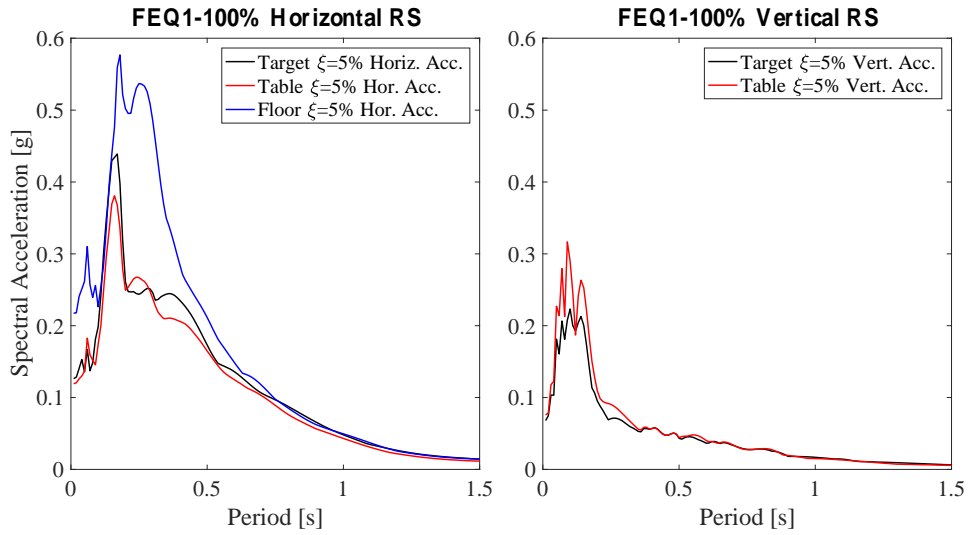


Figure 5.43 FEQ1-100%: Theoretical-experimental 5% damped response spectra.

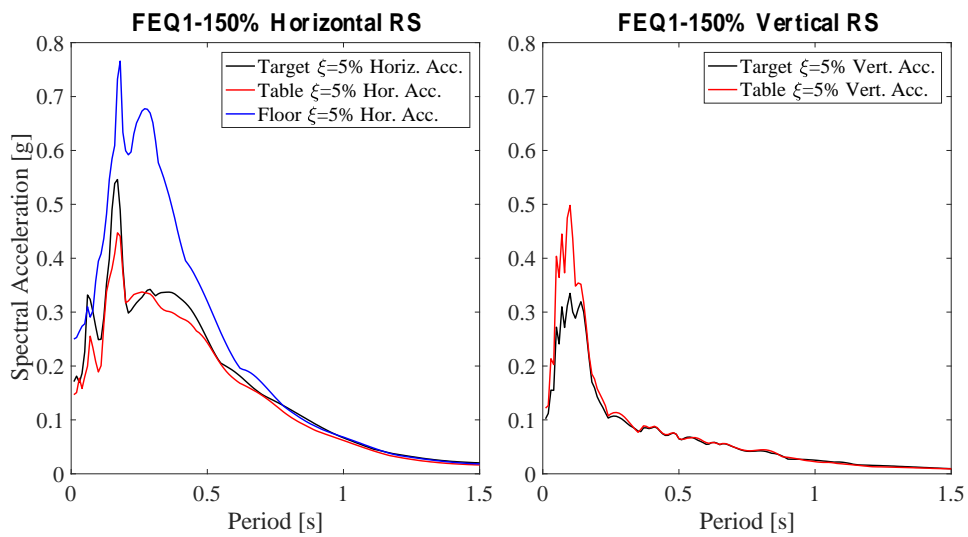


Figure 5.44 FEQ1-150%: Theoretical-experimental 5% damped response spectra.

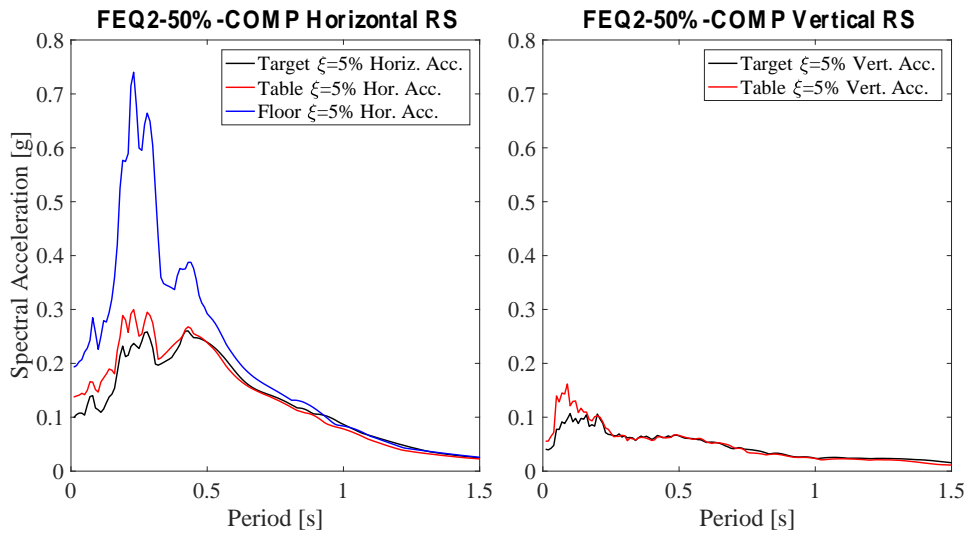


Figure 5.45 FEQ2-50%-COMP: Theoretical-experimental 5% damped response spectra.

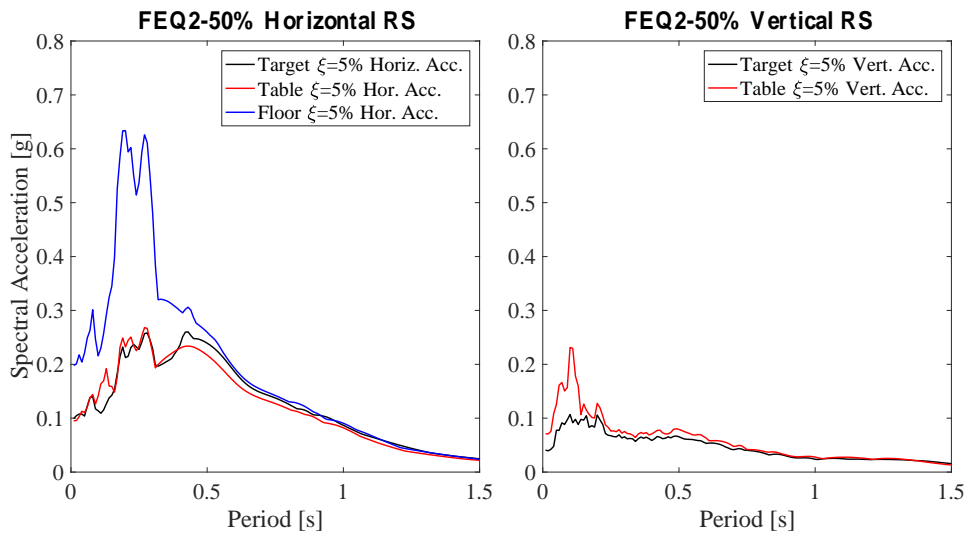


Figure 5.46 FEQ2-50%: Theoretical-experimental 5% damped response spectra.

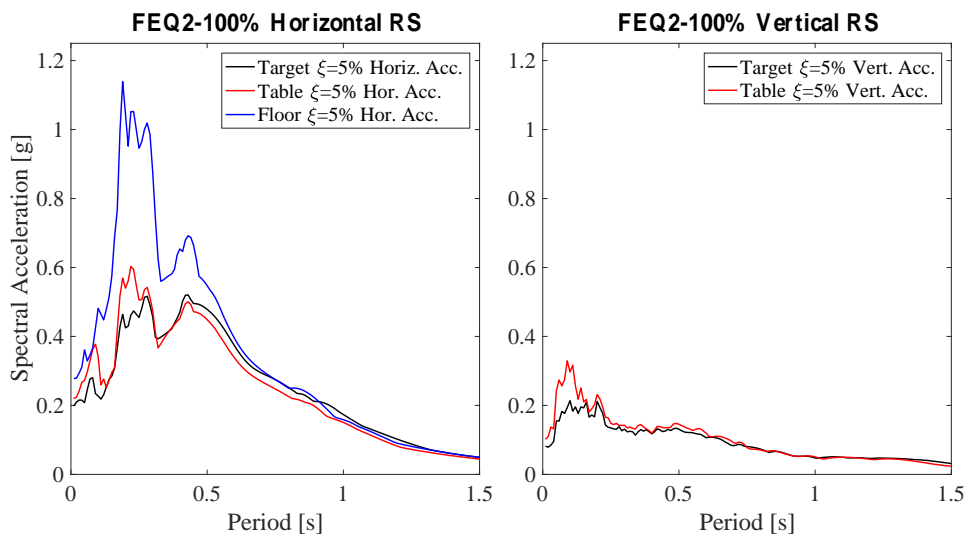


Figure 5.47 FEQ2-100%: Theoretical-experimental 5% damped response spectra.

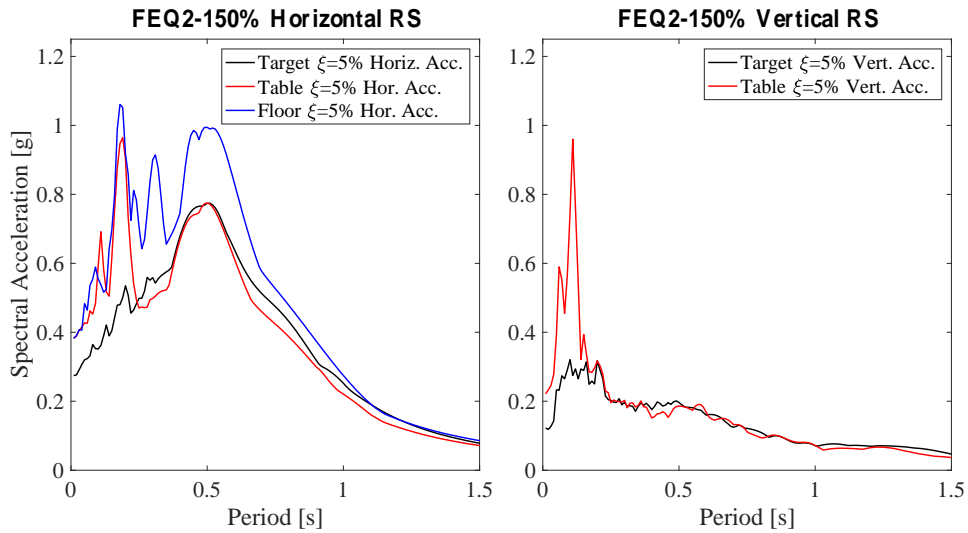


Figure 5.48 FEQ2-150%: Theoretical-experimental 5% damped response spectra.

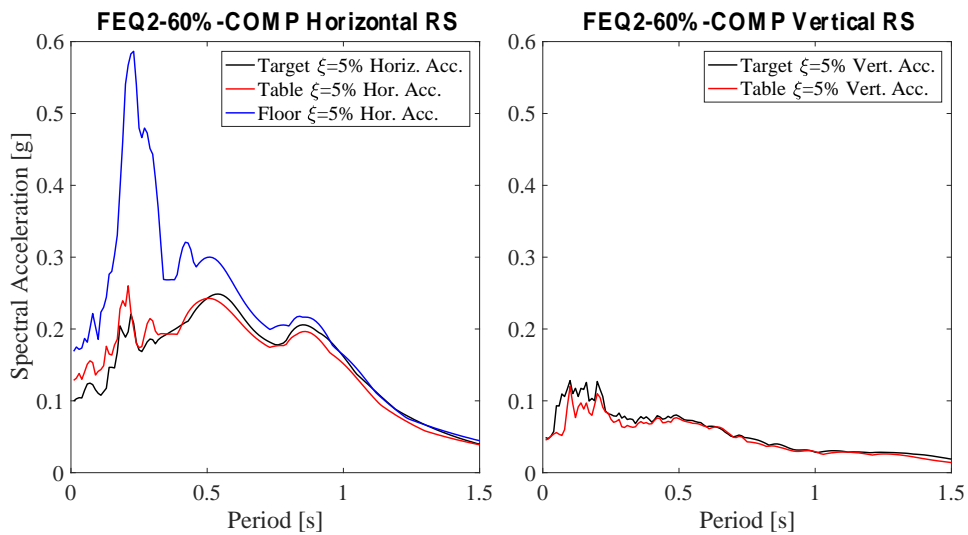


Figure 5.49 FEQ2-60%-COMP: Theoretical-experimental 5% damped response spectra.

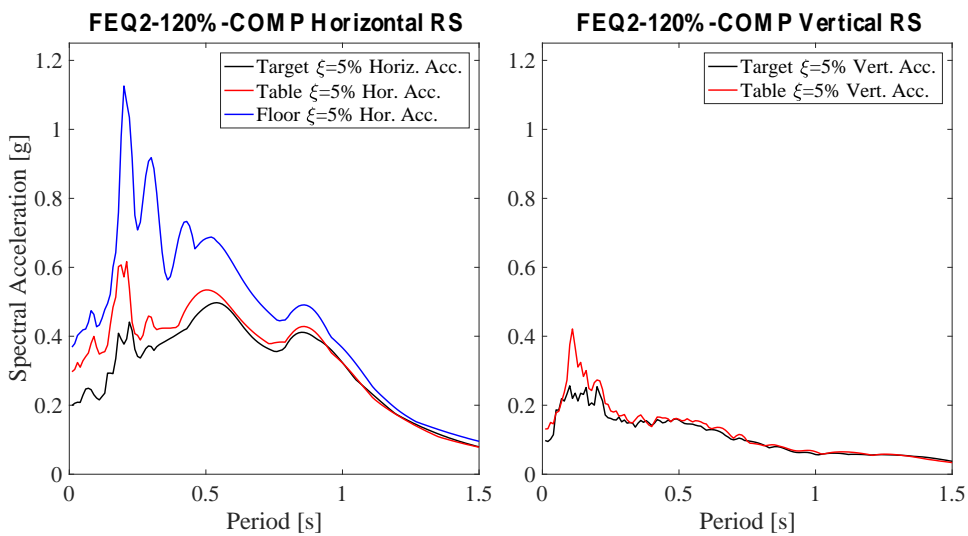


Figure 5.50 FEQ2-120%-COMP: Theoretical-experimental 5% damped response spectra.

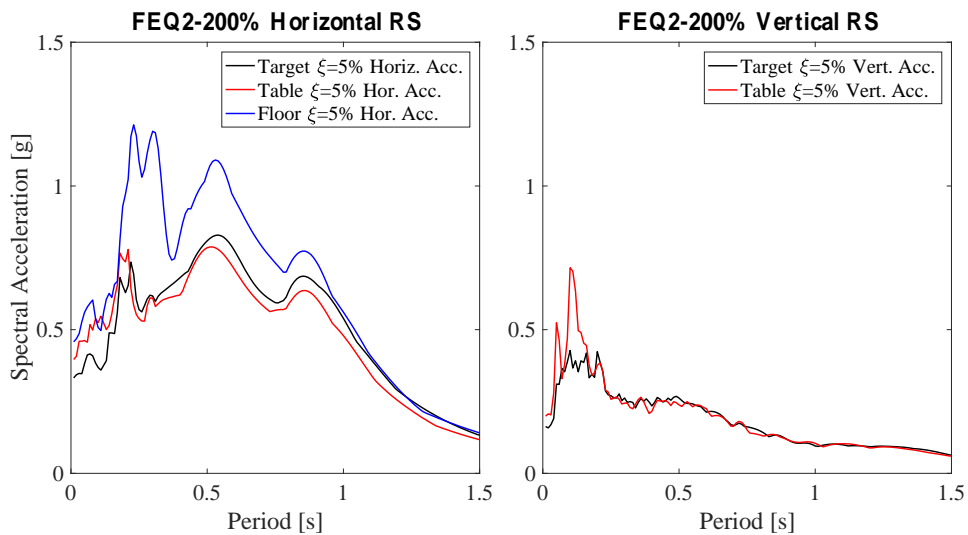


Figure 5.51 FEQ2-200%: Theoretical-experimental 5% damped response spectra.

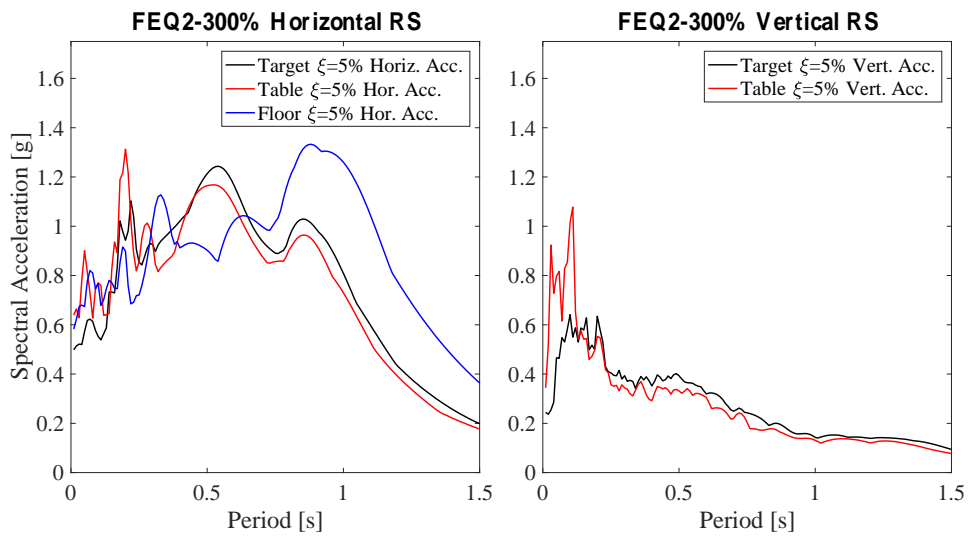


Figure 5.52 FEQ2-300%: Theoretical-experimental 5% damped response spectra.

5.6 Displacement and Acceleration Histories

The horizontal displacement and acceleration histories of the floor and of the ridge beam are shown from Figure 5.53 to Figure 5.63, as well as the horizontal and vertical table accelerations.

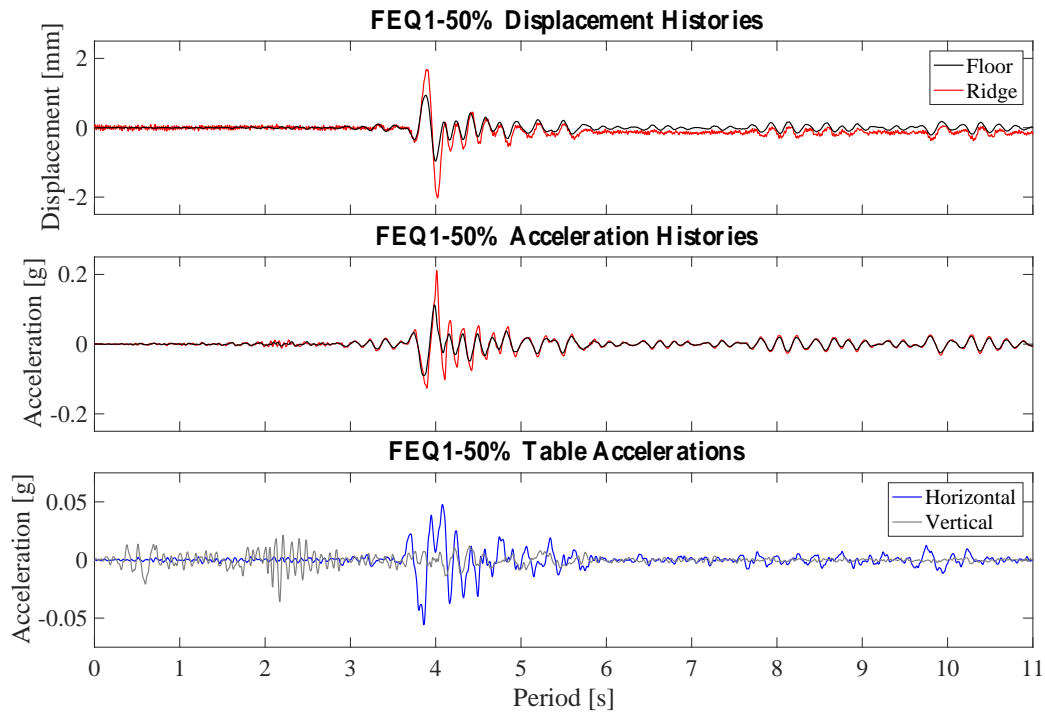


Figure 5.53 FEQ1-50%: Displacement and acceleration histories.

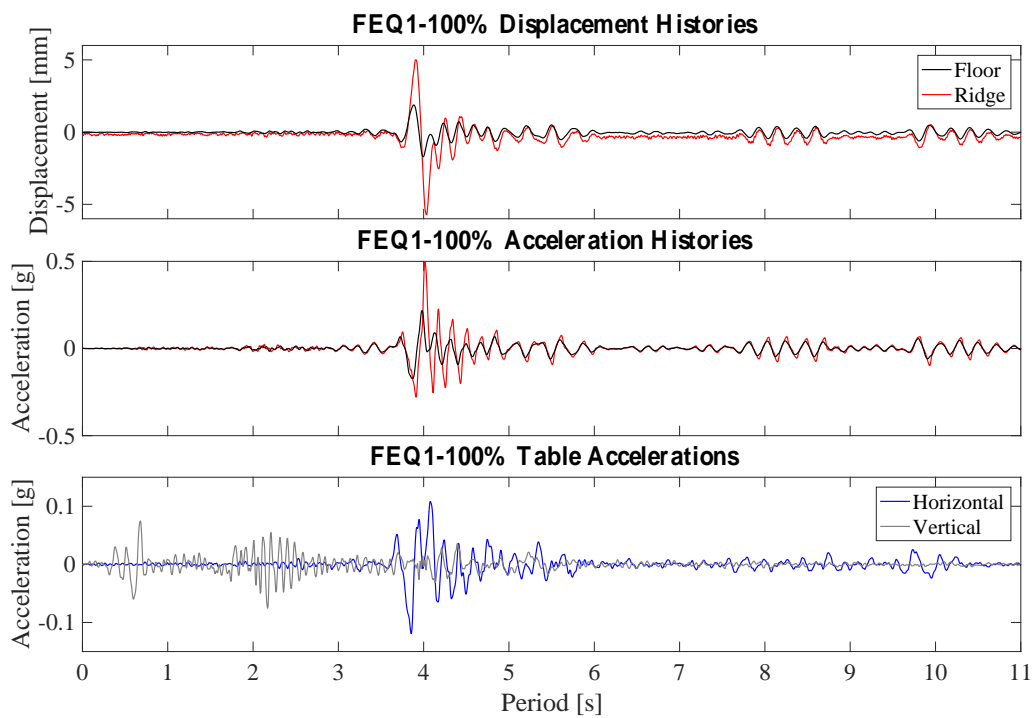


Figure 5.54 FEQ1-100%: Displacement and acceleration histories.

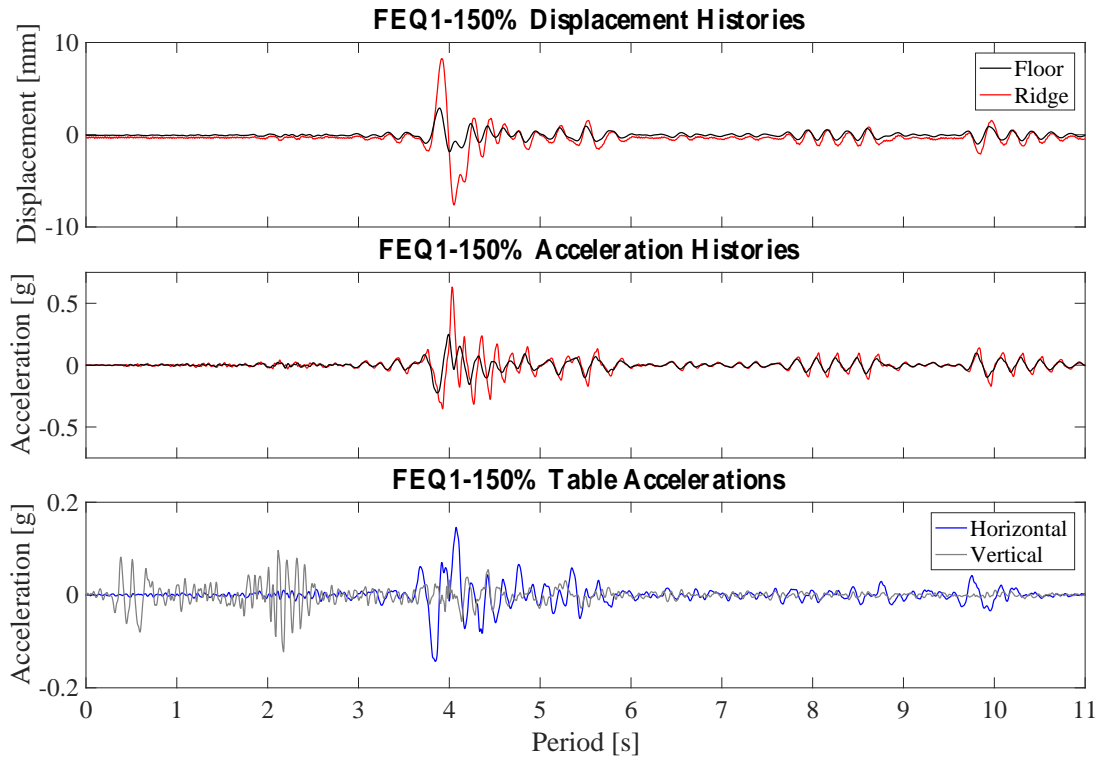


Figure 5.55 FEQ1-150%: Displacement and acceleration histories.

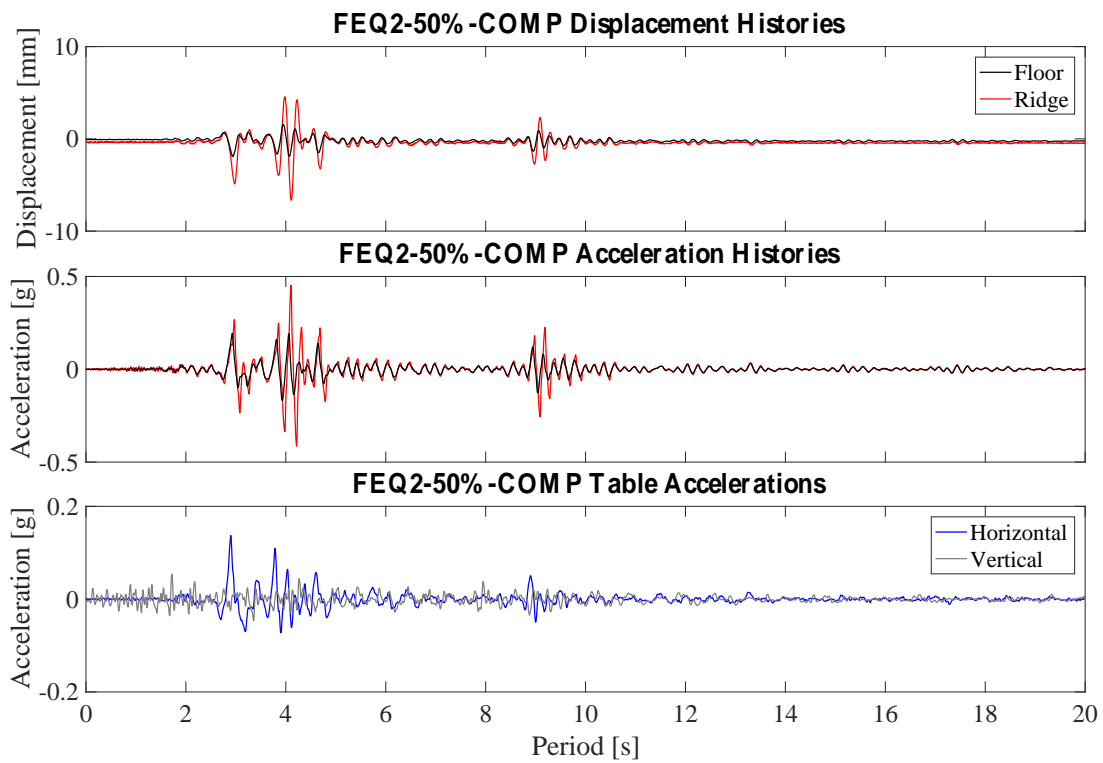


Figure 5.56 FEQ1-50%-COMP: Displacement and acceleration histories.

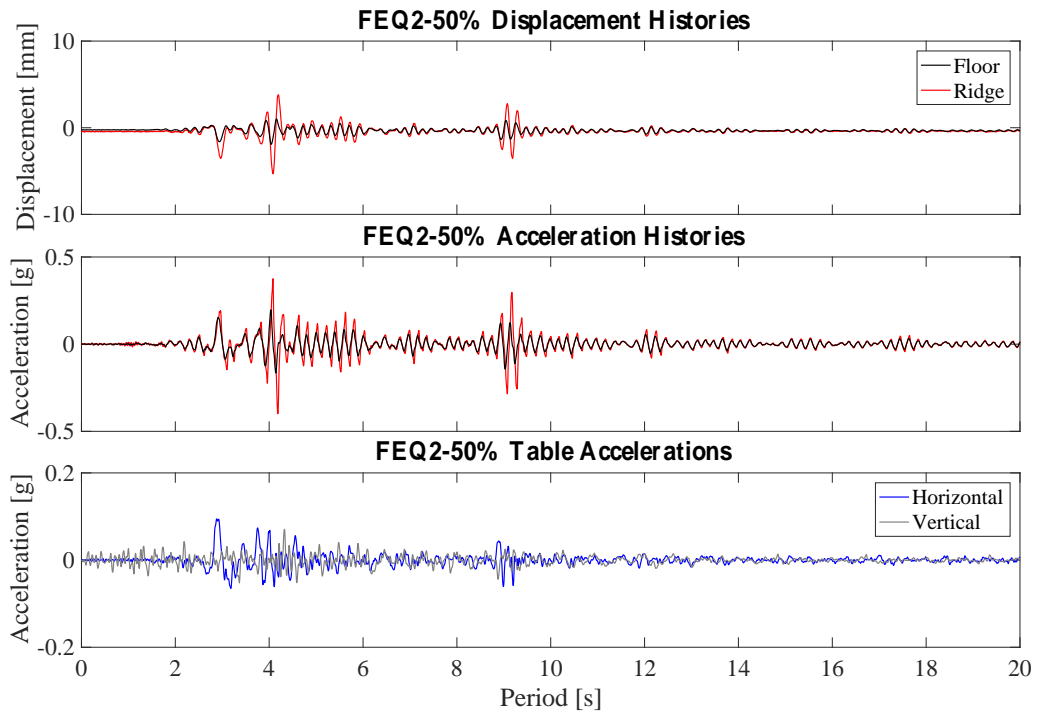


Figure 5.57 FEQ2-50%: Displacement and acceleration histories.

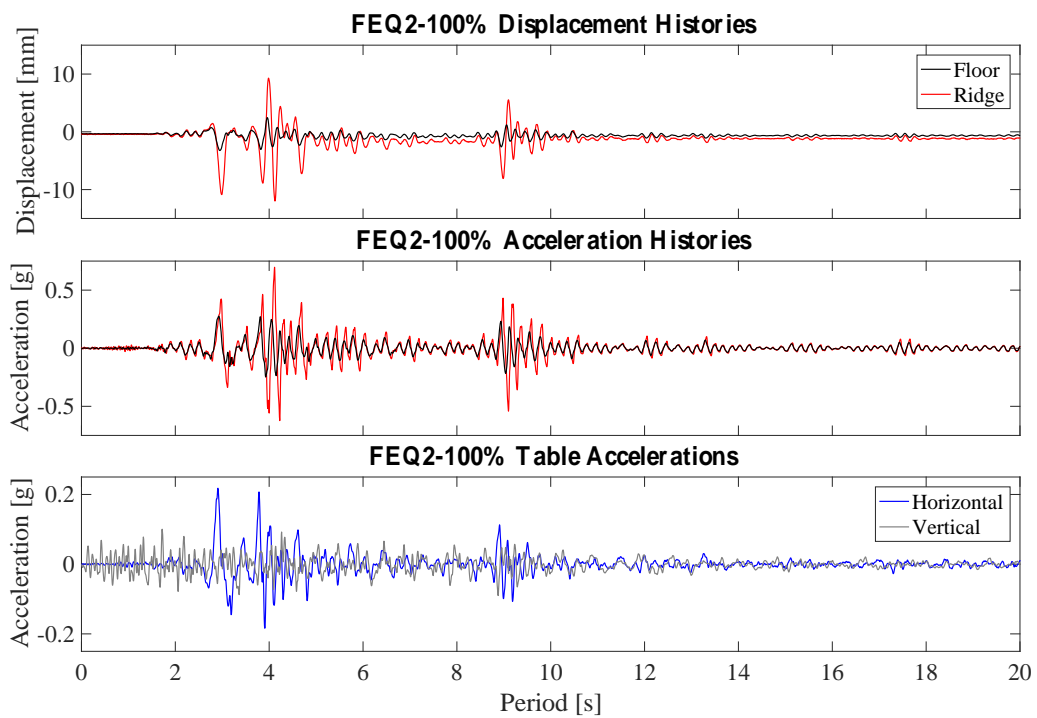


Figure 5.58 FEQ2-100%: Displacement and acceleration histories.

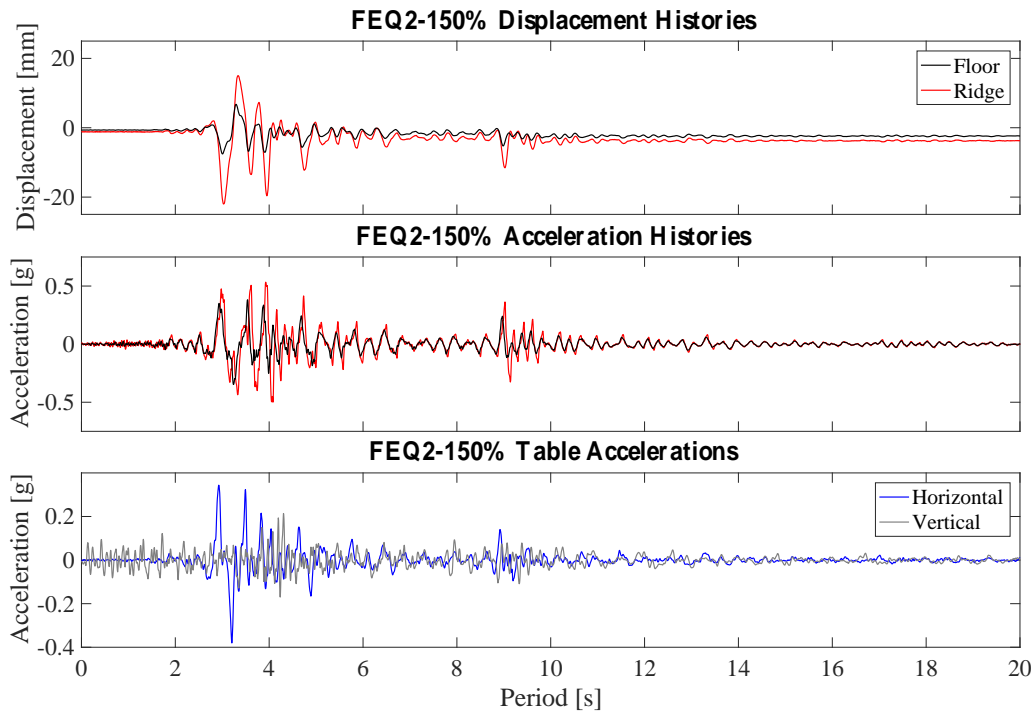


Figure 5.59 FEQ2-150%: Displacement and acceleration histories.

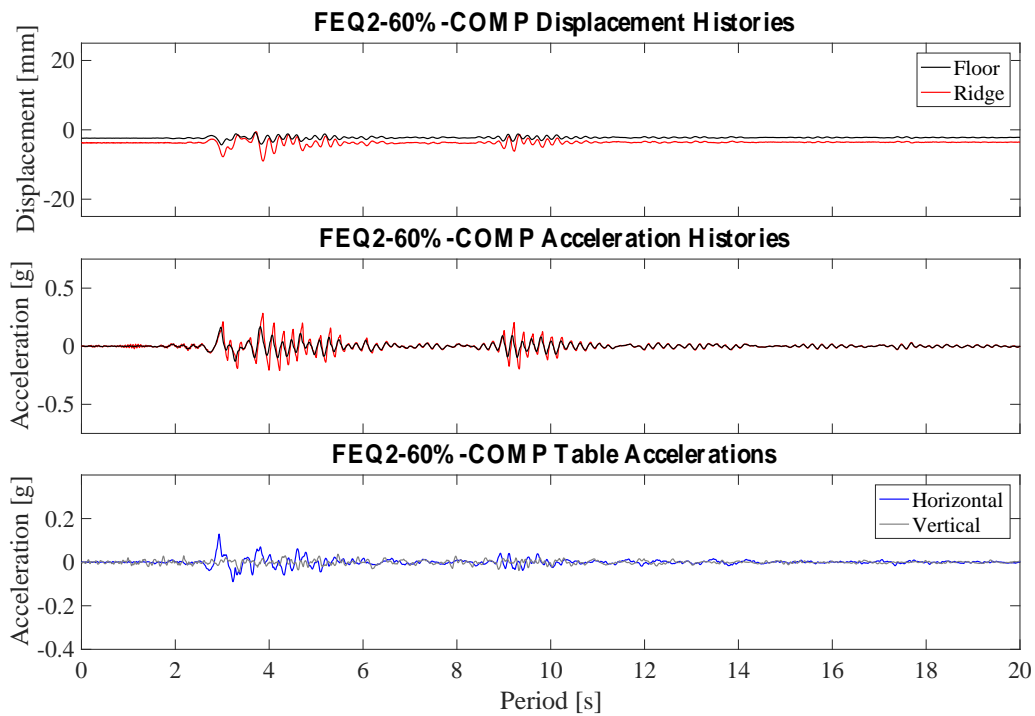


Figure 5.60 FEQ2-60%-COMP: Displacement and acceleration histories.

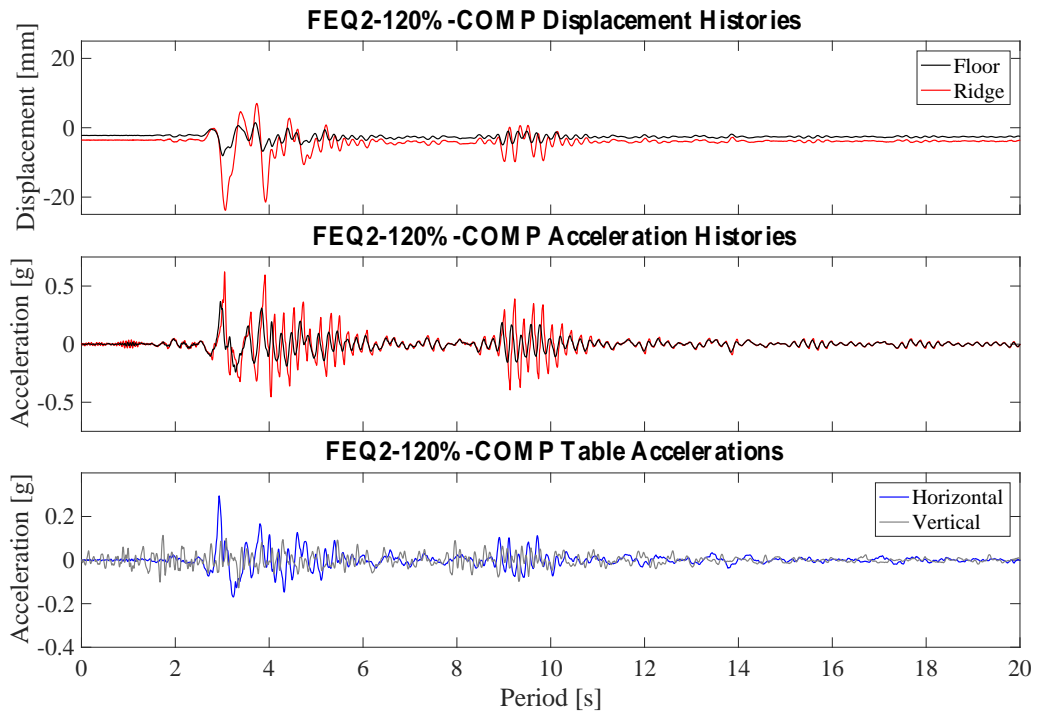


Figure 5.61 FEQ2-120%-COMP: Displacement and acceleration histories.

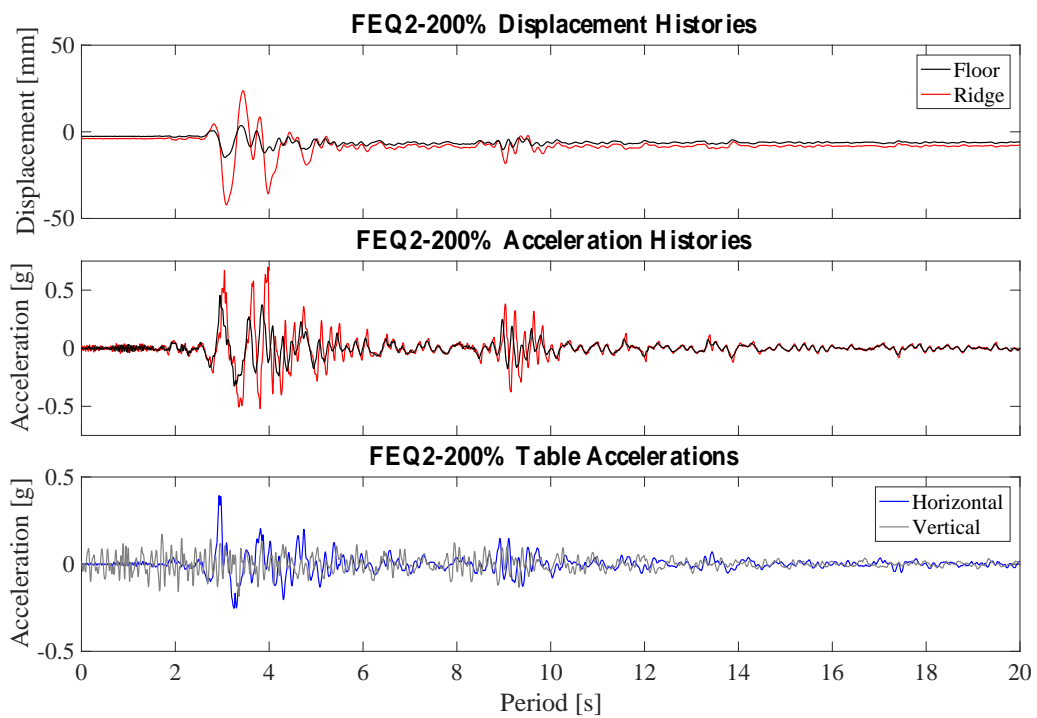


Figure 5.62 FEQ2-200%: Displacement and acceleration histories.

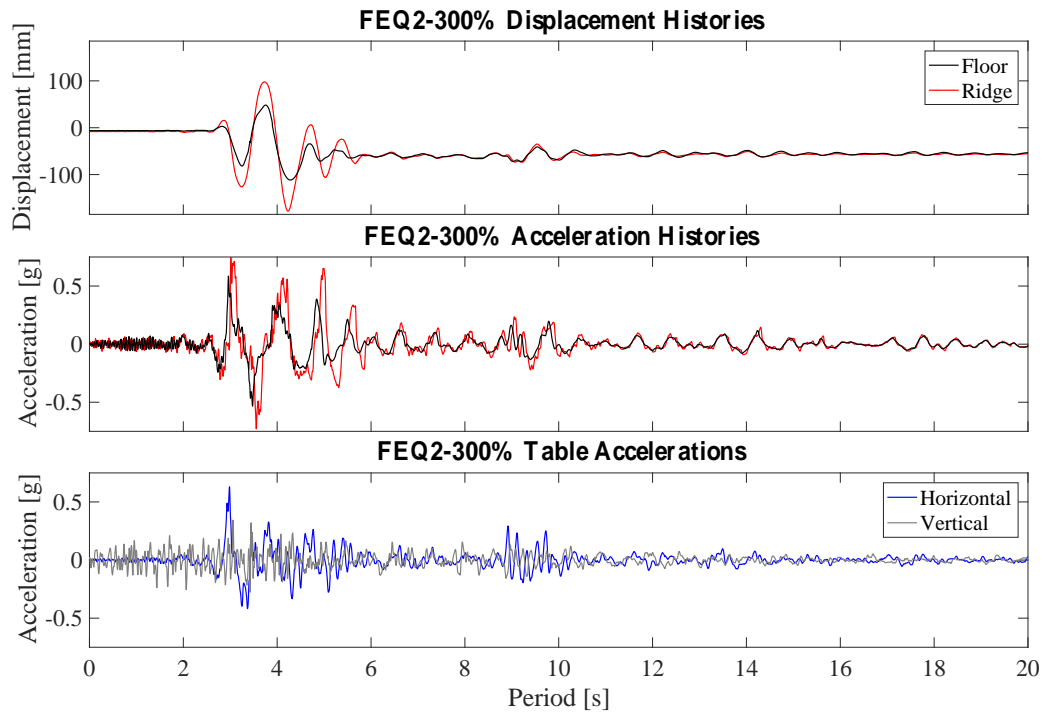


Figure 5.63 FEQ2-300%: Displacement and acceleration histories.

5.7 Deformed shape

Deformed shapes in elevation have been generated by plotting the average horizontal displacements recorded by the traditional potentiometers mounted on the floors and the wire potentiometers located at the level of the storey mid-height, at the floor level (recording the out-of-plane displacement of the clay wall) and at the ridge of the roof. The following figures (from Figure 5.64 to Figure 5.73) represent the out-of-plane deflected shape of a longitudinal cross section of the specimen at the instants of peak floor displacement and peak roof displacement, respectively. The deflected shapes have been amplified by a scaling factor indicated in the figures. In all tests, except for the FEQ2-300% one, the higher drifts were observed at the roof level. This sub-structure, indeed, resulted, as in Graziotti et al. (2015), significantly more flexible.

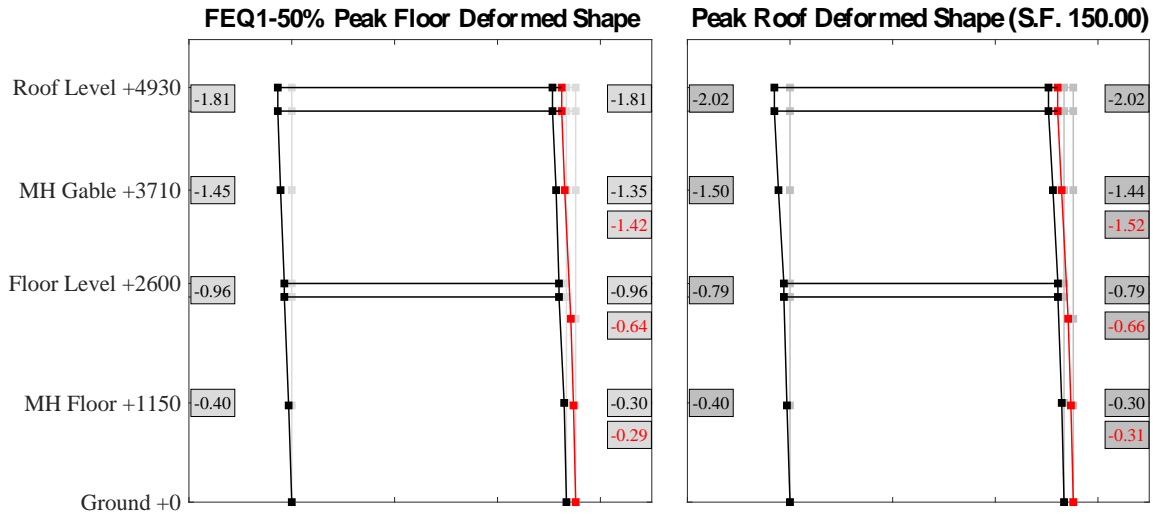


Figure 5.64 FEQ1-50%: Longitudinal cross section deflected shape.

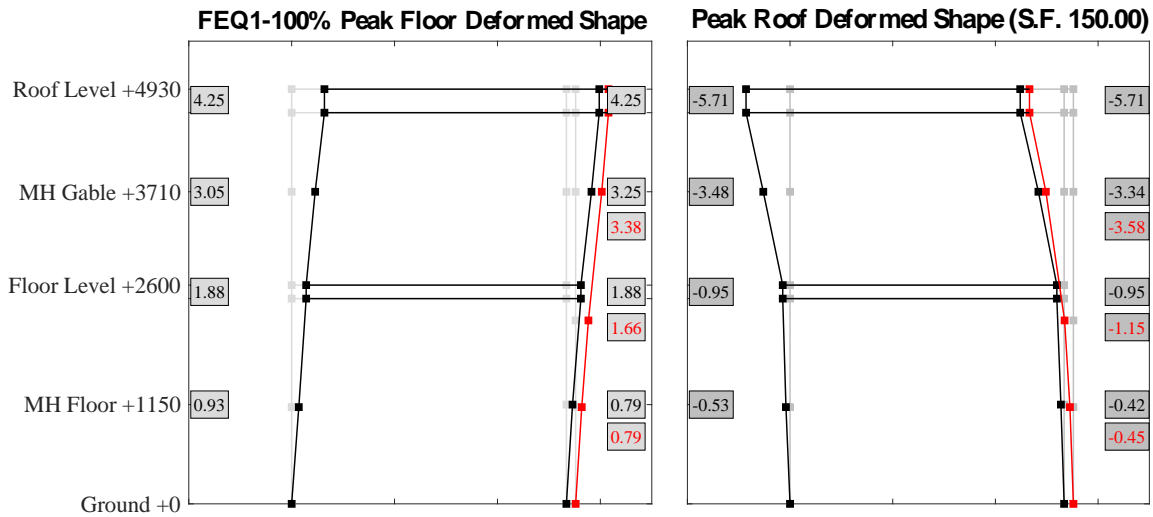


Figure 5.65 FEQ1-100%: Longitudinal cross section deflected shape.

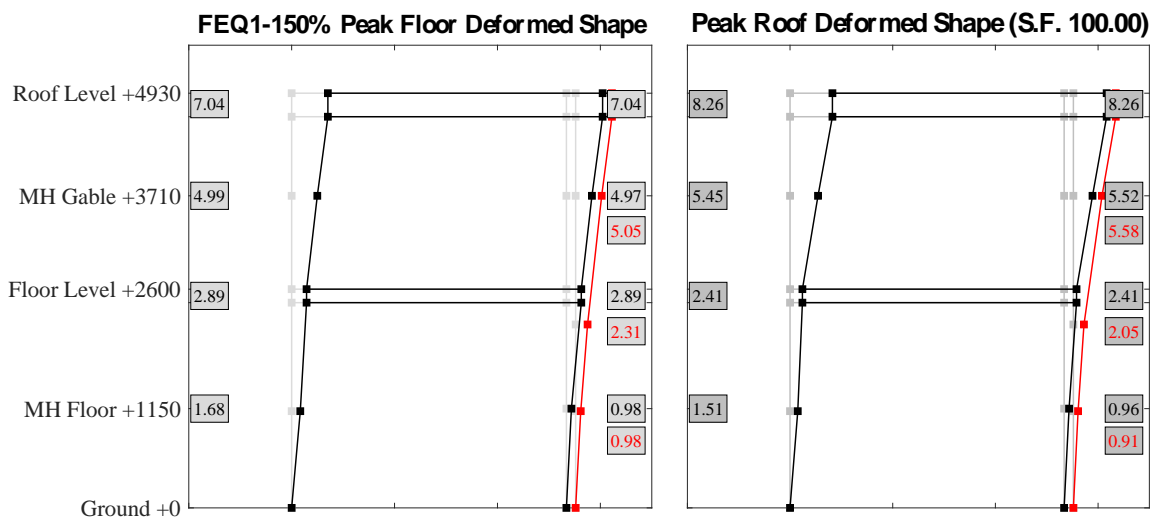


Figure 5.66 FEQ1-150%: Longitudinal cross section deflected shape.

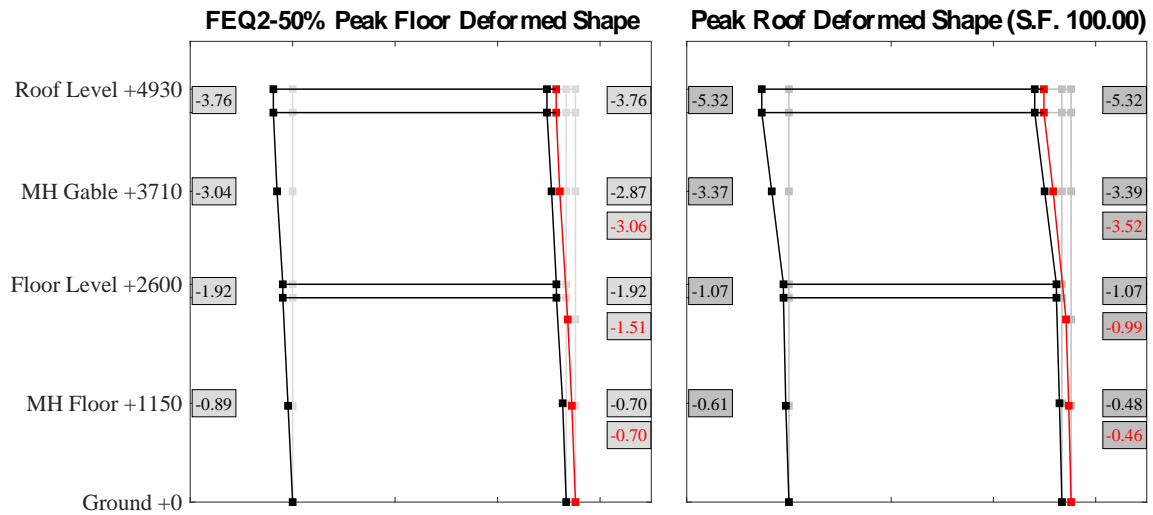


Figure 5.67 FEQ1-150%: Longitudinal cross section deflected shape.

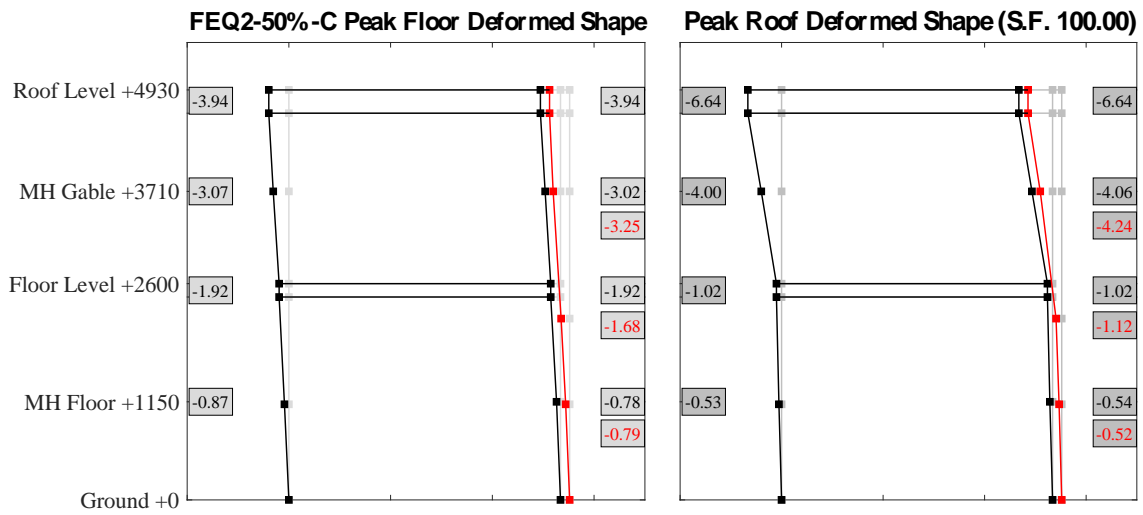


Figure 5.68 FEQ2-50%-COMP: Longitudinal cross section deflected shape.

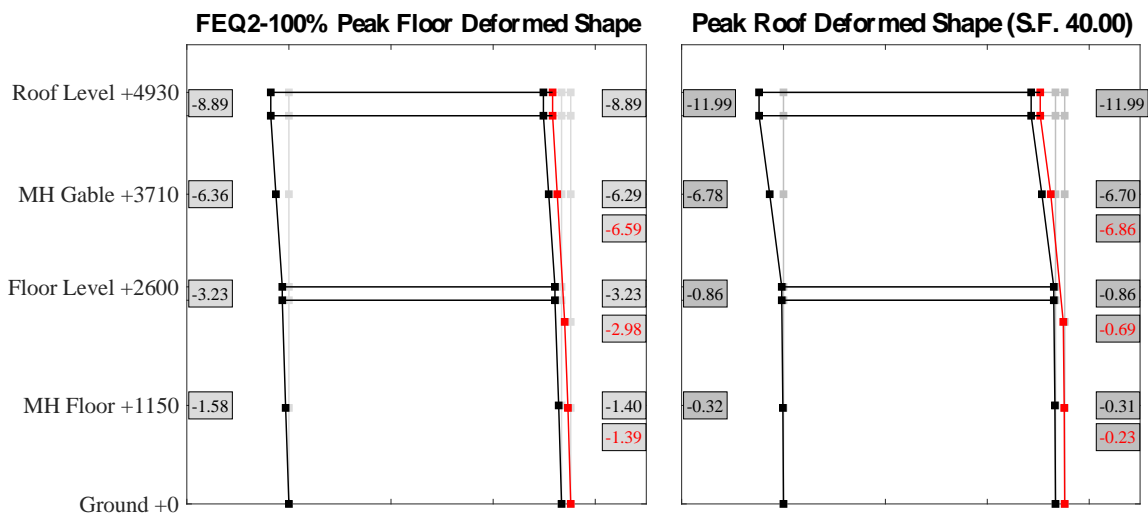


Figure 5.69 FEQ2-100%: Longitudinal cross section deflected shape.

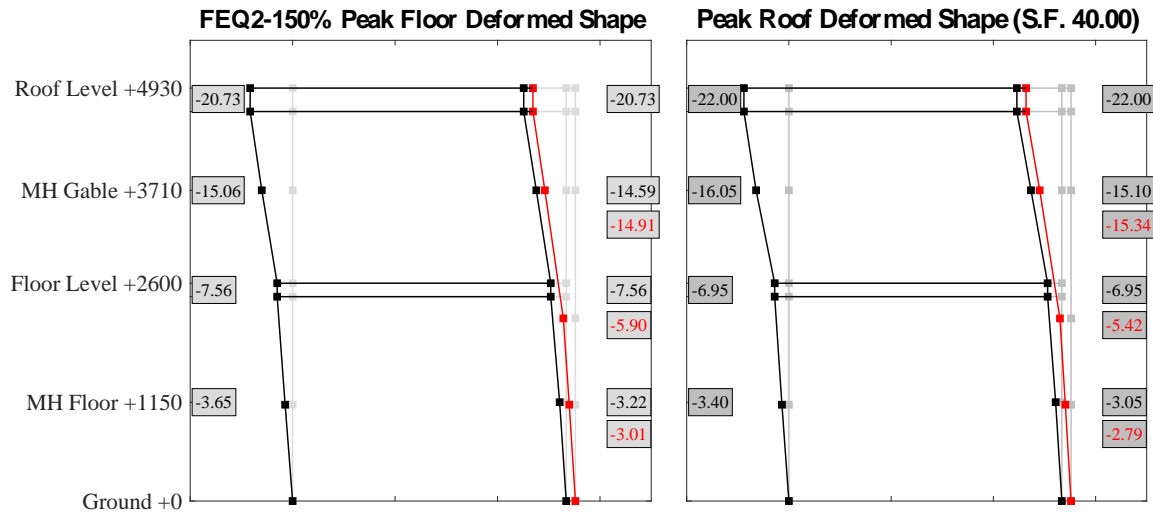


Figure 5.70 FEQ2-150%: Longitudinal cross section deflected shape.

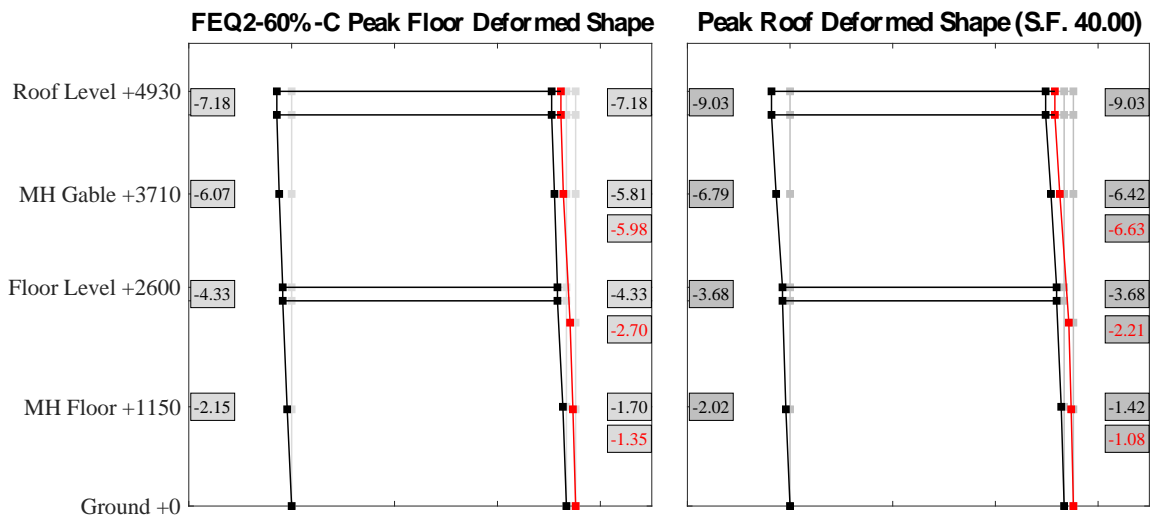


Figure 5.71 FEQ2-60%-COMP: Longitudinal cross section deflected shape.

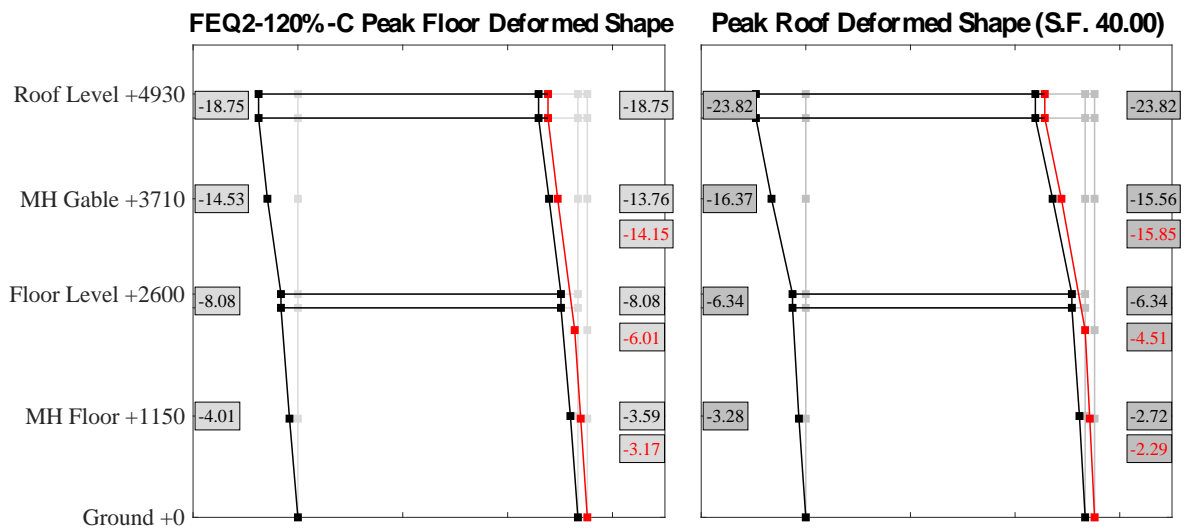


Figure 5.72 FEQ2-120%-COMP: Longitudinal cross section deflected shape.

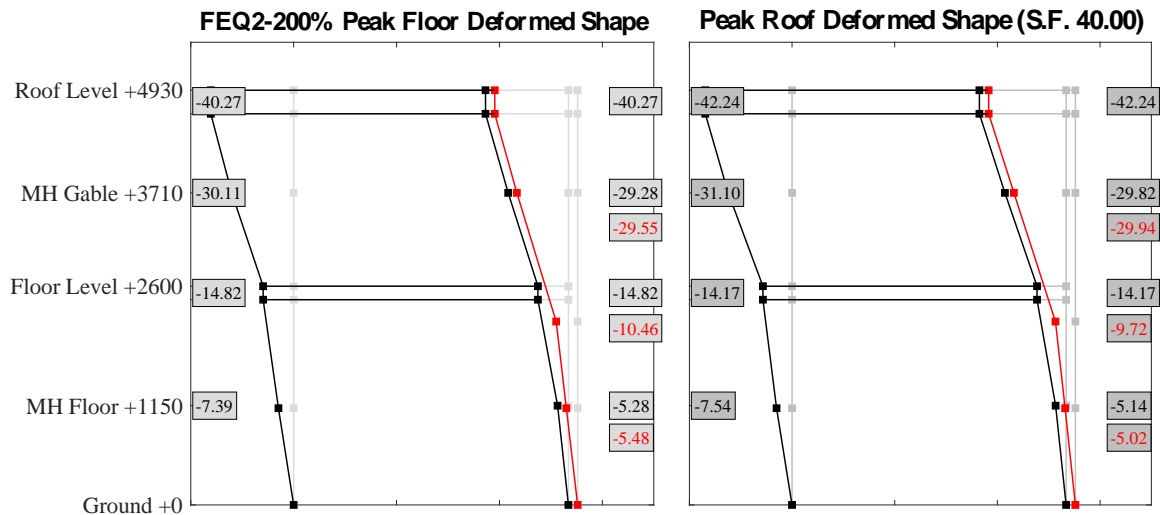


Figure 5.73 FEQ2-200%: Longitudinal cross section deflected shape.

The transportation of the specimen on the shaking table caused the failure of the interface between the top of the clay wall and the timber wall plates; consequently a clear relative displacement was observed in all tests between the timber plate (well attached to the slab) and the clay veneer, showing that the presence of cavity ties was not sufficient to ensure the collaboration between the two leaves. Most of the ties were permanently bent after the first tests.

On the other hand, the specimen transportation caused also the damage of the interface between the top of the CS longitudinal walls and RC slab. The bar plots in Figure 5.74 and Figure 5.75 compare the floor displacements with the differential displacements recorded between the top of CS longitudinal piers and the ones recorded between the timber plate and the top of clay longitudinal piers, respectively. Figure 5.74 shows as initially Piers 2 and 5 (Pot. Col. 21 and 17) displaced at the same way of the RC slab, while a significant differential displacement is recorded on top of Pier 1 (Pot. Col. 20). Increasing the ground motion intensity, it can be observed as the differential displacement of the Pier 1 is limited by the connection with the East OOP wall, while Piers 2 and 5 exhibited rather significant differential displacements.

Figure 5.75 confirms instead as the failure of the mortar bed-joint between the timber plate and the top of the clay wall caused the complete decoupling of the longitudinal veneer piers which were not involved in the oscillation of the overall building.

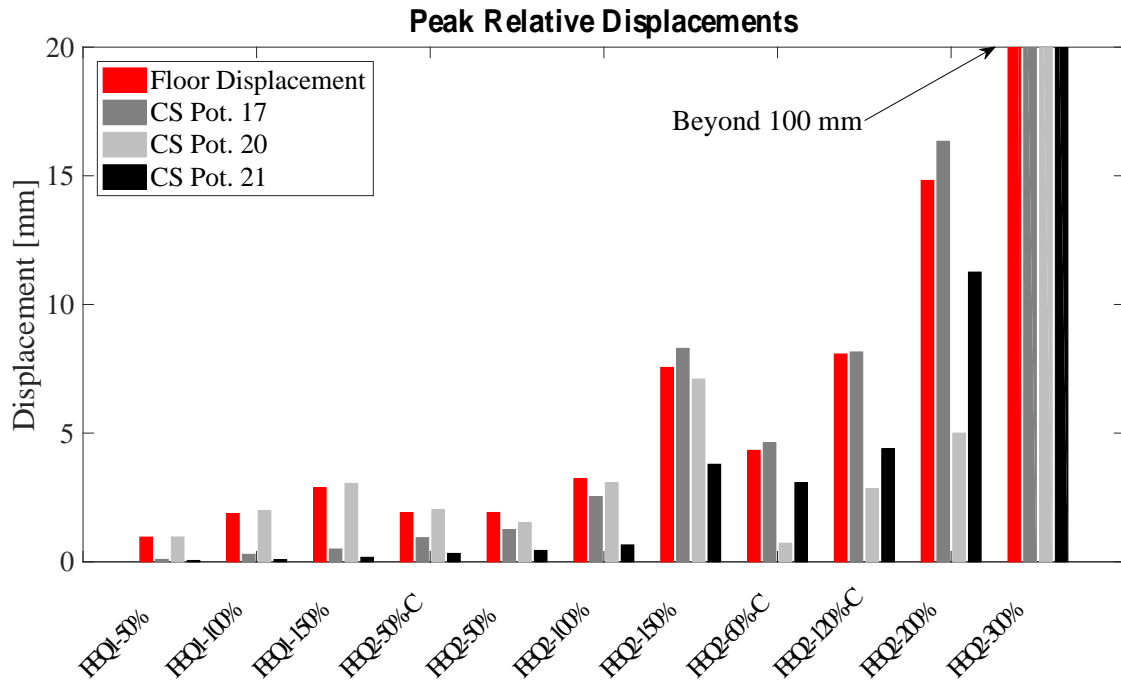


Figure 5.74 Differential displacement recorded between the top of the CS longitudinal piers and the RC slab.

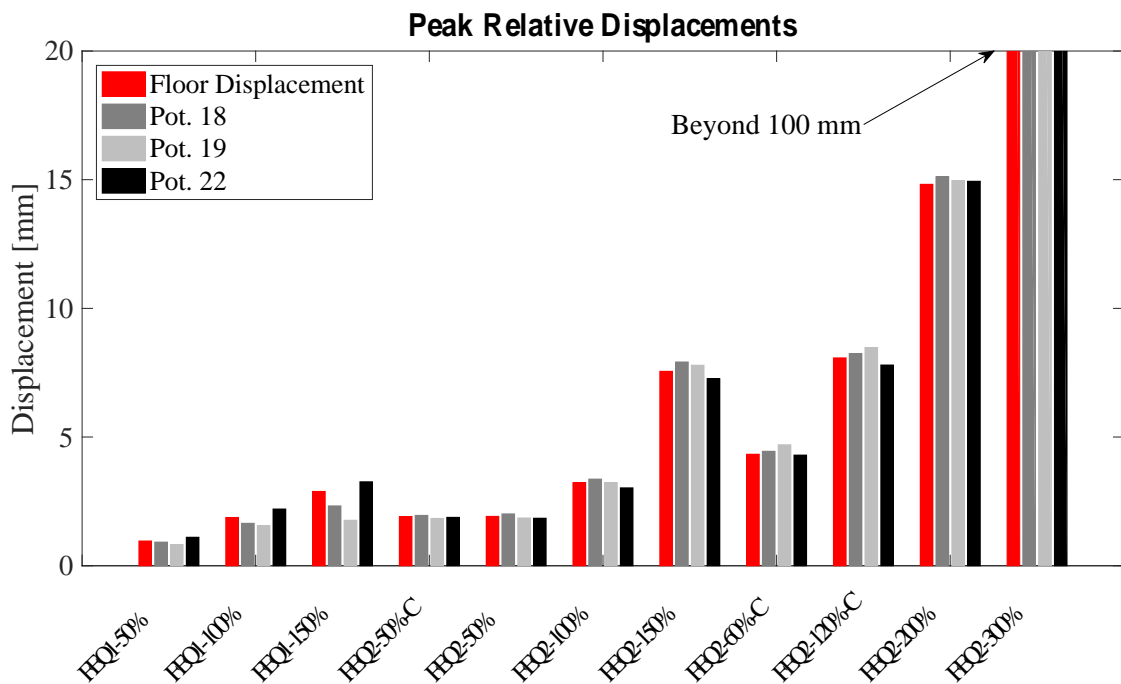


Figure 5.75 Differential displacement recorded between the top of the longitudinal clay piers and the timber plate.

5.8 Post-processing of the experimental data of the FEQ2-300% test

With the partial collapse occurred in test FEQ2-300%, the specimen displaced significantly in the longitudinal and transverse directions, several instruments got damaged or saturated, some of them were attached to the specimen portion which failed out-of-plane; many acceleration and displacement histories, resulted, hence, affected by the damage of the building prototype. The attempt of obtaining reliable displacement histories started from integrating the recorded acceleration histories.

In particular, the present section shows the post-processing operations carried out in order to obtain a reliable horizontal displacement history of the ridge beam, since the wire potentiometer 8 (col. 16) saturated without recording displacements beyond 140 mm. Figure 5.76 shows the comparison between recorded and integrated absolute horizontal displacement histories of the ridge beam; the former has been obtained by summing up the horizontal displacement history recorded by the wire potentiometer 8 (col.16) and the horizontal one of the shaking table (col. 1); the latter represent the displacement histories obtained by integrating and correcting the acceleration histories recorded by accelerometers 12 and 18 (col. 46 and 52). The integrated and corrected displacement histories cannot capture eventual sliding (e.g. constant velocity or displacement phases of the response) during the motion as well as the permanent residual displacement.

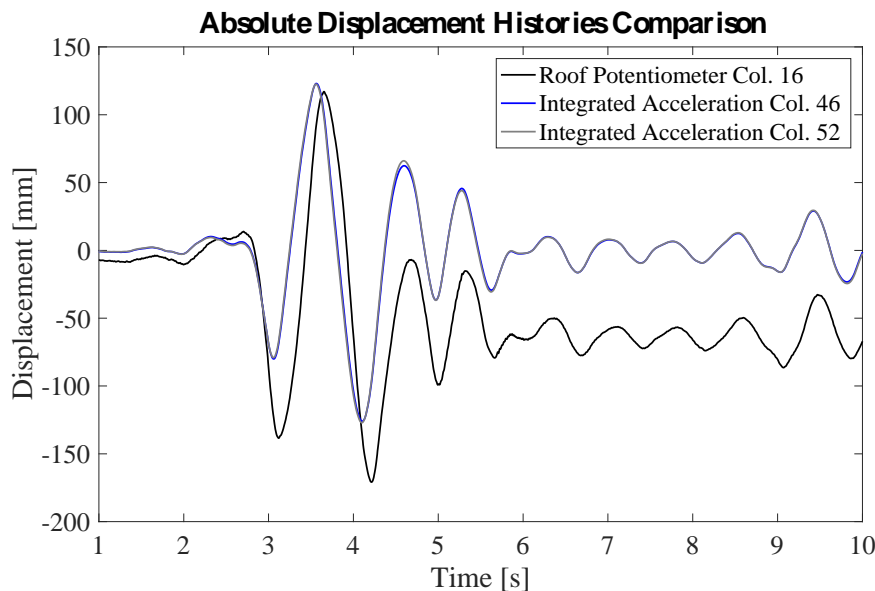


Figure 5.76 Comparison between roof recorded and integrated absolute horizontal displacement histories.

Figure 5.77 proposes the same comparison showing relative measurements (subtracting from the displacement time histories presented in Figure 5.76 the shaking table displacement). The recorded (black line) and integrated (grey line) histories appear considerably different, the wire potentiometer saturated around 4.2 s and seem to impact with some object between seconds 5 and 6. The integrated acceleration has been synchronised with the recorded displacement and shifted in order to match the residual displacement measured by the wire potentiometer; the modified integrated (grey dashed line) history showed a good match with the measured one beyond the 4 seconds of response; assuming that the sliding of the specimen (not captured by the integration) happened between seconds 2 and 4, the cleaned displacement history has been obtained adopting the recorded one and substituting the saturated region with a spline having as negative displacement peak the one given by the modified integrated history.

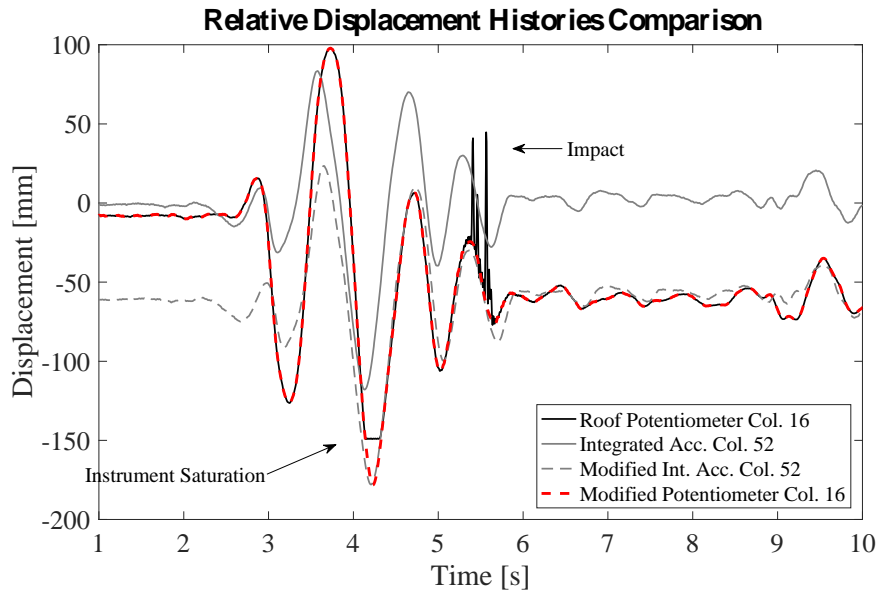


Figure 5.77 Comparison between roof recorded and integrated relative horizontal displacement histories.

This section shows, instead, the post-processing operations carried on in order to obtain a reliable horizontal displacement history of first-floor slab, since all the wire potentiometers (col. 24, 25 and 26) saturated without recording displacements beyond 55 mm. Figure 5.78 shows the comparison between recorded and integrated (col. 61 and 63) absolute horizontal displacement histories of the floor; the former has been obtained by summing up the floor horizontal displacement history recorded by the traditional potentiometers (col.1 xy) and the horizontal one of the shaking table (col. 1); the latter represent the displacement histories obtained by integrating and correcting the acceleration histories recorded by accelerometers 27 and 29 (col. 61 and 63). The integrated and corrected displacement histories cannot capture eventual sliding (e.g. constant velocity or displacement phases of the response) during the motion as well as permanent residual displacements.

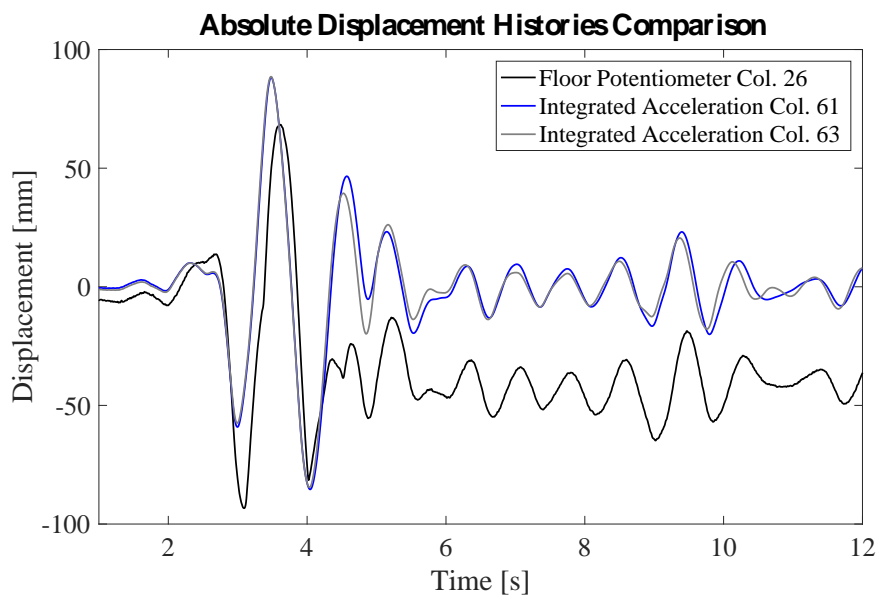


Figure 5.78 Comparison between floor recorded and integrated absolute horizontal displacement histories.

Figure 5.79 proposes the comparison in terms of relative displacement histories; The three displacement histories recorded by the potentiometers (col. 24, 25 and 26) are shown by the lines of different types in black. The potentiometer of column 24 saturated recording a positive residual displacement that cannot be considered reliable if compared with the observed slab residual displacement in the negative direction. The potentiometers 25 and 26 (located on the north and south sides, respectively) measured negative residual displacements partially capturing the torsional response exhibited by the floor slab. A reliable average residual displacement of the slab has been obtained, hence, taking into account the residual recorded by the roof potentiometers and assuming no permanent displacement of the system gables and roof diaphragm (according to visual inspection). The Integrated acceleration (col. 63) has been modified (dashed blue line) by summing to the integrated response the displacement modification line shown in yellow (accounting for sliding and a reliable residual), in order to match the displacement recorded by the potentiometers in the non-saturated regions. The final floor displacement (dashed red line) has been obtained from the modification of the displacement recorded by the potentiometer 18 (col. 26); the displacement peak around second 2.5 has been substituted with a spline having as negative peak value the one given by the modified integrated history; the second negative peak is slightly lower than the one given by the modified integrated history to better match the recorded displacement histories while final part of the response was obtained by translating the recorded history to match the residual given by the roof wire potentiometer (considered more reliable and centred with respect to the specimen geometry).

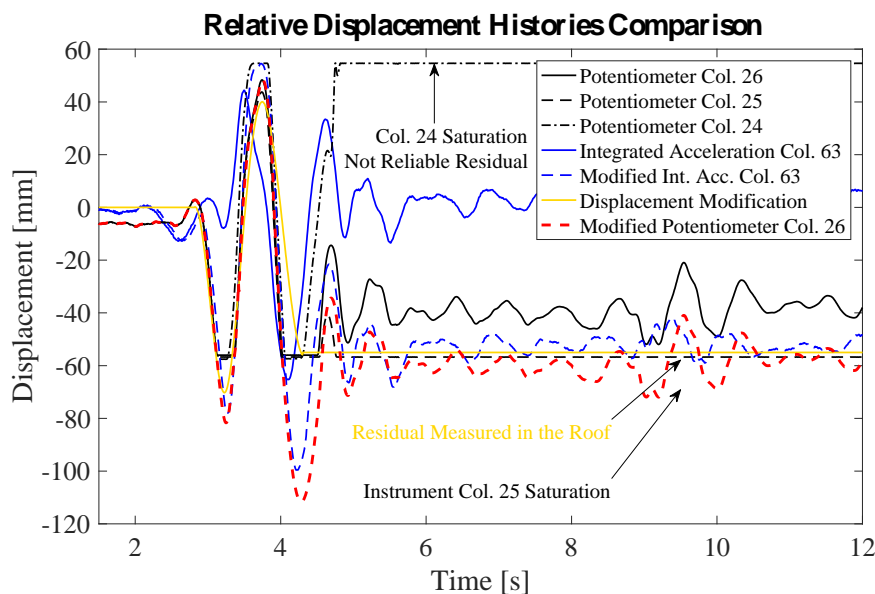


Figure 5.79 Comparison between floor recorded and integrated relative horizontal displacement histories.

Figure 5.80 shows the available acceleration and displacement histories monitoring the East wall during the last test FEQ2-300% when it collapsed out-of-plane. The recorded histories have been stopped at second 4.86 when during loss of equilibrium of the East wall the mid-height displacement was large enough (-136 mm) to saturate the wire potentiometer (col 9).

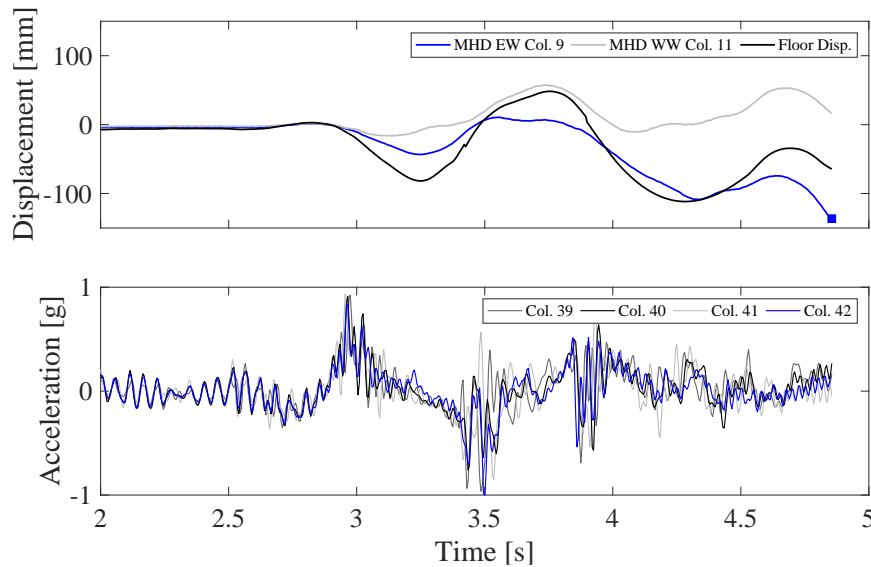


Figure 5.80 Displacement and acceleration histories of the East wall during the attainment of the OOP collapse.

5.9 Hysteretic Response

The evolution of the specimen's hysteretic response is shown in Figure 5.81, in terms of base shear, V , versus first-floor drift, θ_1 , which take into account the residual displacements. The time histories of the base shear have been computed as the sum of the products of each acceleration recording times the tributary mass of the corresponding accelerometer. Masses are assumed to be lumped at the accelerometer locations and listed in Table 3.1. The mass of the masonry body from the foundation level to the mid-height of the ground storey (at 1.22 m from the base) was assigned to the ground floor (and hence multiplied by the base acceleration time history). The base shear coefficient BSC is defined as:

$$BSC = \frac{V}{M \cdot g} \quad (23)$$

where Mg is the total weight of the specimen. In each plot of Figure 5.81, the hysteretic response of preceding tests is reported in grey. The red dots represent the positive and negative peak force responses with the corresponding displacements. The proportion between the two axes of all the plots is the same. In this way the eventual progressive specimen stiffness degradation and the consequent fundamental period elongation may be appreciable.

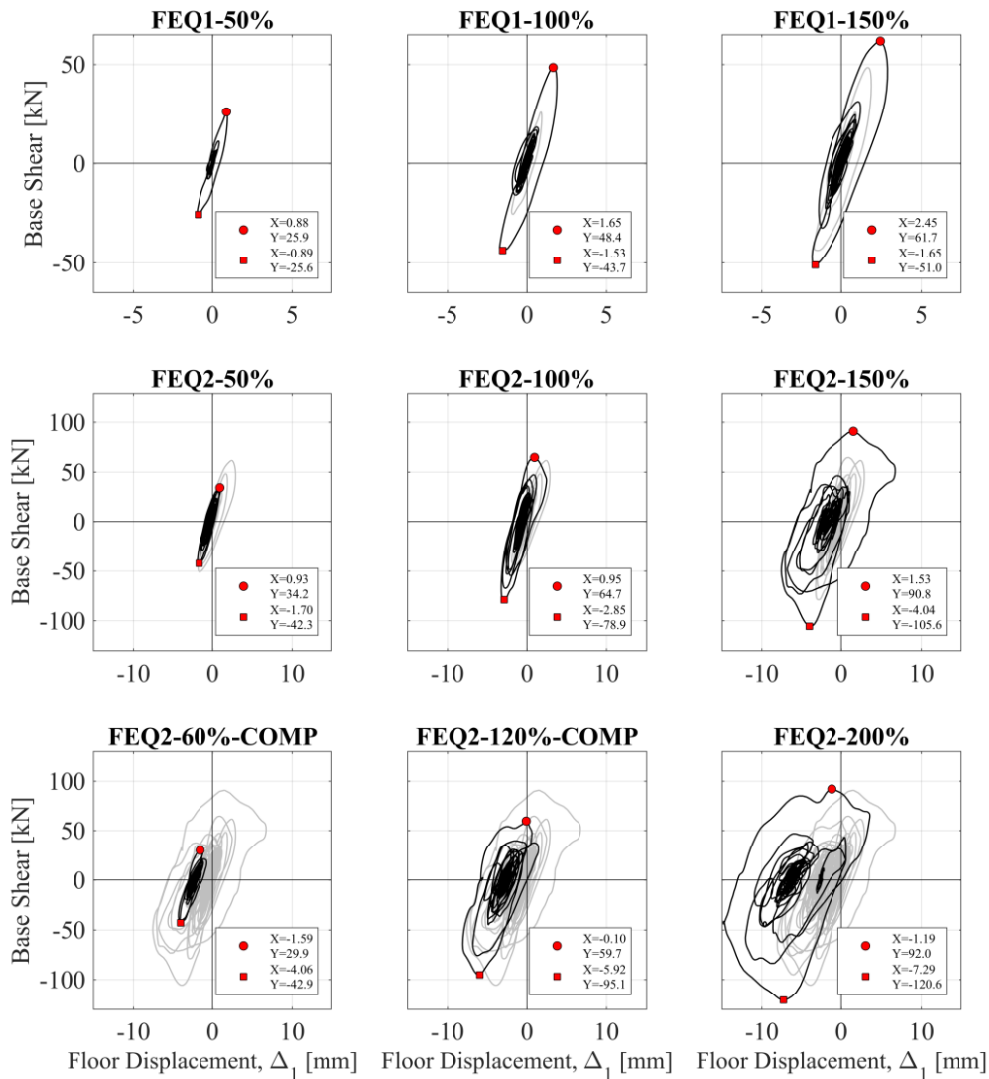


Figure 5.81 Evolution of specimen hysteretic response.

Figure 5.82 compares the hysteretic response exhibited by the specimen up to test FEQ2-200%. Figure 5.83 shows, instead, the hysteretic response related to the last test FEQ2-300%. The displacement and base shear histories have been truncated at the instant of the peak floor horizontal displacement.

The dynamic force-displacement backbone curve (shown by Figure 5.84) can be obtained by connecting the peak points of the experimental curves. In other words, it is defined as the plot of the maximum resisted base shear, V_{max} , and the corresponding first-floor drift depurated from residual displacements (e.g. each test floor displacement starts from 0), $\bar{\theta}_1$, for each stage of testing. The last point of both the positive and negative branch was obtained as the pair of the maximum drift attained and the corresponding base shear. The attainment of the higher base shear occurred for sway towards the negative direction (towards the single-leaf side, South). In particular, the base shear attained for southward motion ($V_{max}^- = 159.5$ kN) was 42% higher than the force reported for motion towards the double-leaf side of the structure ($V_{max}^+ = 111.6$ kN). The asymmetry in the envelope response curve could be attributed to the northward “spike” of the applied accelerogram FEQ2 and to the asymmetry of the structure.

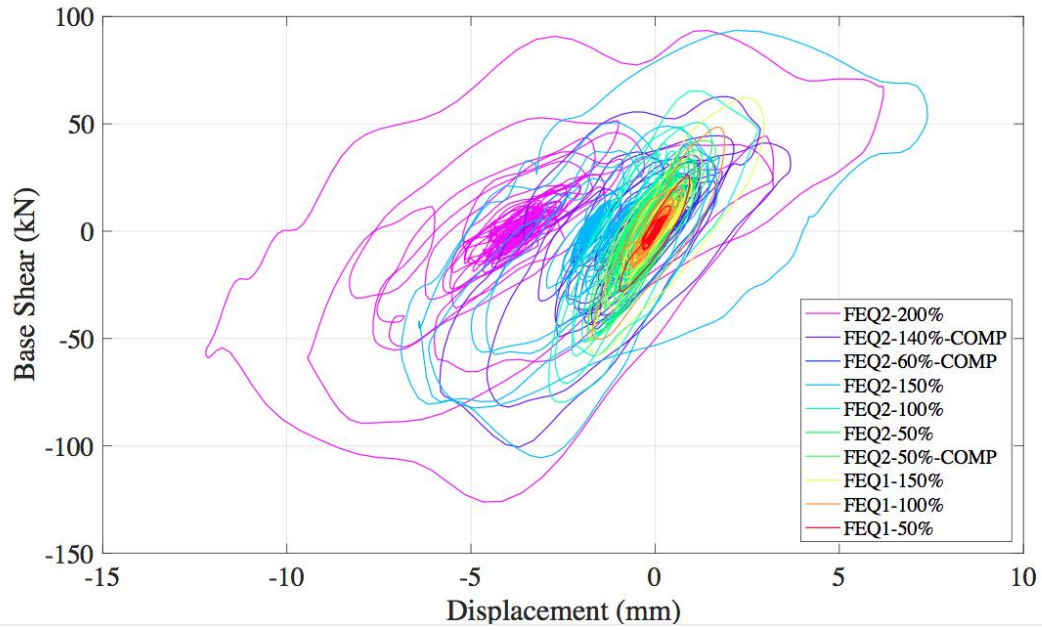


Figure 5.82 Evolution of specimen hysteretic response.

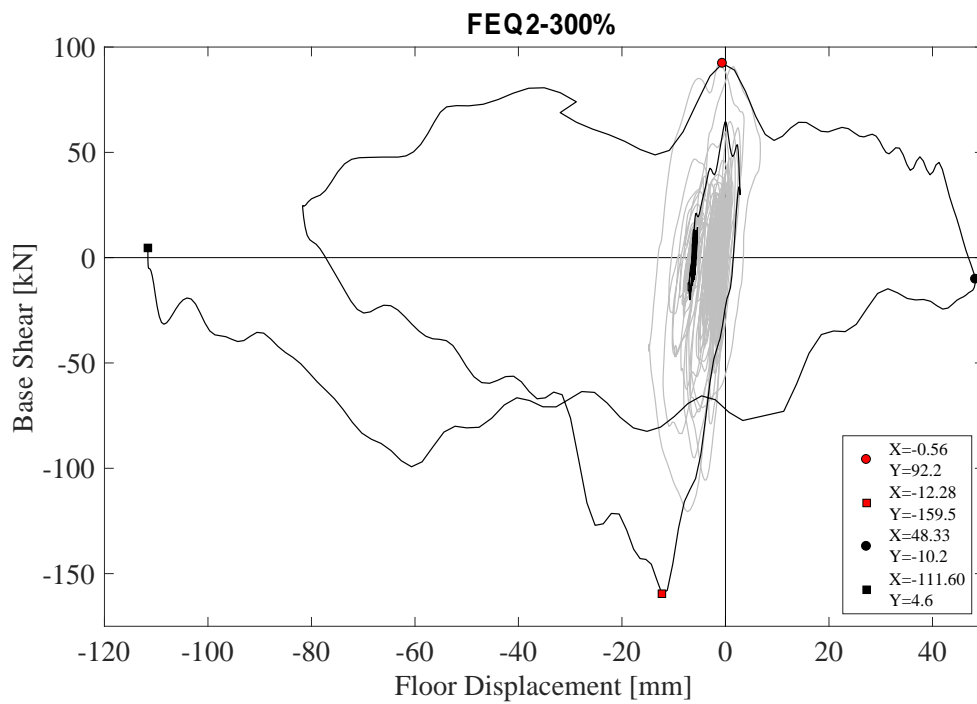


Figure 5.83 Hysteretic response during the FEQ2-300%.

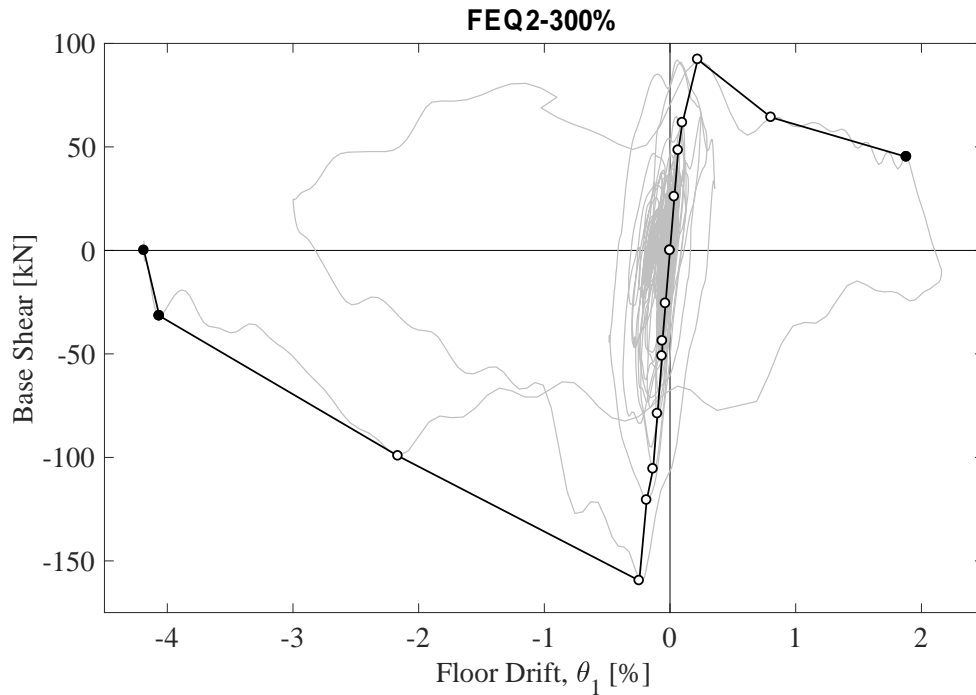


Figure 5.84 Backbone capacity curve.

Table 5.11 lists the coordinates of the peak resisted base shear with the associated floor displacement (depurated from residuals) and the peak displacement with the associated base shear, in the negative and positive directions, for each stage of testing.

Table 5.11 List of the backbone curve coordinates.

Test Name	Max Force, V, [kN]	Ass. Floor Disp. $\tilde{\Delta}_1$ [mm]	Min Force V, [kN]	Ass. Floor Disp. $\tilde{\Delta}_1$ [mm]	Max Floor Disp. $\tilde{\Delta}_1$ [mm]	Ass. Force V, [kN]	Min Floor Disp. $\tilde{\Delta}_1$ [mm]	Ass. Force V, [kN]
FEQ1-50%	25.9	0.88	-25.6	-0.89	0.94	22.5	-0.96	-23.4
FEQ1-100%	48.4	1.66	-43.7	-1.52	1.89	38.7	-1.71	-42.3
FEQ1-150%	61.7	2.51	-51.0	-1.59	2.95	48.0	-1.78	-46.6
FEQ2-50%-C	40.8	1.42	-48.8	-1.66	1.64	36.5	-1.84	-43.9
FEQ2-50%	34.2	1.17	-42.3	-1.46	1.27	32.3	-1.68	-40.1
FEQ2-100%	64.7	1.30	-78.9	-2.50	2.81	42.0	-2.89	-65.8
FEQ2-150%	90.8	2.19	-105.6	-3.38	7.40	50.7	-6.90	-49.8
FEQ2-60%-C	29.9	0.81	-42.9	-1.66	1.65	16.9	-1.93	-35.7
FEQ2-140%-C	59.7	2.13	-95.1	-3.69	3.68	31.5	-5.85	-64.6
FEQ2-200%	92.0	1.43	-120.6	-4.67	6.20	64.2	-12.20	-43.4
FEQ2-300%	92.2	5.57	-159.5	-6.15	54.45	-10.2	-105.47	4.6

5.10 Roof Response

The gable-roof system response was of particular interest for further investigation. The detailed response of the roof in the course of the shaking table testing is illustrated in Figure 5.85, in terms of acceleration versus relative displacement curves. The first quantity regards the acceleration, a_R , recorded by the accelerometers located at the ridge beam level, whereas the second refers to the relative displacement of the ridge, δ_R , with respect to the first-floor level.

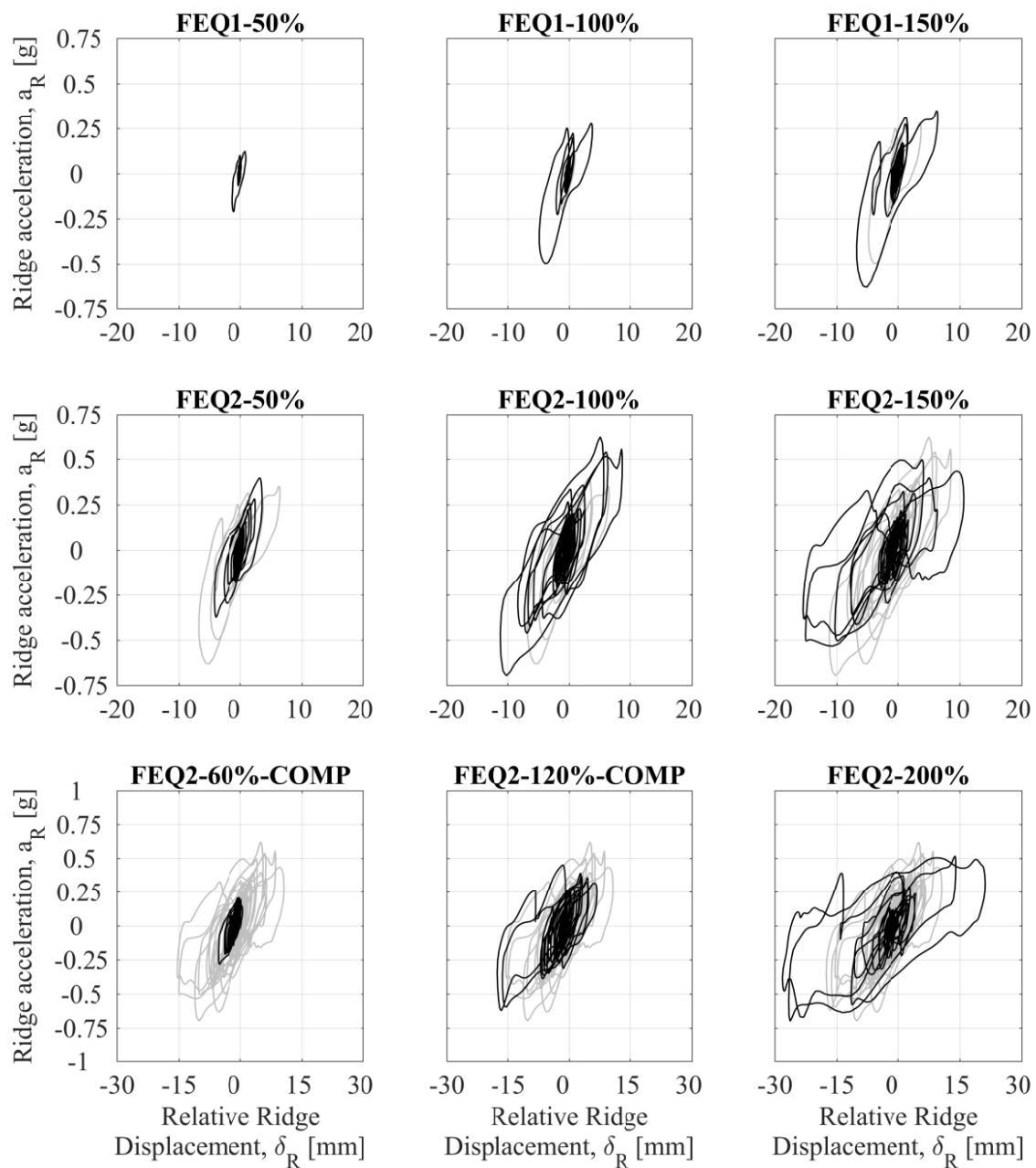


Figure 5.85 Evolution of the roof response.

Figure 5.86 shows the roof response during the last test FEQ2-300%. A peak ridge horizontal displacement beyond 60 mm has been recorded in the negative direction.

The dynamic force-displacement backbone curve of the roof (shown by Figure 5.84) can be obtained by connecting the peak points of the maximum resisted roof shear, $V_{R,max}$, and the corresponding relative displacement depurated from residual displacements (e.g. each test floor displacement starts from 0), δ_R , for each stage of testing. The last point of both the positive and negative branch was obtained as the pair of the maximum displacement attained and the corresponding roof shear.

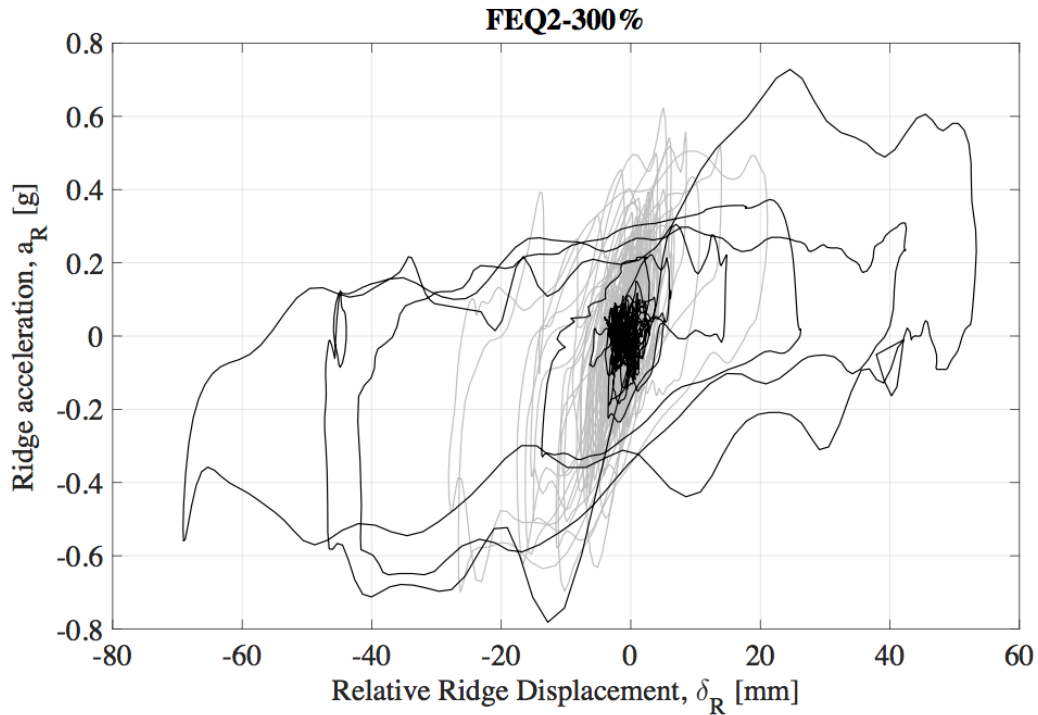


Figure 5.86 Roof response during FEQ2-300%.

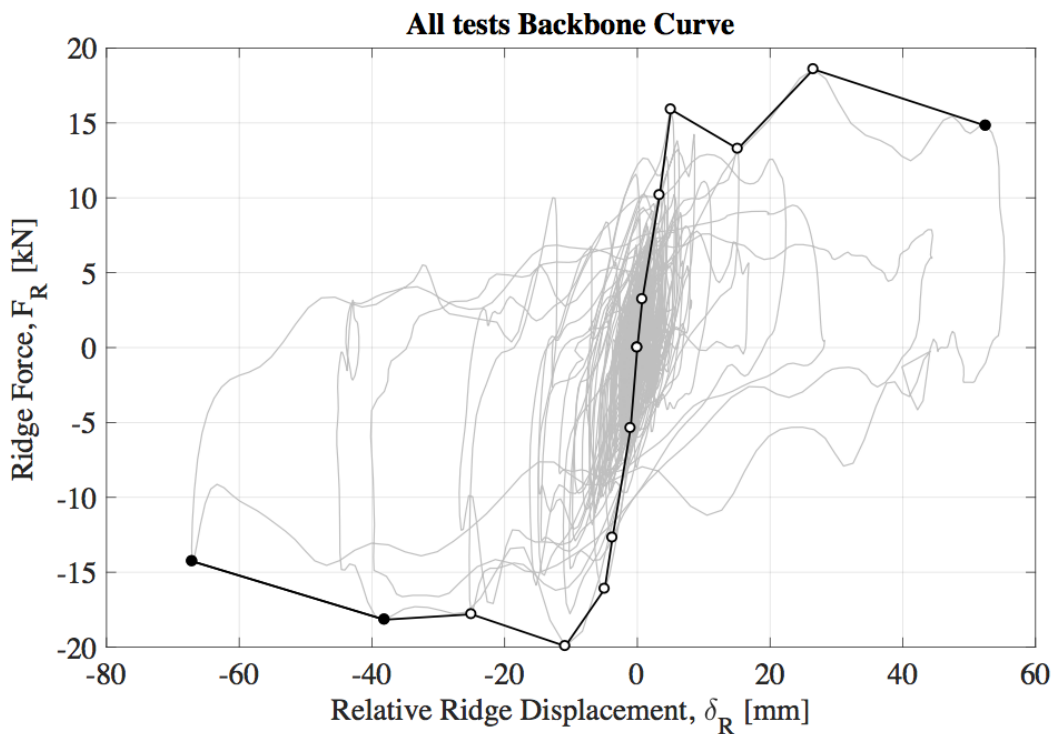


Figure 5.87 Roof backbone curve.

Table 5.12 lists the coordinates of the peak resisted roof shear with the associated roof relative displacement (depurated from residuals) and the peak roof relative displacement with the associated roof shear, in the negative and positive directions, for each stage of testing.

Table 5.12 List of the roof backbone curve coordinates.

Test Name	Max Force, V_R , [kN]	Ass. Floor Disp. $\tilde{\delta}_R$ [mm]	Min Force V_R , [kN]	Ass. Floor Disp. $\tilde{\delta}_R$ [mm]	Max Floor Disp. $\tilde{\delta}_R$ [mm]	Ass. Force V_R , [kN]	Min Floor Disp. $\tilde{\delta}_R$ [mm]	Ass. Force V_R , [kN]
FEQ1-50%	3.2	0.76	-5.4	-1.01	0.91	1.8	-1.3	-4.03
FEQ1-100%	7.1	3.67	-12.7	-3.75	3.88	6.4	-4.7	-9.71
FEQ1-150%	9.0	6.48	-16.1	-4.91	6.67	7.7	-6.6	-10.07
FEQ2-50%-C	10.6	3.80	-11.5	-5.15	4.21	7.5	-5.5	-6.92
FEQ2-50%	10.2	3.36	-9.6	-3.89	3.74	7.5	-4.1	-6.98
FEQ2-100%	15.9	5.07	-17.8	-10.16	8.64	13.1	-11.2	-11.88
FEQ2-150%	12.7	4.38	-13.6	-10.19	11.15	7.5	-14.9	-8.71
FEQ2-60%-C	5.3	1.15	-7.3	-3.85	1.94	2.7	-4.1	-6.30
FEQ2-140%-C	11.6	-0.23	-15.9	-15.25	8.04	6.3	-16.2	-8.77
FEQ2-200%	13.3	15.15	-17.8	-25.00	22.39	8.3	-26.8	-9.69
FEQ2-300%	18.6	26.55	-19.9	-10.85	55.32	5.9	-67.2	-13.39

5.11 Identification of specimen Damage Limit States

In this section, the identification of global quantitative thresholds that adequately describe the overall structural damage state of the building is attempted. Six damage states (DS) were considered: DS0, completely undamaged; DS1, no structural damage; DS2, minor structural damage; DS3, moderate structural damage; DS4, extensive structural damage; and DS5, very heavy structural damage, total or local collapse. As earlier mentioned in section 5.2, the building prototype experienced damage due to transportation before the starting of the dynamic testing sequence. A crack was observed at the base of the CS central pier (Pier 2) of the North façade, starting from the bottom edge of the window, two minor cracks appeared in the South Wall; for this reason, the building can be initially classified in DS2, having a slight structural damage. Although the pre-existing damage slightly affected the building response at low excitation amplitudes, DS0 and DS1 have been identified analysing the damage observed after the firsts stages of testing. The damage limits (DL), defining quantitative boundaries in terms of inter-storey drift between the aforementioned damage states, have been defined as follow:

- DL0 is defined as the maximum achieved level of displacement with no visible seismic damage (structural or non-structural). It has been identified with the peak floor drift equal to 0.04% achieved during FEQ1-50% (H-PGA=0.056g, V-PGA=0.036g) which did not cause any further damage; (H-PGV=33mm/s, V-PGV=8.5mm/s);
- DL1 is defined as the maximum achieved level of displacement with no visible structural damage. After tests FEQ1-150% (H-PGA=0.146g, V-PGA=0.122g), with a peak floor drift experienced by the specimen equal to 0.11%, only minor cracks (0.2 mm thick) on the plaster layer of the South wall were observed; the northern wall (without plaster) did not show any further damage, for this reason the surveyed damage was considered limited only to the specimen finishing; (H-PGV=86mm/s, V-PGV=28.9mm/s);
- DL2 is defined as the maximum achieved level of displacement with minor/slight structural damage. It has been identified at the end of the test FEQ2-100%, when a crack appeared at the bottom of Pier 1 in the North wall. The recorded peak floor drift was equal to 0.13%; (H-PGV=141mm/s, V-PGV=45mm/s);
- DL3 is defined as the maximum achieved level of displacement with moderate structural damage (but still repairable). This state was associated with damage observed in all the piers contributing to the longitudinal resistance of the

specimen after test FEQ2-150% (H-PGA = 0.380g, V-PGA= 0.214g) due to a peak floor drift equal to 0.30% (H-PGV=201mm/s, V-PGV=56mm/s);

- DL4 is defined as the maximum achieved level of displacement with extensive structural damage (e.g. not repairable). The limit could be considered as a collapse-prevention threshold. Generally, at this stage, small variations in the input intensities could lead to significantly different peak displacements. DL4 was addressed after a peak floor displacement of 0.59% recorded during test FEQ2-200% (H-PGA = 0.393g, V-PGA= 0.184g, H-PGV=273mm/s, V-PGV=66mm/s);
- DL5 is defined as the displacement associated with the loss of equilibrium of the specimen (or part of it). It has been identified with the peak floor displacement (4.43%) of the last test, FEQ2-300% (H-PGA = 0.630g, V-PGA= 0.343g), when the East wall collapsed out-of-plane (H-PGV=420mm/s, V-PGV=85mm/s).

Figure 5.88 identifies the DLs on the experimental backbone curve defined in terms of *BSC* and floor drift (taking into account the residuals).

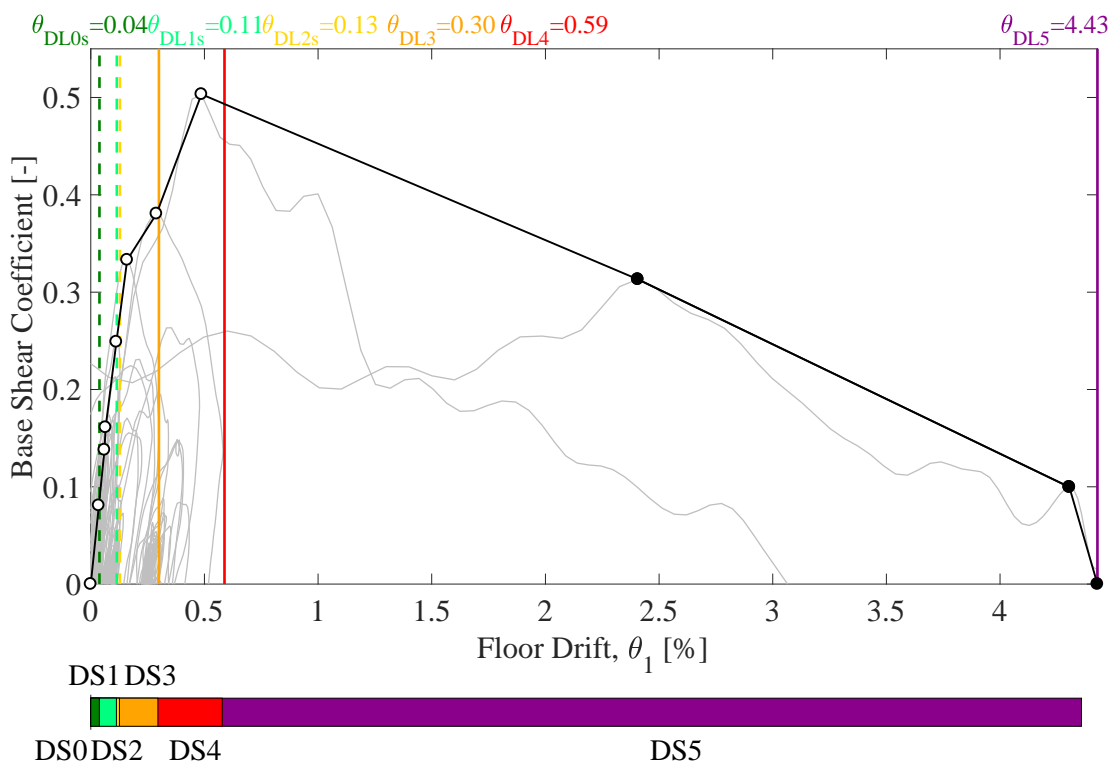


Figure 5.88 Identification of the DLs on the building backbone curve.

5.12 Derivation of EDP according to specimen performance

Figure 5.89 reports the building performance in terms of peak displacements (Δ_I and Δ_R), IDR (θ_I and roof diaphragm shear deformation γ_R) usually strictly connected to the in-plane damage occurring in structural elements like piers and spandrels, and RIDR very often associated with a general damage and damage accumulation. The response in terms of PFA/PGA is also shown. This EDP could be correlated with the OOP performance of masonry (or more in general secondary) components or the damage occurring to acceleration sensitive non-structural components. The evolution of the building fundamental period of vibration during all test phases is also shown.

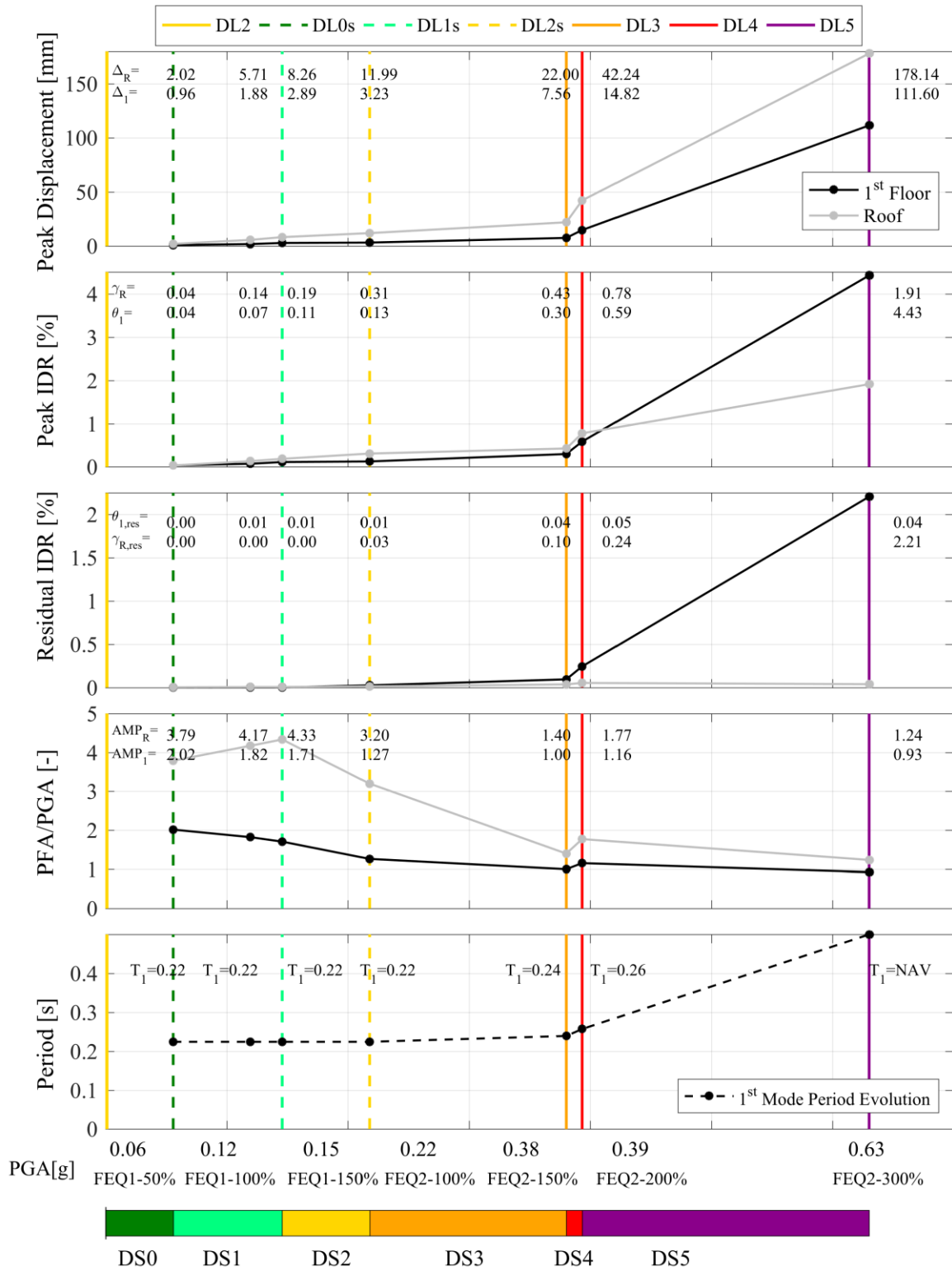


Figure 5.89 Summary of the performance of the building specimen.

REFERENCES

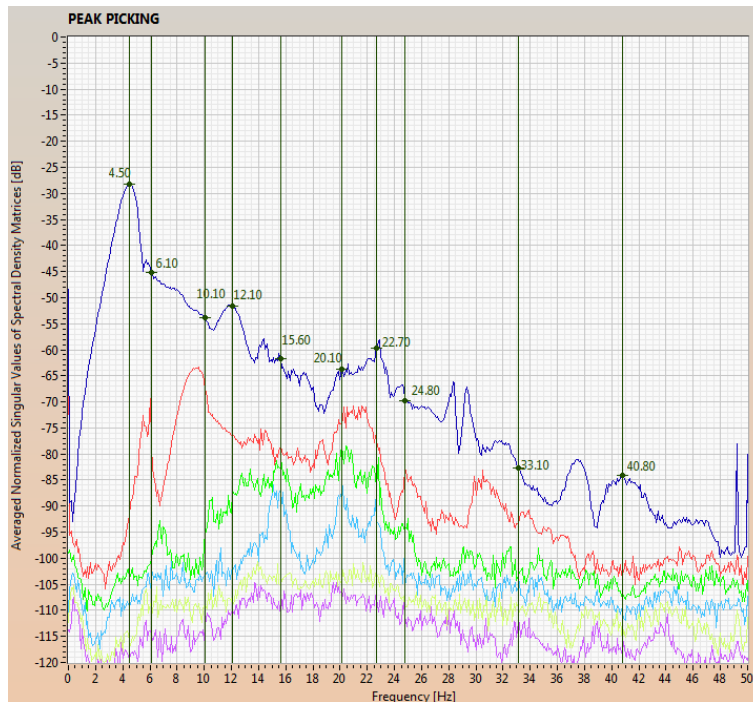
- Allemang, R.J., Brown, D.L. (1982) "A Correlation Coefficient for Modal Vector Analysis," Proceedings of the 1st International Modal Analysis Conference (IMAC I), Orlando, USA.
- Bendat, J.S., Piersol, A.G. (2010) "Random Data: Analysis and Measurement Procedures," 4th Edition, ISBN: 0470248777, Wiley Series in Probability and Statistics.
- Brincker, R., Ventura, C., et al. (2001) "Damping Estimation by Frequency Domain Decomposition," Proceedings of the 19th International Modal Analysis Conference (IMAC XIX), Kissimmee, USA.
- Graziotti, F., Tomassetti, U., Rossi, A., Kallioras, S., Mandirola, M., Cenja, E., Penna, A., Magenes, G. (2015) "Experimental campaign on cavity-wall systems representative of the Groningen building stock", Technical Report EUC318/2015U, Eucentre, Pavia, Italy. Available on URL: <http://www.eucentre.it/project-nam/>
- Graziotti, F., Tomassetti, U., Penna, A., Magenes, G. (2016b) "Out-of-plane shaking table tests on URM single leaf and cavity walls", Engineering Structures, 125, 455-470, doi:10.1016/j.engstruct.2016.07.011.
- Magenes, G., Penna, A., Senaldi, I.E., Rota, M., Galasco, A. (2014) "Shaking Table Test of a Strengthened Full-Scale Stone Masonry Building with Flexible Diaphragms", International Journal of Architectural Heritage: Conservation, Analysis, and Restoration, 8:3, 349-375.
- Mendes, L., Campos Costa, A., (2007) "LNEC-SPA – Signal Processing and Analysis Tool for Civil Engineers. Version 1.0 – Build 12," Report LNEC 29
- Tomažević, M., Weiss, P. and Velechovsky, T. (1991) "The influence of rigidity of floors on the seismic behaviour of old stone-masonry buildings," European Earthquake Engineering, 3.
- Tondelli, M., Graziotti, F., Rossi, A., Magenes, G. (2015) "Characterisation of masonry materials in the Groningen area by means of in-situ and laboratory testing", Technical Report, Eucentre, Pavia, Italy. Available on URL: <http://www.eucentre.it/project-nam>

ANNEXES

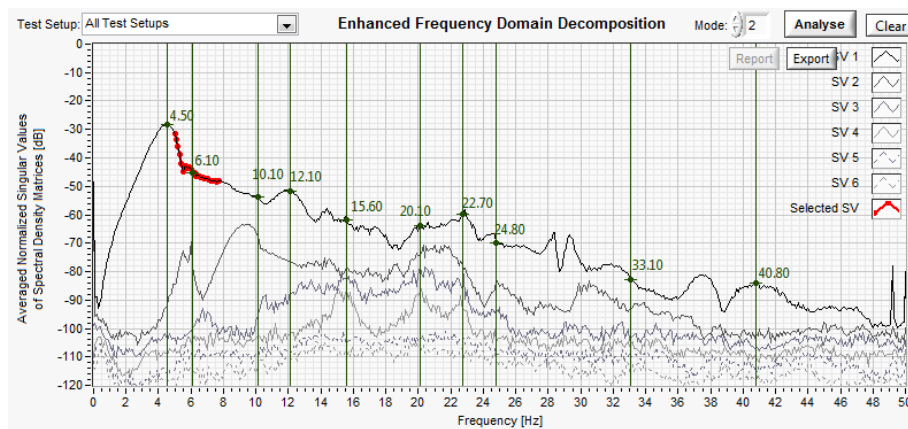
ANNEX I

Additional dynamic identification tests on the shaking table

3rd dynamic identification (Test 5)



FDD results for 3rd dynamic identification (Test 5)



EFDD results for 3rd dynamic identification (Test 5)

Summary of vibration modes' characteristics for 3rd dynamic identification (Test 5):

Mode	FDD Frequency [Hz]	EFDD Frequency [Hz]	Damping [%]
1	4.50	4.46	4.28
2	6.10	5.69	4.34
3	10.10	10.12	2.02
4	12.10	12.13	1.78
5	15.60	15.60	1.33

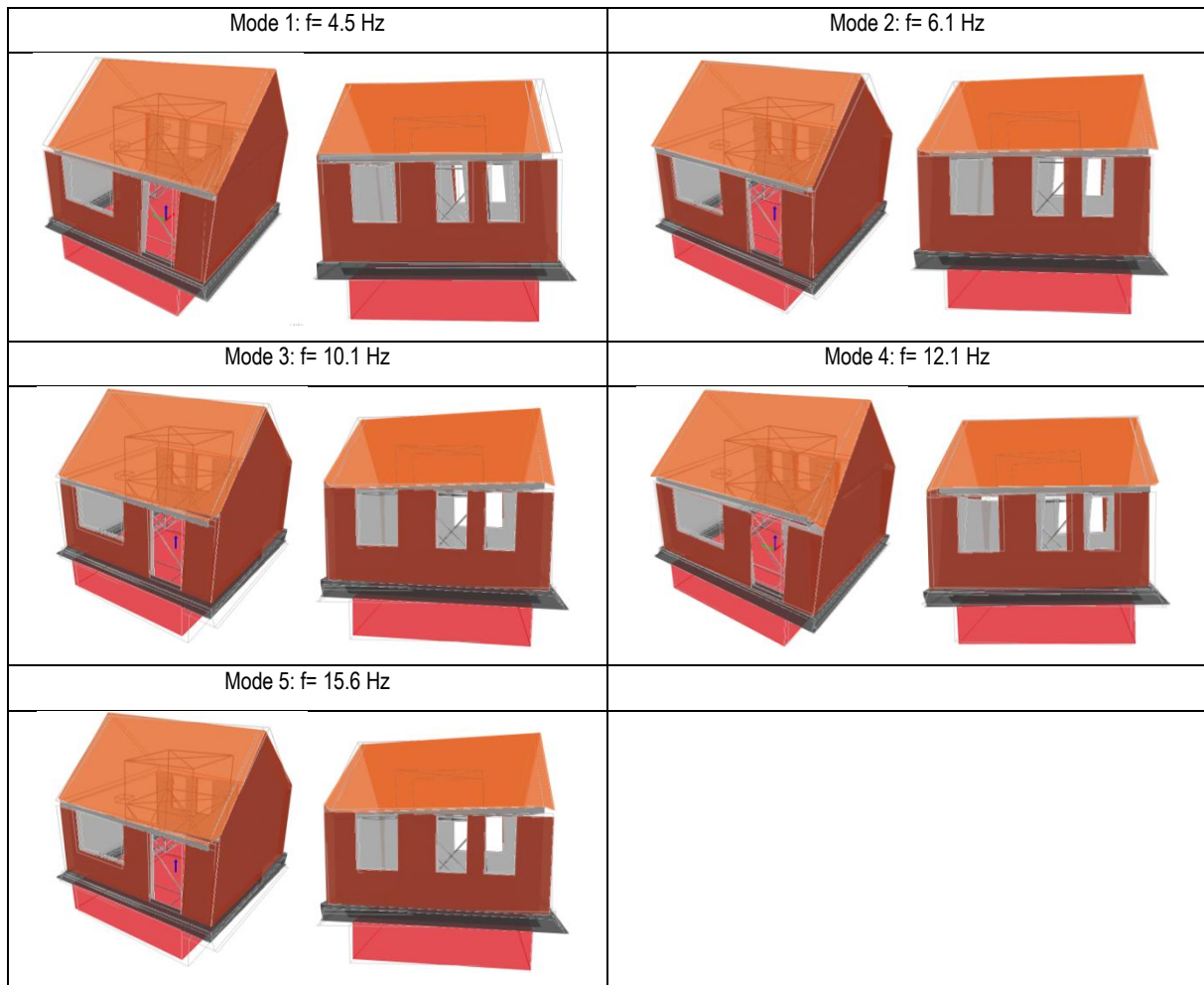
174 Collapse Shaking Table Test on URM Cavity Wall Structure representative of a Dutch Terraced House

MAC coefficients for 3rd dynamic identification (Test 5):

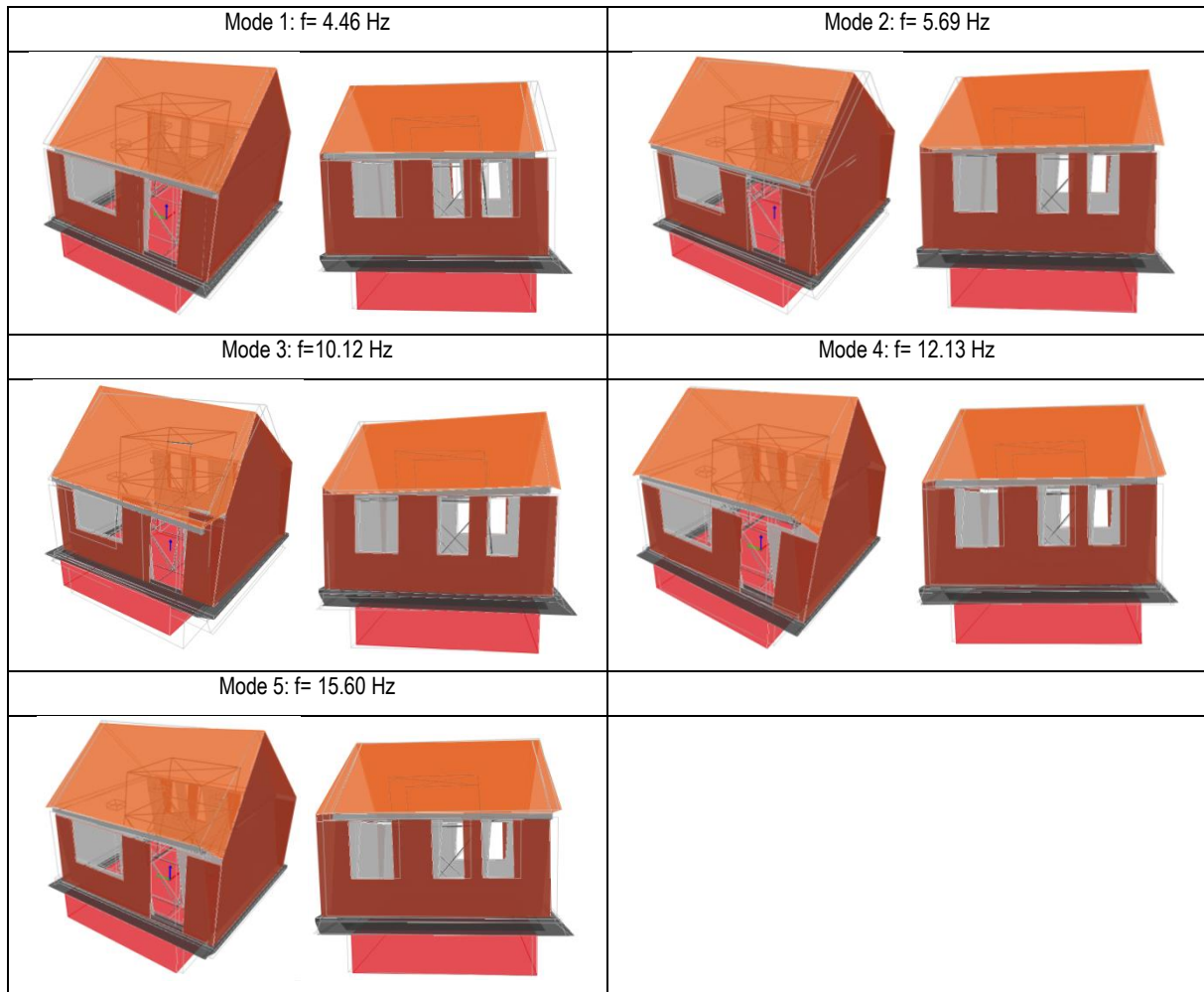
MODE i_j		MODE_01_03	MODE_02_03	MODE_03_03	MODE_04_03	MODE_05_03
	Frequency [Hz]	4.5	5.7	10.1	12.1	15.6
MODE_01_02	4.5	1.00	0.86	0.59	0.45	0.57
MODE_02_02	5.8	0.92	0.99	0.51	0.33	0.40
MODE_03_02	9.3	0.63	0.60	0.83	0.76	0.75
MODE_04_02	12.1	0.42	0.34	0.69	1.00	0.88
MODE_05_02	15.3	0.58	0.47	0.58	0.81	0.98

i Mode

j dynamic identification

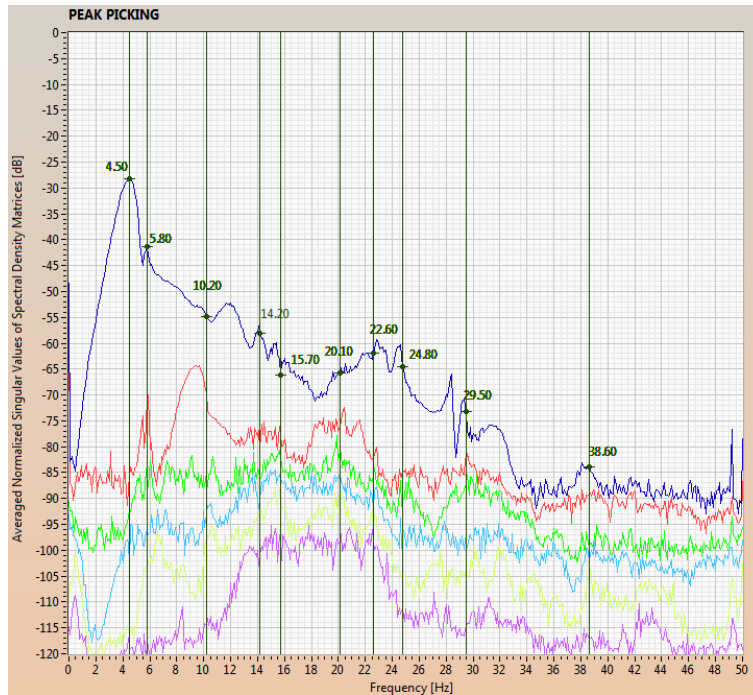


FDD mode shapes for 3rd dynamic identification (Test 5)

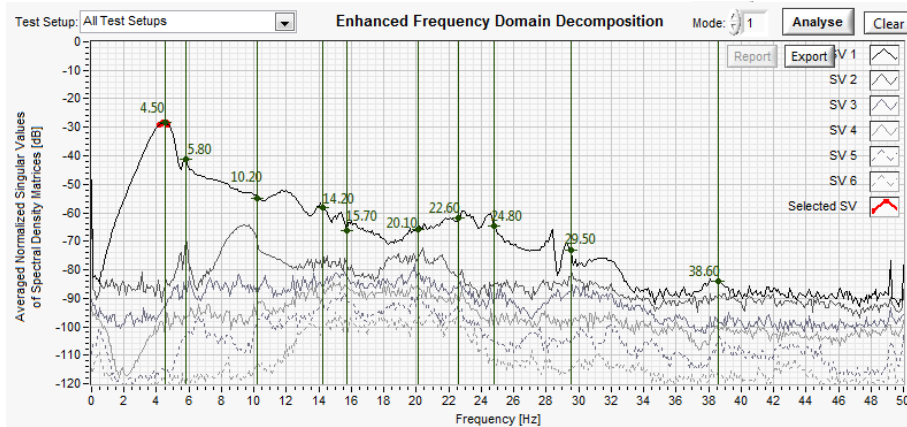


EFDD mode shapes for 3rd dynamic identification (Test 5)

4th dynamic identification (Test 7)



FDD results for 4th dynamic identification (Test 7)



EFDD results for 4th dynamic identification (Test 7)

Summary of vibration modes' characteristics for 4th dynamic identification (Test 7):

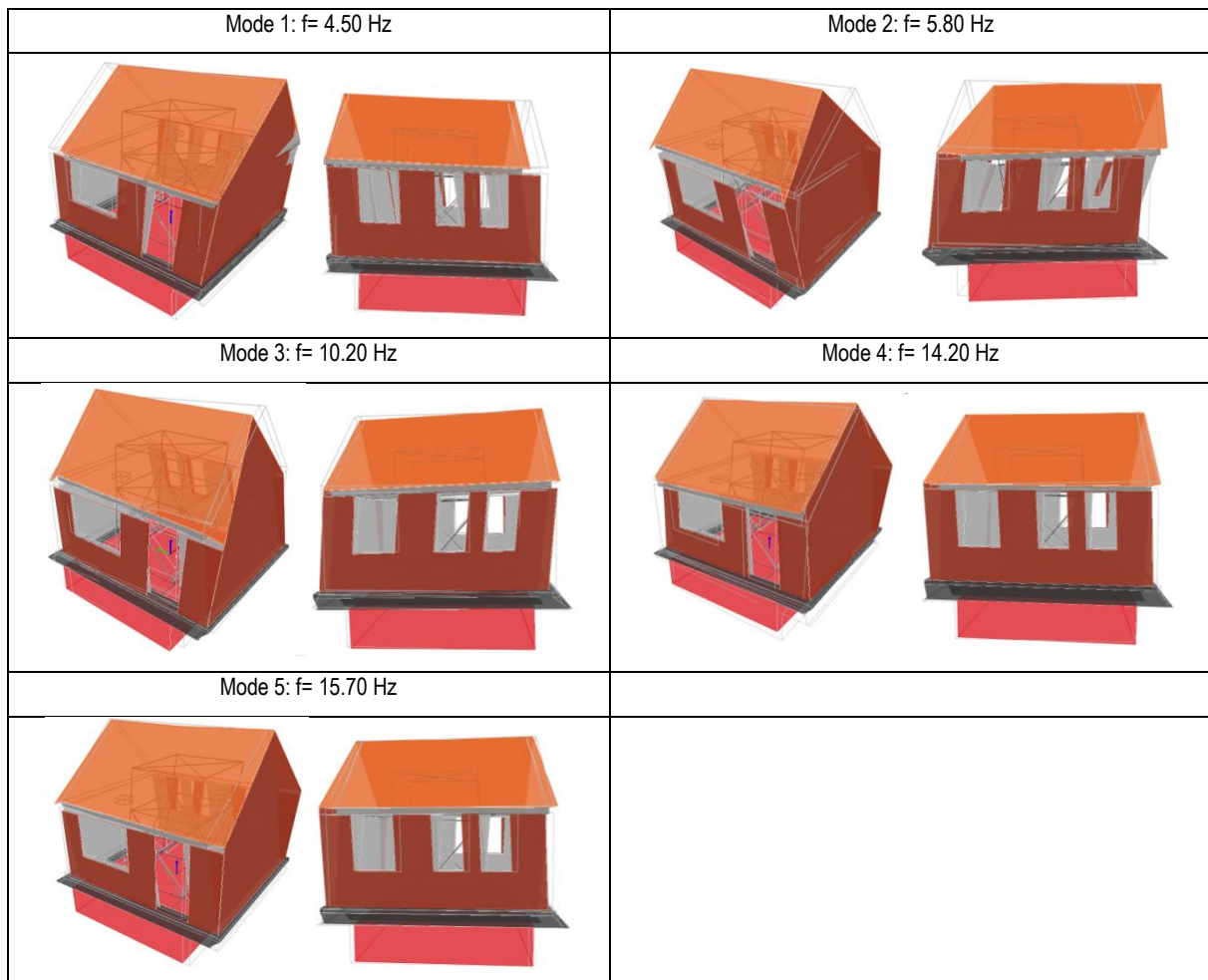
Mode	FDD Frequency [Hz]	EFDD Frequency [Hz]	Damping [%]
1	4.50	4.45	4.29
2	5.80	5.81	3.47
3	10.20	10.28	1.76
4	14.20	14.21	1.51
5	15.70	15.74	1.41

MAC coefficients for 4th dynamic identification (Test 7):

MODE i_j		MODE_01_04	MODE_02_04	MODE_03_04	MODE_04_04	MODE_05_04
	Frequency [Hz]	4.5	5.8	10.2	14.2	15.7
MODE_01_02	4.5	1.00	0.94	0.57	0.57	0.52
MODE_02_02	5.8	0.92	1.00	0.51	0.48	0.41
MODE_03_02	9.3	0.62	0.58	0.80	0.78	0.74
MODE_04_02	12.1	0.41	0.33	0.71	0.89	0.84
MODE_05_02	15.3	0.57	0.46	0.59	0.94	0.94

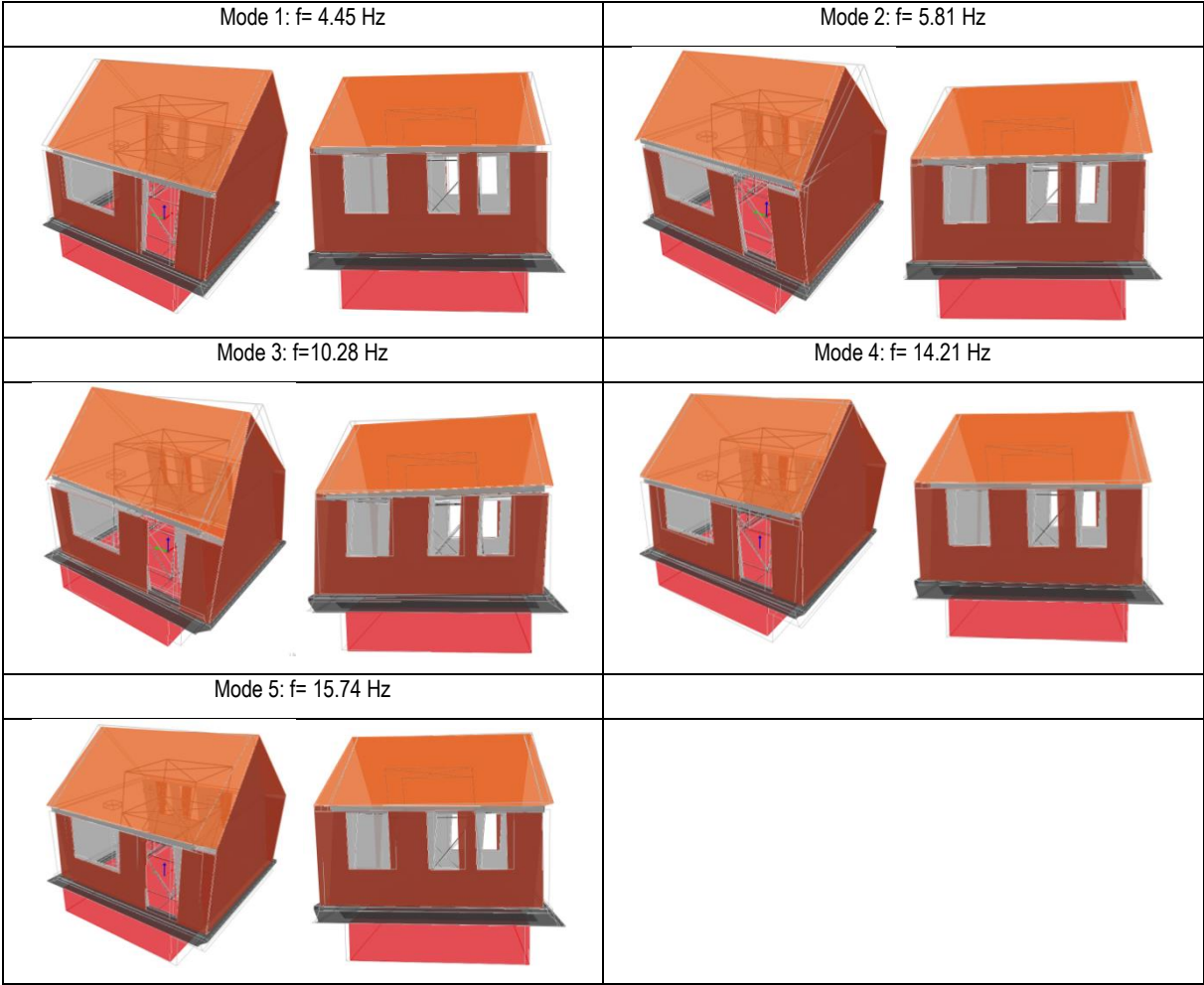
i Mode

j dynamic identification



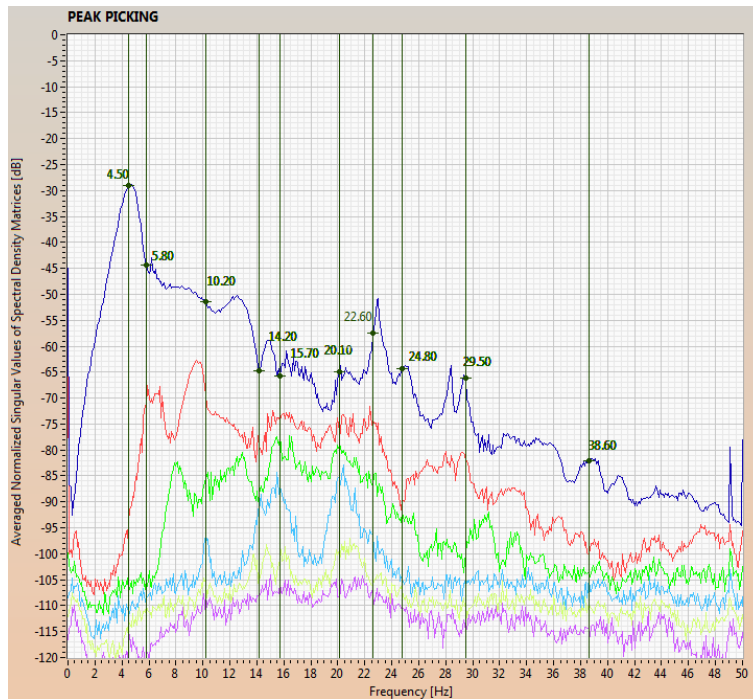
FDD mode shapes for 4th dynamic identification (Test 7)

178 Collapse Shaking Table Test on URM Cavity Wall Structure representative of a Dutch Terraced House

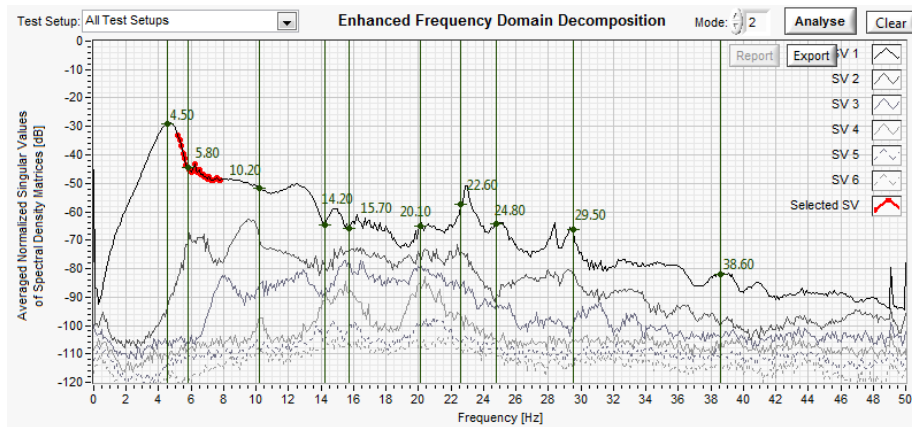


EFDD mode shapes for 4th dynamic identification (Test 7)

5th dynamic identification (Test 9)



FDD results for 5th dynamic identification (Test 9)



EFDD results for 5th dynamic identification (Test 9)

Summary of vibration modes' characteristics for 5th dynamic identification (Test 9):

Mode	FDD Frequency [Hz]	EFDD Frequency [Hz]	Damping [%]
1	4.50	4.48	4.28
2	5.80	5.79	3.70
3	10.20	10.22	2.05
4	14.20	14.33	0.73
5	15.70	15.78	1.37

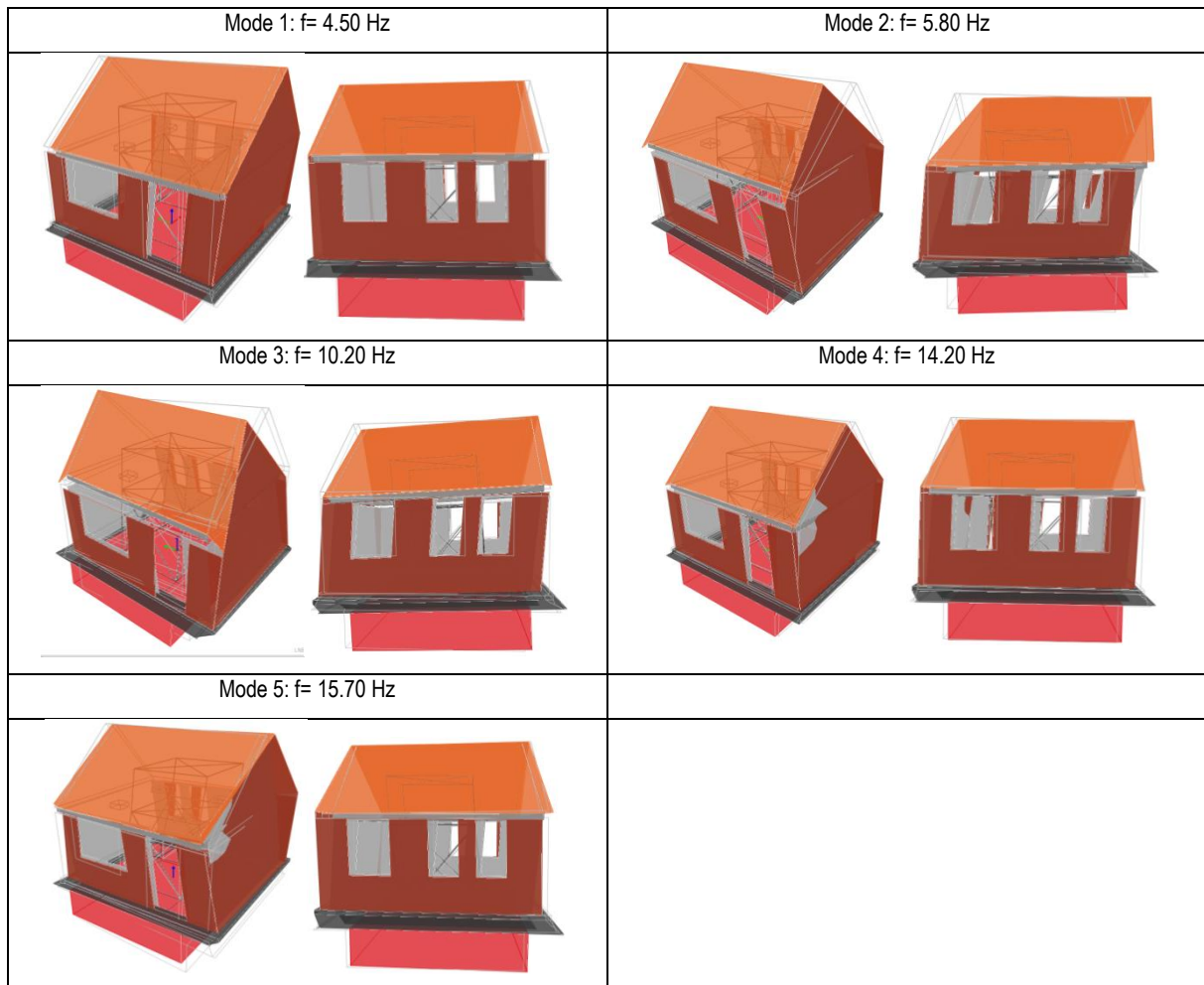
180 Collapse Shaking Table Test on URM Cavity Wall Structure representative of a Dutch Terraced House

MAC coefficients for 5th dynamic identification (Test 9):

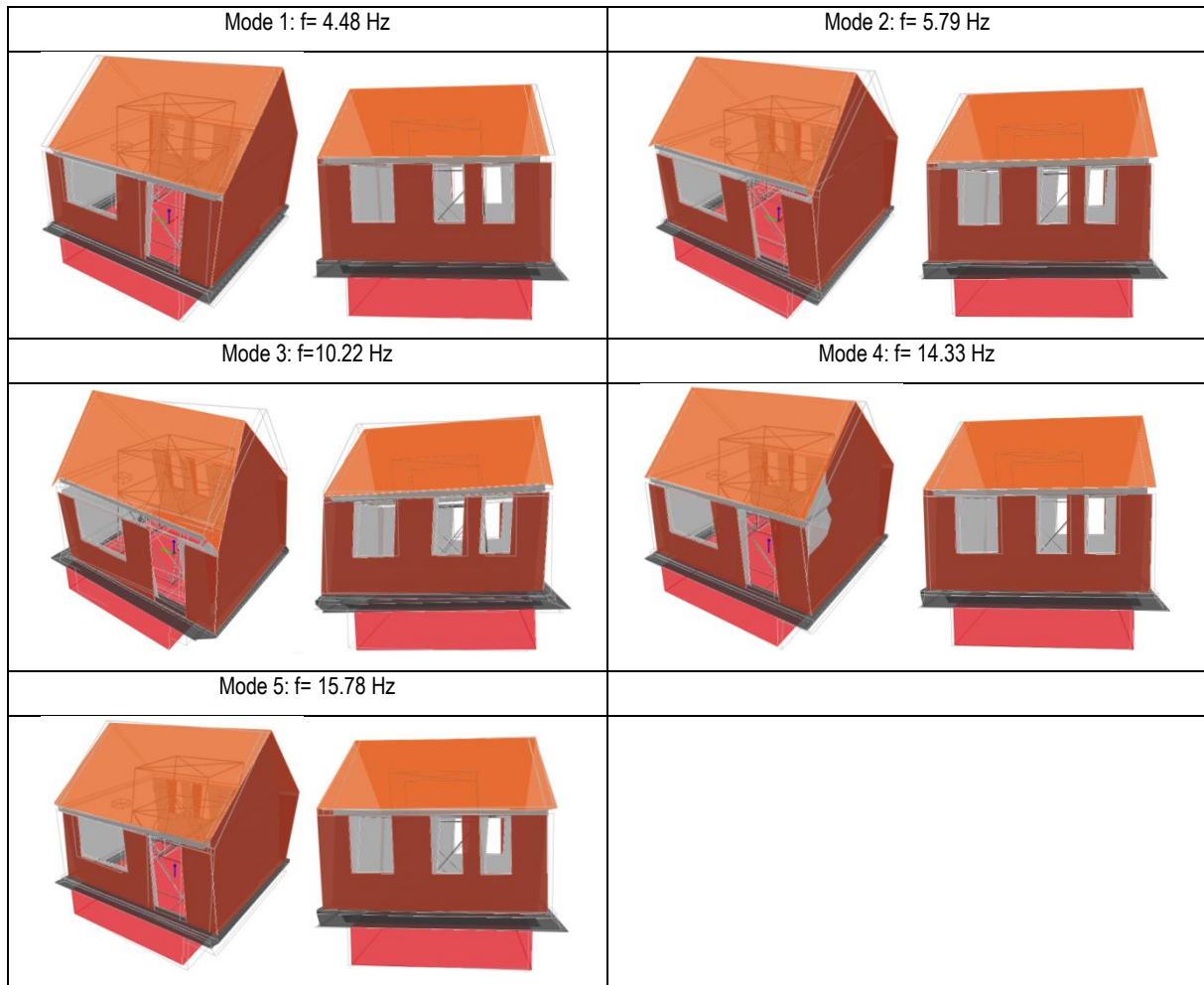
MODE i_j		MODE_01_05	MODE_02_05	MODE_03_05	MODE_04_05	MODE_05_05
	Frequency [Hz]	4.5	5.8	10.2	14.2	15.7
MODE_01_02	4.5	0.99	0.94	0.64	0.73	0.56
MODE_02_02	5.8	0.91	1.00	0.61	0.63	0.49
MODE_03_02	9.3	0.65	0.58	0.83	0.77	0.76
MODE_04_02	12.1	0.45	0.32	0.67	0.64	0.89
MODE_05_02	15.3	0.62	0.47	0.66	0.66	0.90

i Mode

j dynamic identification

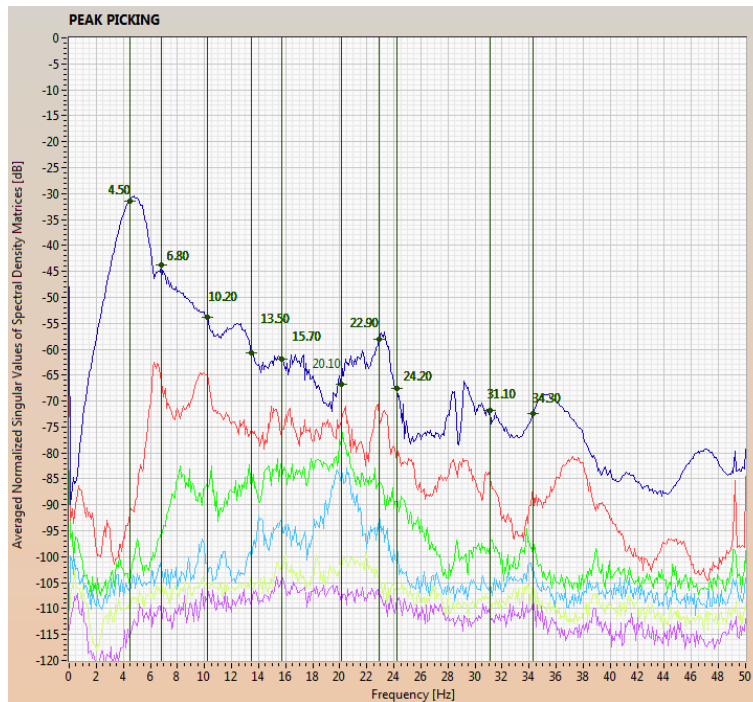


FDD mode shapes for 5th dynamic identification (Test 9)

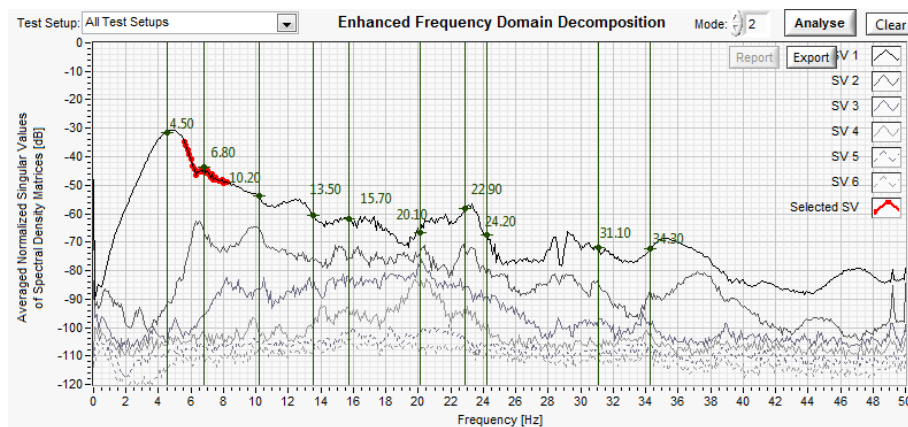


EFDD mode shapes for 5th dynamic identification (Test 9)

6th dynamic identification (Test 12)



FDD results for 6th dynamic identification (Test 12)



EFDD results for 6th dynamic identification (Test 12)

Summary of vibration modes' characteristics for 6th dynamic identification (Test 12):

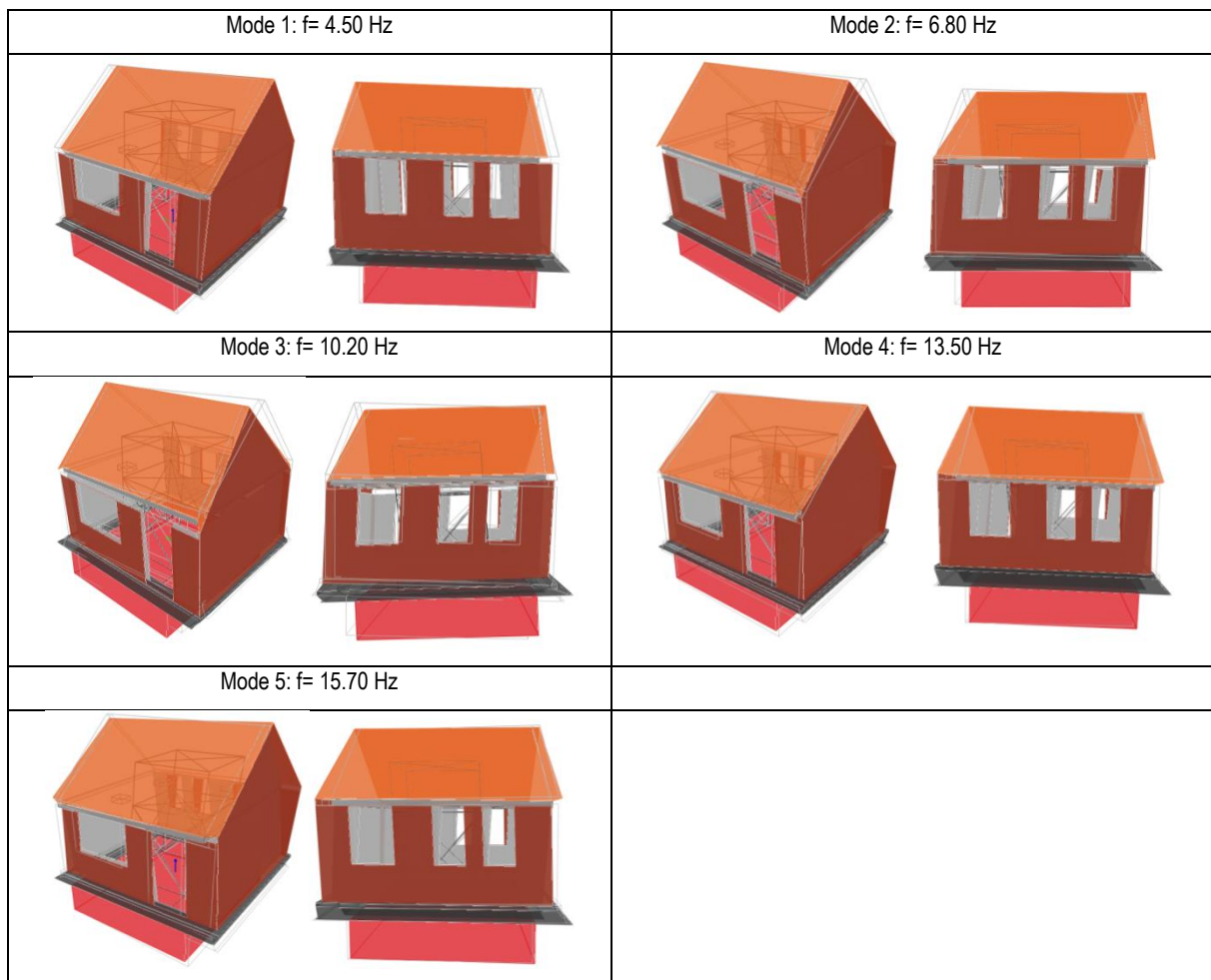
Mode	FDD Frequency [Hz]	EFDD Frequency [Hz]	Damping [%]
1	4.50	4.47	4.36
2	6.80	6.84	3.03
3	10.20	10.15	0.69
4	13.50	13.39	1.54
5	15.70	15.72	1.35

MAC coefficients for 6th dynamic identification (Test 12):

MODE _i _j		MODE_01_06	MODE_02_06	MODE_03_06	MODE_04_06	MODE_05_06
	Frequency [Hz]	4.5	6.8	10.2	13.5	15.7
MODE_01_02	4.5	0.98	0.96	0.54	0.41	0.60
MODE_02_02	5.8	0.89	0.99	0.47	0.31	0.55
MODE_03_02	9.3	0.69	0.64	0.83	0.72	0.74
MODE_04_02	12.1	0.50	0.39	0.72	0.91	0.84
MODE_05_02	15.3	0.67	0.55	0.64	0.73	0.96

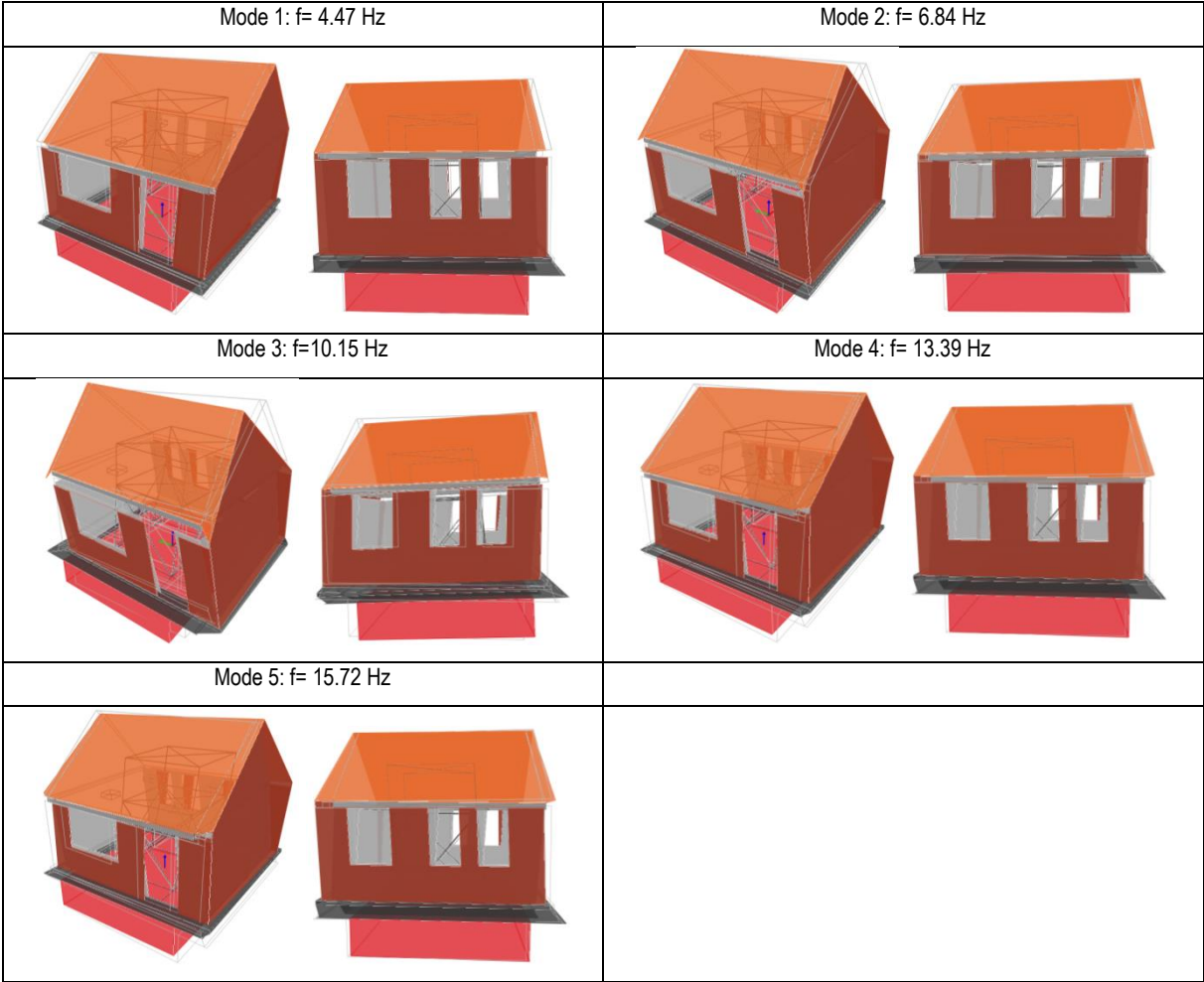
i Mode

j dynamic identification



FDD mode shapes for 6th dynamic identification (Test 12)

184 Collapse Shaking Table Test on URM Cavity Wall Structure representative of a Dutch Terraced House



EFDD mode shapes for 6th dynamic identification (Test 12)

ANNEX II
Additional information on mortar characterisation tests

Characteristics of mortar specimens for calcium silicate blocks (MS) selected for the tests:

Sample	Specimen	Length [mm]	Width [mm]	Height [mm]	Mass [g]
MS_1_1	MS_1_1_1	160.07	40.03	40.71	419.24
	MS_1_1_2	160.22	40.01	40.76	421.95
	MS_1_1_3	160.29	40.11	40.91	424.45
MS_1_2	MS_1_2_19	159.99	39.98	40.56	417.15
	MS_1_2_20	160.18	40.06	40.85	416.43
	MS_1_2_21	160.19	39.99	41.35	412.97
MS_C_1	MS_C_1_31	160.15	40.09	40.53	482.96
	MS_C_1_32	160.28	40.09	40.78	482.27
	MS_C_1_33	160.48	40.08	40.58	480.20
MS_C_2	MS_C_2_43	160.17	40.00	40.57	424.25
	MS_C_2_44	160.09	40.05	40.68	424.06
	MS_C_2_45	190.09	40.06	40.72	419.29
MS_2_1	MS_2_1_55	160.90	40.04	41.18	425.11
	MS_2_1_56	160.55	40.19	41.23	432.26
	MS_2_1_57	160.59	39.99	41.20	431.47
MS_1_1	MS_1_1_4	160.19	39.97	40.89	412.81
	MS_1_1_5	160.24	40.01	41.35	418.06
	MS_1_1_6	160.07	39.97	40.75	409.17
MS_1_2	MS_1_2_22	160.03	39.97	40.53	403.59
	MS_1_2_23	160.24	39.91	40.86	406.64
	MS_1_2_24	160.06	39.88	40.81	408.12
MS_C_1	MS_C_1_34	159.86	40.10	40.69	444.53
	MS_C_1_35	159.81	40.17	40.88	448.03
	MS_C_1_36	159.88	40.22	41.12	450.30
MS_C_2	MS_C_2_46	160.00	40.04	40.91	413.83
	MS_C_2_47	160.03	40.06	40.76	415.34
	MS_C_2_48	160.26	39.99	40.95	415.66
MS_2_1	MS_2_1_58	154.90	35.02	36.12	413.90
	MS_2_1_59	155.01	35.04	36.22	416.57
	MS_2_1_60	155.22	40.31	41.29	419.32
MS_1_1	MS_1_1_7	160.12	40.01	40.97	410.97
	MS_1_1_8	160.15	40.20	40.85	410.09
	MS_1_1_9	160.11	40.05	40.82	410.44
	MS_1_1_10	160.25	40.29	41.12	413.03
	MS_1_1_11	160.12	40.16	41.17	412.95
	MS_1_1_12	160.51	40.35	40.95	409.94
MS_1_2	MS_1_2_25	160.08	40.25	40.93	406.38
	MS_1_2_26	160.08	40.14	40.70	405.28
	MS_1_2_27	160.03	40.11	40.64	402.14
	MS_1_2_28	160.50	40.14	40.80	403.38
	MS_1_2_29	160.29	40.30	41.00	404.07
	MS_1_2_30	160.16	40.08	40.80	400.46
MS_C_1	MS_C_1_37	159.81	40.13	41.11	457.70
	MS_C_1_38	159.94	40.29	41.02	452.95
	MS_C_1_39	159.78	40.37	40.83	455.57
	MS_C_1_40	160.38	40.12	40.94	465.06
	MS_C_1_41	160.25	40.20	41.26	468.05
	MS_C_1_42	160.36	40.13	41.12	464.36
MS_C_2	MS_C_2_49	160.06	40.58	40.95	415.99
	MS_C_2_50	160.43	40.21	40.99	415.85
	MS_C_2_51	160.24	40.23	40.98	417.15
	MS_C_2_52	161.06	40.21	41.08	417.97
	MS_C_2_53	161.61	40.40	41.17	416.96

Sample	Specimen	Length [mm]	Width [mm]	Height [mm]	Mass [g]
	MS_C_2_54	161.37	40.26	41.31	415.69
MS_2_1	MS_2_1_61	159.77	40.21	40.83	415.45
	MS_2_1_62	159.74	40.11	41.18	415.46
	MS_2_1_63	159.97	40.09	41.14	416.60
	MS_2_1_64	160.11	40.29	41.44	418.25
	MS_2_1_65	160.01	40.33	41.31	419.84
	MS_2_1_66	160.28	40.31	41.43	419.34

Characteristics of mortar specimens for clay bricks (MCL) selected for the tests:

Sample	Specimen	Length [mm]	Width [mm]	Height [mm]	Mass [g]
MCL_1_1	MCL_1_1_1	159.97	40.05	40.84	482.17
	MCL_1_1_2	160.20	40.06	41.18	494.66
	MCL_1_1_3	160.17	39.99	41.35	493.25
MCL_C_1	MCL_C_1_19	160.30	40.12	40.76	478.26
	MCL_C_1_20	160.22	40.13	41.26	481.88
	MCL_C_1_21	160.16	40.00	40.54	478.30
MCL_C_2	MCL_C_2_31	159.78	40.12	40.95	513.61
	MCL_C_2_32	159.96	40.05	41.16	508.12
	MCL_C_2_33	160.04	40.16	40.93	504.95
MCL_2_1	MCL_2_1_43	160.23	40.34	41.80	525.07
	MCL_2_1_44	160.04	40.42	41.59	525.88
	MCL_2_1_45	160.05	40.12	41.51	520.29
MCL_1_1	MCL_1_1_4	160.10	39.97	40.54	472.38
	MCL_1_1_5	160.05	39.90	40.56	474.18
	MCL_1_1_6	160.22	39.97	40.85	475.75
MCL_C_1	MCL_C_1_22	160.13	40.08	41.29	480.95
	MCL_C_1_23	160.12	40.09	41.10	476.70
	MCL_C_1_24	159.90	40.06	40.94	473.12
MCL_C_2	MCL_C_2_34	160.06	40.13	41.60	507.50
	MCL_C_2_35	160.08	40.05	40.79	499.01
	MCL_C_2_36	160.17	40.10	41.40	505.83
MCL_2_1	MCL_2_1_46	159.90	40.33	41.47	499.38
	MCL_2_1_47	160.37	40.16	41.25	499.22
	MCL_2_1_48	160.61	40.46	41.58	502.54
MCL_1_1	MCL_1_1_7	160.44	40.48	41.20	477.49
	MCL_1_1_8	160.52	40.43	40.84	475.93
	MCL_1_1_9	160.10	40.33	41.10	475.65
	MCL_1_1_10	160.67	40.28	41.03	469.44
	MCL_1_1_11	160.66	40.21	40.99	470.14
	MCL_1_1_12	160.26	40.31	41.12	470.14
MCL_C_1	MCL_C_1_25	160.81	40.50	41.11	473.59
	MCL_C_1_26	161.16	40.57	41.22	471.59
	MCL_C_1_27	191.04	40.62	41.10	474.05
	MCL_C_1_28	160.21	40.46	41.32	473.89
	MCL_C_1_29	160.13	40.73	41.33	475.52
	MCL_C_1_30	160.29	40.33	41.41	475.64
MCL_C_2	MCL_C_2_37	160.08	40.58	41.57	513.61
	MCL_C_2_38	160.06	40.34	41.64	515.22
	MCL_C_2_39	160.16	40.41	41.48	510.60
	MCL_C_2_40	159.89	40.28	41.00	503.79
	MCL_C_2_41	159.89	40.14	40.88	495.11
	MCL_C_2_42	160.00	40.38	40.86	496.69

Sample	Specimen	Length [mm]	Width [mm]	Height [mm]	Mass [g]
MCL_2_1	MCL_2_1_49	160.01	40.44	41.22	492.05
	MCL_2_1_50	160.10	40.28	41.05	492.54
	MCL_2_1_51	160.30	40.72	41.35	497.18
	MCL_2_1_52	159.88	40.28	41.54	495.94
	MCL_2_1_53	160.02	40.51	41.81	501.93
	MCL_2_1_54	159.89	40.12	41.22	492.00

Test results for the determination of the dynamic modulus of elasticity after 10 days, 20 days and 28 days of the bedding mortar of calcium silicate blocks (MS):

Specimen	Date of test	Age of specimen [days]	Density [kg/m ³]		Frequency of resonance [Hz]		Dynamic modulus of elasticity [MPa]	
			Individual values	Average	Individual values	Average	Individual values	Average
MS_1_1_1	2017-03-02	10	1607	1612	7256.8	7226.9	8674	8642
MS_1_1_2			1615		7209.2		8619	
MS_1_1_3			1614		7214.7		8633	
MS_1_2_19	2017-03-02	10	1608	1585	7132.9	7129.8	8377	8264
MS_1_2_20			1589		7151.4		8339	
MS_1_2_21			1559		7105.1		8077	
MS_C_1_31	2017-03-06	12	1854	1845	9449.0	9357.2	16978	16677
MS_C_1_32			1842		9284.3		16315	
MS_C_1_33			1840		9338.3		16739	
MS_C_2_43	2017-03-06	12	1632	1621	7449.5	7578.1	9229	9528
MS_C_2_44			1626		7726.0		9951	
MS_C_2_45			1606		7558.9		9405	
MS_2_1_55	2017-03-03	10	1602	1619	7305.5	7359.8	8855	9089
MS_2_1_56			1625		7314.5		8962	
MS_2_1_57			1630		7459.3		9449	
MS_1_1_4	2017-03-13	21	1577	1577	7356.9	7347.5	8759	8734
MS_1_1_5			1577		7414.6		8905	
MS_1_1_6			1576		7271.1		8539	
MS_1_2_22	2017-03-13	21	1557	1564	7323.7	7312.2	8552	8576
MS_1_2_23			1569		7308.9		8610	
MS_1_2_24			1567		7303.9		8565	
MS_C_1_34	2017-03-13	20	1704	1705	8454.7	8512.1	12453	12632
MS_C_1_35			1708		8318.8		12071	
MS_C_1_36			1703		8762.9		13372	
MS_C_2_46	2017-03-14	20	1579	1584	7636.0	8373.0	9427	11434
MS_C_2_47			1589		8722.1		12386	
MS_C_2_48			1584		8760.9		12489	
MS_2_1_58	2017-03-13	20	2112	1951	7357.6	7382.2	10974	10211
MS_2_1_59			2118		7357.6		11019	
MS_2_1_60			1623		7431.4		8639	
MS_1_1_7	2017-03-20	28	1566	1560	7372.8	7388.6	8727	8743
MS_1_1_8			1559		7405.8		8774	
MS_1_1_9			1568		7344.0		8671	
MS_1_1_10			1555		7397.5		8744	
MS_1_1_11			1560		7401.6		8764	
MS_1_1_12			1551		7409.9		8777	
MS_1_2_25	2017-03-20	28	1541	1536	7373.1	7304.7	8586	8411
MS_1_2_26			1542		7307.3		8438	
MS_1_2_27			1541		7284.6		8379	
MS_1_2_28			1535		7361.7		8570	

190 Collapse Shaking Table Test on URM Cavity Wall Structure representative of a Dutch Terraced House

Specimen	Date of test	Age of specimen [days]	Density [kg/m ³]		Frequency of resonance [Hz]		Dynamic modulus of elasticity [MPa]	
			Individual values	Average	Individual values	Average	Individual values	Average
MS_1_2_29			1526		7273.2		8294	
MS_1_2_30			1529		7228.0		8196	
MS_C_1_37	2017-03-22	28	1736	1743	8810.3	8956.4	13764	14346
MS_C_1_38			1713		8793.1		13556	
MS_C_1_39			1730		8788.3		13641	
MS_C_1_40			1765		9144.4		15189	
MS_C_1_41			1759		9208.2		15321	
MS_C_1_42			1755		8994.2		14603	
MS_C_2_49			2017-03-22		28		1564	
MS_C_2_50	1573	7721.6		9654				
MS_C_2_51	1576	7818.8		9895				
MS_C_2_52	1571	7637.6		9510				
MS_C_2_53	1552	7573.4		9288				
MS_C_2_54	1561	7552.1		9275				
MS_2_1_61	2017-03-21	28	1574	1573	7424.8	7436.2	8857	8901
MS_2_1_62			1575		7357.3		8700	
MS_2_1_63			1579		7518.1		9137	
MS_2_1_64			1565		7431.9		8861	
MS_2_1_65			1575		7457.0		8970	
MS_2_1_66			1567		7428.3		8883	

Test results for the determination of the dynamic modulus of elasticity after 10 days, 20 days and 28 days of the bedding mortar of clay bricks (MCL):

Specimen	Date of test	Age of specimen [days]	Density [kg/m ³]		Frequency of resonance [Hz]		Dynamic modulus of elasticity [MPa]	
			Individual values	Average	Individual values	Average	Individual values	Average
MCL_1_1_1	2017-03-02	10	1843	1799	7413.1	7388.7	10366	10406
MCL_1_1_2			1872		7365.5		10424	
MCL_1_1_3			1682		7387.5		10428	
MCL_C_1_19	2017-03-06	12	1824	1829	7529.4	7585.1	10629	10805
MCL_C_1_20			1817		7629.8		10862	
MCL_C_1_21			1845		7596.2		10924	
MCL_C_2_31	2017-03-06	12	1940	1929	8833.6	8306.8	12785	12755
MCL_C_2_32			1927		8009.1		12650	
MCL_C_2_33			1919		8077.8		12830	
MCL_2_1_43	2017-03-03	10	1943	1950	7969.6	7976.5	16676	14055
MCL_2_1_44			1955		7977.9		12747	
MCL_2_1_45			1952		7982.1		12742	
MCL_1_1_4	2017-03-13	21	1821	1823	7971.2	7974.4	11863	11892
MCL_1_1_5			1831		7985.8		11963	
MCL_1_1_6			1818		7966.3		11850	
MCL_C_1_22	2017-03-13	20	1816	1809	7992.7	8254.3	11884	12645
MCL_C_1_23			1807		8028.2		11941	
MCL_C_1_24			1805		8741.9		14111	
MCL_C_2_34	2017-03-14	20	1900	1904	8263.0	8288.2	13291	13407
MCL_C_2_35			1908		8310.3		13508	
MCL_C_2_36			1903		8291.3		13422	
MCL_2_1_46	2017-03-13	20	1867	1869	8355.5	8309.2	13333	13260
MCL_2_1_47			1879		8250.3		13158	
MCL_2_1_48			1860		8321.7		13290	
MCL_1_1_7	2017-03-20	28	1785	1781	8102.6		12064	12000

Specimen	Date of test	Age of specimen [days]	Density [kg/m ³]		Frequency of resonance [Hz]		Dynamic modulus of elasticity [MPa]	
			Individual values	Average	Individual values	Average	Individual values	Average
MCL_1_1_8			1796		8206.5	8088.3	12466	
MCL_1_1_9			1793		8143.3		12188	
MCL_1_1_10			1768		7970.5		11598	
MCL_1_1_11			1776		8091.3		12002	
MCL_1_1_12			1770		8015.3		11680	
MCL_C_1_25	2017-03-22	28	1775	1767	8007.4	8211.1	11775	11795
MCL_C_1_26			1750		8023.9		11703	
MCL_C_1_27			1763		8005.0		11719	
MCL_C_1_28			1769		9019.2		11682	
MCL_C_1_29			1765		8116.3		11926	
MCL_C_1_30			1777		8094.9		11967	
MCL_C_2_37	2017-03-22	28	1902	1900	8831.7	8655.8	15205	14582
MCL_C_2_38			1917		8746.1		15024	
MCL_C_2_39			1902		8782.7		15054	
MCL_C_2_40			1908		8555.3		14284	
MCL_C_2_41			1887		8480.5		13879	
MCL_C_2_42			1881		8538.3		14043	
MCL_2_1_49	2017-03-21	28	1845	1852	8441.3	8438.0	13462	13510
MCL_2_1_50			1860		8462.2		13659	
MCL_2_1_51			1842		8424.7		13436	
MCL_2_1_52			1854		8391.5		13348	
MCL_2_1_53			1852		8520.9		13772	
MCL_2_1_54			1861		8387.3		13384	

Test results for flexural and compression strength for the bedding mortar specimen for the calcium silicate blocks (MS) after 10 days, 20 days and 28 days:

Specimen	Date of test	Age of specimen [days]	Bulk density [kg/m ³]		Compressive strength [MPa]		Flexural strength [MPa]		
			Individual values	Average	Individual values	Average	Individual values	Average	
MS_1_1_1	2017-03-02	10	1610	1610	3.90	4.30	1.55	1.42	
MS_1_1_2			1620		4.30	4.15	1.55		
MS_1_1_3			1610		2.70	3.75	1.15		
MS_1_2_19	2017-03-02	10	1610	1590	3.15	3.15	1.35	1.48	
MS_1_2_20			1590		3.40	3.40	1.80		
MS_1_2_21			1560		3.80	3.65	1.30		
MS_C_1_31	2017-03-06	12	1860	1850	8.70	7.75	3.60	3.62	
MS_C_1_32			1840		7.85	7.50	3.60		
MS_C_1_33			1840		7.75	6.60	3.65		
MS_C_2_43	2017-03-06	12	1632	1621	3.35	3.20	2.15	2.05	
MS_C_2_44			1630		4.80	4.55	1.95		
MS_C_2_45			1350		3.90	4.15	2.05		
MS_2_1_55	2017-03-03	10	1600	1620	4.05	4.30	2.05	2.03	
MS_2_1_56			1620		3.95	3.55	2.00		
MS_2_1_57			1630		4.20	3.95	2.05		
MS_1_1_4	2017-03-13	21	1580	1580	6.80	6.35	2.70	2.22	
MS_1_1_5			1580		6.40	6.65	1.10		
MS_1_1_6			1570		6.40	6.35	2.85		
MS_1_2_22	2017-03-13	21	1560	1560	5.80	5.95	2.45	2.67	
MS_1_2_23			1560		6.10	5.70	2.75		
MS_1_2_24			1570		5.85	4.50	2.80		
MS_C_1_34	2017-03-13	20	1700	1700	8.85	9.05	8.62	3.90	3.93

192 Collapse Shaking Table Test on URM Cavity Wall Structure representative of a Dutch Terraced House

Specimen	Date of test	Age of specimen [days]	Bulk density [kg/m ³]		Compressive strength [MPa]		Flexural strength [MPa]	
			Individual values	Average	Individual values	Average	Individual values	Average
MS_C_1_35			1710		8.25	8.85	4.05	
MS_C_1_36			1700		8.30	8.40	3.85	
MS_C_2_46	2017-03-14	20	1580	1580	6.35	5.85	2.85	3.03
MS_C_2_47			1590		5.85	5.60	3.50	
MS_C_2_48			1580		6.00	5.90	2.75	
MS_2_1_58			2110		5.05	5.60	2.65	
MS_2_1_59	2017-03-13	20	2120	1950	5.40	5.60	2.70	2.67
MS_2_1_60			1620		5.70	5.90	2.65	
MS_1_1_7	2017-03-20	28	1570	1562	6.80	6.90	2.85	2.93
MS_1_1_8			1560		6.55	6.60	2.90	
MS_1_1_9			1570		6.30	6.50	2.80	
MS_1_1_10			1560		6.30	6.25	3.10	
MS_1_1_11			1560		6.85	7.00	2.80	
MS_1_1_12			1550		6.90	6.85	3.15	
MS_1_2_25	2017-03-20	28	1540	1537	6.60	6.45	2.80	2.90
MS_1_2_26			1550		6.20	6.35	3.10	
MS_1_2_27			1540		5.55	5.90	3.00	
MS_1_2_28			1530		5.60	5.65	2.75	
MS_1_2_29			1530		5.60	5.65	2.75	
MS_1_2_30			1530		5.65	5.85	3.00	
MS_C_1_37	2017-03-22	28	1740	1743	10.50	9.75	4.70	4.63
MS_C_1_38			1710		9.45	9.90	4.70	
MS_C_1_39			1730		9.60	9.85	4.60	
MS_C_1_40			1770		9.40	11.35	4.10	
MS_C_1_41			1760		11.10	11.90	4.85	
MS_C_1_42			1750		11.60	11.90	4.85	
MS_C_2_49	2017-03-22	28	1560	1563	6.70	6.10	3.80	3.78
MS_C_2_50			1570		6.20	6.80	3.80	
MS_C_2_51			1580		6.20	5.75	4.40	
MS_C_2_52			1570		6.65	6.35	3.40	
MS_C_2_53			1550		6.70	6.20	3.65	
MS_C_2_54			1550		6.95	5.95	3.65	
MS_2_1_61	2017-03-21	28	1580	1573	6.30	5.85	2.80	2.78
MS_2_1_62			1570		6.20	5.90	2.85	
MS_2_1_63			1580		6.60	5.50	2.65	
MS_2_1_64			1560		6.00	6.05	2.90	
MS_2_1_65			1580		6.00	6.10	2.50	
MS_2_1_66			1570		5.90	5.95	2.95	

Test results for the test for flexural and compression strength for the bedding mortar specimen for the clay bricks (MCL) after 10 days, 20 days and 28 days:

Specimen	Date of test	Age of specimen [days]	Bulk density [kg/m ³]		Compressive strength [MPa]		Flexural strength [MPa]	
			Individual values	Average	Individual values	Average	Individual values	Average
MCL_1_1_1	2017-03-02	10	1840	1860	3.90	3.85	1.40	1.43
MCL_1_1_2			1870		3.35	3.90	1.40	
MCL_1_1_3			1860		3.80	3.70	1.50	
MCL_C_1_19	2017-03-06	12	2600	2090	5.25	4.55	1.85	2.00
MCL_C_1_20			1820		4.75	4.90	2.05	
MCL_C_1_21			1840		3.65	3.70	2.10	
MCL_C_2_31	2017-03-06	12	1960	1940	6.10	6.00	2.80	2.47
MCL_C_2_32			1930		5.75	5.95	2.20	

Specimen	Date of test	Age of specimen [days]	Bulk density [kg/m ³]		Compressive strength [MPa]		Flexural strength [MPa]		
			Individual values	Average	Individual values	Average	Individual values	Average	
MCL_C_2_33			1920		6.50	6.35	2.40		
MCL_2_1_43	2017-03-03	10	1940	1950	5.60	5.45	5.59	2.20	2.17
MCL_2_1_44			1950		5.30	6.00		2.30	
MCL_2_1_45			1950		5.65	5.55		2.00	
MCL_1_1_4			1820		7.05	6.85		3.15	
MCL_1_1_5	2017-03-13	21	1830	1820	6.90	6.60	6.83	1.65	2.65
MCL_1_1_6			1820		6.95	6.60		3.15	
MCL_C_1_22			1810		7.45	7.20		3.00	
MCL_C_1_23	2017-03-13	20	1810	1810	7.35	7.25	7.09	1.35	2.25
MCL_C_1_24			1800		6.65	6.65		2.40	
MCL_C_2_34			1900		7.70	7.95		2.20	
MCL_C_2_35	2017-03-14	20	1910	1900	7.45	7.75	7.79	2.15	2.15
MCL_C_2_36			1900		8.00	7.90		2.10	
MCL_2_1_46			1870		8.55	8.45		2.65	
MCL_2_1_47	2017-03-13	20	1880	1870	8.25	7.95	8.30	2.00	2.08
MCL_2_1_48			1860		8.05	8.55		1.60	
MCL_1_1_7			1780		7.60	7.90		2.80	
MCL_1_1_8	2017-03-20	28	1800	1782	8.10	8.25	7.70	3.55	3.10
MCL_1_1_9			1790		7.50	7.75		3.20	
MCL_1_1_10			1770		7.45	7.35		2.95	
MCL_1_1_11			1780		7.75	7.60		3.25	
MCL_1_1_12			1770		7.35	7.80		2.85	
MCL_C_1_25			1770		7.75	7.90		3.15	
MCL_C_1_26	2017-03-22	28	1750	1720	7.30	7.45	7.59	2.90	3.17
MCL_C_1_27			1490		6.85	7.30		3.10	
MCL_C_1_28			1770		7.30	7.25		3.35	
MCL_C_1_29			1760		7.90	8.00		3.00	
MCL_C_1_30			1780		8.30	7.80		3.50	
MCL_C_2_37			1900		10.50	10.15		3.30	
MCL_C_2_38	2017-03-22	28	1920	1900	10.30	10.10	9.75	3.60	3.29
MCL_C_2_39			1900		9.95	9.85		3.45	
MCL_C_2_40			1910		9.65	9.25		2.50	
MCL_C_2_41			1890		9.30	9.10		3.05	
MCL_C_2_42			1880		9.50	9.30		3.85	
MCL_2_1_49			1840		9.30	9.00		3.05	
MCL_2_1_50	2017-03-21	28	1860	1850	9.05	8.50	8.98	2.80	2.96
MCL_2_1_51			1840		9.00	8.95		3.20	
MCL_2_1_52			1850		8.80	8.75		2.80	
MCL_2_1_53			1850		9.10	9.55		2.90	
MCL_2_1_54			1860		9.10	8.70		3.00	

ANNEX III

Additional information on masonry blocks characterisation tests

Characteristics of the two types of blocks selected for the tests:

Specimen	Mass [kg]	Length (L1) [mm]			Width (L2) [mm]			Height (H) [mm]		
		L1 (top)	L1 (down)	Average	L2 (top)	L2 (down)	Average	H1 (left)	H2 (right)	Average
BS_0	2.952	212.72	212.65	212.69	103.36	103.87	103.62	70.67	70.89	70.78
BS_1	2.978	212.65	213.03	212.84	103.37	103.40	103.39	70.84	70.99	70.92
BS_2	2.968	212.86	212.75	212.81	103.39	103.89	103.64	70.82	70.56	70.69
BS_3	2.926	213.21	212.99	213.10	102.95	103.43	103.19	70.88	71.23	71.06
BS_4	2.915	213.05	212.82	212.94	102.99	103.13	103.06	71.08	71.28	71.18
BS_5	2.761	212.71	212.61	212.66	102.08	102.16	102.12	70.82	70.98	70.90
BS_6	2.967	212.73	212.62	212.68	103.46	103.66	103.56	71.00	71.17	71.09
BS_7	2.961	212.82	212.79	212.81	103.27	103.51	103.39	70.21	70.87	70.54
BS_8	3.008	212.69	212.86	212.78	104.25	103.51	103.88	70.32	70.23	70.28
BS_9	2.964	212.71	212.68	212.70	103.70	103.76	103.73	71.12	71.01	71.07
BS_10	2.943	213.26	212.88	213.07	103.35	103.58	103.47	70.57	70.76	70.57
BS_11	2.743	212.36	212.34	212.35	102.36	102.38	102.37	70.64	70.53	70.59
BS_12	2.887	212.66	212.21	212.44	102.69	102.84	102.77	70.97	71.04	71.01
BS_13	2.802	212.66	212.21	212.44	102.60	102.19	102.40	70.23	70.67	70.45
BS_14	2.738	212.48	212.60	212.54	102.60	101.93	102.27	70.27	70.45	70.36
BS_15	2.886	212.62	212.75	212.69	102.45	102.24	102.35	70.21	70.25	70.23
BS_16	2.798	212.66	212.53	212.60	102.31	102.07	102.19	69.97	69.86	69.92
BCL_0	1.698	213.31	211.20	212.26	99.65	100.57	100.11	50.53	45.00	47.77
BCL_1	1.708	209.97	209.83	209.90	101.27	101.56	101.42	50.21	50.32	50.27
BCL_2	1.699	209.47	210.15	209.81	101.26	101.58	101.42	50.39	50.47	50.43
BCL_3	1.638	210.95	208.80	209.88	99.01	100.11	99.56	49.86	50.03	49.95
BCL_4	1.686	213.17	211.72	212.45	100.53	99.54	100.04	50.31	50.18	50.25
BCL_5	1.735	213.83	213.17	213.50	101.61	102.73	102.17	50.27	50.12	50.20
BCL_6	1.686	213.06	211.80	212.43	100.40	99.75	100.08	50.78	50.89	50.84
BCL_7	1.711	209.91	209.86	209.89	100.80	101.96	101.38	49.76	49.71	49.74
BCL_8	1.675	213.72	211.16	212.44	98.97	99.60	99.29	49.94	49.86	49.90
BCL_9	1.669	215.89	211.88	213.89	98.37	98.54	98.46	50.03	50.15	50.09
BCL_10	1.678	212.92	210.41	211.67	99.70	100.54	100.12	49.76	49.87	49.82
BCL_11	1.727	210.23	210.49	210.36	102.16	101.3	101.73	49.89	50.01	49.95

198 Collapse Shaking Table Test on URM Cavity Wall Structure representative of a Dutch Terraced House

Specimen	Mass [kg]	Length (L1) [mm]			Width (L2) [mm]			Height (H) [mm]		
		L1 (top)	L1 (down)	Average	L2 (top)	L2 (down)	Average	H1 (left)	H2 (right)	Average
BCL_12	1.728	210.36	210.09	210.23	101.71	102.27	101.99	50.37	50.55	50.46
BCL_13	1.733	210.55	210.89	210.72	102.06	102.81	102.44	50.21	50.45	50.33
BCL_14	1.736	209.95	209.91	209.93	102.01	101.52	101.77	50.12	50.45	50.29
BCL_15	1.728	210.53	210.12	210.33	101.51	102.28	101.90	49.99	49.67	49.83
BCL_16	1.730	210.45	210.62	210.54	102.06	101.61	101.84	50.34	50.56	50.45

Determination of bulk density for calcium silicate blocks:

Specimen	Length [m]	Width [m]	Height [m]	Mass [kg]	Bulk density [kg/m ³]
BS_0	0.21269	0.10362	0.07078	2.952	1892.41
BS_1	0.21284	0.10339	0.07092	2.978	1908.20
BS_2	0.21281	0.10364	0.07069	2.968	1903.65
BS_3	0.21310	0.10319	0.07106	2.926	1872.53
BS_4	0.21294	0.10306	0.07118	2.915	1866.09
BS_5	0.21266	0.10212	0.07090	2.761	1793.18
BS_6	0.21268	0.10356	0.07109	2.967	1894.92
BS_7	0.21281	0.10339	0.07054	2.961	1907.80
BS_8	0.21278	0.10388	0.07028	3.008	1936.35
BS_9	0.21270	0.10373	0.07107	2.964	1890.25
BS_10	0.21307	0.10347	0.07057	2.943	1891.62
BS_11	0.21235	0.10237	0.07059	2.743	1787.55
BS_12	0.21244	0.10277	0.07101	2.887	1862.19
BS_13	0.21244	0.10240	0.07045	2.802	1828.31
BS_14	0.21254	0.10227	0.07036	2.738	1790.27
BS_15	0.21269	0.10235	0.07023	2.886	1887.73
BS_16	0.21260	0.10219	0.06992	2.798	1841.94
Average [kg/m³]					1867.94
Standard deviation [kg/m ³]					44.95
Coefficient of variation [-]					0.02

Determination of bulk density for clay blocks:

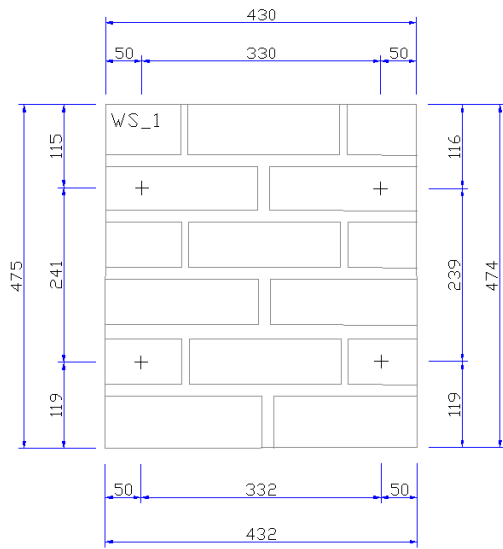
Specimen	Length [m]	Width [m]	Height [m]	Mass [kg]	Bulk density [kg/m ³]
BCL_0	0.21226	0.10011	0.04777	1.698	1672.77
BCL_1	0.20990	0.10142	0.05027	1.708	1596.04
BCL_2	0.20981	0.10142	0.05043	1.699	1583.27
BCL_3	0.20988	0.09956	0.04995	1.638	1569.36
BCL_4	0.21245	0.10004	0.05025	1.686	1578.67
BCL_5	0.21350	0.10217	0.05020	1.735	1584.44
BCL_6	0.21243	0.10008	0.05084	1.686	1559.87
BCL_7	0.20989	0.10138	0.04974	1.711	1616.59
BCL_8	0.21244	0.09929	0.04990	1.675	1591.37
BCL_9	0.21389	0.09846	0.05009	1.669	1582.18
BCL_10	0.21167	0.10012	0.04982	1.678	1589.31
BCL_11	0.21036	0.10173	0.04995	1.727	1615.64
BCL_12	0.21023	0.10199	0.05046	1.728	1597.18
BCL_13	0.21072	0.10244	0.05033	1.733	1595.21

Specimen	Length	Width	Height	Mass	Bulk density
	[m]	[m]	[m]	[kg]	[kg/m ³]
BCL_14	0.20993	0.10177	0.05029	1.736	1615.83
BCL_15	0.21033	0.10190	0.04983	1.728	1618.11
BCL_16	0.21054	0.10184	0.05045	1.730	1599.42
Average [kg/m³]					1597.96
Standard deviation [kg/m ³]					25.50
Coefficient of variation [-]					0.02

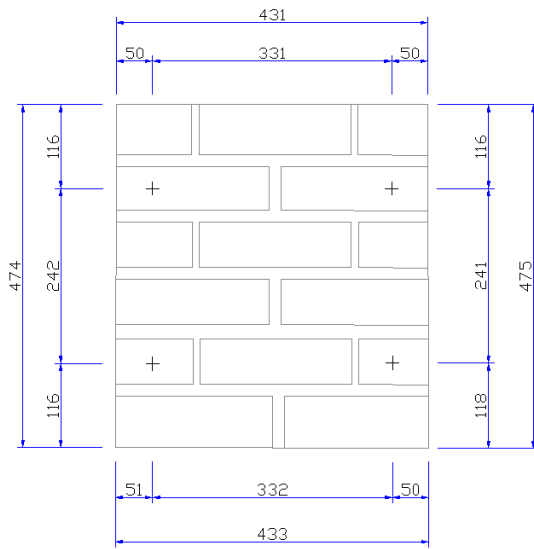
ANNEX IV

Geometry, instrumentation layout and additional information on *wallettes* and *triplets* for material characterisation tests

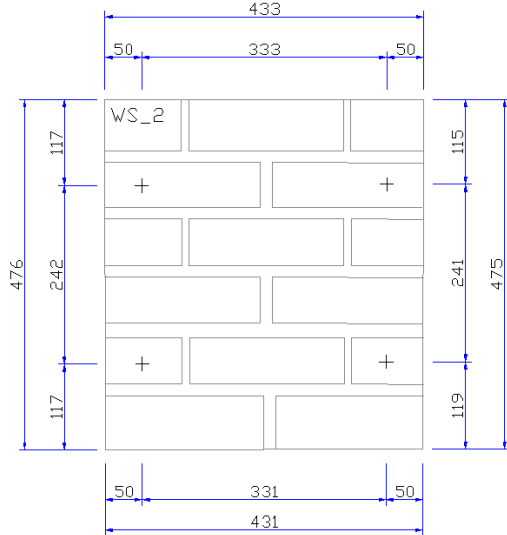
Geometry and instrumentation layout in calcium silicate *wallettes* for compressive strength tests:



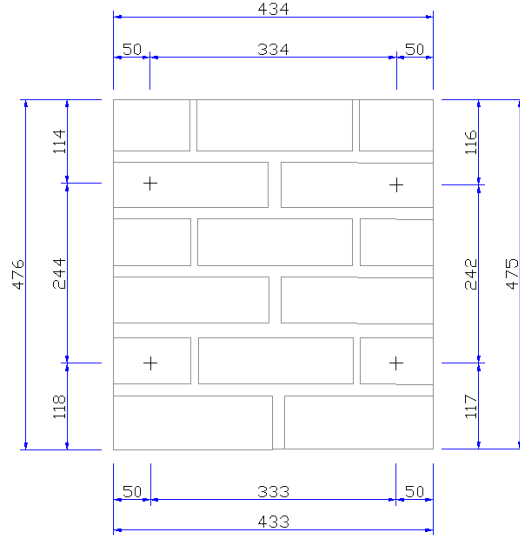
Wallette WS_1 – front side



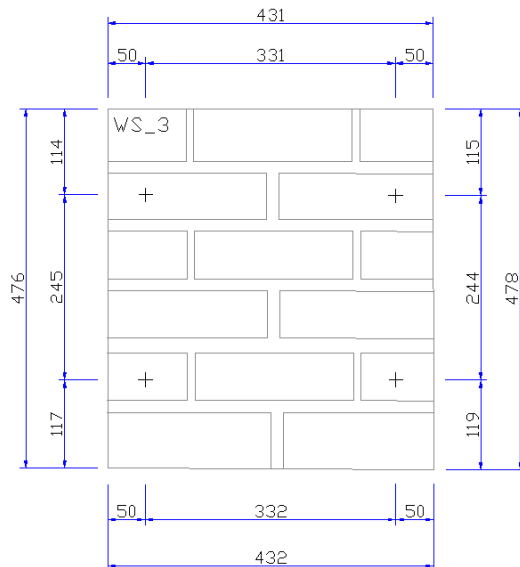
Wallette WS_1 – back side



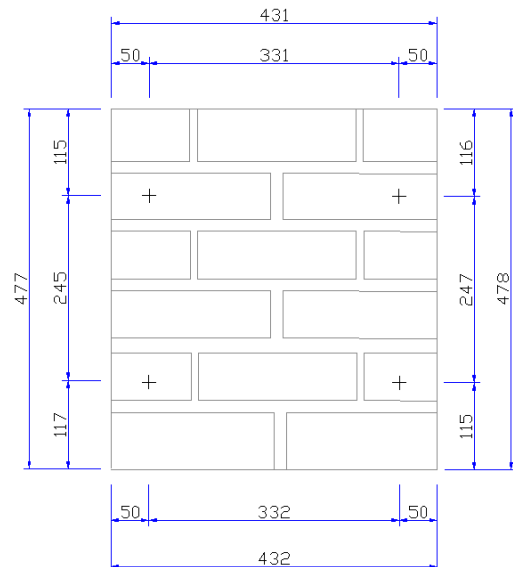
Wallette WS_2 – front side



Wallette WS_2 – back side

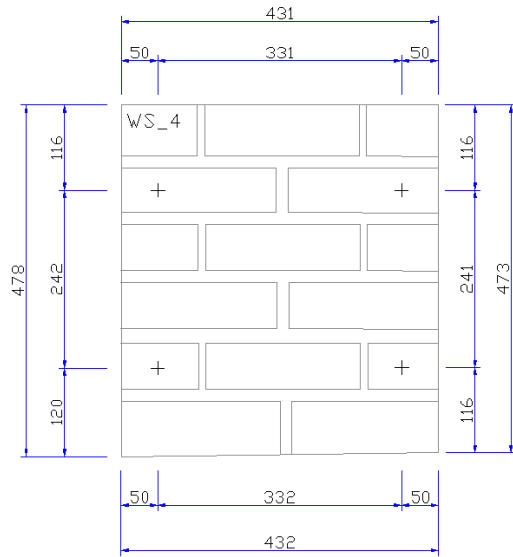


Wallette WS_3 – front side

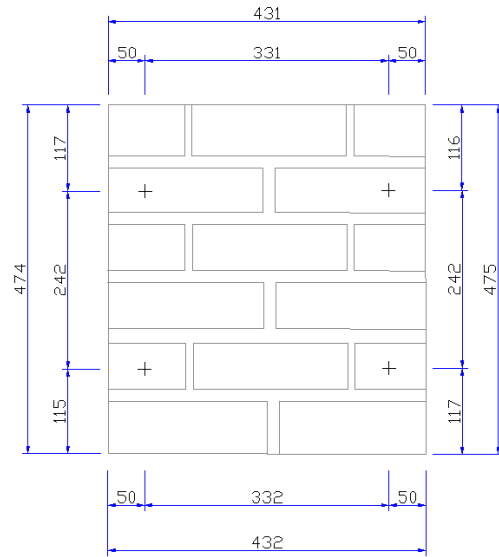


Wallette WS_3 – back side

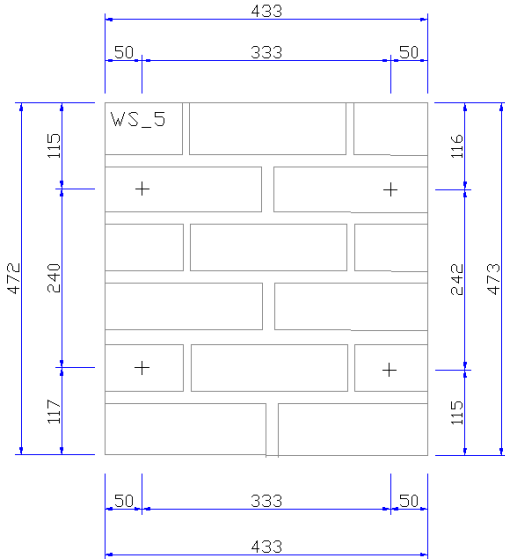
204 Collapse Shaking Table Test on URM Cavity Wall Structure representative of a Dutch Terraced House



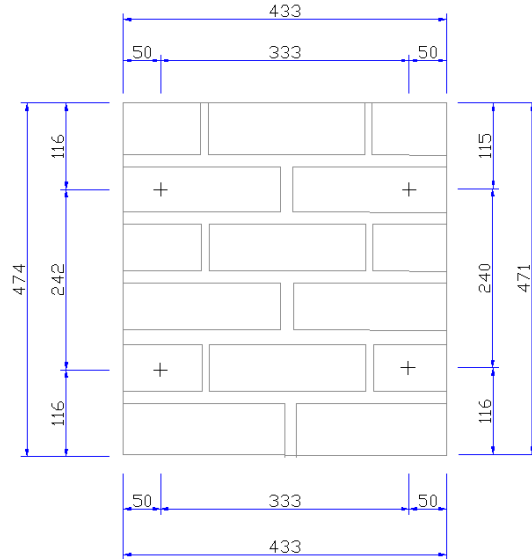
Wallette WS_4 – front side



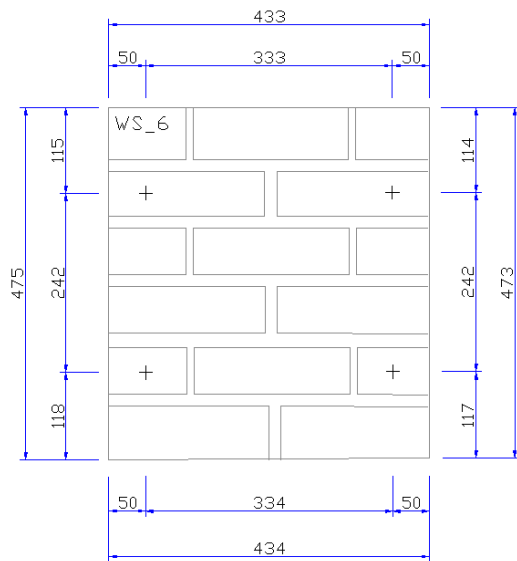
Wallette WS_4 – back side



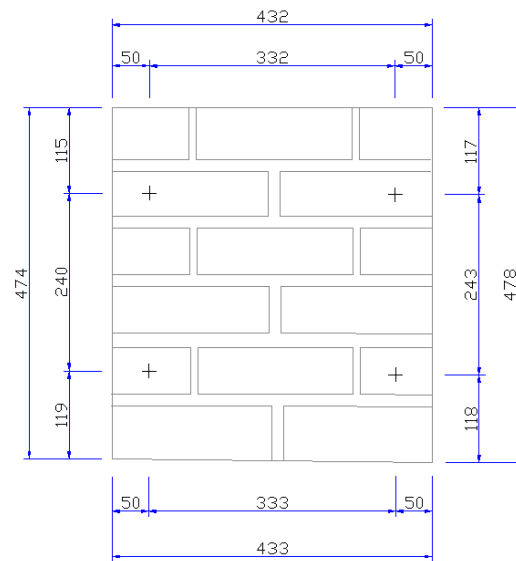
Wallette WS_5 – front side



Wallette WS_5 – back side

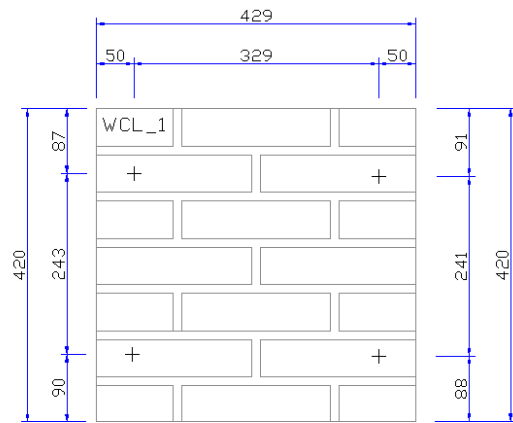


Wallette WS_6 – front side

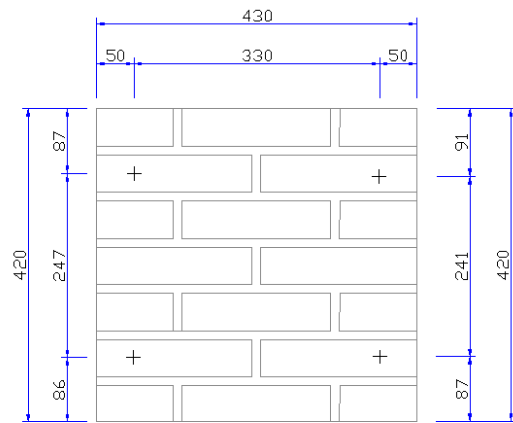


Wallette WS_6 – back side

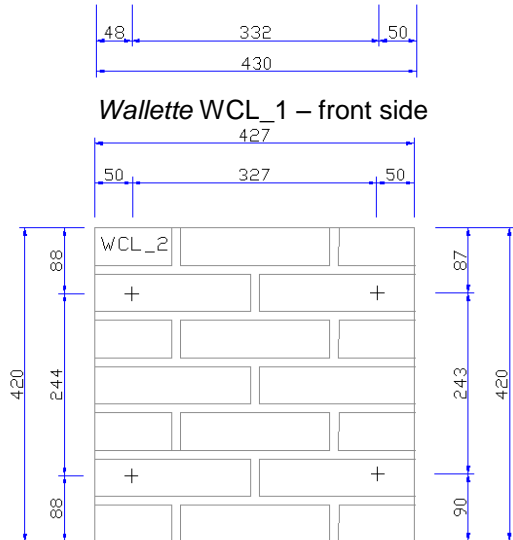
Geometry and instrumentation layout in clay *wallettes* for compressive strength tests:



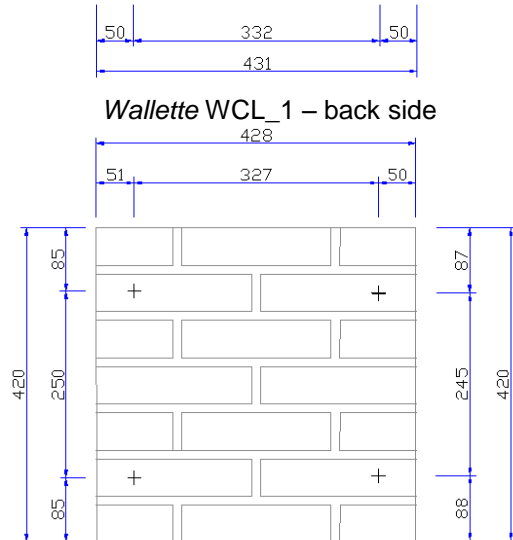
Wallette WCL_1 – front side



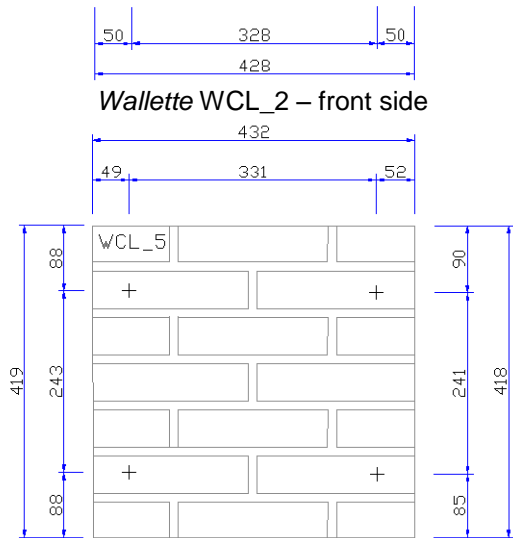
Wallette WCL_1 – back side



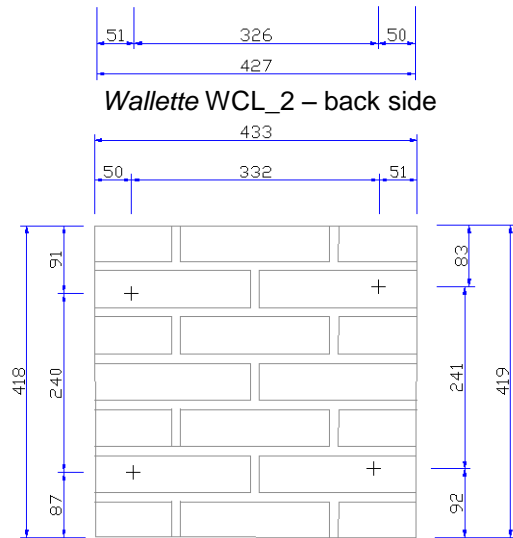
Wallette WCL_2 – front side



Wallette WCL_2 – back side

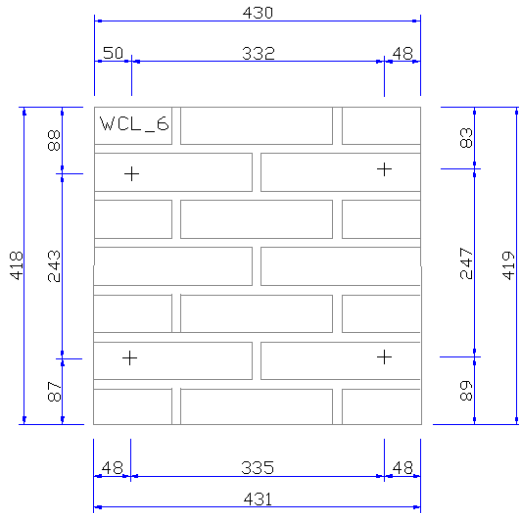


Wallette WCL_5 – front side

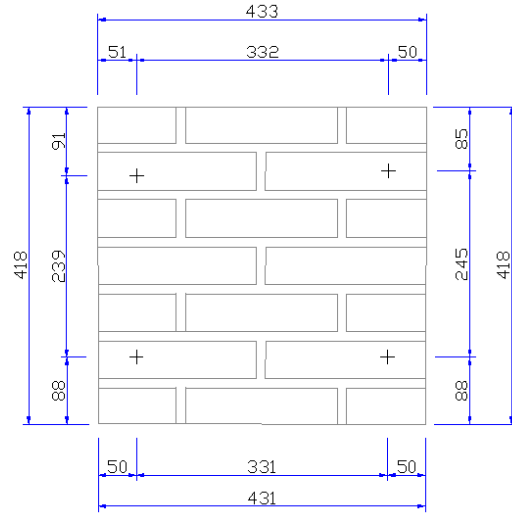


Wallette WCL_5 – back side

206 Collapse Shaking Table Test on URM Cavity Wall Structure representative of a Dutch Terraced House

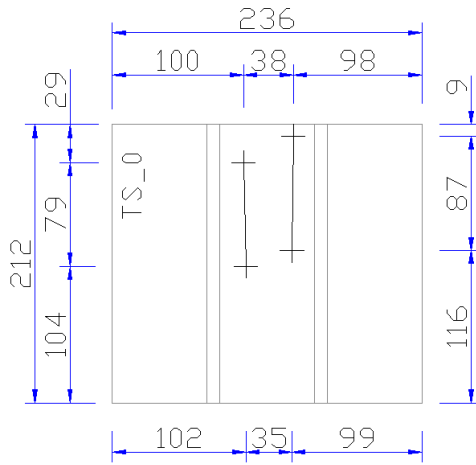


Wallette WCL_6 – front side

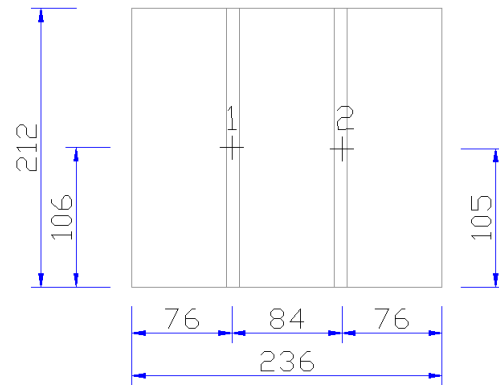


Wallette WCL_6 – back side

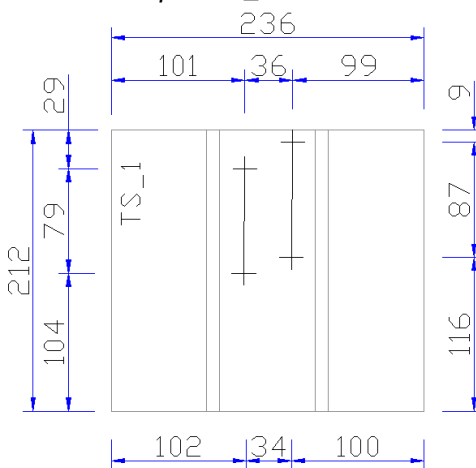
Geometry and instrumentation layout in calcium silicate triplets for shear strength tests:



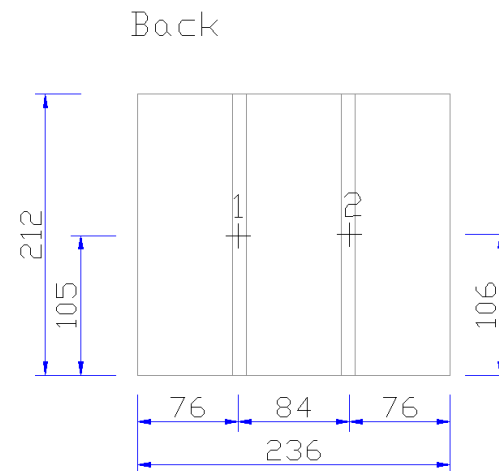
Triplet TS_0 – front side



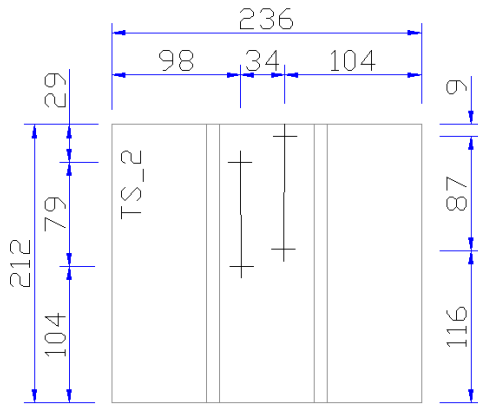
Triplet TS_0 – back side



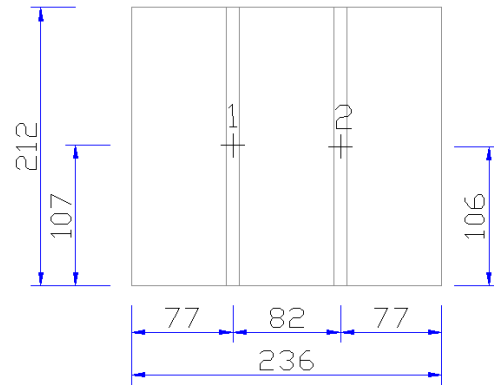
Triplet TS_1 – front side



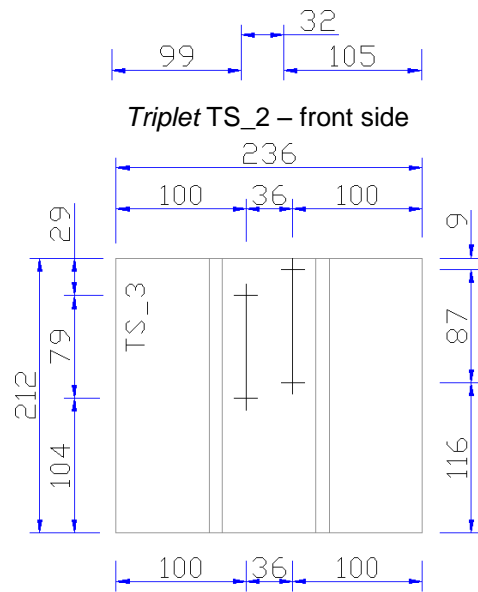
Triplet TS_1 – back side



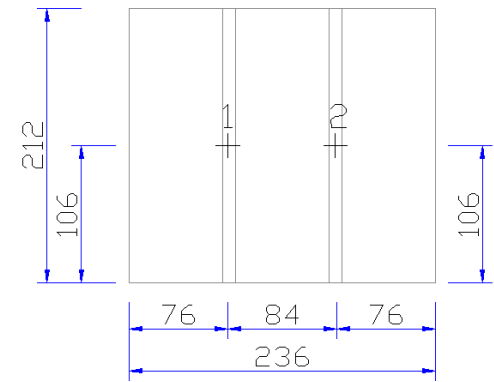
Triplet TS_2 – front side



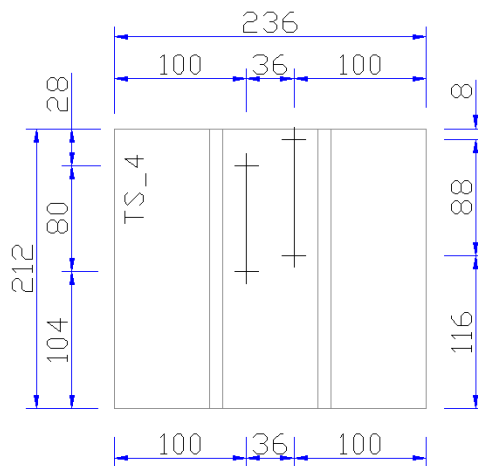
Triplet TS_2 – back side



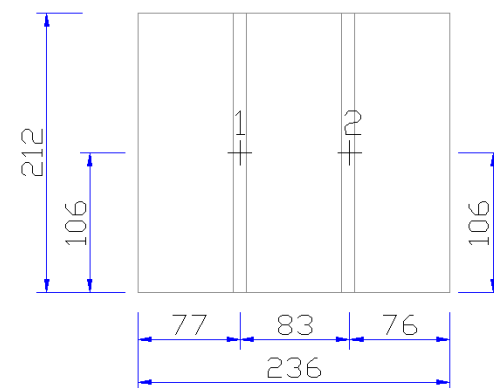
Triplet TS_3 – front side



Triplet TS_3 – back side

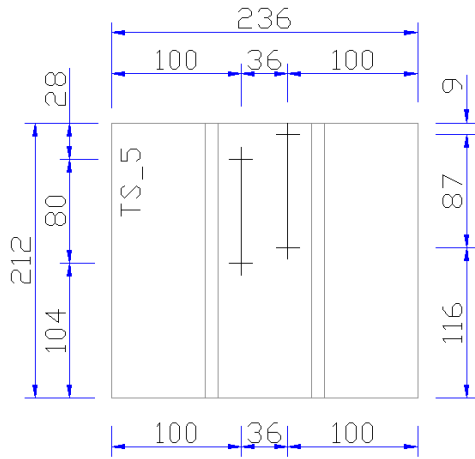


Triplet TS_4 – front side

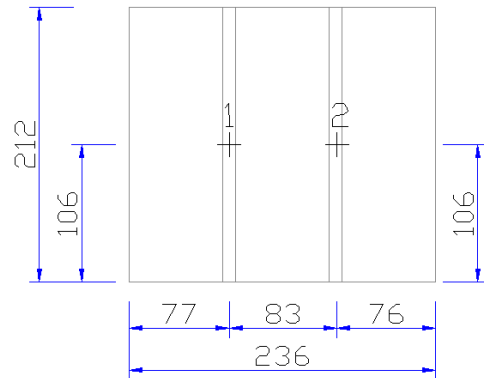


Triplet TS_4 – back side

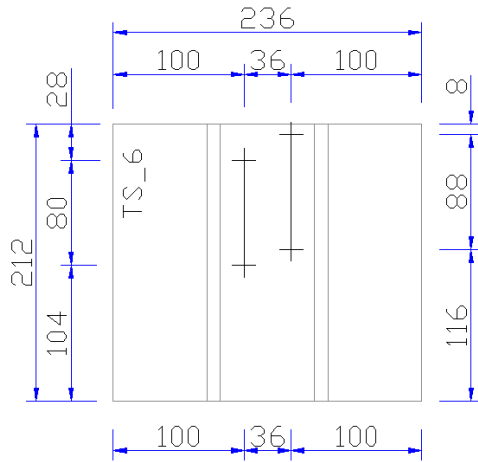
208 Collapse Shaking Table Test on URM Cavity Wall Structure representative of a Dutch Terraced House



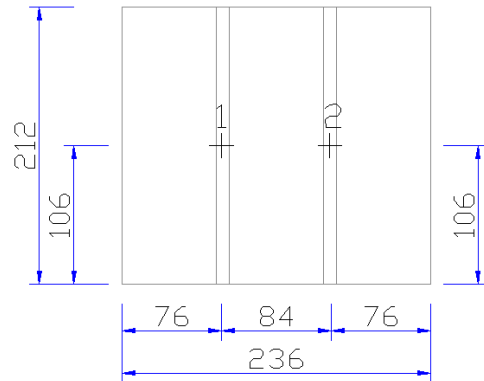
Triplet TS_5 – front side



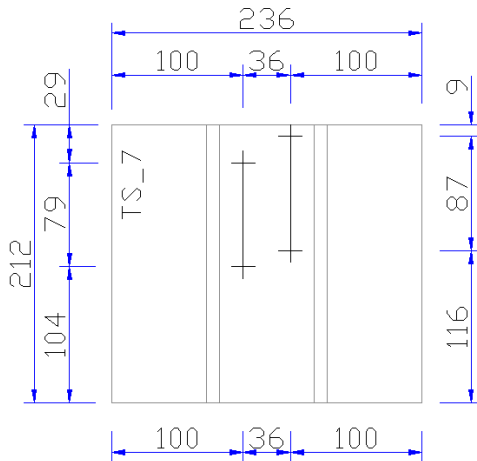
Triplet TS_5 – back side



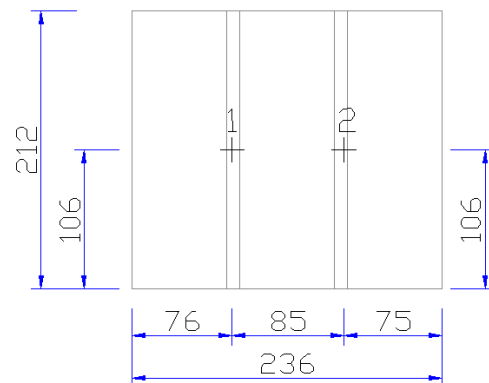
Triplet TS_6 – front side



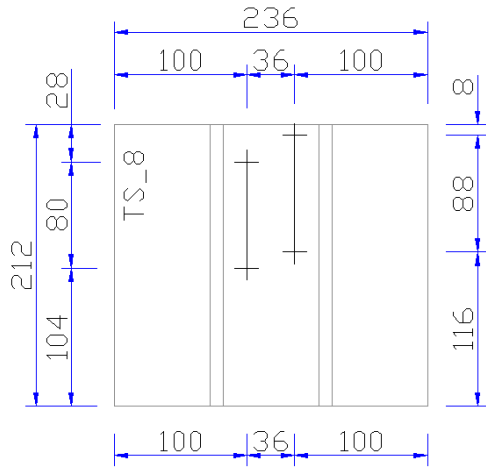
Triplet TS_6 – back side



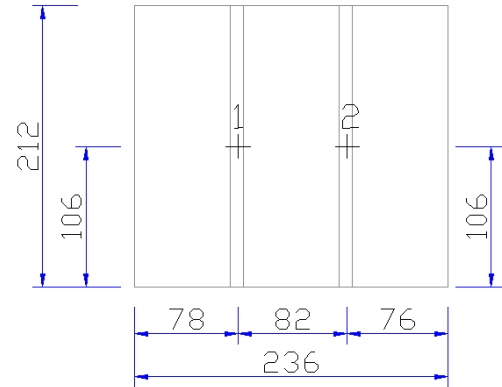
Triplet TS_7 – front side



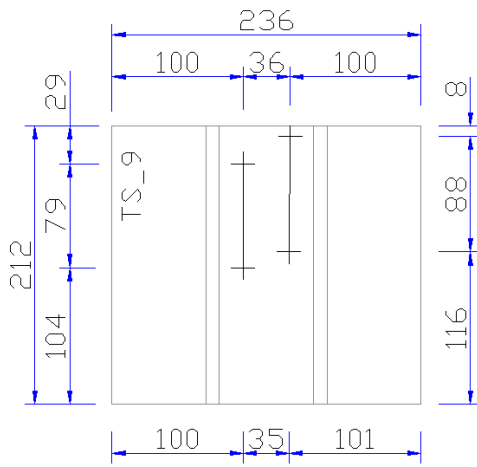
Triplet TS_7 – back side



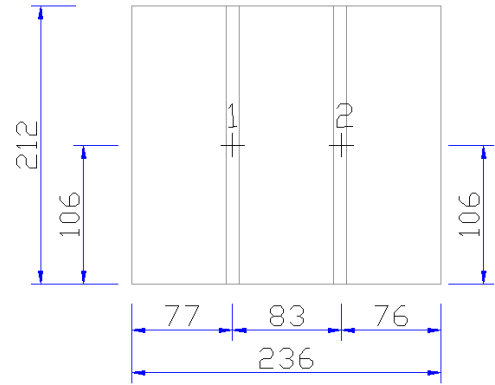
Triplet TS_8 – front side



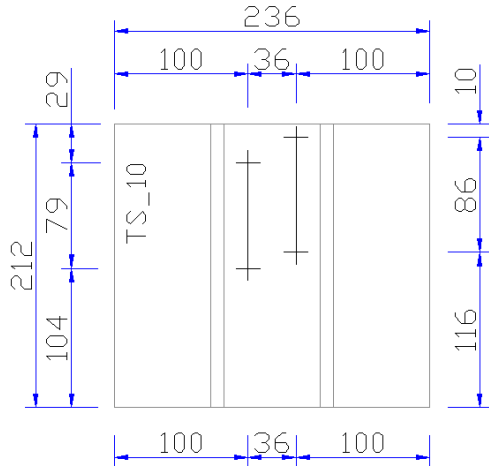
Triplet TS_8 – back side



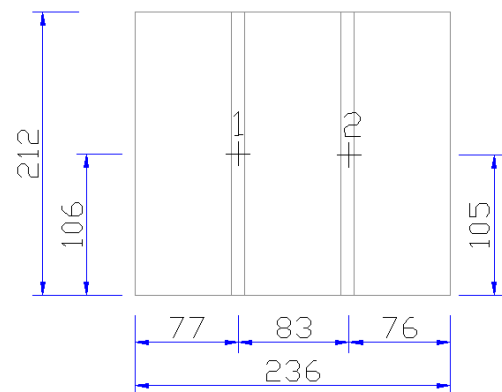
Triplet TS_9 – front side



Triplet TS_9 – back side

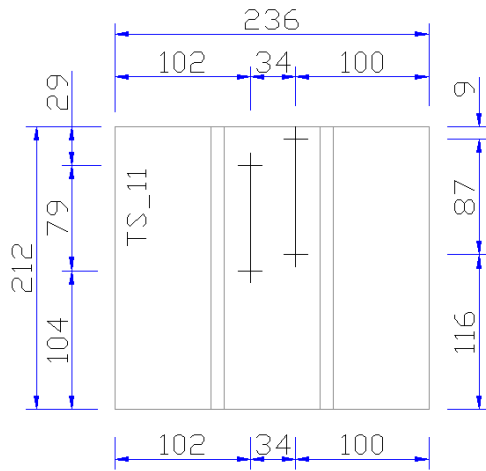


Triplet TS_10 – front side

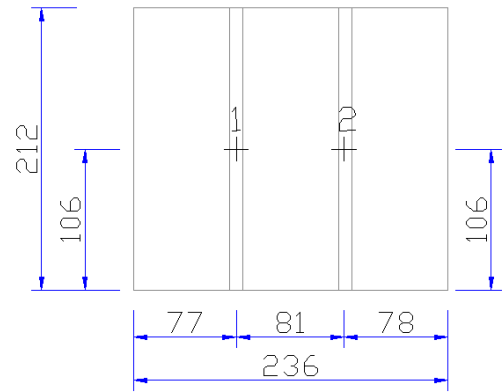


Triplet TS_10 – back side

210 Collapse Shaking Table Test on URM Cavity Wall Structure representative of a Dutch Terraced House

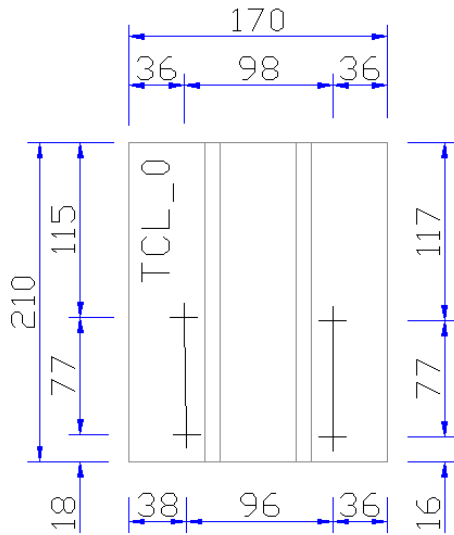


Triplet TS_11 – front side

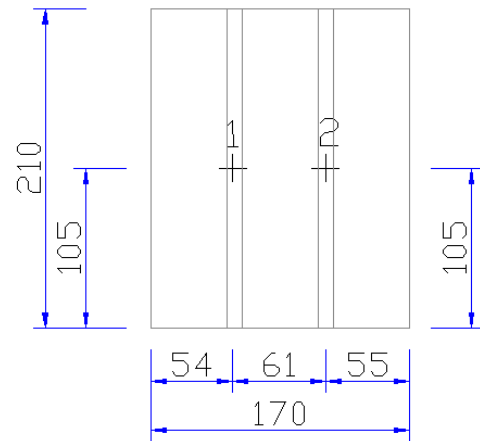


Triplet TS_11 – back side

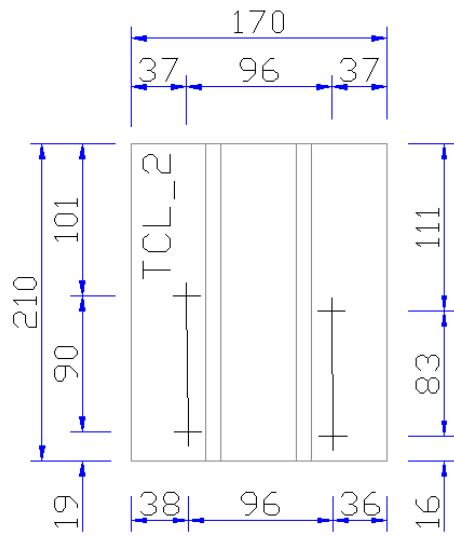
Geometry and instrumentation layout in clay triplets for shear strength tests:



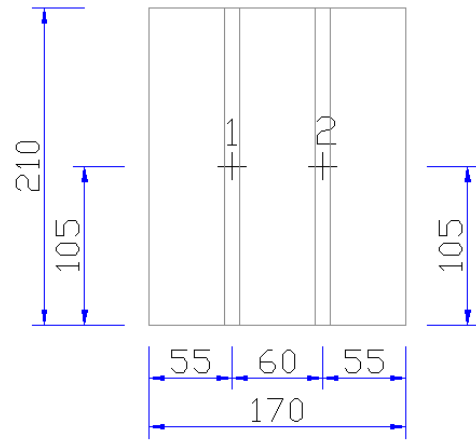
Triplet TCL_1 – front side



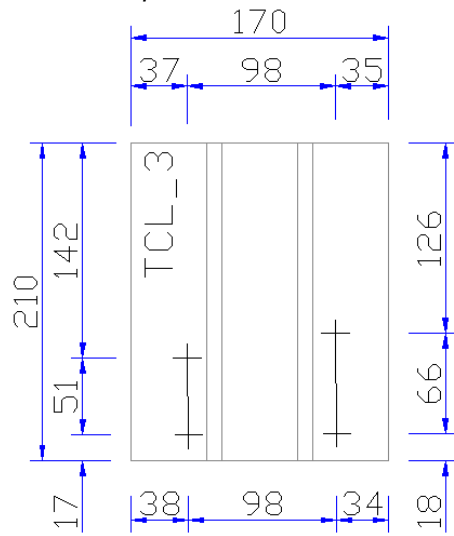
Triplet TCL_1 – back side



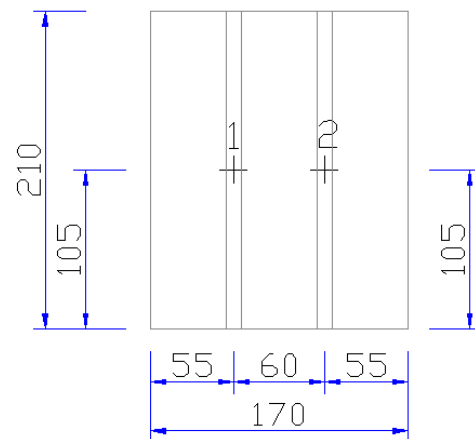
Triplet TCL_2 – front side



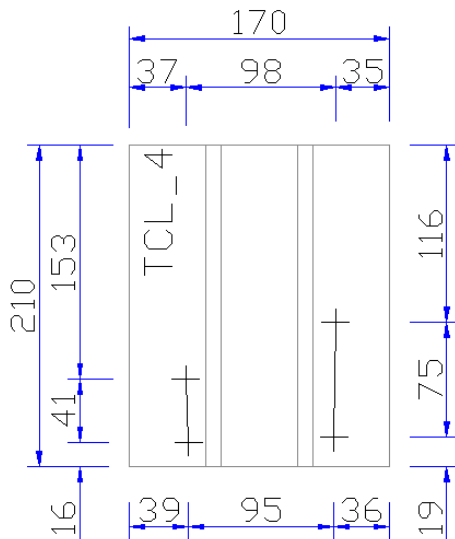
Triplet TCL_2 – back side



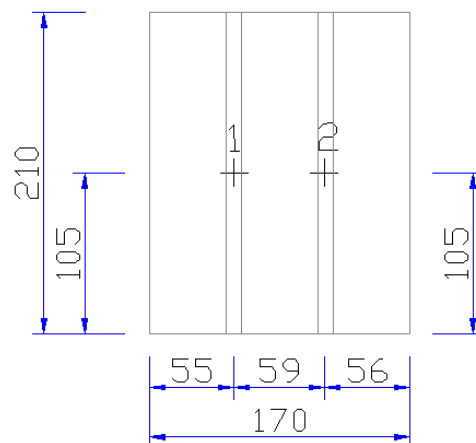
Triplet TCL_3 – front side



Triplet TCL_3 – back side

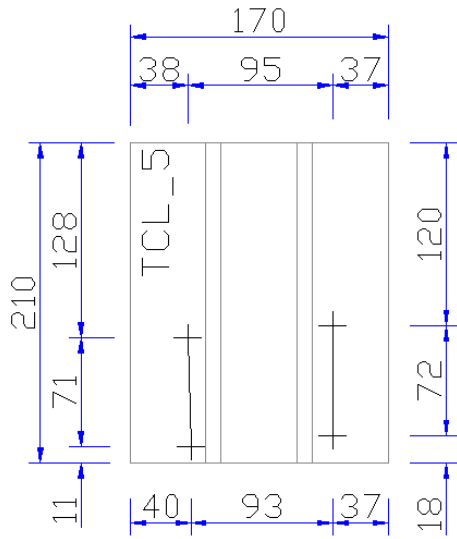


Triplet TCL_4 – front side

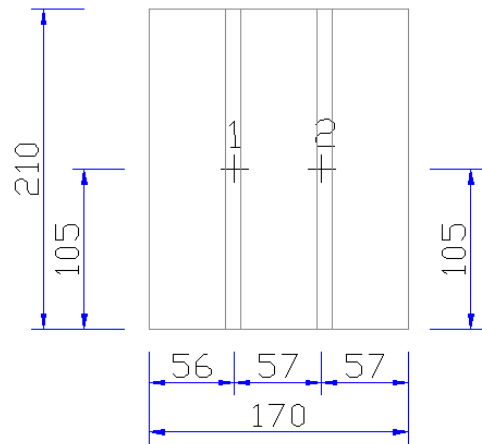


Triplet TCL_4 – back side

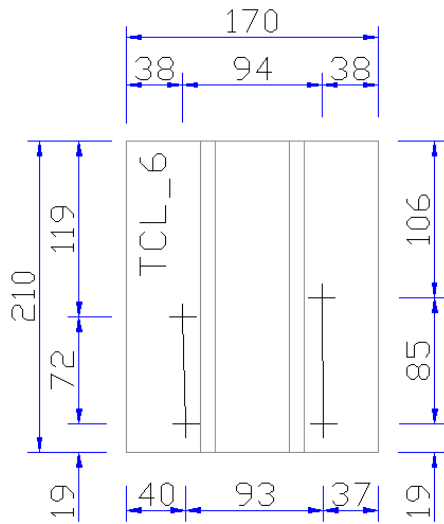
212 Collapse Shaking Table Test on URM Cavity Wall Structure representative of a Dutch Terraced House



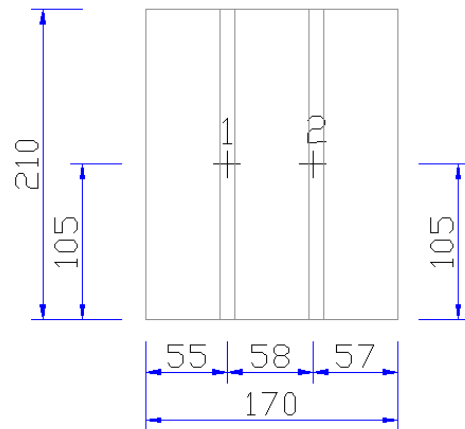
Triplet TCL_5 – front side



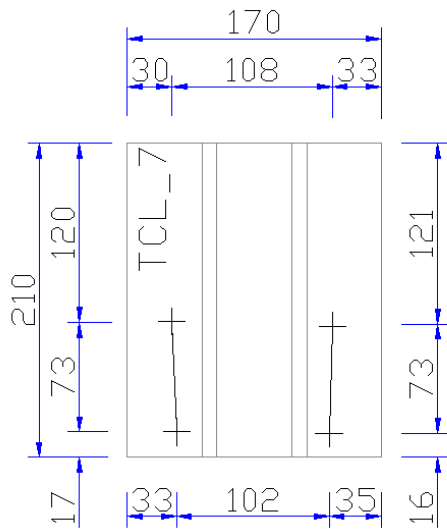
Triplet TCL_5 – back side



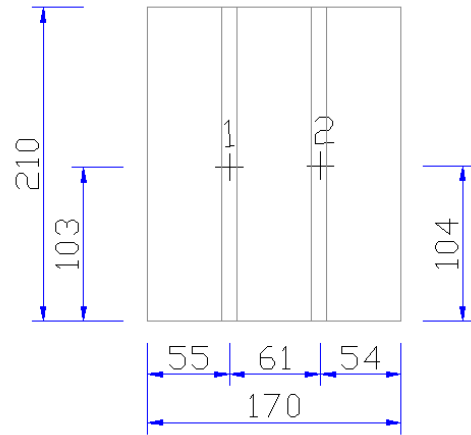
Triplet TCL_6 – front side



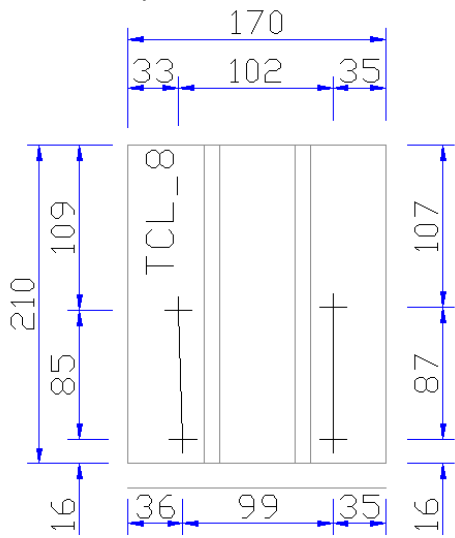
Triplet TCL_6 – back side



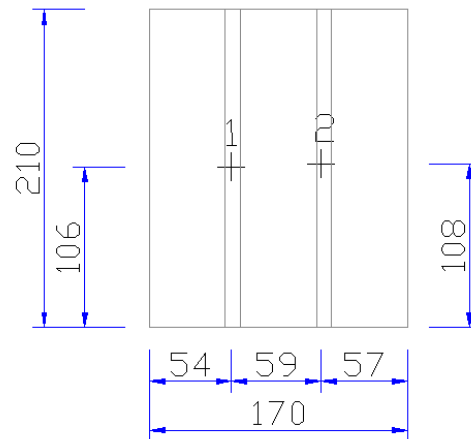
Triplet TCL_7 – front side



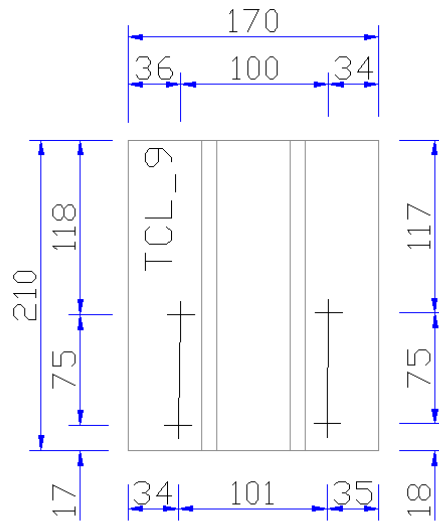
Triplet TCL_7 – back side



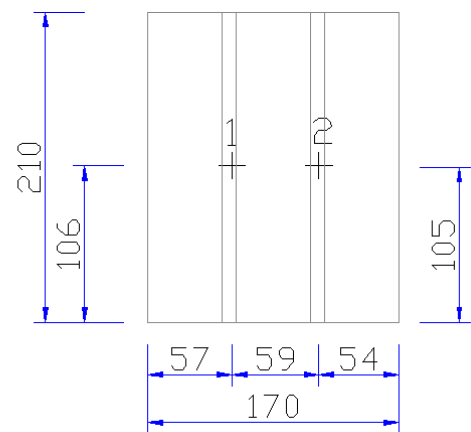
Triplet TCL_8 – front side



Triplet TCL_8 – back side



Triplet TCL_9 – front side



Triplet TCL_9 – back side

214 *Collapse Shaking Table Test on URM Cavity Wall Structure representative of a Dutch Terraced House*

Dimensions and masses of the two types of wallettes constructed for the compression strength tests:

Specimen		Length [mm]			Average	Width [mm]			Average	Height [mm]			Mass [kg]
		Up	Down			Top	Bottom			Left	Right		
WS_0	Front	433.20	434.05	433.43	Left	101.89	102.32	101.95	473.50	474.00	473.75	37.837	
	Back	432.35	434.10		Right	101.51	102.06						
WS_1	Front	429.10	435.00	432.06	Left	102.75	103.90	102.82	474.50	474.00	474.25	38.178	
	Back	429.05	435.10		Right	102.75	101.88						
WS_2	Front	434.00	435.30	434.36	Left	102.20	103.35	102.76	475.00	475.00	475.00	38.071	
	Back	434.05	434.10		Right	102.21	103.26						
WS_3	Front	430.35	435.24	432.45	Left	103.05	102.99	104.28	477.50	477.50	477.50	38.316	
	Back	430.30	433.90		Right	108.08	103.01						
WS_4	Front	432.15	435.45	433.74	Left	102.67	102.76	102.98	476.00	474.00	475.00	38.325	
	Back	432.15	435.20		Right	103.18	103.30						
WS_5	Front	436.25	434.00	435.45	Left	102.13	102.93	102.40	476.00	474.00	475.00	38.129	
	Back	437.09	434.44		Right	101.32	103.21						
WS_6	Front	434.70	434.00	434.34	Left	101.63	102.99	102.71	474.50	473.50	474.00	37.978	
	Back	434.82	433.84		Right	103.56	102.67						
WCL_0	Front	425.70	429.01	427.95	Left	99.30	99.98	100.12	410.00	410.50	410.25	32.557	
	Back	428.07	429.00		Right	100.13	101.06						
WCL_1	Front	429.00	430.35	430.29	Left	99.62	101.27	100.93	412.50	410.50	411.50	32.676	
	Back	430.64	431.15		Right	101.48	101.35						
WCL_2	Front	426.92	428.10	427.60	Left	100.22	100.60	99.92	411.00	411.50	411.25	32.790	
	Back	428.08	427.30		Right	98.79	100.08						
WCL_3	Front	428.04	429.72	429.40	Left	101.15	100.16	100.31	412.50	412.00	412.25	32.767	
	Back	428.64	431.20		Right	101.66	98.26						
WCL_4	Front	431.36	430.00	431.37	Left	101.13	100.29	101.04	411.50	407.50	409.50	32.483	
	Back	432.96	431.15		Right	101.63	101.11						
WCL_5	Front	432.27	431.38	431.80	Left	100.79	101.06	100.81	408.00	410.50	409.25	32.655	
	Back	433.05	430.48		Right	100.74	100.65						
WCL_6	Front	430.84	431.84	431.76	Left	99.44	101.36	100.59	409.00	409.00	409.00	32.487	
	Back	433.03	431.31		Right	100.38	101.17						

Dimensions and masses of calcium silicate triplets built for the shear strength tests:

Specimen	Block	Height [mm]			Width [mm]				Length [mm]			Thickness of bed joint [mm]				Mass [kg]	
		Left	Right	Average	Block	Top	Middle	Bottom	Average	Individual values		Bed joint 1		Bed joint 2			
										Top	Bottom	Front	Back	Front	Back		
TS_0	1	212.98	212.86	212.84	1	102.18	102.25	103.00	102.95	Top	234.00	233.50	11.23	12.32	12.28	11.03	9.445
	2	212.91	212.93		2	103.01	X	103.19		Bottom	233.00		11.04	12.69	10.49	10.20	
	3	212.60	212.77		3	103.42	103.53	103.01									
TS_1	1	212.92	212.98	212.75	1	103.61	103.99	103.40	102.83	Top	234.00	234.50	11.56	11.35	10.97	10.51	9.307
	2	212.67	212.71		2	102.51	X	102.01		Bottom	235.00		12.19	10.92	12.44	13.00	
	3	212.48	212.74		3	102.49	102.32	102.30									
TS_2	1	212.51	212.66	212.70	1	103.04	103.19	103.42	102.96	Top	237.00	236.00	10.94	13.27	13.72	14.33	9.520
	2	212.87	212.78		2	102.35	X	102.91		Bottom	235.00		12.04	12.56	12.56	13.52	

216 Collapse Shaking Table Test on URM Cavity Wall Structure representative of a Dutch Terraced House

Specimen	Block	Height [mm]			Width [mm]				Length [mm]			Thickness of bed joint [mm]				Mass [kg]	
		Left	Right	Average	Block	Top	Middle	Bottom	Average	Individual values		Average	Bed joint 1		Bed joint 2		
													Front	Back	Front		Back
	3	212.59	212.80		3	103.36	102.70	102.72									
TS_3	1	212.65	212.55	212.61	1	102.68	102.95	103.02	102.76	Top	232.00	232.50	10.65	10.87	12.18	12.43	9.351
	2	212.75	212.60		2	102.09	X	102.63		Bottom	233.00		12.00	10.84	11.44	11.07	
	3	212.54	212.57		3	103.20	102.86	102.64									
TS_4	1	212.89	212.89	212.78	1	102.17	102.23	102.36	101.97	Top	236.00	235.50	11.48	11.91	13.47	14.97	9.187
	2	212.71	212.73		2	102.29	X	102.25		Bottom	235.00		12.23	12.12	13.20	13.08	
	3	212.63	212.84		3	101.33	101.52	101.59									
TS_5	1	212.76	213.07	212.80	1	102.38	102.17	102.20	102.20	Top	236.00	237.00	11.57	12.08	15.06	14.13	9.319
	2	212.87	212.79		2	102.56	X	102.25		Bottom	238.00		13.00	11.95	15.49	12.69	
	3	212.62	212.66		3	101.89	101.92	102.20									
TS_6	1	212.57	212.89	212.64	1	102.25	102.27	102.16	102.51	Top	233.00	233.50	10.87	11.93	13.13	12.11	9.263
	2	212.65	212.57		2	102.17	X	102.60		Bottom	234.00		11.50	11.41	12.43	10.74	
	3	212.51	212.62		3	103.13	102.89	102.64									
TS_7	1	213.05	212.79	212.91	1	102.89	103.02	102.94	103.03	Top	233.00	233.50	10.35	10.81	11.56	10.88	9.506
	2	212.97	213.12		2	102.83	X	103.08		Bottom	234.00		10.32	9.76	12.37	11.65	
	3	212.67	212.88		3	103.10	103.46	102.91									
TS_8	1	212.51	213.02	212.69	1	103.25	103.12	103.34	102.88	Top	235.00	236.50	11.63	11.53	14.57	14.87	9.478
	2	212.54	212.57		2	102.23	X	102.00		Bottom	238.00		12.07	11.39	15.77	14.06	
	3	212.89	212.60		3	102.98	102.98	103.13									
TS_9	1	212.72	212.76	212.67	1	102.65	102.83	103.11	102.81	Top	237.00	237.00	11.24	12.71	14.26	14.22	9.531
	2	212.67	212.62		2	102.96	X	103.32		Bottom	237.00		12.00	12.58	14.14	14.11	
	3	212.54	212.71		3	102.21	102.56	102.86									
TS_10	1	212.76	213.00	212.74	1	104.31	103.34	102.94	103.07	Top	234.54	233.74	9.12	10.24	9.47	12.09	9.324
	2	212.88	212.52		2	102.35	X	101.97		Bottom	232.93		9.13	10.26	9.12	10.96	
	3	212.51	212.79		3	102.93	103.57	103.11									
TS_11	1	212.17	212.75	212.38	1	103.59	102.48	102.90	103.09	Top	238.93	238.42	15.59	9.21	14.36	10.30	9.642
	2	212.53	212.42		2	103.58	X	102.63		Bottom	237.90		15.61	10.54	13.48	11.76	
	3	212.04	212.34		3	103.64	102.06	103.82									

Dimensions and masses of clay triplets built for the shear strength tests:

Specimen	Block	Height [mm]			Block	Width [mm]			Length [mm]			Thickness of bed joint [mm]				Mass [kg]	
		Left	Right	Average		Top	Middle	Bottom	Average	Individual values		Average	Bed joint 1		Bed joint 2		
										Front	Back		Front	Back			
TCL_0	1	210.92	211.18	210.48	1	100.64	102.19	102.03	101.38	Top	172.00	171.50	13.12	12.94	14.81	13.19	6.689
	2	210.64	210.13		2	101.62	X	100.92		Bottom	171.00		13.25	12.90	12.13	12.07	
	3	209.70	210.29		3	100.19	102.00	101.43									
TCL_1	1	209.96	211.55	210.54	1	99.73	99.24	98.84	100.34	Top	171.00	170.50	12.76	12.77	13.47	11.49	6.610
	2	209.62	210.62		2	101.04	X	99.85		Bottom	170.00		11.98	13.11	11.23	12.14	
	3	210.46	211.05		3	100.58	101.99	101.45									
TCL_2	1	210.55	211.12	210.60	1	101.84	102.43	100.89	101.32	Top	171.00	171.00	11.49	11.37	15.07	14.29	6.674
	2	210.79	210.31		2	100.82	X	101.59		Bottom	171.00		11.71	11.43	11.65	13.32	
	3	209.87	210.93		3	100.42	101.25	101.28									
TCL_3	1	209.74	211.37	210.48	1	99.78	99.35	99.03	100.56	Top	169.00	169.00	11.78	11.55	11.40	12.46	6.590
	2	210.38	210.84		2	100.60	X	101.70		Bottom	169.00		10.34	13.23	10.95	12.64	
	3	210.31	210.21		3	100.85	101.55	101.64									
TCL_4	1	210.48	209.92	210.26	1	101.16	101.17	100.77	101.34	Top	171.00	171.00	13.66	14.85	12.83	11.10	6.676
	2	210.24	209.89		2	101.28	X	100.65		Bottom	171.00		12.37	13.77	11.32	12.33	
	3	210.51	210.54		3	100.47	102.72	102.53									
TCL_5	1	210.69	209.87	210.56	1	99.16	99.94	99.48	100.63	Top	175.00	174.00	12.44	16.96	16.11	14.89	6.679
	2	211.27	210.60		2	101.21	X	101.93		Bottom	173.00		14.07	13.88	12.22	14.69	
	3	210.89	210.05		3	100.75	101.24	101.31									
TCL_6	1	207.71	209.78	210.06	1	100.29	99.68	99.35	100.67	Top	173.00	173.00	13.85	15.40	16.72	14.95	6.726
	2	210.70	211.71		2	100.90	X	101.69		Bottom	173.00		14.90	14.05	12.15	13.28	
	3	210.22	210.21		3	100.68	101.61	101.14									
TCL_7	1	209.52	210.60	210.22	1	100.02	101.07	101.04	100.92	Top	170.00	170.00	12.55	13.28	13.71	11.63	6.538
	2	209.83	210.70		2	100.28	X	101.25		Bottom	170.00		12.40	12.75	11.23	12.37	
	3	210.10	210.56		3	101.39	101.57	100.76									
TCL_8	1	209.11	209.87	209.99	1	100.78	100.05	99.54	100.33	Top	171.00	171.50	14.44	14.53	13.13	12.56	6.612
	2	209.96	210.66		2	101.30	X	100.37		Bottom	172.00		15.58	14.34	10.75	11.58	
	3	209.25	211.08		3	100.01	101.01	99.57									
TCL_9	1	208.27	209.17	209.55	1	100.95	100.46	99.17	100.15	Top	172.00	171.50	13.87	12.40	13.86	13.90	6.557
	2	209.99	210.04		2	101.45	X	100.21		Bottom	171.00		11.49	12.53	12.55	12.91	
	3	209.03	210.82		3	100.28	99.40	99.28									

218 Collapse Shaking Table Test on URM Cavity Wall Structure representative of a Dutch Terraced House

Dimensions and masses of the two types of wallettes built for the bond strength tests:

Specimen	Height [mm]			Width [mm]			Length [mm]			Thickness of bed joint [mm]				Mass [kg]
	Left	Right	Average	Top	Bottom	Average	Front	Back	Average	Bed joint 1		Bed joint 2		
										Front	Back	Front	Back	
BWS_0	237.00	236.00	236.50	102.32	102.21	102.27	214.00	213.00	213.50	11.44	11.63	13.20	13.11	9.239
										11.74	10.63	14.41	13.38	
BWS_1	235.00	234.00	234.50	102.55	102.81	102.68	213.00	213.00	213.00	10.79	11.64	12.82	12.76	9.379
										9.92	11.21	12.42	12.32	
BWS_2	235.00	234.00	234.50	102.08	103.04	102.56	212.00	213.00	212.50	12.47	10.83	10.38	10.14	9.306
										13.04	11.76	10.11	10.66	
BWS_3	233.00	234.00	233.50	102.49	101.96	102.23	213.00	213.00	213.00	12.03	11.65	10.60	10.89	9.401
										11.95	11.34	9.76	10.12	
BWS_4	238.00	239.00	238.50	102.02	102.28	102.15	215.00	215.00	215.00	10.91	11.93	13.95	15.16	9.425
										12.09	12.41	13.69	13.48	
BWS_5	240.00	238.00	239.00	102.16	102.04	102.10	214.00	212.00	213.00	11.66	11.23	15.13	14.16	9.508
										11.51	12.35	14.21	13.04	
BWCL_1	171.94	173.33	172.64	100.58	98.55	99.57	210.62	208.67	209.65	13.99	13.88	13.91	12.16	6.526
										14.70	13.81	12.81	11.97	
BWCL_2	175.70	176.42	176.06	98.53	102.05	100.29	210.35	211.81	211.08	13.27	12.66	16.91	15.74	6.677
										14.48	13.79	15.16	12.07	
BWCL_3	170.74	171.87	171.31	101.69	101.82	101.76	210.94	211.12	211.03	13.20	13.33	14.09	12.04	6.671
										10.86	11.11	12.71	11.85	
BWCL_4	172.13	173.31	172.72	102.38	98.62	100.50	210.32	210.73	210.53	12.82	12.72	13.51	11.18	6.495
										13.55	12.99	11.60	8.65	
BWCL_5	173.19	173.80	173.50	98.31	101.01	99.66	210.21	211.75	210.98	11.84	10.85	16.46	14.95	6.502
										13.28	12.84	13.14	12.20	
BWCL_6	170.06	170.74	170.40	102.14	101.56	101.85	210.81	211.04	210.93	10.96	11.49	14.68	13.82	6.640
										10.62	10.73	12.86	11.03	
BWCL_7	171.96	171.29	171.63	100.48	98.40	99.44	210.99	209.32	210.16	12.07	13.86	13.64	9.56	6.463
										12.04	9.53	11.49	9.85	
BWCL_8	174.18	175.05	174.62	100.44	101.27	100.86	210.17	209.00	209.59	13.99	15.35	15.55	13.72	6.543
										15.05	13.81	14.58	10.99	

Determination of bulk density for calcium silicate wallettes and triplets:

Specimen	Length	Width	Height	Mass	Bulk density
	[m]	[m]	[m]	[kg]	[kg/m ³]
WS_0	0.43343	0.10195	0.47375	37.837	1807.43
WS_1	0.43206	0.10282	0.47425	38.178	1812.11
WS_2	0.43436	0.10276	0.47500	38.071	1795.67
WS_3	0.43245	0.10428	0.47750	38.316	1779.38
WS_4	0.43374	0.10298	0.47500	38.325	1806.37
WS_5	0.43545	0.10240	0.47500	38.129	1800.21
WS_6	0.43434	0.10271	0.47400	37.978	1796.02
	Average				1799.60
TS_0	0.23350	0.10295	0.21284	9.445	1846.02
TS_1	0.23450	0.10283	0.21275	9.307	1814.17
TS_2	0.23600	0.10296	0.21270	9.520	1842.00
TS_3	0.23250	0.10276	0.21261	9.351	1840.89
TS_4	0.23550	0.10197	0.21278	9.187	1797.96
TS_5	0.23700	0.10220	0.21280	9.319	1808.00
TS_6	0.23350	0.10251	0.21264	9.263	1819.93
TS_7	0.23350	0.10303	0.21291	9.506	1855.89
TS_8	0.23650	0.10288	0.21269	9.478	1831.50
TS_9	0.23700	0.10281	0.21267	9.531	1839.28
TS_10	0.23374	0.10307	0.21274	9.324	1819.23

Specimen	Length	Width	Height	Mass	Bulk density
	[m]	[m]	[m]	[kg]	[kg/m ³]
TS_11	0.23842	0.10309	0.21238	9.642	1847.12
Average					1830.16
BWS_0	0.21350	0.10227	0.23650	9.239	1789.15
BWS_1	0.21300	0.10268	0.23450	9.379	1828.72
BWS_2	0.21250	0.10256	0.23450	9.306	1820.89
BWS_3	0.21300	0.10223	0.23350	9.401	1848.97
BWS_4	0.21500	0.10215	0.23850	9.425	1799.35
BWS_5	0.21300	0.10210	0.23900	9.508	1829.30
Average					1819.40

Determination of bulk density for clay bricks wallettes and triplets:

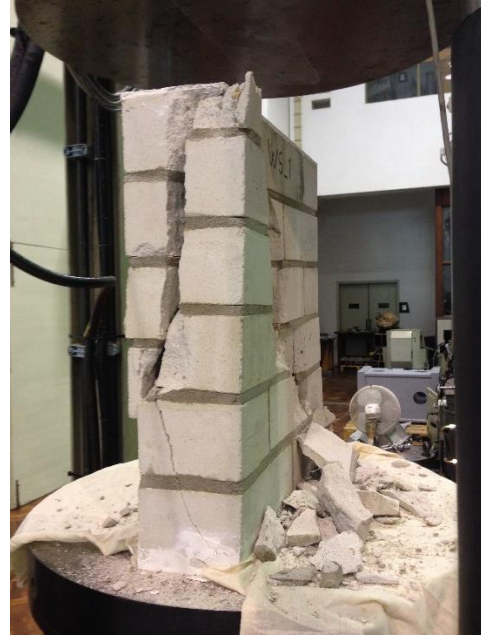
Specimen	Length	Width	Height	Mass	Bulk density
	[m]	[m]	[m]	[kg]	[kg/m ³]
WCL_0	0.42795	0.10012	0.41025	32.557	1852.17
WCL_1	0.43029	0.10093	0.41150	32.676	1828.43
WCL_2	0.42760	0.09992	0.41125	32.790	1866.14
WCL_3	0.42940	0.10031	0.41225	32.767	1845.31
WCL_4	0.43137	0.10104	0.40950	32.483	1819.95
WCL_5	0.43180	0.10081	0.40925	32.655	1833.05
WCL_6	0.43176	0.10059	0.40900	32.487	1828.90
Average					1839.14
TCL_0	0.17150	0.10138	0.21048	6.689	1827.82
TCL_1	0.17050	0.10034	0.21054	6.610	1835.14
TCL_2	0.17100	0.10132	0.2106	6.674	1829.10
TCL_3	0.16900	0.10056	0.21048	6.590	1842.31
TCL_4	0.17100	0.10134	0.21026	6.676	1832.24
TCL_5	0.17400	0.10063	0.21056	6.679	1811.59
TCL_6	0.17300	0.10067	0.21006	6.726	1838.52
TCL_7	0.17000	0.10092	0.21022	6.538	1812.78
TCL_8	0.17150	0.10033	0.20999	6.612	1829.95
TCL_9	0.17150	0.10015	0.20955	6.557	1821.81
Average					1828.12
BWCL_1	0.20965	0.09957	0.17264	6.526	1810.85
BWCL_2	0.21108	0.10029	0.17606	6.677	1791.50
BWCL_3	0.21103	0.10176	0.17131	6.671	1813.37
BWCL_4	0.21053	0.10050	0.17272	6.495	1777.28
BWCL_5	0.21098	0.09966	0.17350	6.502	1782.32
BWCL_6	0.21093	0.10185	0.17040	6.640	1813.84
BWCL_7	0.21016	0.09944	0.17163	6.463	1801.90
BWCL_8	0.20959	0.10086	0.17462	6.543	1772.53
Average					1795.45

ANNEX V
Collapse mechanisms in material characterisation tests

Failure mechanisms of calcium silicate *wallettes* for compressive strength tests:



Wallette WS_1 – front side



Wallette WS_1 – lateral side



Wallette WS_2 – front side



Wallette WS_2 – lateral side

224 Collapse Shaking Table Test on URM Cavity Wall Structure representative of a Dutch Terraced House



Walette WS_3 – front side



Walette WS_3 – lateral side



Walette WS_4 – front side



Walette WS_4 – lateral side



Walette WS_5 – front side



Walette WS_5 – lateral side



Walette WS_6 – front side



Walette WS_6 – lateral side

226 Collapse Shaking Table Test on URM Cavity Wall Structure representative of a Dutch Terraced House

Failure mechanisms of clay *walletes* for compressive strength tests:



Wallette WCL_1 – front side



Wallette WCL_1 – lateral side



Wallette WCL_2 – front side



Wallette WCL_2 – lateral side



Walette WCL_5 – front side



Walette WCL_5 – lateral side



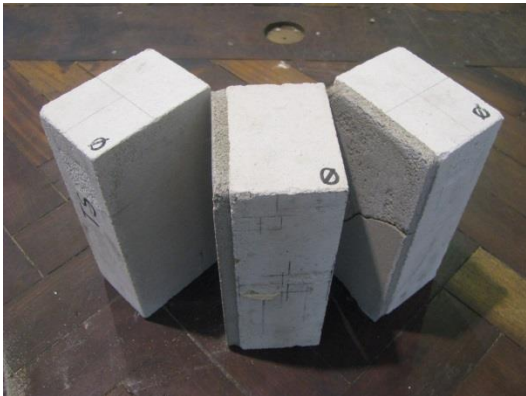
Walette WCL_6 – front side



Walette WCL_6 – lateral side

228 Collapse Shaking Table Test on URM Cavity Wall Structure representative of a Dutch Terraced House

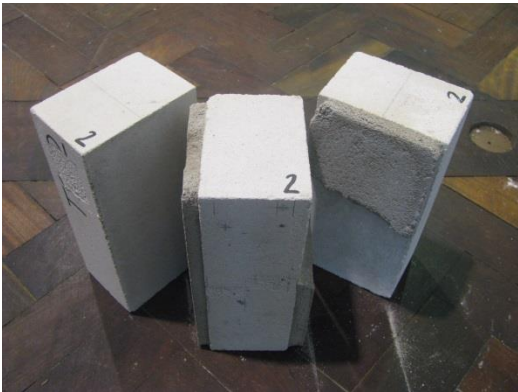
Failure mechanisms of calcium silicate triplets for shear strength tests:



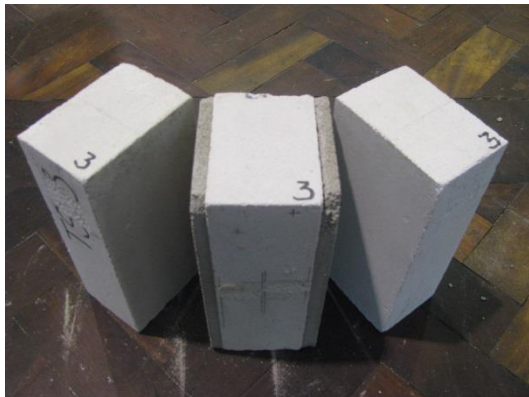
Triplet TS_0



Triplet TS_1



Triplet TS_2



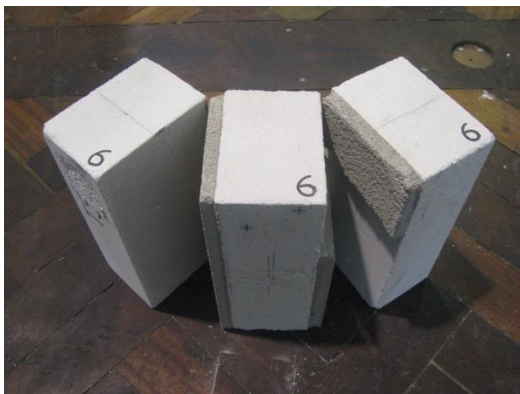
Triplet TS_3



Triplet TS_4



Triplet TS_5



Triplet TS_6



Triplet TS_7



Triplet TS_8



Triplet TS_9



Triplet TS_10

Triplet TS_11

230 Collapse Shaking Table Test on URM Cavity Wall Structure representative of a Dutch Terraced House

Failure mechanisms of clay triplets for shear strength tests:



Triplet TCL_0



Triplet TCL_2



Triplet TCL_3



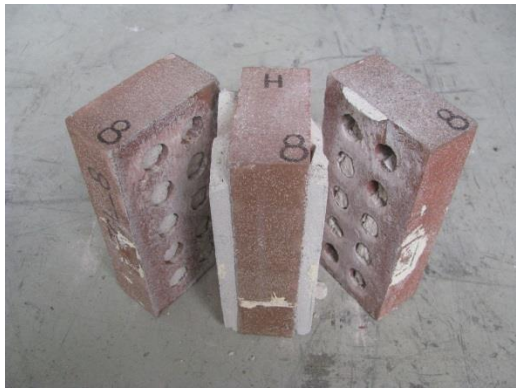
Triplet TCL_4



Triplet TCL_5



Triplet TCL_6



Triplet TCL_7

Triplet TCL_8



Triplet TCL_9

232 Collapse Shaking Table Test on URM Cavity Wall Structure representative of a Dutch Terraced House

Failure mechanisms of calcium silicate triplets for bond wrench tests:



Triplet BWS_0



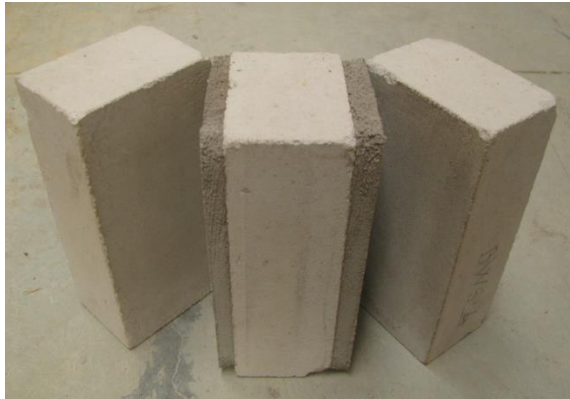
Triplet BWS_1



Triplet BWS_2



Triplet BWS_3



Triplet BWS_4



Triplet BWS_5

Failure mechanisms of clay triplets for bond wrench tests:



Triplet BWCL_1



Triplet BWCL_2



Triplet BWCL_3



Triplet BWCL_4



Triplet BWCL_5



Triplet BWCL_6

234 Collapse Shaking Table Test on URM Cavity Wall Structure representative of a Dutch Terraced House



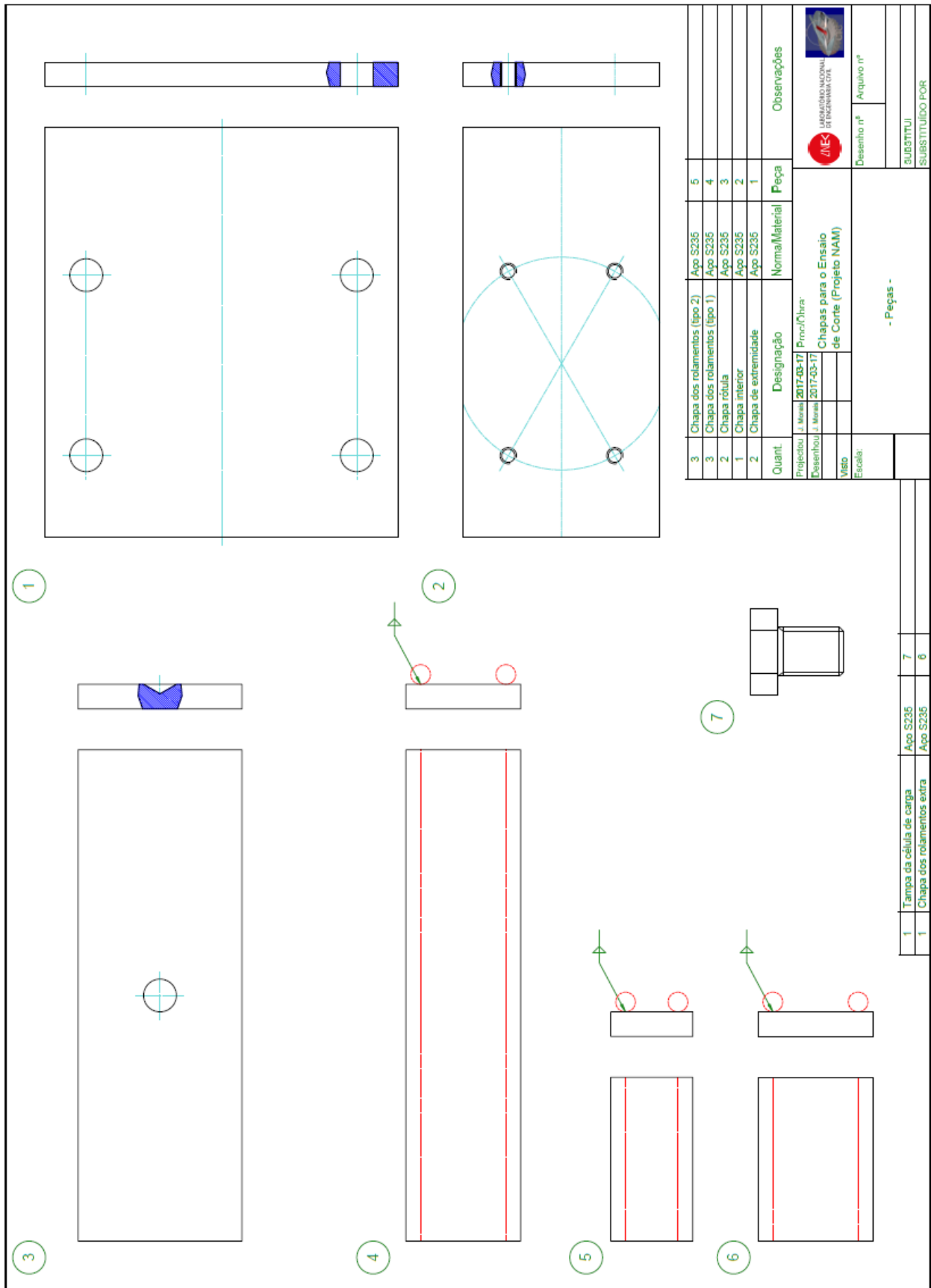
Triplet BWCL_7

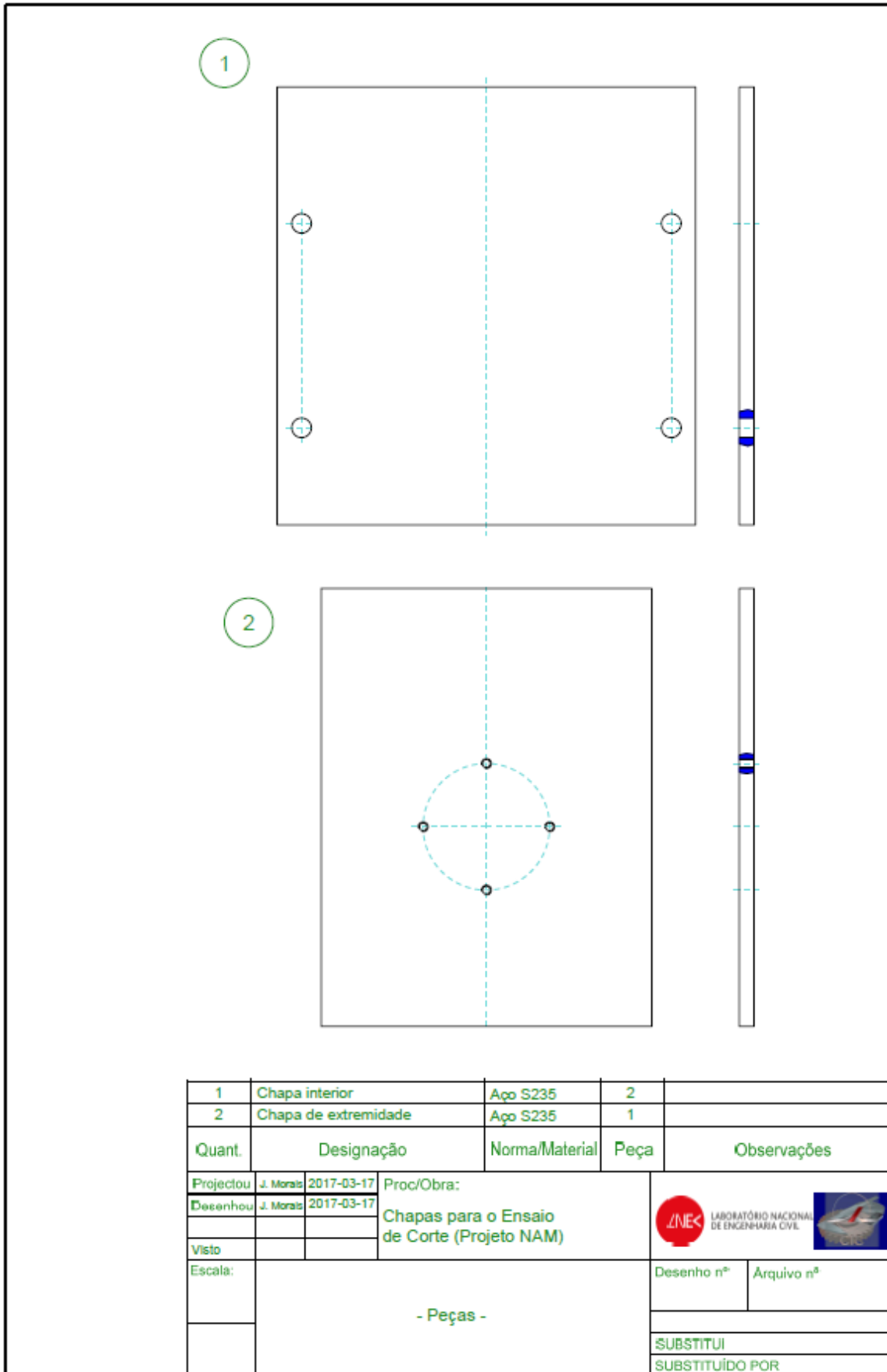


Triplet BWCL_8

ANNEX VI
Design of test devices for material characterisation tests

Device for shear strength tests:

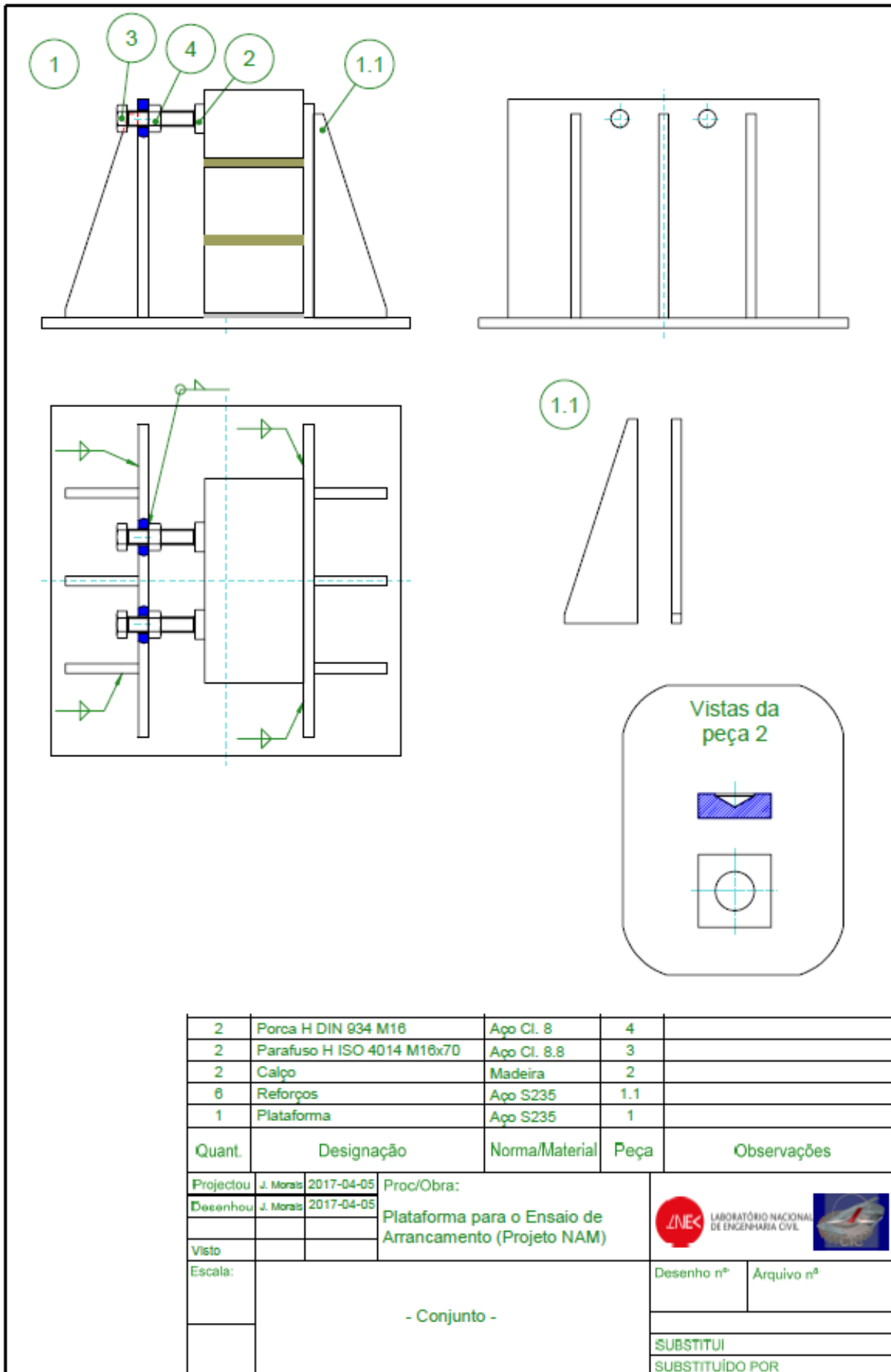




1	Chapa interior	Aço S235	2	
2	Chapa de extremidade	Aço S235	1	
Quant.	Designação	Norma/Material	Peça	Observações
Projectou	J. Morais	2017-03-17	Proc/Obra:	
Desenhou	J. Morais	2017-03-17	Chapas para o Ensaio de Corte (Projeto NAM)	
Visto			 	
Escala:				
	- Peças -			
			SUBSTITUI	
			SUBSTITUÍDO POR	

Device for bond wrench tests:

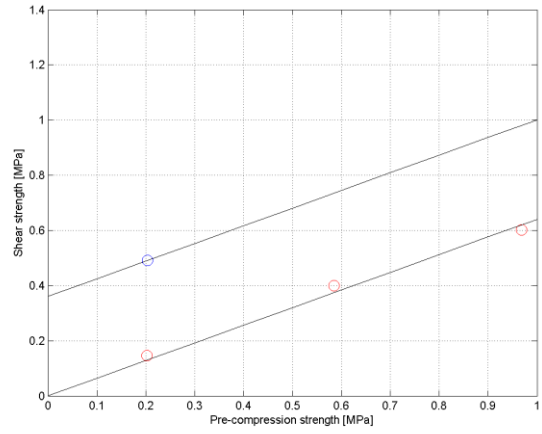
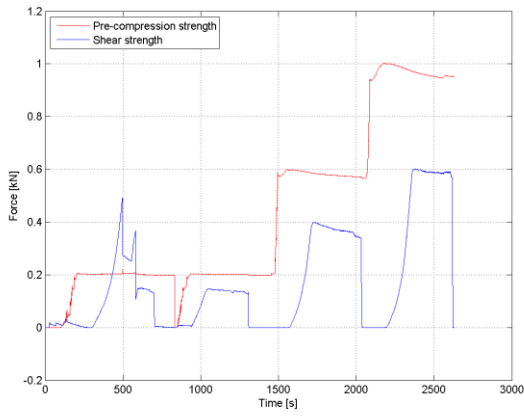
3	Forca H DIN 934 M16	Aço Cl. 8	7
4	Parafuso H ISO 4014 M10x40	Aço Cl. 8.8	6
3	Parafuso H ISO 4014 M16x70	Aço Cl. 8.8	5
1	Casquilho	Aço S235	4
2	Calço	Madeira	3
2	Placa de enchimento	Madeira	2
1	Garra	Aço S235	1
Quant.	Designação	Normal/Material	Peça
Projecto: J. Ivoval 2017-04-05 Proc/Obras:			
Desenho: J. Ivoval 2017-04-05			
Garra para o Ensaio de Arrancamento (Projeto NAM)			
- Conjunto -			
Desenho nº		Arquivo nº	
SUBSTITUI		SUBSTITUIDO POR	
Observações			



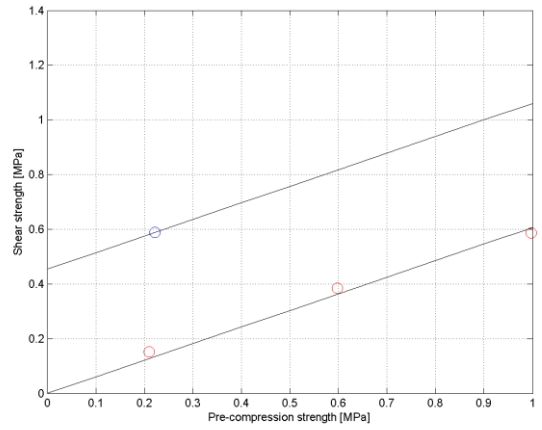
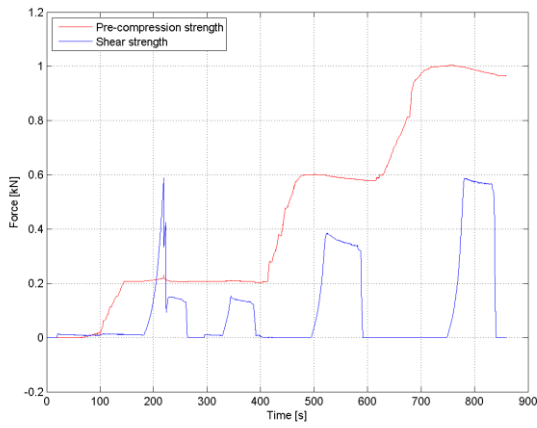
ANNEX VII
Individual results from shear strength tests

244 Collapse Shaking Table Test on URM Cavity Wall Structure representative of a Dutch Terraced House

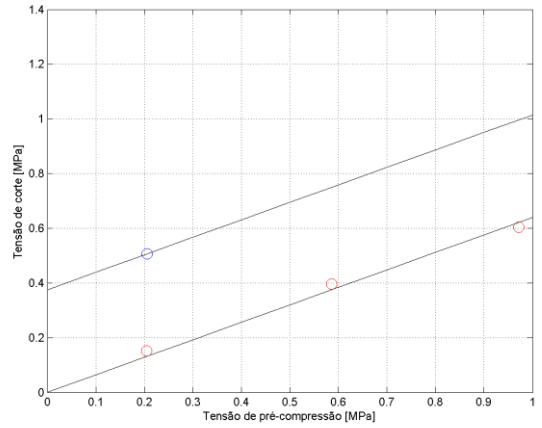
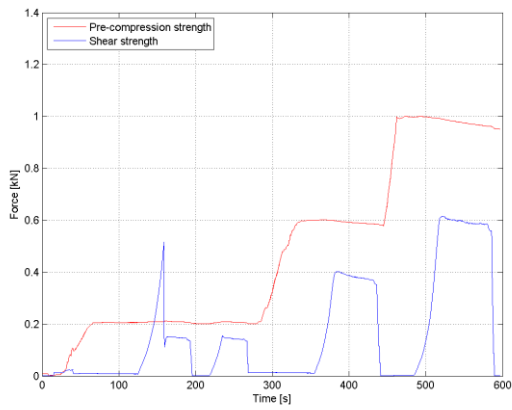
Results for calcium silicate triplets from shear strength tests:



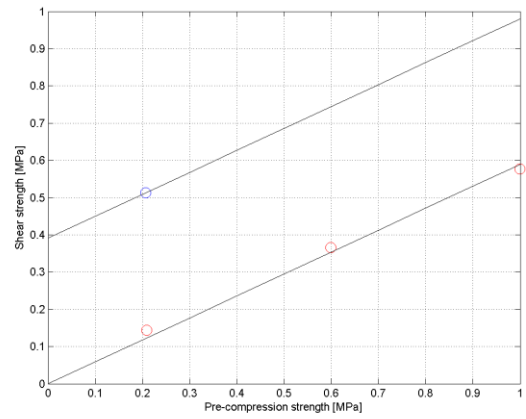
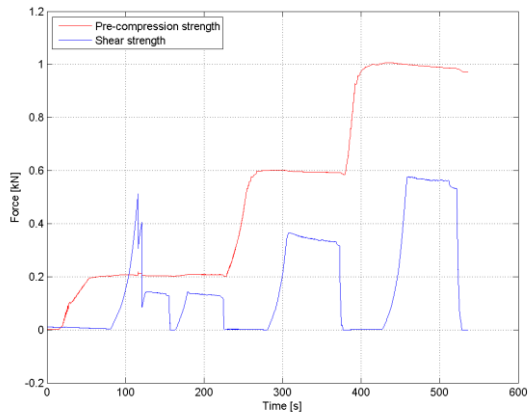
Triplet TS_1



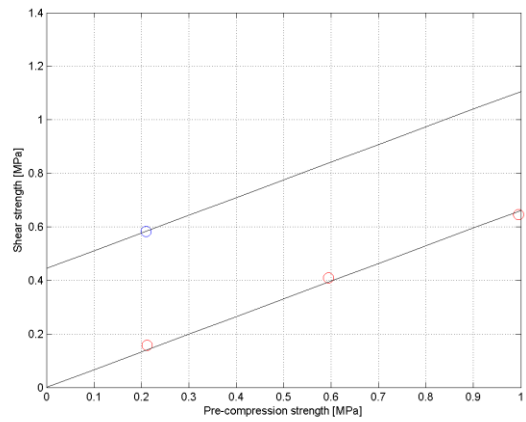
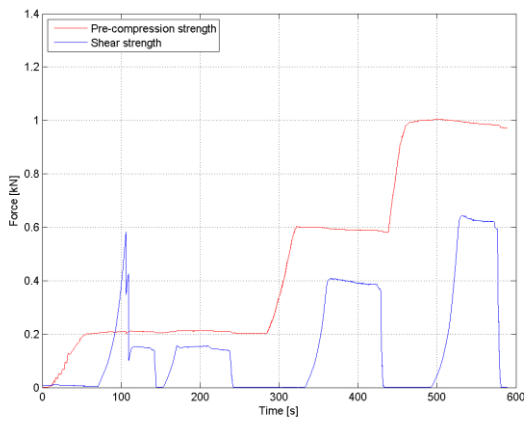
Triplet TS_2



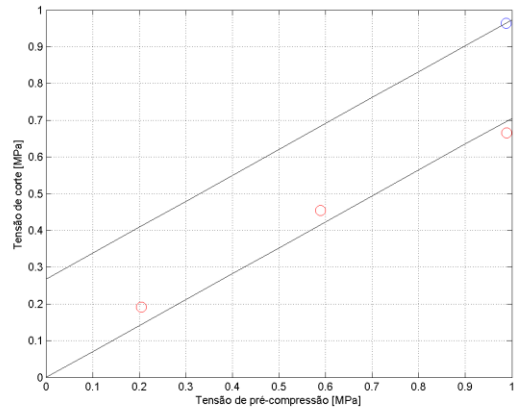
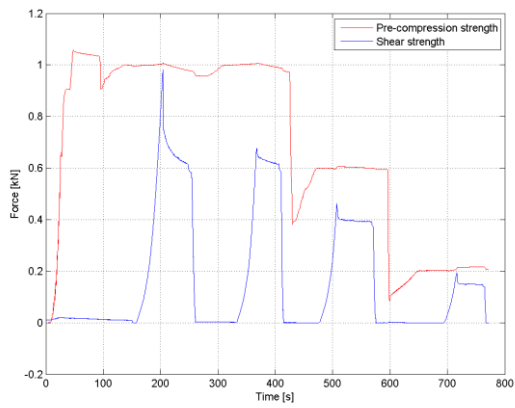
Triplet TS_3



Triplet TS_4

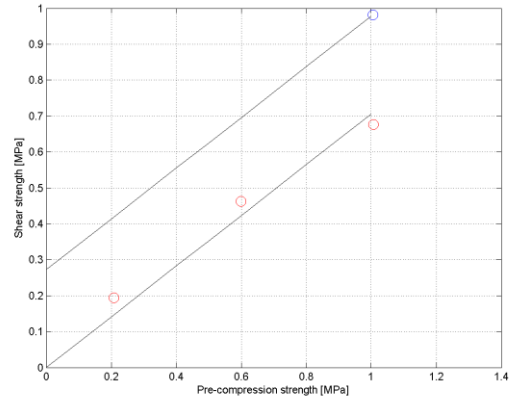
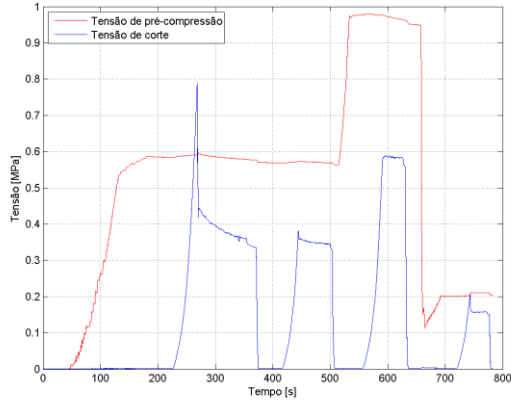


Triplet TS_5

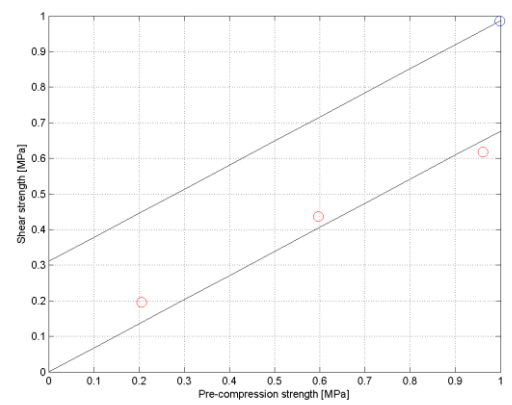
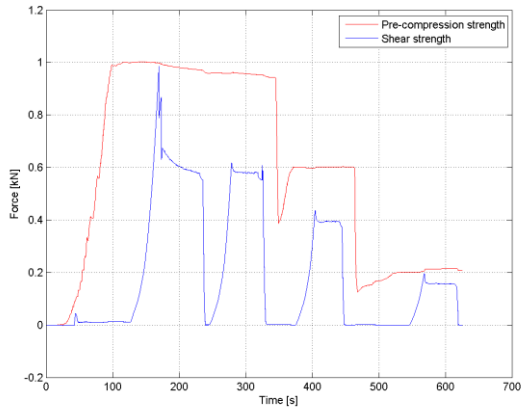


Triplet TS_6

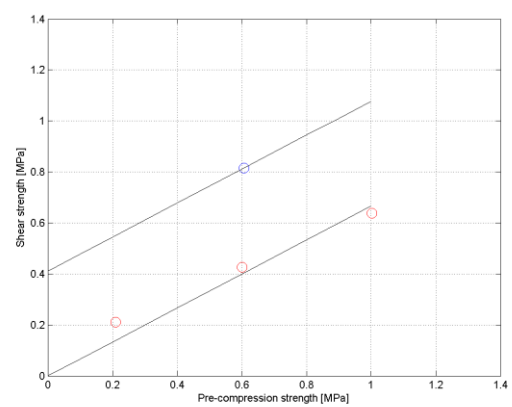
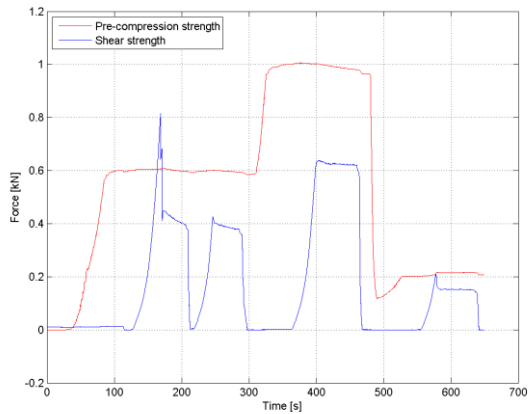
246 Collapse Shaking Table Test on URM Cavity Wall Structure representative of a Dutch Terraced House



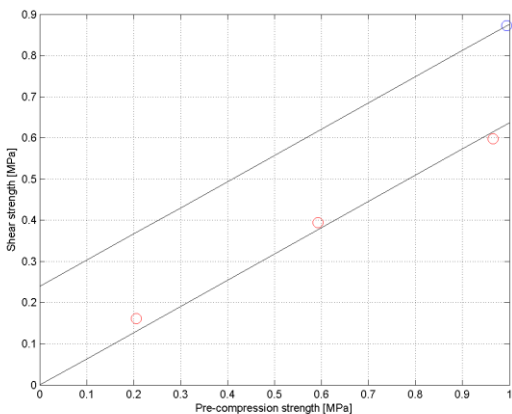
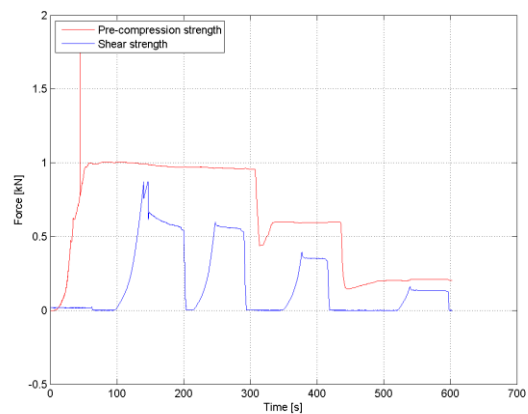
Triplet TS_7



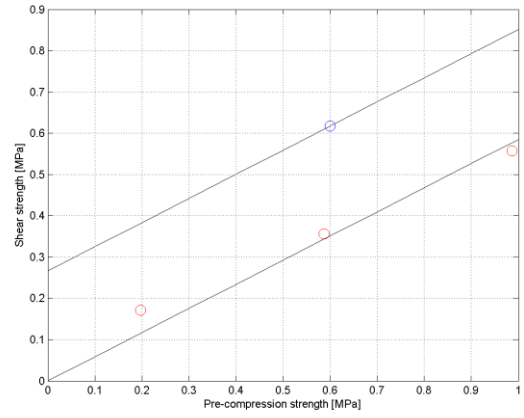
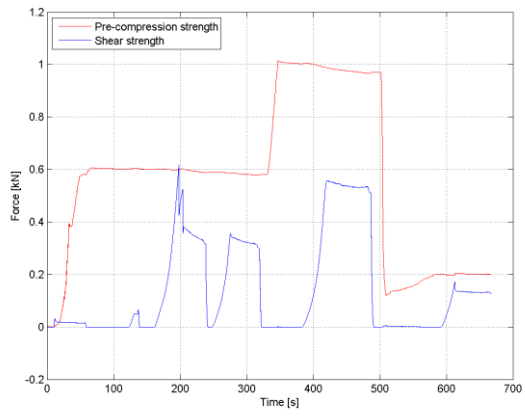
Triplet TS_8



Triplet TS_9



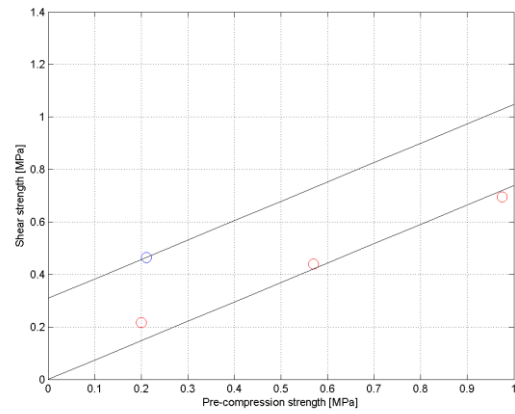
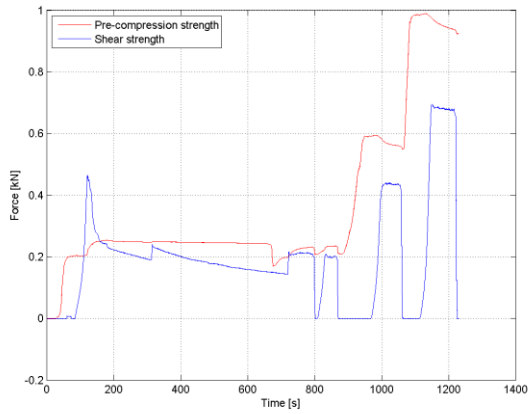
Triplet TS_10



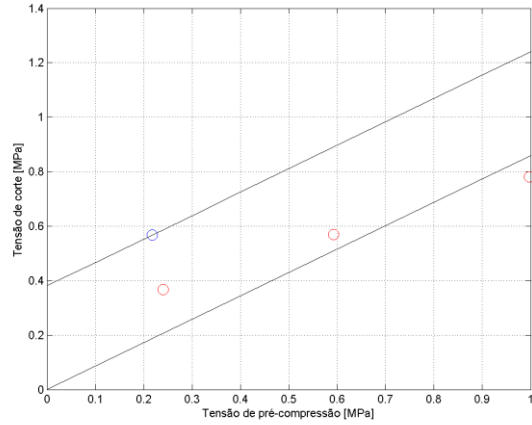
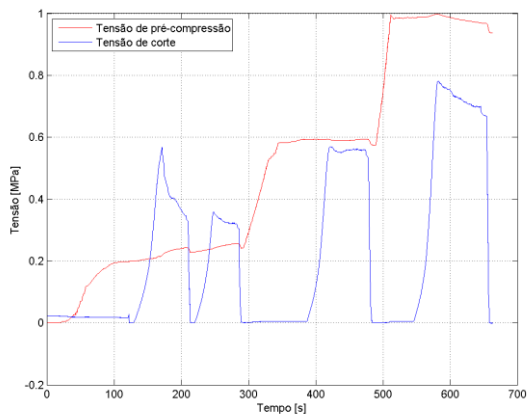
Triplet TS_11

248 Collapse Shaking Table Test on URM Cavity Wall Structure representative of a Dutch Terraced House

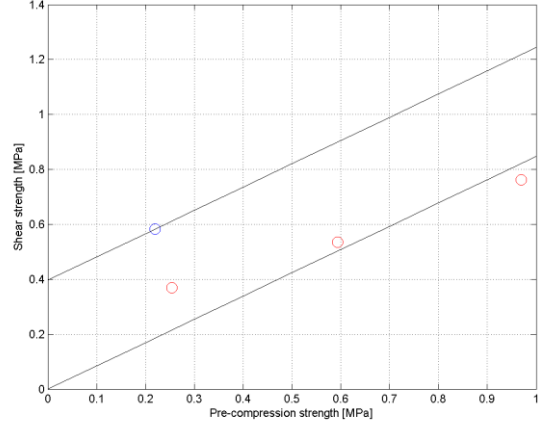
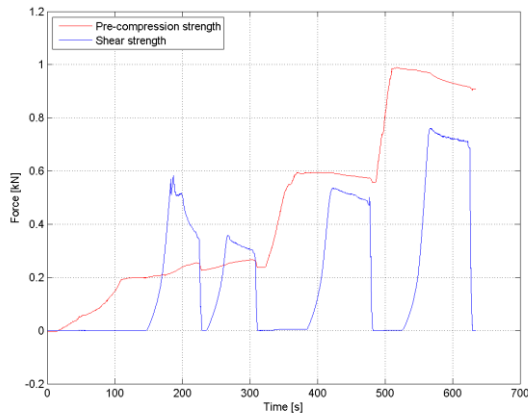
Results for clay triplets from shear strength tests:



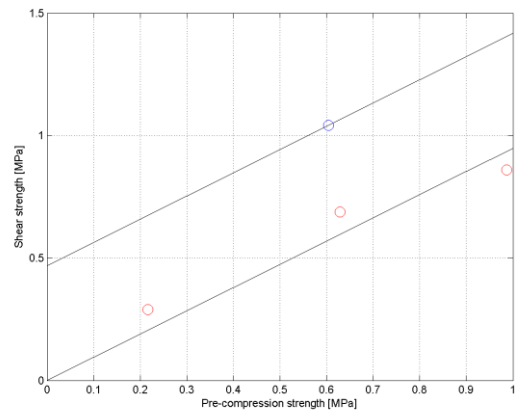
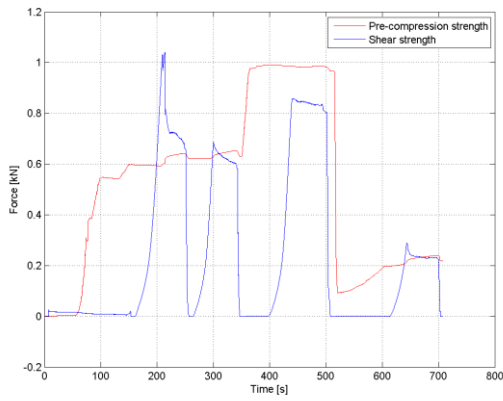
Triplet TCL_0



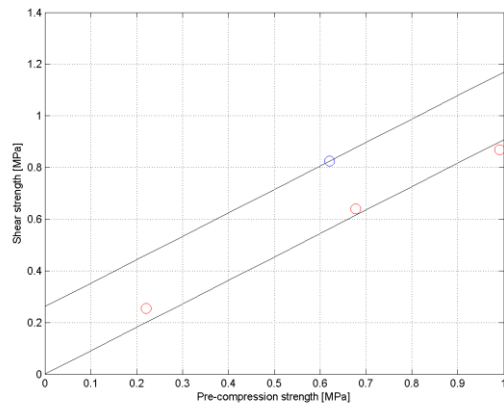
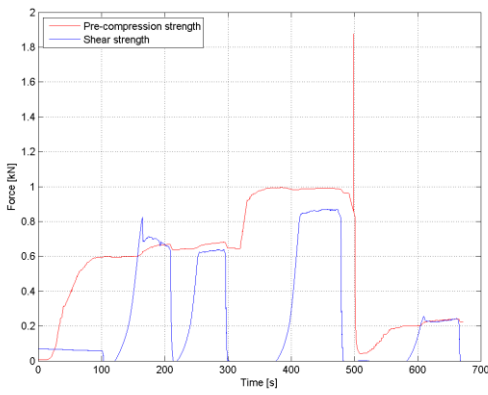
Triplet TCL_2



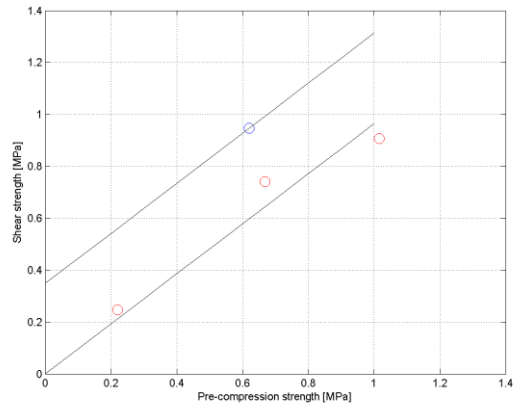
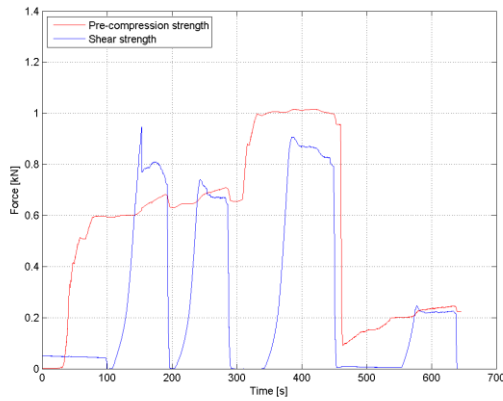
Triplet TCL_3



Triplet TCL_4

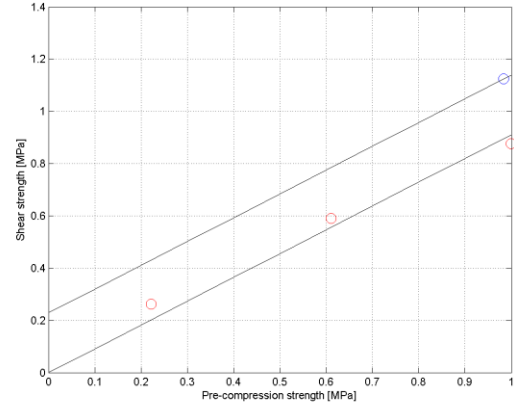
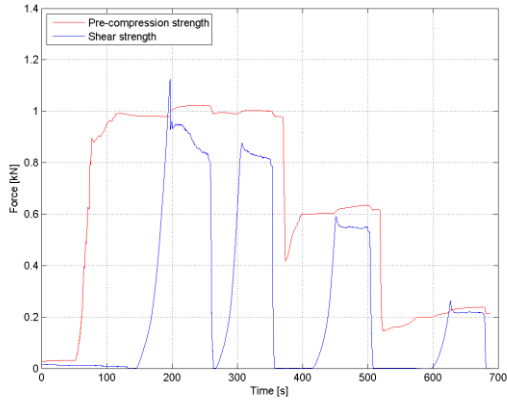


Triplet TCL_5

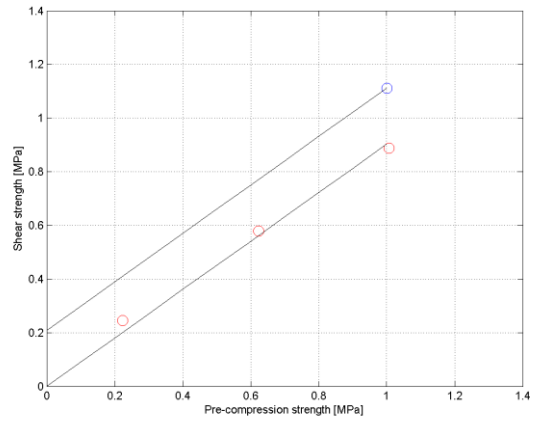
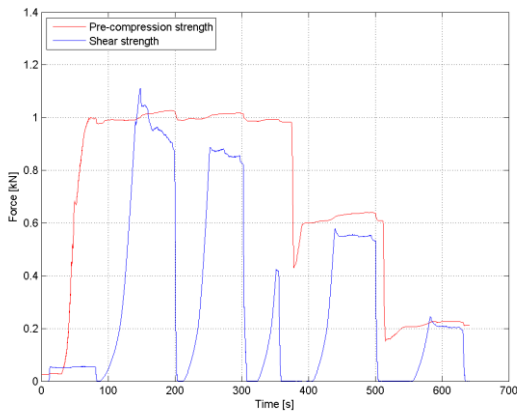


Triplet TCL_6

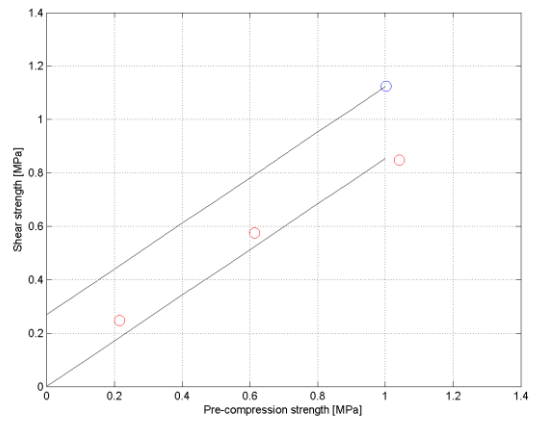
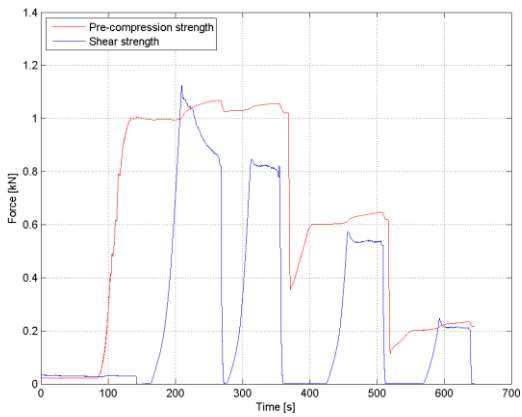
250 Collapse Shaking Table Test on URM Cavity Wall Structure representative of a Dutch Terraced House



Triplet TCL_7



Triplet TCL_8



Triplet TCL_9



Research Report
